NEW MEXICO BUREAU OF GEOLOGY AND MINERAL RESOURCES

Hydrogeologic Investigation of the Southern Taos Valley, Taos County, New Mexico

Peggy S. Johnson
Paul W. Bauer
Brigitte Felix

Final Technical Report
August 2016 (updated November 2016)
Open-File Report 581

New Mexico Bureau of Geology and Mineral Resources

A division of New Mexico Institute of Mining and Technology

Socorro, NM 87801
(575) 835 5490
Fax (575) 835 6333
geoinfo.nmt.edu

Hydrogeologic Investigation of the Southern Taos Valley, Taos County, New Mexico

Peggy S. Johnson
Paul W. Bauer
Brigitte Felix

Final Technical Report
August 2016 (updated November 2016)
Open-File Report 581

AQUIFER MAPPING PROGRAM

New Mexico Bureau of Geology and Mineral Resources

PROJECT FUNDING

Taos County
New Mexico Bureau of Geology and Mineral Resources, Aquifer Mapping Program
Healy Foundation

Cover photograph: View north down the Picuris piedmont in an area where Quaternary sand and gravel deposits cover a complex system of buried Embudo faults and Picuris-Pecos faults. Proterozoic rocks of the Sangre de Cristo Mountains are on the right horizon, and isolated volcanoes of the Taos Plateau volcanic field in the Rio Grande rift are on the left horizon. The water well being drilled in the fall of 2015 penetrated 1200 feet of Santa Fe Group and Picuris Formation sedimentary rocks. *Photograph by Paul Bauer*

CONTENTS

Figures

Tables

Plates

Appendices

(Available in digital format)

View west across the Picuris piedmont from just east of Ponce de Leon spring. The orange rocks in the foreground are Proterozoic rocks of the Miranda Granite. Arroyo Miranda runs from left to right in the middle distance, with the homes of the Ponce de Leon neighborhood built on Tertiary rocks of the Picuris Formation. On the left horizon are the Proterozoic rocks of the Picuris Mountains, which grade northward down the Picuris piedmont to the Rio Pueblo de Taos canyon. On the distant skyline to the right are the Proterozoic rocks of the Tusas Mountains. *Photo by Paul Bauer*.

EXECUTIVE SUMMARY

The southern Taos Valley hydrogeologic study area is bounded to the south by the Picuris Mountains, to the north by the Rio Pueblo de Taos, and to the east approximately by the west boundary of the Town of Taos. It contains the neighborhoods of Ranchos de Taos, Talpa, Los Cordovas, Llano Quemado, Ranchito, La Cordillera, and Tierra Blanca, as well as the mostly undeveloped land to the west. The study area also includes Miranda Canyon, south of Llano Quemado.

For the approximately 3000 residents of the study area, 100% of their domestic (self-supplied private wells) and public (MDWCA, subdivisions, mobile home parks) water supplies come from groundwater. Although the number of private wells in the area is unknown, it probably exceeds 1000. The major public water suppliers are the Ranchos de Taos MDWCA, the Talpa MDWCA, the Llano Quemado MDWCA, and the Ranchitos MDWCA.

The study area also contains over 20 acequias and irrigation ditches, the Taos Country Club (18-hole golf course), the Taos Regional Wastewater Treatment Plant, Town of Taos production wells, several deep exploration wells, the Ponce de Leon geothermal area, Carson National Forest lands, and a large area of private land that could potentially be subdivided in the future.

The southern Taos Valley has experienced high growth in the last few decades, and population projections suggest that the population could double by the year 2050. As population increases, so will the demand for sustainable sources of potable groundwater. In addition, the Abeyta Settlement includes provisions for drilling and developing a number of deep supplemental wells that would be operated to offset depletions agreed upon in the settlement. An important component of managing such groundwater development involves developing a detailed understanding of the geology and hydrogeology of the local aquifers. Such is the goal of this investigation.

The hydrogeologic field investigation of the southern Taos Valley, conducted between January 2011 and October 2015, is the first comprehensive assessment of local groundwater conditions and interactions between local aquifers and the Rio Pueblo de Taos and the Rio Grande. The key to deciphering the groundwater network is development of a geologic model that is capable of depicting the complexities of the local stratigraphy combined with the local structural geology. Our approach to this problem is to integrate state-of-the-art geologic mapping with the latest subsurface information and high-resolution geophysics to create a network of intersecting geologic cross sections of the study area. These cross sections then become the foundation for developing the hydrogeologic model. These studies advance our understanding of the groundwater system in the southern Taos Valley, and the interconnection of groundwater and surface water along the Rio Grande basin in southern Taos County.

The geology and hydrogeology of the study area are enormously complex; the aquifers and the quality of water range from excellent to poor, and the depth to water in wells ranges from

deep to shallow and flowing artesian. The results of this study will demonstrate the complex hydrogeologic conditions that create such remarkable groundwater variations.

This report contains eight detailed hydrogeologic cross sections, a detailed geologic map and ten geologic cross sections, locations of inventoried wells, and data tables of well characteristics, water-level measurements, and results of geochemical sampling. It also contains interpretive maps of a regional water-table surface, the physical, chemical and isotopic characteristics of groundwater including temperature, distribution of dissolved ions and elements, and apparent ^{14}C and tritium (^{3}H) ages of groundwater. Interpretive plots of groundwater geochemistry provide insight into controlling hydrogeochemical processes, sources of groundwater, and groundwater flow paths. When combined, these multiple data sets support a conceptual hydrogeologic model of the groundwater and surface water systems of the southern Taos Valley.

This technical report is expected be a useful resource for subdivision applicants, county officials, and the interested public, as it contains much of the supporting geologic and hydrogeologic information for any site-specific area within the southern Taos Valley. Report findings can help the county make defensible, science-based decisions on water supply and water quality, assist local communities in maintaining adequate water supplies, and guide future use of shallow and deep groundwater supplies.

I. INTRODUCTION

Background

The southern Taos Valley, located just southwest of the Town of Taos, has experienced high growth in the last few decades. The increasing demand for domestic water is dependent on the long-term availability of groundwater. Much of the study area (Fig. 1) is unincorporated, and therefore the county government is responsible for approving or disapproving residential developments. Recently, a variety of residents (homeowners, farmers, developers, county officials, scientists, and others) have expressed concerns about the vulnerability of the groundwater aquifers in the region. The study area contains over 20 acequias and irrigation ditches, the Taos Country Club (18-hole golf course), the Taos Regional Wastewater Treatment Plant, Town of Taos production wells, several deep exploration wells, the Ponce de Leon geothermal area, and a vast amount of private land that could potentially be subdivided in the future. The geology and hydrogeology of the study area are complex; the aquifers and the quality of water range from excellent to poor, and the depth to water in wells ranges from shallow to deep and flowing artesian. The results of this study will demonstrate the complex hydrogeologic conditions that create such remarkable groundwater variations.

The origin of this study dates back to perceived threats to groundwater by a large, proposed development of 150 home sites on about 2,000 acres of a 5,000-acre parcel in Miranda Canyon. In May 2009, the Taos County Planning Commission denied the proposal, and in July 2009 the Taos County Commission unanimously voted down the proposal citing a number of issues, with water supply at the top of the list. The commissioners concluded that their understanding of the groundwater system in Miranda Canyon, and its connection to Llano Quemado and the Rio Pueblo de Taos, was not adequate to evaluate their water-related concerns. In August 2009, the commissioners invited Paul Bauer and Peggy Johnson to present a seminar on the geology and hydrogeology of Taos County, and then initiated a discussion on whether the New Mexico Bureau of Geology (NMBGMR) could perform a comprehensive hydrogeologic study of the southern Taos Valley. In May 2010, the County Commission discussed enacting a three-year moratorium on subdivisions and major developments, during which they could collect independent hydrogeologic information on the area. However, in July 2010, the County Commission tabled the moratorium. In August of 2010, the Taos County Manager (Adam Baker) requested a scope of work from the NMBGMR for a hydrogeologic investigation of the southern Taos Valley, and in January 2011, we began a three-year, $150,000 study of the area. At about the same time, the Trust for Public Land, a non-profit organization dedicated to land conservation, took ownership of the Miranda Canyon property, and in October 2012 the U.S. Forest Service began a process that led to the purchase of the entire 5,000 acres.

Taos County's land use regulations (Ordinance No. 2014-1, adopted in 2014) state that for major developments the applicant must demonstrate a 50-year water supply and submit a detailed geohydrologic report that "*shall contain maps and cross-sections showing geology, depth to the water-bearing formation, water-level contours, and the estimated thickness of saturation in the aquifer.*" (Ordinance appendix 2, section 1B). Furthermore, appendix 2, section 1A of the ordinance states that applications may be rejected in areas where: 1)"*the Office of the State Engineer (OSE) determines groundwater will be supplied from geologic formations that yield minimal amounts of water, fail to recover adequately from pump tests, experience seasonal depth to water, or experience excessive draw downs*"; or 2) "*the groundwater is to be supplied from geologic formations where wells have been determined to produce three gallons per minute or less or where available information suggests the likelihood of low yielding wells*"; or 3) "*the seasonal high water table is four feet or less.*"

This technical report is expected be a useful resource for applicants, county officials, and the interested public, as it contains much of the supporting geologic and hydrogeologic information for any site-specific area within the southern Taos Valley. Report findings can help the county make defensible,

science-based decisions on water supply and water quality, assist local communities in maintaining adequate water supplies, and guide future use of deep groundwater supplies.

Previous Work

Studies of the geology of the Taos County region have been reported in a variety of formats. A series of geologic quadrangle maps has been produced by the NMBGMR (http://geoinfo.nmt.edu/publications/maps/geologic/ofgm/home.cfm), including maps of the entire southern Taos Valley study area

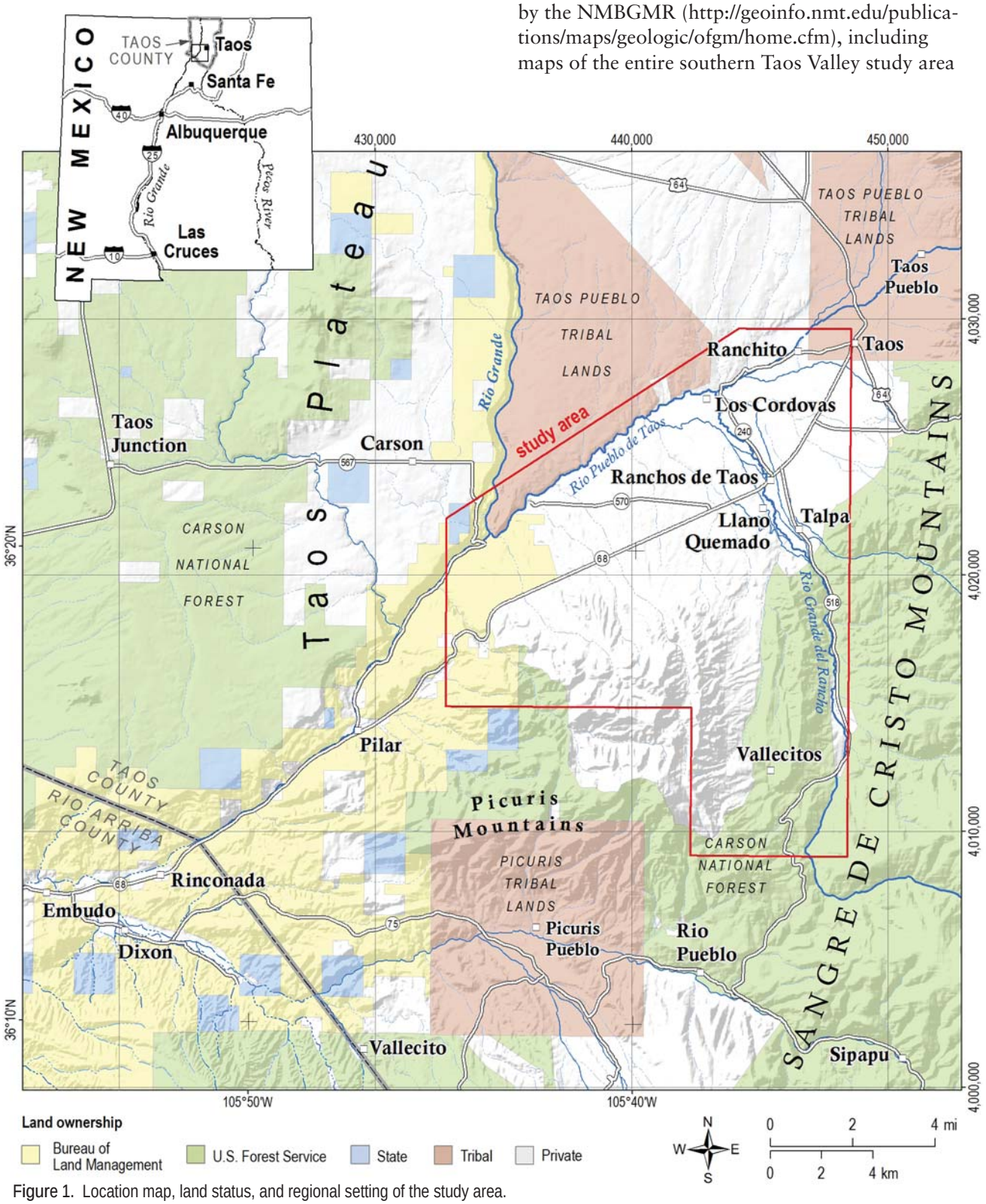

Figure 1. Location map, land status, and regional setting of the study area.

(Bauer et al., 2016). Regional geologic maps (Miller et al., 1963; Lipman and Mehnert, 1975; Machette and Personius, 1984; Garrabrant, 1993) and thesis maps of generally small areas or specialized subjects (Chapin, 1981; Peterson, 1981; Leininger, 1982; Rehder, 1986; Kelson, 1986; Bauer, 1988) also exist for the study area.

A great variety of geologic and hydrogeologic topics are covered in the 2004 New Mexico Geological Society Guidebook (Brister et al., 2004), and by references therein. Several of those papers pertain to the faulting in the study area, including an analysis of the Embudo fault zone (Kelson et al., 2004a) and an evaluation of the rates of extension along the Embudo fault and across the rift (Bauer and Kelson, 2004a). Kelson et al. (1997) published a study of the earthquake potential of the Embudo fault zone. The study included detailed geomorphic mapping and kinematic analysis of faults on the Picuris piedmont from Pilar to Talpa. Drakos et al. (2004a) described the subsurface stratigraphy of the southern San Luis Basin. Grauch and Keller (2004), Bankey et al. (2006) and Grauch et al. (2015) provided updated interpretations of regional geophysical studies of the southern San Luis Basin. USGS scientists are currently working on a major revision of the gravity model for the entire San Luis Basin (Drenth et al., 2015).

Published literature on regional water resources includes a report on the availability and quality of water in Taos County (Wilson et al., 1978), a general water resource inventory of Taos County (Garrabrant, 1993), a surface water assessment of Taos County (Johnson, 1998), a summary of the groundwater geology of Taos County (Benson, 2004), a regional groundwater flow model related to the Abeyta water rights settlement (Burck et al., 2004), and a summary of the hydrology and water supply of the Taos valley (Shomaker and Johnson, 2005). The Taos Regional Water Plan (Daniel B. Stephens and Assoc., 2008) also contains compilations and summaries of water resource data.

Previously published hydrogeology studies that encompass the southern Taos Valley area include the following. Bryan (1938) summarized the geology and hydrogeology of the San Luis Basin. Coons and Kelly (1984) proposed a regional hydrogeologic conceptual model for groundwater/surface water flow in the San Luis Basin of New Mexico. Hearne and Dewey (1988) published a regional hydrologic analysis of the San Luis Basin of Colorado and New Mexico. A preliminary hydrogeologic analysis of the southeastern Taos Valley (Bauer et al., 1999) slightly overlaps with the eastern edge of the current study area. Drakos et al. (2004b) published a summary of the hydrologic characteristics of the southern San Luis Basin, and Drakos et al. (2004c) presented a hydrogeochemical study of the aquifers in the southern San Luis Basin. Benson (2004) compiled water levels from drillers' records, and created a regional, contoured groundwater map of Taos County. Bauer et al. (2007) inventoried the springs of the Rio Grande gorge in Taos County.

Purpose and Scope

The principle objective of this study was to characterize and interpret the shallow three-dimensional geology and hydrogeology of the southern Taos Valley. The methodology used involved compiling existing geologic, geophysical and hydrologic data, collecting new hydrologic and geochemical data, and interpreting it all in a geologic context.

Field work in the southern Taos Valley was conducted by staff of the NMBGMR primarily between January 2011 and September 2013, although data have been collected as recently as the fall of 2015. Field data collection included locating water wells in the study area, surveying their locations, and measuring groundwater levels and collecting samples at suitable sites. The second phase of work included compiling geologic maps, interpreting existing geophysical data, incorporating new geophysical data, drawing hydrogeologic cross sections, and developing a 3-dimensional geologic model. During the final phase of the project, we analyzed the hydrologic and geochemical data, integrated these data into the geologic model, and developed a conceptual model of groundwater flow for the southern Taos Valley.

The report contains a detailed geologic map, ten geologic cross sections, eight hydrogeologic cross sections, locations of inventoried wells, and data tables of well characteristics, water-level measurements, and results of geochemical sampling and laboratory analyses of groundwater chemistry. It also contains interpretive maps of a regional potentiometric surface, the physical, chemical and isotopic characteristics of groundwater including temperature, distribution of dissolved ions and elements, and the apparent carbon-14 (^{14}C) and tritium (^{3}H) ages of groundwater. Interpretive plots of groundwater geochemistry provide additional insight into controlling hydrogeochemical processes, sources of groundwater, and groundwater flow paths. The resulting conceptual hydrogeologic model of the

groundwater flow system will advance understanding of the groundwater system and the interconnection of groundwater and surface water among the Picuris Mountains, the Picuris piedmont, the Rio Grande del Rancho, the Rio Pueblo de Taos, and the Rio Grande.

Description of the Study Area

Geography

The southern Taos Valley study area is situated at the southern end of the San Luis Basin of northern New Mexico and southern Colorado. The Rio Grande occupies a deep canyon that has been cut into the basin. In New Mexico, the Rio Grande gorge separates the Taos Plateau to the west from the piedmont slopes to the east, which rise gently eastward to join the Taos Range of the Sangre de Cristo Mountains (Fig. 1). The Taos Plateau is a low-relief landscape that is punctuated by broad, high-relief volcanoes.

The highlands in the southern part of the study area are the Picuris Mountains, a westward prong of the Sangre de Cristo Mountains. The Picuris Mountains drain northward across large alluvial fan deposits to the Rio Pueblo de Taos. For the purposes of this report, the area between the mountains and the Rio Pueblo de Taos will be referred to as the "Picuris piedmont."

The study area (92 mi^2, 238 km^2) includes the foothills of the Picuris Mountains (including much of Miranda Canyon) and the Picuris piedmont, which extends northward to the Rio Pueblo de Taos, eastward to just past the Rio Grande del Rancho valley, and westward to the Rio Grande gorge (Fig. 1). The area includes the unincorporated traditional communities of Ranchos de Taos, Talpa, Llano Quemado, Los Cordovas, and Ranchito, as well as eight Taos County neighborhood associations (Fig. 2).

Geomorphology and surface hydrology

The southern Taos Valley displays a well-integrated system of streams and arroyos (Fig. 3). The Rio Pueblo de Taos flows southwestward across the northern study area, whereupon it joins the Rio Grande near the Taos Junction Bridge. The Rio Pueblo de Taos originates high in the Sangre de Cristo Mountains, with a watershed area of about 418 mi^2 (Fig. 4). In the north-central part of the study area, the Rio Pueblo de Taos changes from a low-gradient meandering stream in a small canyon to a high-gradient stream that has cut a deep canyon through the basalts.

The principal tributary to the Rio Pueblo de Taos is the Rio Grande del Rancho, a perennial stream with a medium-sized watershed (150 mi^2) in the Proterozoic, Paleozoic, and Tertiary rocks of the northwestern Picuris Mountains (Fig. 4). The stream drains several high peaks (nearly 12,000 ft in elevation) in the Sangre de Cristo Mountains. A secondary tributary is the Rio Fernando de Taos, a perennial stream with a watershed area of about 68 mi^2 in the Paleozoic sedimentary rocks of the Sangre de Cristo Mountains. Both of these tributaries join the Rio Pueblo de Taos in the area of the community of Los Cordovas, in the northeastern part of the study area. In hydrologic discussions, we refer to this area as "the confluence".

The Rio Grande del Rancho is joined by two small perennial tributaries near Talpa, the Rio Chiquito and Arroyo Miranda. The Rio Chiquito has a small watershed in the Paleozoic rocks east of Talpa. Arroyo Miranda drains the Proterozoic, Paleozoic, and Tertiary rocks of the Picuris Mountains, and is an ephemeral stream above the Ponce de Leon springs, and a perennial stream below the springs.

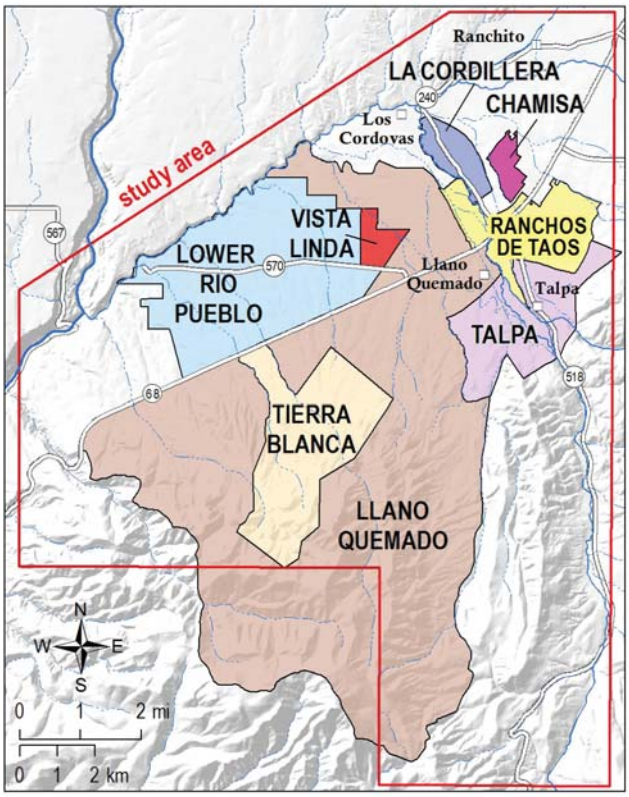

Figure 2. Neighborhood associations of the study area. Courtesy of the Taos County Planning Department.

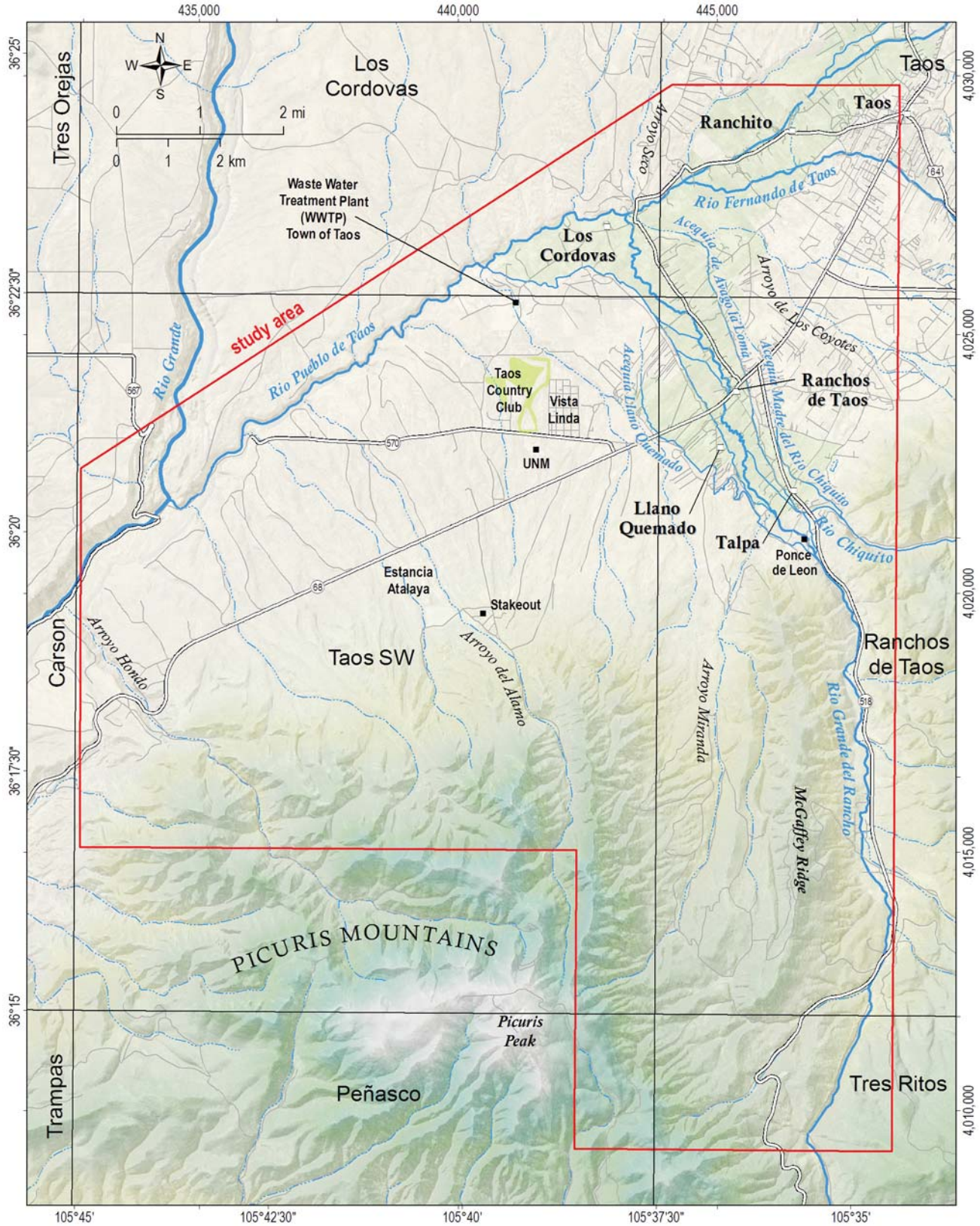

Figure 3. Physiographic features of the southern Taos Valley, with acequias and sites of interest. The study area is outlined in red.

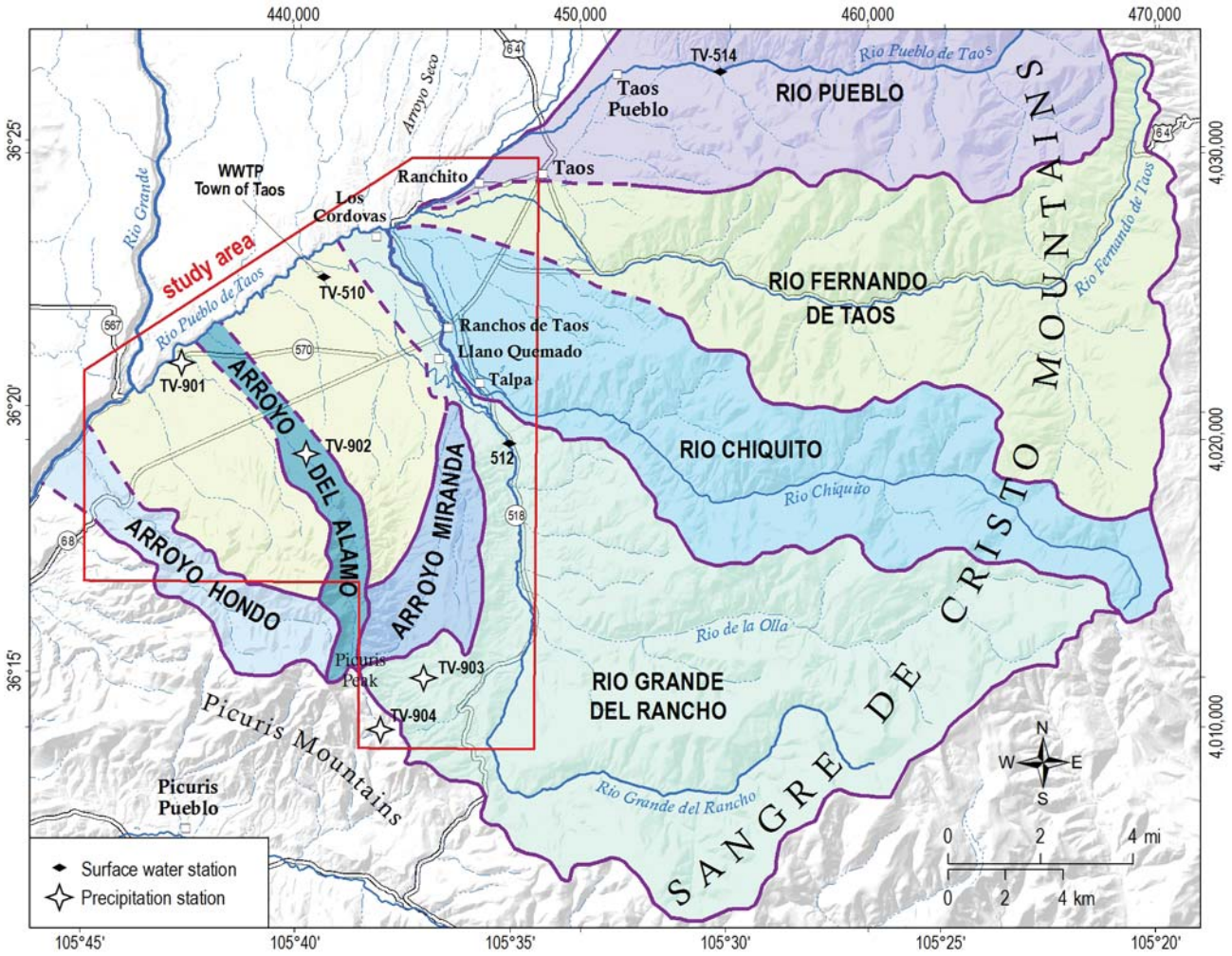

Figure 4. Watersheds of the Taos Valley, with surface water sample sites and precipitation collection stations.

Two other named ephemeral drainages exist within the study area. Arroyo del Alamo drains the Proterozoic rocks of the Picuris Mountains in the central study area. Although Arroyo del Alamo is typically dry where it crosses the Picuris piedmont, local reaches in the upper canyon may be wet. The second drainage is Arroyo Hondo, along the western edge of the study area, which drains the interior of the Picuris Mountains. Although some reaches of Arroyo Hondo in the mountains are perennial, it is typically dry from NM-68 to the confluence with the Rio Grande.

According to information provided by the Taos Valley Acequia Association, the Rio Grande del Rancho, Rio Chiquito, and Rio Fernando de Taos supply water to 24 acequias and ditches, which distribute water to 966 acres of irrigated land in the study area (Fig. 3). Some of these acequias and ditches are continually flowing during the irrigation season, whereas others flow intermittently or not at all.

Land status and accessibility

The study area (Fig. 1) consists principally of private land, although several recent land transfers have significantly increased the federal land area. In 2003, the BLM acquired 2,581 acres of land between NM-68 and the Rio Grande gorge. This Taos Valley Overlook is now part of the Rio Grande del Norte National Monument. In 2013, the BLM also acquired 78 acres of contiguous land at the west end of County Road 110. In 2012–2013, 5,000 acres in Miranda Canyon were purchased by the U.S. Forest Service. This parcel is contiguous with Carson National Forest lands that extend eastward from Arroyo Miranda. Within the map area, all of the land north of the Rio Pueblo de Taos and east of the Rio Grande is part of Tract A of the Pueblo of Taos.

Much of the study area is accessible by road, with permission of landowners on the private parcels and private roads.

II. METHODS

This section describes the methods applied to collection and analysis of the geologic, hydrologic, and geochemical data used in the southern Taos Valley groundwater study. Hydrogeologic field work was conducted by NMBGMR staff between January 2011 and October 2015. The data used in this investigation include:

- published and unpublished geologic map data,
- subsurface geologic data from water-well records and lithologic logs,
- groundwater level and water quality data collected from wells by the NMBGMR in 2011–2015,
- water quality data collected from Rio Grande gorge springs by NMBGMR in 2006–2009, and
- historical groundwater level and water quality data from published and unpublished sources.

Details about data sources, methods and site characteristics are described below.

Geologic Mapping and Cross Sections

Understanding the nature, characteristics, relative age and distribution of geologic strata is essential to any groundwater study. The geologic map used in this study integrates parts of six geologic maps of 7.5-minute quadrangles that were completed under the NMBGMR STATEMAP Program. The maps are credited as follows:

1. Taos SW quadrangle (Bauer et al., 1997)
2. Ranchos de Taos quadrangle (Bauer et al., 2000)
3. Taos quadrangle (Bauer and Kelson, 2001)
4. Los Cordovas quadrangle (Kelson and Bauer, 2003)
5. Peñasco quadrangle (Bauer et al., 2005)
6. Tres Ritos quadrangle (Aby et al., 2007)

Geologic mapping was done principally by Paul Bauer, Keith Kelson, and Scott Aby between 1997 and 2007. Bauer focused on mapping basement (Proterozoic, Paleozoic, and Tertiary) rocks and structures. Kelson focused on air photo interpretation, geologic and geomorphic mapping of surficial deposits and Tertiary rocks, and fault scarps in Quaternary deposits. Aby focused on mapping the Tertiary Santa Fe Group sedimentary units.

The 1:24,000-scale compilation map (Plate 1) shows the distribution of rock units and unconsolidated, surficial, sand and gravel deposits, as well as the locations of known and inferred faults. Some of the geologic units shown in the cross sections are not exposed at the surface in the study area, but are exposed in nearby areas where they have been mapped and analyzed. The physical characteristics of some of these units (such as composition, thickness, texture, and lateral extent) are based on work in these nearby areas. Geologic unit descriptions are included in Appendix 1.

A primary goal of the geologic component of the investigation was to provide a conceptual model of the large-scale geologic structure of the basin beneath the southern Taos Valley. Our approach was to understand the surficial structural geology around the edge of the basin by detailed mapping, and then to infer the subsurface basin structure using that knowledge and all other available data sets, including:

- photographic imagery,
- boreholes,
- geophysics,
- surface structure,
- geomorphology,
- hydrology.

We created ten new geologic cross sections for this study (Plate 2). The locations of the sections were chosen to optimize hydrogeologic understanding, maximize the number of useful wells that could be incorporated into the section lines, and utilize the geophysical insights provided by colleagues Tien Grauch and Ben Drenth of the U.S. Geological Survey. The topographic profiles were generated by ArcGIS software. Geologic cross sections in Plate 2 have no vertical exaggeration in order to accurately depict the stratigraphic and structural relationships.

Some of the same cross sections are shown later in this report at three times vertical exaggeration, and to a depth of 3,500 feet, to better illustrate the details of the wells and the hydrology.

The geologic units shown in the cross sections originated from three principal data sources:

1. 1:24,000 geologic quadrangle maps,
2. Interpretations from borehole geology and borehole geophysics, and
3. Interpretations from three geophysical data sets—a high-resolution aeromagnetic survey, ground-magnetic surveys, and gravity modeling.

The relevance of the various data in creating the geologic map and cross sections is briefly summarized below.

Aerial photogrammetry and field mapping

As part of delineating bedrock units, faults, and basin-fill sediments, the mappers analyzed multiple sets of photographic imagery, all of which have a high degree of clarity and provide good information on surficial deposits and fault-related features. Because of their good coverage and high quality, the air-photo analysis primarily utilized 1:15,840-scale color images taken for the USFS from 1973–1975. Following our analysis of aerial photography, we conducted detailed mapping of geologic units and geomorphic features at scales of 1:12,000 and 1:6,000, especially in the Talpa area. Our mapping delineated Quaternary deposits and surfaces, and Quaternary faults, fault scarps, and lineaments. Analysis of faults in all units (Proterozoic to Quaternary) included evaluations of fault geometries and kinematic data. On bedrock faults, fault striations (slickenlines) were combined with kinematic indicators such as offset piercing lines or planes, and calcite steps to infer slip directions. Because of limited fault exposures in Quaternary deposits, we inferred slip directions based on fault scarp geometry, the map pattern of fault strands, and deflected drainages.

Boreholes

The geologic and geophysical data attached to the drill holes in the study area ranged from wells with no data, to wells with extensive analyses of lithologic cuttings, different types of borehole geophysics, and a variety of aquifer and water-quality tests. Domestic well records in the study area are marginally useful for defining the subsurface stratigraphy, as most well drillers do not record the detailed characteristics of well cuttings. In contrast, geologic logs created by on-site geologists who examined well cuttings are generally very helpful for defining the subsurface stratigraphy.

Geophysics

A number of existing and new geophysical studies in the area were incorporated into this investigation. Each of these geophysical techniques can be used alone to provide useful constraints on the subsurface geology, but the real value of these techniques is that when they are interpreted collectively by a geophysicist, they can provide immensely valuable, detailed information on the subsurface geology. Each of the geophysical studies used in the current study are summarized below.

1. Existing high-resolution aeromagnetic survey (Dr. V.J.S. Grauch, USGS). In 2003, Dr. Grauch began a regional aeromagnetic survey of the San Luis Basin (Grauch et al., 2004; Bankey et al., 2006; Grauch et al., 2015). For the current study, she reexamined parts of the existing data set in order to develop an aeromagnetic anomaly map of the study area that shows buried faults and buried volcanic rocks. This method can be effective at delineating buried, large-scale, horizontal and vertical variations in rock type.
2. New ground-magnetic surveys (Dr. V.J.S. Grauch, USGS). Dr. Grauch ran select ground-based magnetic traverses across the Picuris piedmont. This method can precisely locate buried faults and other features that juxtapose materials with different magnetic properties.
3. Gravity surveys and regional gravity model (Dr. Benjamin J. Drenth, USGS). Dr. Drenth has been collecting detailed gravity data, and incorporating these data into a regional gravity model interpretation of the San Luis Basin (Drenth et al., 2015). His main goal was to improve understanding of the thickness of the basin-fill materials and the geometry of the rift basin. The gravity method is especially useful for estimating the general depth to basement rocks and for locating large-offset basement faults.

Development of cross sections

The following list describes the general steps that were taken to create the geologic cross sections developed for this study:

1. **Geologic contacts are picked off of the geologic map.** The surface geology is taken from the geologic map and placed on the topographic profile

of the cross section. Geologic contacts that are buried by thin surficial deposits were estimated. Some of the thinnest Quaternary surficial deposits are not shown on the cross sections.

2. **The gravity model is used to define the depth to basement rocks in the cross sections.** The base of each cross section is constrained by the depth-to-basement curve derived from the USGS gravity model. The depth-to-basement curve depicts a highly smoothed contact between basin-fill sediments and bedrock. In the model, both Paleozoic sedimentary rocks and Proterozoic crystalline rocks are considered to be bedrock.
3. **Geologic information derived from wells and boreholes is added to the cross sections.** Expertly studied wells can help control the regional thicknesses and depths of key stratigraphic formations, including some of the basin-fill units such as the Lama formation and thick clay horizons. Most of the basin-fill stratigraphy (Tesuque Formation (Tt), Chamita Formation (Tc), and Lama formation (QTl)) consist of poorly sorted, clay-to-boulder sized, alluvial material that was eroded from the nearby mountains. Unless the compositions and proportions of rock clasts and the color of the sediment are well described, it is not possible to tell them apart in drill holes. Although the depictions of these units on the cross sections are based principally on borehole data, local stratigraphic relationships, and an understanding of the sedimentary systems and geologic processes of the area, it is possible that the thicknesses of the various basin-fill units are still not accurately represented. For example, in many areas where there is no Servilleta Basalt in the subsurface, it is not possible to confidently place the contact between the Chamita Formation (Tc) and the Lama formation (QTl).
4. **Mapped and inferred faults are drawn onto the cross sections.** For the purposes of this study, the dips of the inferred Embudo faults were estimated to be between 70 and 80 degrees northward, unless evidence existed for some other orientation. In all cases, the geometries of the normal faults drawn in the cross sections are intentionally simplified as single inclined planes, when in fact all of the mapped normal faults in this area have much more complex geometries. They are typically curved, segmented, branched, and composed of multiple overlapping fault planes. Where exposed, faults in bedrock typically display wide fracture zones with high permeabilities, whereas faults in basin-fill sediments commonly display narrow, clay-rich cores with lower permeabilities.
5. **Interpretations from geophysics are added to cross sections.** With consultations from the USGS geophysicists, any additional information gleaned from the geophysics is added to the cross section. For example, this could include evidence for deeply buried volcanic rocks.
6. **Conceptual models of volcanic and sedimentary processes are incorporated into the cross sections.** For example, in this part of the basin, Servilleta Basalt lavas flowed predominantly south and southeast, and therefore would be expected to thin across Embudo fault scarps and interact in complex ways with north- and northwest-prograding alluvial fans from the Picuris and Sangre de Cristo Mountains.
7. **Information from the hydrology is added to the cross sections.** Hydrologic information such as the locations of spring zones, water levels in wells, the locations of streams and acequias, and variations in field parameters such as groundwater temperature, are included on report figures of the hydrogeologic cross sections. Where we have studied the hydrogeology of springs in Taos County, we have found that the location and characteristics of springs are strongly influenced by the geology (Bauer et al., 2007). Specifically, springs tend to occur where contrasts in the hydraulic properties of the rocks exist. Such contrasts can be created by faults, by original variations in rock properties, and by post-depositional effects such as cementation.
8. **Formation contacts are drawn onto the cross sections.** Due to a lack of stratigraphic markers in the southern Taos Valley, the dips of the geologic units are generally unknown. Therefore, unless evidence exists for depicting local dips, contacts have been drawn as sub-horizontal. In most of the study area, thicknesses of buried basin-fill units are poorly constrained, and so the cross sections show approximate formation thicknesses.
9. **The cross sections are checked against the geophysical models.** After each cross section has been drawn, it is checked by our USGS colleagues against the geophysical models from the aeromagnetic and gravity surveys. Where the geophysical model is robust, this is an excellent way to fine tune the geologic model. For example, the aeromagnetic model might suggest that a volcanic layer shown in a cross section should be thicker or thinner, or that a fault must juxtapose materials with more extreme variations in magnetic properties. This iterative

process between geologist and geophysicist is a powerful tool for developing well-constrained geologic models.

Depiction of faults in the cross sections

The fault structures depicted in the cross sections were established from three data sources:

1. *Mapped faults from the geologic map*. These faults are displayed with a high degree of certainty and are referred to as "mapped faults."
2. *Faults inferred from the magnetic and gravity surveys*. These faults are displayed with a moderate to high degree of certainty and referred to as "geophysical faults."
3. *A conceptual model of the geometry and kinematics of the northern Rio Grande rift*. Such faults must exist, but their exact locations are shown with a low degree of certainty. They are referred to as "inferred faults."

Imposing a vertical exaggeration on a cross section results in an apparent steepening of faults and contacts, therefore, the apparent fault dips shown in the exaggerated hydrogeologic cross sections are considerably steeper than those shown on the geologic cross sections. The geologic map (Plate 1) shows a large number of mapped faults, including: 1) segmented oblique-slip fault splays of the Embudo fault zone along the north flank of the Picuris Mountains; 2) normal faults of the Sangre de Cristo fault zone in the northeastern study area; 3) intrabasinal normal faults of the Los Cordovas fault zone; and 4) bedrock strike-slip faults of the Picuris-Pecos fault system.

Modern geophysical techniques using high-resolution magnetic data and gravity data are capable of defining buried faults in Rio Grande rift basins, such as in the southern Taos Valley. Drs. Grauch and Drenth have refined these techniques in the Rio Grande rift. They are currently capable of processing the data in ways that allow them to accurately draw the locations of faults that create geophysical anomalies. There is good correspondence between the mapped faults and the geophysically defined faults, which elevates our confidence in the delineation of buried faults by such geophysical techniques.

Recent gravity modeling by Dr. Drenth also provides an extremely useful tool for estimating the thickness of basin-fill deposits in the rift basin. This technique yields a depth-to-basement curve for the cross sections. As the basement deepens away from the edge of the rift, numerous buried (inferred) faults must exist in order to deepen the basement.

Water-Level Measurements, Water-Table Map, and Groundwater Hydrographs

Water-level measurements from observation wells are the principal source of information about the hydrologic stresses acting on aquifers and how these stresses affect groundwater recharge, storage, and discharge (Taylor and Alley, 2001). A major component of this study was to collect water-level data from a network of wells tapping the basin and mountain aquifers (Fig. 5, Tables 1 and 2). Current and historic water-level data were used to: 1) characterize groundwater flow in the regional basin-fill aquifer; 2) characterize groundwater flow in the shallow aquifers near streams, acequias, and irrigated lands; and 3) establish how groundwater levels have changed over time in various aquifer zones. Groundwater data and hydrographs are presented in report Figures 20–25 and in Appendix 2.

Measurement and inventory methods

Periodic water levels were measured using a graduated steel tape for pump-equipped wells and a Solinst™ electronic sounder for unequipped wells. Measurements were made to a repeatable accuracy of 0.02 ft. Continuous monitoring of water levels was accomplished using automatic sensing and recording instruments. The instrumentation combines a pressure sensor to measure total water and atmospheric pressure at a specified frequency and memory for storing data. In this study, measurements were taken at 12-hour intervals (00:00 and 12:00 hours, midnight and noon) and recorded using a Schlumberger Water Services Diver DI502 20-meter and Mini-Diver DI501 10-meter. Changes in total pressure due to atmospheric variations were corrected using an on-site Schlumberger Baro-Diver DI500 and software. Wells and springs were located in the field with a handheld GPS device and assigned site identification numbers, which are used throughout this report. Elevations of measured wells and springs were calculated in ArcGIS using a 10-meter DEM and GPS-derived coordinates.

Water-table map

A water-table map shows lines of equal elevation of the water table for an unconfined aquifer, or the potentiometric surface for a confined aquifer. It is used to interpret several important aspects of groundwater flow and conditions. Interpretations that can be made from a water-table map include hydraulic gradient, horizontal flow direction, changes in aquifer

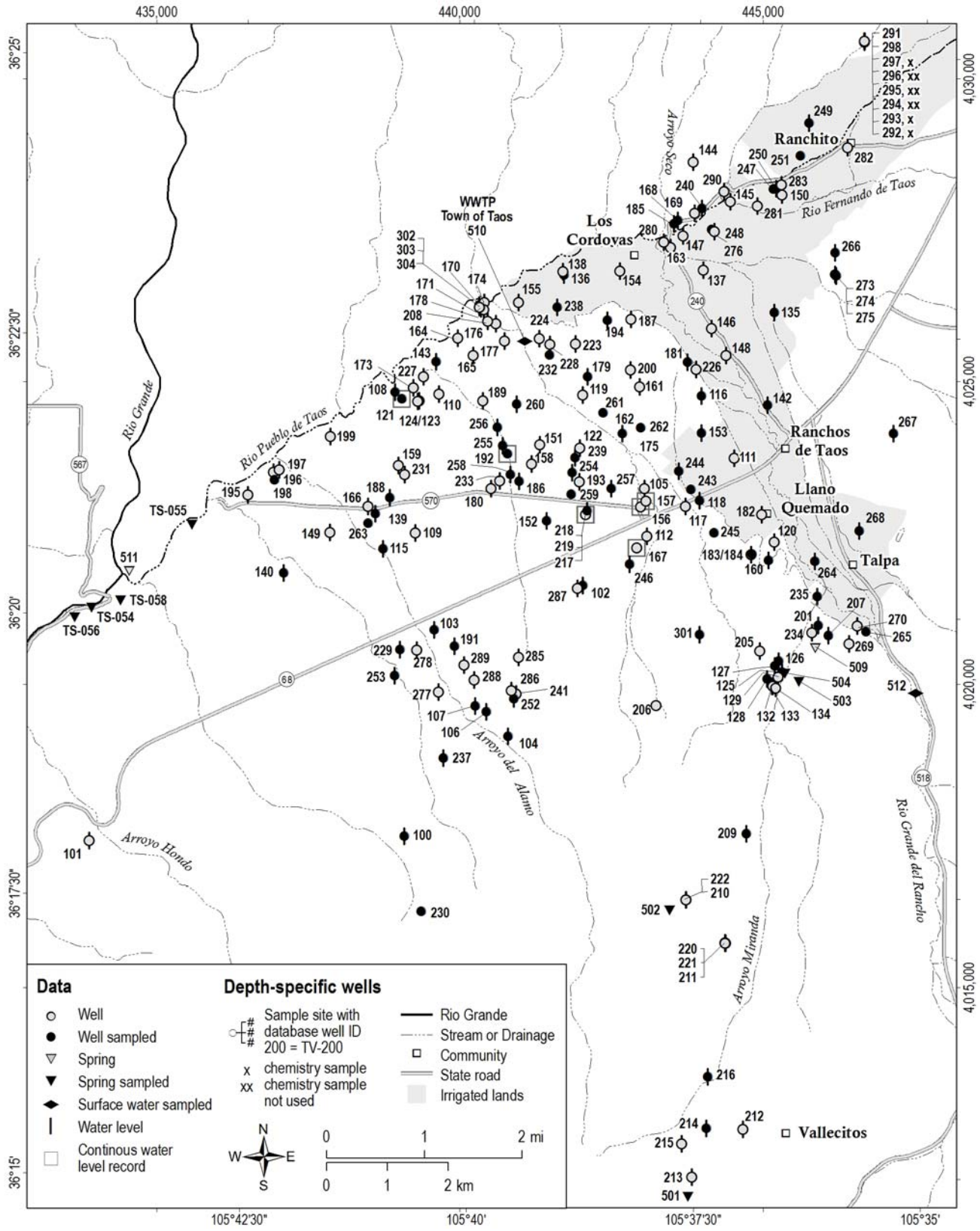

Figure 5. Map of wells, springs, and surface-water sites used in the study. Well, spring, and surface water information is displayed in Tables 1 and 2.

Table 1. Inventory of wells shown on Figure 5, with location, site and construction information.—Continued

WELL LOCATION				SITE INFORMATION					WELL CONSTRUCTION						
Site ID	UTM easting NAD83	UTM northing NAD83	Elevation (ft asl)	NMOSE well record	Water sample	Water level	Site visit	Water bearing formation †	Well depth (ft bls)	Screen top (ft bls)	Screen bottom (ft bls)	Drill date	Driller static water level (ft bls)	Static water elevation (ft asl)	Well yield (gpm)
TV-100	439079	4017493	7751	RG-83352	x	x	x	Tpl	1000	880	1000	11/19/04	505	7246	25
TV-101	433880	4017420	7153	RG-16717		x		Tc	450	380	450	9/26/69	400	6753	
TV-102	442027	4021635	7049	RG-87241	x	x	x	Ttc	460	360	440	7/10/06	330	6719	15
TV-103	439575	4020899	7086	RG-88886	x	x	x	Tto	1000	790	970	3/16/07	651	6435	25
TV-104	440789	4019142	7440	RG-52607-CLW	x	x	x	Ttc	1080	980	1080	10/7/97	980	6460	25
TV-105	443044	4023239	6930	none		x	x	Tc	320			5/11/05	220	6710	
TV-106	440432	4019553	7352	RG-27921	x	x	x	Ttc	972	870	970	1/28/77	850	6502	10
TV-107	440249	4019644	7313	RG-37157	x	x	x	Ttc	955	868	955	2/1/82	870	6443	25
TV-108	438929	4024831	6731	RG-68034	x	x	x	QTlb	185	145	185	10/10/97	120	6611	25
TV-109	439266	4022500	6912	RG-45676		x	x	Tc	330	300	330	9/13/86	290	6622	6
TV-110	439656	4024799	6760	RG-88016		x	x	Tsb	298	238	298	8/7/06	103	6657	15
TV-111	444522	4023739	6943	RG-50511		x	x	Tc	125	80	125	4/17/89	80	6863	20
TV-112	443087	4022445	6974	RG-51249		x	x	Ttc	325	290	320	11/23/89	220	6754	20
TV-115	438728	4022238	6883	RG-55576	x	x	x	Tc	600	190	600	1/20/92	460	6423	15
TV-116	443986	4024762	6898	RG-90552	x	x	x	QTl	260	160	240	6/18/08	83	6815	20
TV-117	443718	4022942	6959	none		x	x	Tc							15
TV-118	443951	4023035	6978	RG-18848	x	x	x	Tc	175	145	175	6/30/71	135	6843	
TV-119	442022	4024782	6852	RG-64885		x	x	QTl	150	60	150	8/1/96	87	6765	25
TV-120	445183	4022350	7020	RG-37919		x	x	Ttc	125	64	125	4/3/84	85	6935	8
TV-121	439043	4024718	6732	RG-67154	x	DL	x	QTlb, Tsb	215	155	215	12/12/97	120	6612	53
TV-122	441974	4023904	6882	RG-81894		x	x	QTl	160	100	160	2/6/04	45	6837	15
TV-123	439328	4024683	6752	RG-83208		x	x	QTlb	220	180	220	4/7/05	120	6632	30
TV-124	439301	4024674	6749	RG-83204		x	x	QTlb	215	175	215	4/9/05	139	6610	15
TV-125	445310	4020203	7214	RG-82804	x	x	x	Xhu	280	240	280	7/21/04	0	7214	25
TV-126	445254	4020385	7204	RG-44015	x	x	x	Tp	420	350	420	7/3/85	10	7194	5
TV-127	445193	4020308	7205	RG-45679	x	x	x	Xmg	400	380	385	8/2/86	20	7185	0.5
TV-128	445068	4020094	7242	RG-57268	x	x	x	Tp	500	440	500	11/9/93	390	6852	15
TV-129	445250	4020120	7227	RG-26087-CLW		x		Xmg	440	380	400	6/10/81	0	7227	3
TV-132	445150	4019970	7252	RG-78874-CLW	x	x		Xhu(f)	400			7/16/03	0	7252	30
TV-133	445160	4019970	7252	RG-81518		x		Xmg(f)	383			6/10/05	0	7252	60
TV-134	445208	4019938	7248	RG-83373		x		Xhu(f)	294			4/26/05	0	7248	45
TV-135	445189	4026137	6875	RG-71955	x	x	x	QTl	112	72	112	6/22/99	18	6857	25
TV-136	441717	4026765	6733	RG-75773	x	x	x	QTlb	122	82	122	5/15/01	15	6718	15
TV-137	444018	4026841	6781	none		x	x	QTlb, Tsb							
TV-138	441701	4026814	6730	RG-89795		x	x	QTl, Tsb	100			2/28/11	42	6688	15
TV-139	438605	4022824	6840	RG-88461	x	x	x	QTlb, Tsb	400	260	360	9/29/06	175	6665	30
TV-140	437092	4021843	6845	RG-76925	x	x	x	QTl, Tc	260	220	260	12/17/02	190	6655	20
TV-142	445074	4024612	6886	RG-35148	x	x	x	QTl, Tc	65	45	65	11/26/80	20	6866	10
TV-143	439606	4025327	6726	RG-83661	x	x	x	QTlb, Tsb	300	240	300	8/10/06	121	6605	15
TV-144	443847	4028625	6910	none		x	x	QTl							
TV-145	444459	4027975	6763	RG-41884		x	x	QTl	80	20	80	6/1/84	25	6738	10
TV-146	444153	4025875	6806	RG-85313		x	x	QTl	60	40	60	5/26/05	54	6752	15
TV-147	443682	4027403	6739	none		x	x	QTl, Tsb							
TV-148	444389	4025434	6812	RG-91630		x		QTl	100	80	100	9/12/10	40	6772	25
TV-149	437854	4022511	6843	RG-77935		x	x	Tc	575	515	575	5/15/03	300	6543	20
TV-150	445312	4028085	6806	RG-78943		x	x	QTl	84	42	84	10/7/02	30	6776	30
TV-151	441313	4023957	6869	RG-60090		x	x	QTl	160	140	160	8/7/94	131	6738	10

Table 1. Continued

WELL LOCATION				SITE INFORMATION					WELL CONSTRUCTION						
Site ID	UTM easting NAD83	UTM northing NAD83	Elevation (ft asl)	NMOSE well record	Water sample	Water level	Site visit	Water bearing formation †	Well depth (ft bls)	Screen top (ft bls)	Screen bottom (ft bls)	Drill date	Driller static water level (ft bls)	Static water elevation (ft asl)	Well yield (gpm)
TV-152	441426	4022701	6969	RG-59563-X	x	x	x	Tc, Tto	1200	997	1187	11/5/95	310	6659	100
TV-153	443983	4024152	6933	RG-75582	x	x	x	QTl, Tc	245	140	200	3/9/01	104	6829	45
TV-154	442635	4026829	6760	RG-49046		x	x	QTl	40	20	40	4/25/88	8	6752	15
TV-155	440968	4026311	6749	RG-39866		x	x	QTlb, Tsb	120						
TV-156	442983	4022935	6934	RG-88306		DL	x	Tc	400	280	380	8/23/06	171	6763	40
TV-157	443068	4023026	6925	RG-87082		DL	x	Tc	230	300	340	3/28/06			20
TV-158	441180	4023644	6890	RG-73735		x	x	QTl	280	180	280	5/10/00	140	6750	15
TV-159	438986	4023615	6787	RG-83900		x	x	Tsb	280	200	260	3/8/05	240	6547	10
TV-160	445094	4022051	7036	none	x	x	x	Ttc	125						
TV-161	442967	4024915	6872	RG-56518		x	x	QTl	120	60	120	1/6/93	84	6788	15
TV-162	442680	4024140	6887	RG-78996	x	x	x	QTl	160	140	160	12/20/02	120	6767	15
TV-163	443478	4027212	6731	none		x	x	Tsb	80				0	6731	
TV-164	439960	4025718	6685	RG-67818		x	x	Tsb(f)	100	60	100	10/1/97	20	6665	50
TV-165	440217	4025434	6732	RG-69193		x	x	Tsb(f)	120	90	120	4/13/98	60	6672	25
TV-166	438483	4022941	6823	RG-79997		x	x	QTlb, Tsb	300						
TV-167	442917	4022252	7000	RG-87080		DL	x	Ttc	460	400	460	3/28/06	260	6740	20
TV-168	443597	4027664	6759	RG-30133	x	x	x	Tsb	50	30	50	3/31/78	15	6744	5
TV-169	443870	4027780	6783	none		x	x	Tsb							
TV-170	440310	4026257	6658	RG-73668	x		x	Tto	2527	1384	2520	11/20/00	152	6506	500
TV-171	440344	4026206	6667	RG-37303-S	x		x	Tto, Ttc	3180	2497	3160	7/18/07	205	6462	325
TV-173	439230	4024897	6732	RG-83207		x	x	QTlb	200	160	200	4/18/05	95	6637	15
TV-174	440398	4026308	6661	none		x	x	QTlb	144	88	143.5	1/25/95	29	6632	
TV-176	440594	4025959	6686	none		x	x	QTl	40				21	6665	
TV-177	440735	4025672	6753	none		x	x	QTl	93				69	6684	
TV-178	440395	4026185	6669	none		x	x	QTl	34				16	6653	
TV-179	442102	4025079	6850	RG-39658	x	x	x	QTl	180			1/1/85			
TV-180	440513	4023235	6904	RG-05213-CLW		x	x	QTlb, Tc	440	380	440		320	6584	
TV-181	443750	4025324	6848	RG-35970	x	x	x	QTl	150	90	150	4/21/81	100	6748	20
TV-182	444981	4022809	7008	RG-03894-S		x	x	Tc	244	224	244	3/15/76	94	6914	20
TV-183	444800	4022144	7057	RG-03894		x	x	Ttc	185	115	195	9/17/53	137	6920	20
TV-184	444810	4022151	7056	RG-65037	x		x	Ttc	255	175	220	5/28/97	140	6916	20
TV-185	443531	4027603	6745	RG-26574	x	x	x	QTlb	180	120	180	10/1/75	125	6620	20
TV-186	440972	4023357	6901	RG-80614	x	x	x	QTl	280	240	280	9/2/03	200	6701	15
TV-187	442824	4026031	6806	RG-90026		x	x	QTl	100	60	100	2/27/08	30	6776	15
TV-188	438841	4023087	6802	RG-81317	x	x	x	Tc	395	335	395	1/6/05	320	6482	8
TV-189	440377	4024683	6804	RG-91705		x	x	Tsb							
TV-191	439911	4020631	7146	RG-91446	x	x	x	Tto	1002	760	920	7/30/09	700	6446	30
TV-192	440787	4023808	6841	RG-50140	x	DL	x	QTl, Tsb	240	190	240	12/9/88	190	6651	35
TV-193	441972	4023344	6908	RG-62319		x	x	QTl	200	180	200	7/20/95	112	6796	10
TV-194	442432	4026017	6812	none	x	x	x	QTl	100						
TV-195	436504	4023133	6699	RG-87837		x	x	Tsb(f)	480	360	420	4/12/07	290	6409	30
TV-196	436925	4023507	6693	RG-80207		x	x	QTlb, Tsb	450	350	450	5/28/03	295	6398	20
TV-197	437019	4023546	6659	RG-65392		x	x	QTlb, Tsb	300	240	300	7/10/96	233	6426	
TV-198	436937	4023381	6687	RG-80117	x		x	QTlb, Tsb	480	400	480	5/22/03	294	6393	20
TV-199	437863	4024095	6698	RG-87207		x	x	Tsb	400	300	400	3/19/07	177	6521	10
TV-200	442816	4025197	6855	RG-83851		x	x	QTl	160						
TV-201	445909	4020976	7134	RG-62881	x	x	x	/Pu	260	200	260	7/28/95	23	7111	20

Table 1. Continued

WELL LOCATION				SITE INFORMATION					WELL CONSTRUCTION						
Site ID	UTM easting NAD83	UTM northing NAD83	Elevation (ft asl)	NMOSE well record	Water sample	Water level	Site visit	Water bearing formation †	Well depth (ft bls)	Screen top (ft bls)	Screen bottom (ft bls)	Drill date	Driller static water level (ft bls)	Static water elevation (ft asl)	Well yield (gpm)
TV-205	444949	4020549	7182	none		x	x	Tp	60			8/31/06			<5
TV-206	443234	4019655	7296	RG-92034			x	Tp	860			4/21/10	dry		<2
TV-207	446075	4020810	7178	RG-75724	x	x	x	Tpl	598	540	598	4/30/01	30	7148	50
TV-208	440458	4025995	6688	none		x	x	QTl	78			3/1/03			
TV-209	444721	4017534	7500	RG-83482	x	x	x	Tp	295			9/20/04	38	7462	
TV-210	443726	4016447	7853	RG-85779		x	x	Tp	895	815	895	10/1/06	112	7741	
TV-211	444378	4015730	7840	RG-85777		x	x	Tp	673	118	668	11/6/11	88	7751	
TV-212	444670	4012658	8365	RG-85776		x	x	Tp	420	360	420	9/6/05	189	8176	3
TV-213	443824	4011868	8492	RG-85775		x	x	Tp				10/24/05	115	8378	
TV-214	444063	4012668	8531	RG-85772	x	x	x	Tp	580	540	580	8/26/05	422	8109	9
TV-215	443658	4012416	8666	RG-85771		x	x	Xmg	420	380	420	8/31/05	214	8452	6.5
TV-216	444087	4013519	8120	RG-85773	x	x	x	Tpl	420	360	420	10/31/05	72	8048	23
TV-217	442074	4022809	6959	RG-73095a	x	DL	x	Ttc	2003	1492	2003	11/14/99			200
TV-218	442074	4022809	6959	RG-73095b		DL	x	Tc	460	418	460	11/22/99			
TV-219	442093	4022868	6948	RG-72824	x	x	x	Tto, Ttc	1400	978	1381	10/14/99	270	6678	60
TV-220	444376	4015734	7840	none		x	x	Tp	210						
TV-221	444372	4015730	7840	none		x	x	Tp	31						
TV-222	443726	4016447	7853	none		x	x	Tp	175						
TV-223	441902	4025623	6796	RG-26656		x	x	QTl	70	25	70	1/5/75	19	6777	20
TV-224	441308	4025714	6772	RG-44282		x	x	QTl	105	60	105	5/1/86	60	6712	20
TV-226	443896	4025205	6840	RG-57735-S		x	x	QTl	103	63	103	7/7/05	25	6815	50
TV-227	439398	4025086	6719	RG-83209		x	x	QTlb	185	145	185	4/21/05	105	6614	15
TV-228	441481	4025615	6782	RG-78246		x	x	QTl	140			1/1/08			
TV-229	439009	4020576	7103	RG-63879	x	x	x	Tto	1070	870	1015	5/14/96	663	6441	100
TV-230	439362	4016255	8151	RG-76468	x		x	Xhu	1400	1220	1400	6/10/02	1105	7046	10
TV-231	439088	4023468	6798	RG-83697		x	x	Tsb	191	151	191	12/19/04	135	6663	15
TV-232	441479	4025438	6806	RG-39071	x		x	QTl	120	40	120	1/29/83	40	6766	25
TV-233	440656	4023366	6888	RG-83497		x	x	QTlb, Tsb	347	269	347	12/20/04	245	6643	12
TV-234	445805	4020855	7139	RG-62881POD2		x	x	Tp	760			9/15/11	210	6929	1
TV-235	445894	4021455	7023	RG-62881POD3	x	x	x	Ttc	220	100	200	1/26/12	72	6951	30
TV-237	439727	4018783	7508	RG-67560	x	x	x	Ttc	1290	900	1240	12/23/97	1047	6461	10
TV-238	441602	4026232	6751	RG-67648	x	x	x	Tsb	105	55	105	8/23/97	10	6741	15
TV-239	441899	4023741	6891	RG-73272	x	x		QTl, Tc	300	180	300	2/5/00	105	6786	30
TV-240	443993	4027861	6801	RG-72518	x	x	x	QTlb, Tsb	200	120	200	8/9/99	131	6670	15
TV-241	440929	4019847	7329	RG-74535		x		Ttc	1205	1000	1200	9/10/00	845	6484	32
TV-243	443811	4023222	6978	RG-25111	x		x	Tc	138	100	138	9/8/75	40	6938	10
TV-244	443611	4023520	6951	RG-33852	x	x	x	Tc	320	240	320	3/2/04	154	6797	20
TV-245	444194	4022503	7020	RG-44301	x			Ttc	120	80	120		60	6960	15
TV-246	442801	4021984	7022	RG-70527	x	x	x	Ttc	400	325	380	9/17/98	325	6697	12
TV-247	445170	4028179	6794	RG-59834	x		x	QTl	60	30	60	5/4/95	50	6744	15
TV-248	444152	4027510	6757	RG-82912	x			QTlb	180	160	180	7/14/04	1	6756	40
TV-249	445760	4029271	6829	none	x	x	x	QTl	130			1/1/91			
TV-250	445214	4028188	6798	none	x	x	x	QTl	60			1/1/55			
TV-251	445612	4028725	6810	RG-66311	x		x	Tsb	280	230	270	7/14/97	168	6642	15
TV-252	440890	4019767	7349	RG-79085	x	x		Ttc	1190	1100	1180	10/21/02	873	6476	25
TV-253	438917	4020148	7137	RG-74404	x	x	x	Tto	1048	840	1020	8/24/00	560	6577	50
TV-254	441847	4023497	6884	RG-71587	x	x	x	QTl	210	150	210	6/29/99	136	6748	15

Table 1. Continued

WELL LOCATION				SITE INFORMATION					WELL CONSTRUCTION						
Site ID	UTM easting NAD83	UTM northing NAD83	Elevation (ft asl)	NMOSE well record	Water sample	Water level	Site visit	Water bearing formation †	Well depth (ft bls)	Screen top (ft bls)	Screen bottom (ft bls)	Drill date	Driller static water level (ft bls)	Static water elevation (ft asl)	Well yield (gpm)
TV-255	440707	4023945	6830	RG-77698	x	x		QTlb, Tsb	286	180	286	8/17/02	180	6650	20
TV-256	440619	4024247	6803	RG-73559	x	x	x	QTlb, Tsb	260	200	260	3/10/00	180	6623	20
TV-257	442495	4023234	6915	RG-82811	x	x		Tc	280	240	280	10/8/04	140	6775	30
TV-258	440834	4023468	6864	none	x	x	x	QTl							
TV-259	441837	4023142	6918	none	x			Tc							
TV-260	440935	4024629	6844	RG-80824	x	x		QTl	275	235	275	8/8/03	200	6644	15
TV-261	442358	4024483	6865	none	x		x	QTl	140	100	140	11/10/88	80	6785	20
TV-262	442983	4024240	6897	none	x			QTl	200						
TV-263	438479	4022658	6857	RG-81875	x		x	Tsb, Tc	700	300	690	5/25/04	150	6707	5
TV-264	445853	4022032	6969	RG-59636	x	x		Ttc	210	110	210	9/18/02	50	6919	50
TV-265	446695	4020868	7061	RG-62255	x		x	Qal, Tp	72				53	7008	
TV-266	446191	4027125	6847	RG-64539	x	x	x	QTl	75	40	75	5/9/96	24	6823	15
TV-267	447149	4024143	7027	RG-74887	x	x	x	Tc	182	142	182	11/20/00	60	6967	20
TV-268	446589	4022531	7079	RG-76630	x	x	x	Tc	215	20	215	10/11/01	130	6949	20
TV-269	446417	4020675	7150	RG-51208		x	x	Tp	109	60	109	11/16/89	60	7090	
TV-270	446556	4020963	7058	RG-68552		x		/Pu	420	360	400	11/25/97	60	6998	20
TV-272	446180	4026771	6869	RG-74545	x		x	Ttc	2109	1604	2088	9/30/00	278	6591	
TV-273	446201	4026744	6871	RG-74545	x	x	x	QTl	291	253	291	3/16/00	61	6810	45
TV-274	446187	4026767	6870	RG-74545	x	x	x	Tc, Ttc	1480	1040	1480	5/3/00	83	6787	67
TV-275	446208	4026746	6870	RG-74545	x	x	x	Ttc	2020	1608	2010	5/3/00	276	6594	
TV-276	444199	4027480	6753	RG-82913		x		QTlb, Tc	290	180	290	9/20/04	0	6753	5
TV-277	439648	4019873	7204	RG-79449		x	x	Ttc	1010	720	920	3/29/03	766	6438	25
TV-278	439290	4020567	7110	RG-79302		x	x	Tto	1042	820	940	1/18/03	666	6444	30
TV-280	443366	4027305	6726	RG-74971		x		QTlb, Tsb	140	120	140	11/17/00	10	6716	15
TV-281	444905	4027904	6777	RG-86273		x		QTl	130			11/26/12	27	6750	15
TV-282	446396	4028865	6846	RG-82234		x		QTl	85	65	85	10/5/93	10	6836	15
TV-283	445305	4028253	6804	RG-52846		x		QTl	112	70	90	6/16/97	20	6784	15
TV-285	440965	4020450	7250	RG-59779		x		Tto	1120	900	1120	6/14/96	670	6580	33
TV-286	440850	4019903	7331	RG-80427		x		Ttc	1200	1095	1200	9/25/03	833	6498	25
TV-287	441938	4021590	7059	RG-82695		x		Ttc	480	340	420	6/12/07	340	6719	10
TV-288	440231	4020074	7257	RG-91449		x		Ttc	1005	820	980	7/24/09	801	6456	25
TV-289	440066	4020322	7217	RG-91454		x		Ttc	1000	920	980	8/3/09	762	6455	30
TV-290	444358	4028143	6775	none		x		Tc	1400				-4	6779	
TV-291	446675	4030604	6918	none		x		QTl	100	75	100	8/1/92	34	6884	
TV-292	446675	4030626	6920	none	x	x		Ttc	1942	1921	1942	8/1/92	165	6756	
TV-293	446675	4030626	6920	none	x	x		Tc	1117	1096	1117	8/1/92	247	6673	
TV-294	446675	4030626	6920	none	*	x		Tc	854	833	854	8/1/92	240	6680	
TV-295	446675	4030626	6920	none	*	x		Tsb	672	651	672	8/1/92	66	6854	
TV-296	446675	4030626	6920	none	*	x		QTlb	508	487	508	8/1/92	32	6888	
TV-297	446675	4030626	6920	none	x	x		QTlb, Tsb	348	327	348	8/1/92	27	6894	
TV-298	446675	4030626	6920	none		x		QTl	206	185	206	8/1/92	35	6885	
TV-301	443954	4020825	7134	RG-95474	x	x	x	Ttc	1185	1000	1075	9/30/15	375	6759	
TV-302	440324	4026228	6664	none		x		Tc	1180	1000	1180				
TV-303	440324	4026228	6664	none		x		Tc, Tto	1370	1300	1370				
TV-304	440324	4026228	6664	none		x		Tto	2000	1750	2000				

asl—above sea level; bls—below land surface; †—see Table 3 for formation codes and descriptions;
DL—continuous measurements with data logger; *—water chemistry data not used in analyses, see Appendix 3

Table 2. Inventory of spring and surface-water sites shown on Figure 5.

SITE INFORMATION							
Site ID	UTM easting NAD83	UTM northing NAD83	Elevation (ft asl)	Site type	Water bearing formation*	Water sample	Site visit
TS-054	433924	4021264	6060	SP	Tc	x	x
TS-055	435573	4022633	6473	SP	QTLb	x	x
TS-056	433641	4021102	6115	SP	Tc	x	x
TS-058	434401	4021378	6200	SP	Tc	x	x
TV-501	443761	4011531	8480	SP	Tp	x	x
TV-502	443457	4016260	7975	SP	Tp, Xmg	x	x
TV-503	445589	4020038	7280	SP	Xmg	x	x
TV-504	445363	4020171	7179	SP	Qal, Tp	x	x
TV-509	445864	4020595	7250	SP	Tp, /Pu		x
TV-510	441066	4025662	6728	O		x	x
TV-511	434544	4021864	6181	SP	Tc		x
TV-512	447515	4019855	7096	PS		x	x
TV-513	452454	4040459	8051	PS		x	x
TV-514	454864	4032809	7380	PS		x	x

asl–above sea level; PS–perennial stream; SP–spring; O–effluent outfall;
*–see Table 3 for formation codes and descriptions

transmissivity, recharge and discharge zones, and approximate locations of groundwater mounds and groundwater divides (Brassington, 2007).

A groundwater map for the basin aquifer was constructed primarily from water levels measured by NMBGMR field staff in 88 wells between March 2011 and January 2013 (the majority of wells were measured in March and April 2012), and the elevations of 5 springs emerging along the eastern wall of the Rio Grande gorge. Depth-to-water data from another 54 wells measured prior to the study (taken from unpublished geologic reports and drilling records) provided water-table control in data-poor areas and at study area boundaries. A second groundwater map was constructed for the mountain aquifer using 19 measured water levels, combined with 5 spring elevations, and 7 measurements from unpublished geologic reports and drilling records. Site information for wells and springs is presented in Tables 1 and 2; locations are shown on Figure 5.

Well locations and water-level elevations were plotted in ArcGIS. Groundwater elevation contours were drawn by hand and digitized. The placement of water-table elevation contours was checked against land-surface and stream-channel elevations to ensure accuracy in lowland and wetland areas. Groundwater flow lines showing horizontal flow direction were constructed normal to water-table elevation contours (assuming the aquifer is horizontally isotropic). Converging flow lines delineate zones of groundwater discharge to streams. Diverging flow lines delineate zones of groundwater recharge from streams.

Groundwater-level fluctuations

Monitoring groundwater-level fluctuations, seasonally, annually, and over long periods of time, is an important aspect of studying groundwater systems and sustainability (Taylor and Alley, 2001). Repeat water-level measurements were taken in 54 wells between Talpa, Los Cordovas, and the western end of county road 570 to evaluate annual (2011–2012) and short-term (2 to 4½ years) variations in groundwater levels. Continuous groundwater-level fluctuations were monitored in seven wells over periods of 2 to 4 years using the automated technology described above. Results were evaluated spatially for the period 2011 to 2012 and with hydrographs showing changes in groundwater level over time.

Geochemical Methods

Over the last several decades, a variety of chemical, isotopic, and dating methods have been developed to trace groundwater movement through the hydrologic cycle. For summaries of data collection, application and interpretation see Hounslow (1995), Clark and Fritz (1997), Mazor (2004), and Timmons et al. (2013). Only one previous study of the basin-fill aquifer in the Taos region has applied chemical and isotopic data from streams and groundwater to evaluate source waters and connectivity of aquifers in the basin (Drakos et al., 2004c).

This report provides the first comprehensive hydrogeology study in the southern Taos Valley that utilizes a dense network of geochemical data. Chemical and age data collected from springs and wells were examined for relationships and spatial patterns useful in identifying groundwater sources, flow patterns, recharge and discharge zones, mixing, and residence time. Chemical attributes are presented in contoured plots constructed by kriging concentration values followed by manual smoothing of contours. Surface-water sites were not used to control concentration contours, but appear on figures for comparison. Differences in ion chemistry among groundwater zones are illustrated using a trilinear Piper diagram (Piper, 1944).

Groundwater residence time is evaluated using radiocarbon (^{14}C) dating of the dissolved inorganic carbon and tritium (^{3}H). Radioisotopes of ^{14}C and ^{3}H are produced in the atmosphere by natural and

anthropogenic processes, become entrained in the hydrologic cycle, enter the groundwater system with recharge, and slowly decay as groundwater flows through the aquifer. Large volumes of anthropogenic ^{3}H and ^{14}C produced between 1951 and 1962 by atmospheric testing of thermonuclear weapons created a "bomb" spike of these radioisotopes in groundwater that has been used as a tracer of groundwater movement. Carbon-14 has a relatively long half-life (5,730 years) and is used to detect groundwater with residence times of several 100s to many 1,000s of years. Results are reported as radiocarbon years before present, RCYBP, where "before present" means prior to 1950. Tritium has a relatively short half-life (12.43 years) and its presence in groundwater proves that recharge occurs on a time scale of years to decades. The average tritium content in mountain front streams of the Sangre de Cristo and Picuris Mountains in the southern Taos Valley is 7.7 tritium units (TU). By measuring both the ^{3}H content and ^{14}C activity in groundwater, and comparing to modern levels, we can estimate how long groundwater has resided in the aquifer and detect whether the water represents a mixture of sources with different ages. In some geologic settings, chemical interactions between dissolved carbonate and carbonate-rich sediments or rocks in the aquifer can dilute the amount of ^{14}C measured in a water sample, and provide an anomalously old age. No corrections for geochemical effects have been completed on data collected in this study. The ^{14}C activity and apparent ^{14}C age are used as a relational tool to interpret hydrologic differences between wells and identify groundwater mixing.

CFCs and SF_6 are atmospheric contaminants that are resistant to degradation and soluble in water, making them a useful marker for modern groundwater recharge. Because CFC concentrations have been measured in the atmosphere since the 1940s, and have increased until recently, their input to the aquifer is known, and can, under the right conditions, provide a precise age for groundwater ranging from 0 to 70 years old. In this study, non-atmospheric sources of CFCs from discarded automobiles, refrigerators, and the like have contaminated some samples, making them useless for groundwater dating.

Data collection and analysis

Between April 2011 and October 2015, groundwater samples were collected by NMBGMR from 43 wells and 3 springs in the study area, and from the discharge outflow of the Town of Taos WWTP. Samples were collected from domestic wells using dedicated submersible pumps. Spring waters were sampled using a peristaltic pump and Viton® tubing inserted into a discharge vent or an active spring pool. WWTP discharge outflow was collected as a grab sample.

Waters were field tested for specific conductance (SC), dissolved oxygen (DO), pH, and temperature and were analyzed at NMBGMR for ion and trace element chemistry, and oxygen ($^{18}O/^{16}O$) and hydrogen isotopes ($^{2}H/H$) ratios. Thirty-eight of the samples were analyzed for carbon isotopes (^{14}C and $^{13}C/^{12}C$ ratio) and tritium. Twenty samples were analyzed for CFC and SF_6 recharge ages.

Sample sites are summarized in Tables 1 and 2 and shown on Figure 5. Chemical and isotopic data from water sampling are presented in Appendix 3. Data collection and analysis of are summarized in the following sections.

Field parameters—Groundwater discharge temperature, specific conductance, pH, and dissolved oxygen were measured in the field prior to sampling using a YSI 556 multi-probe system. The probe has a rated accuracy of 0.15°C for temperature, 0.5% for SC, 0.2 units for pH, and 2% for DO. The DO probe was calibrated onsite before measurement. The pH electrode was calibrated weekly against pH 7 and 10 buffers. For springs, field parameters were measured in the spring pool or through an in-line flow cell prior to sampling. For wells, field parameters were monitored continuously during the well purge using an in-line flow cell. Sample collection was initiated following parameter stabilization. Between one and three bore-hole volumes of water were extracted during well purge and sample collection.

Ions and trace metals—Water samples were collected in new, certified clean 125-mL (for trace metals) or 250-mL (for ions) polypropylene containers that were triple rinsed with sample water prior to filling. Trace metal samples were filtered on site through an in-line 0.45 micron filter and acidified to pH less than 2 using ultra-pure nitric acid. All water samples were stored on ice or refrigerated until analysis at the NMBGMR laboratory within one week. Laboratory measurements of pH were performed with an Orion 420A meter, and conductivity was measured using a YSI 3,200 meter. Alkalinity was determined by titration. Major anions (Cl, SO_4, and NO_3) were analyzed using a Dionex DX-600 ion chromatograph (IC). Major cations (Ca, Mg, Na, and K) were analyzed using a Perkin Elmer OPTIMA 5300 DV inductively coupled plasma optical emission

spectrometer (ICP-OES). Trace metals were analyzed by inductively coupled plasma mass spectrometry (ICPMS) using an Agilent 7,500 IS. The quality of chemical analyses was inspected by analyzing blanks, standards, duplicate samples, and checking ion balances. Analytical error for detectable concentrations of major ions and trace metals is generally less than 10 percent using IC, ICP-OES, and ICP-MS. Ion balance errors for analyses conducted by NMBGMR are within ±5%.

Hydrogen and oxygen isotopes—Samples for hydrogen ($^2H/H$, δ^2H) and oxygen ($^{18}O/^{16}O$, $\delta^{18}O$) isotope ratios were collected in 25-mL amber glass bottles that were triple rinsed with sample water prior to filling. Sample bottles were clear of air bubbles, kept from direct sunlight, and stored at room temperature in sealed bottles until analysis at the New Mexico Institute of Mining and Technology, Department of Earth and Environmental Sciences stable isotope laboratory using a cavity ring down spectrometer, Picarro L1102-I isotopic water liquid sampler. Analytical uncertainties for δ^2H and $\delta^{18}O$ are typically less than 1 per mil (‰, parts per thousand) and 0.15‰, respectively.

Carbon isotopes—Select spring and well samples were analyzed for ^{14}C activity and $\delta^{13}C$ to evaluate groundwater age. Water samples were collected in 1-L polypropylene bottles that were tripled rinsed with sample water. Sampling followed protocols described at http://www.radiocarbon.com/groundwater-carbon-dating-sampling.htm. Samples were chilled and stored in a dark environment until shipment to Beta Analytic, Miami, Florida, for analysis. The ^{14}C activity and $^{13}C/^{12}C$ ratios ($\delta^{13}C$) of the water sample were derived from the dissolved inorganic carbon (DIC) by accelerator mass spectrometry. Measured $\delta^{13}C$ values were calculated relative to the PDB-1 standard. Result verification and isotopic fractionation correction using $\delta^{13}C$ were completed by Beta Analytic. Results are reported as ^{14}C activity (in percent of modern carbon (pmC)) and as the apparent radiocarbon age (in radiocarbon years before present (RCYBP), where "present" is 1950 AD), with an uncertainty of one standard deviation.

Tritium (^3H)—Tritium samples were collected in two 500-mL polypropylene bottles that were tripled rinsed with sample water. Sampling followed protocols described at http://www.rsmas.miami.edu/groups/tritium/analytical-services/advice-on-sampling/tritium/. Samples were analyzed at the University of Miami Tritium Laboratory by internal gas proportional counting with electrolytic enrichment. The enrichment step increases tritium concentrations in the sample about 60-fold through volume reduction, yielding lower detection limits. Accuracy of this low-level measurement is 0.10 tritium unit (TU) (0.3 pCi/L of water), or 3.5%, whichever is greater. The standard analytical errors in all samples are 0.09 TU or one standard deviation. Results less than 0.10 TU are shown on figures as <0.1 TU—considered to be below detection—but actual reported values are shown in data tables.

Chlorofluorocarbons (CFCs) and sulfur hexafluoride (SF_6)—CFC and SF_6 samples were collected from well and spring waters into three 250-mL glass bottles with foil-lined caps. Bottles and caps were thoroughly rinsed with sample water and filled and capped underwater in a plastic bucket with no atmospheric exposure. Sampling followed stringent protocols described at www.rsmas.miami.edu/groups/tritium/analytical-services/advice-on-sampling/cfc-and-sf6/. Samples were analyzed at the University of Miami Tritium Laboratory using a purge-and-trap gas chromatograph with an electron capture detector. Limits of detection for CFCs and SF_6 are extremely low, 0.001×10^{-12} moles per kilogram of water (pmol/kg) and 0.01×10^{-15} moles per kilogram of water (fmol/kg), respectively. The accuracy of CFC and SF_6-derived recharge ages from these measurements is three years or less. Calculations of CFC and SF_6 recharge ages assumed recharge elevations of 2,130–2,745 meters (6,988 to 9,006 feet) and recharge temperatures of 5–10°C, which are the estimated elevations and mean annual temperatures for recharge zones between high canyons in the Picuris Mountains and lowlands in the Taos Valley.

Data compilation and data quality

Existing geochemical data from an additional 54 sites were compiled from previous studies by the Taos Soil and Water Conservation District, consulting geologists, and the NMBGMR. Existing isotopic and age data from a study of springs in the Rio Grande gorge (Bauer et al., 2007) and previously unpublished tritium and stable isotope data from Taos-area streams were also incorporated. These data were reviewed and filtered for data quality based on several criteria including an accurate map location or geographical coordinates for the sample site, and ion balance. The data compiled in this study have an ion balance of ±5% or less, with one exception (9.17%).

III. GEOLOGY OF THE SOUTHERN TAOS VALLEY

Regional Geology

Rio Grande rift

The Rio Grande rift in northern New Mexico is composed of a series of north-trending, elongate topographic and structural basins, including the San Luis and Española Basins (Fig. 6). The basins are broad half grabens that are tilted to either the east or west, and typically have a relatively active, north-striking fault system along one border as well as numerous lesser faults within the basin. Current tectonic models and geologic maps show that the basins of the northern Rio Grande rift are separated by northeast-trending fault zones that accommodate the differential sense of basin tilting (Chapin and Cather, 1994).

The 150-mile-long San Luis Basin is bordered by the Sangre de Cristo Mountains on the east, the Tusas and San Juan Mountains on the west, and the Picuris Mountains to the south. The San Luis Basin contains a deep, narrow, structural trough, known as the Taos graben in New Mexico, along the eastern edge of the basin (Bauer and Kelson, 2004). The western edge of the graben (the Gorge fault) lies beneath the Rio Grande (Cordell and Keller, 1984; Bauer and Kelson, 2004), resulting in a graben that is less than half the width of the topographic valley. The structural bench west of the Taos graben rises gently to the Tusas Mountains, and is cut by numerous small-displacement normal faults. The southwestern part of the basin is a physiographically and geologically unique terrain known as the Taos Plateau. The plateau is composed of Pliocene volcanoes and lava flows that have only been mildly deformed by rift processes.

The Sangre de Cristo and Embudo fault zones form the eastern and southern boundaries of the basin (Fig. 6). The Sangre de Cristo fault is a north-striking, west-dipping normal fault system that accommodates asymmetric subsidence of the basin. The Sangre de Cristo fault exhibits geomorphic evidence for multiple surface-rupturing events in the late Quaternary (Machette and Personius, 1984; Menges, 1990; Kelson et al., 2004b). The Embudo fault strikes northeast-southwest, and can be interpreted as a transfer fault or accommodation zone (Faulds and Varga, 1998; Kelson et al., 2004a; Bauer and Kelson, 2004b) that allows differential subsidence between the San Luis Basin to the northeast and the Española Basin to the southwest. Detailed field mapping and geomorphic investigations document late Quaternary and possibly Holocene surface rupture along the northeastern Embudo fault (Kelson et al., 1996, 1997, 2004a).

Unlike the rift basins to the south, the San Luis Basin is relatively undissected. That is, the sedimentary material that fills the basin has not yet been extensively eroded and exposed by the action of rivers and streams. Instead, the Rio Grande and its major eastern tributaries have cut several deep, narrow canyons through the volcanic rocks that cap most of the area. The river canyons provide the only good exposures of the basin-fill rocks in the basin. The Rio Grande gorge contains good exposures of Tertiary volcanic rocks, as well as the interlayered sands and gravels that represent westward-prograding alluvial fans of the Taos Range (Peterson, 1981; Dungan et al., 1984).

Taos Plateau volcanic field

The Pliocene to Pleistocene Taos Plateau volcanic field of northern New Mexico and southern Colorado is the largest and compositionally most diverse volcanic field of the Rio Grande rift. Nearly all of the isolated, rounded mountains scattered across the Taos Plateau are extinct volcanoes that erupted between 6 and 1 million years ago (Lipman and Mehnert, 1979; Appelt, 1998). At least 35 discrete volcanic vents have been identified on the plateau (Dungan et al., 1984; Appelt, 1998).

The volcanoes of the Taos Plateau occur in a variety of sizes and shapes. Shield volcanoes (such as the vents of La Segita Peaks) are shallow-sloped and constructed of successive lava flows that can flow long distances. Lava domes (such as San Antonio Mountain, Ute Mountain, Cerro Chiflo, No Agua Peaks, Cerro del Aire, Cerro de la Olla, and Cerro Montoso)

are large, steep-sided volcanoes that were formed from numerous eruptions of thick, sticky lava. Flood or plateau basalts (such as the Servilleta Basalt) are fluid lavas that erupted out of low-relief vents, and flowed many miles before solidifying.

The volcanoes that flank the Rio Grande gorge span a wide variety of compositions (Lipman and Mehnert, 1979). Although most are mafic to intermediate in composition (basalts, andesites, dacites), rhyolites are not uncommon. Ute Mountain, San Antonio Mountain, Guadalupe Mountain, Cerro de la Olla, Cerro Chiflo, Cerro Montoso, and Cerro de los Taoses are andesite or dacite volcanoes that erupted between approximately 3 to 5 million years ago. The principal rhyolite volcano, No Agua Peaks, is about 4 million years old.

The only rocks of the Taos Plateau volcanic field exposed in the study area are shallow Servilleta Formation basalt flows (3.6 to 5.2 million years old) that exist in the northern half of the map area.

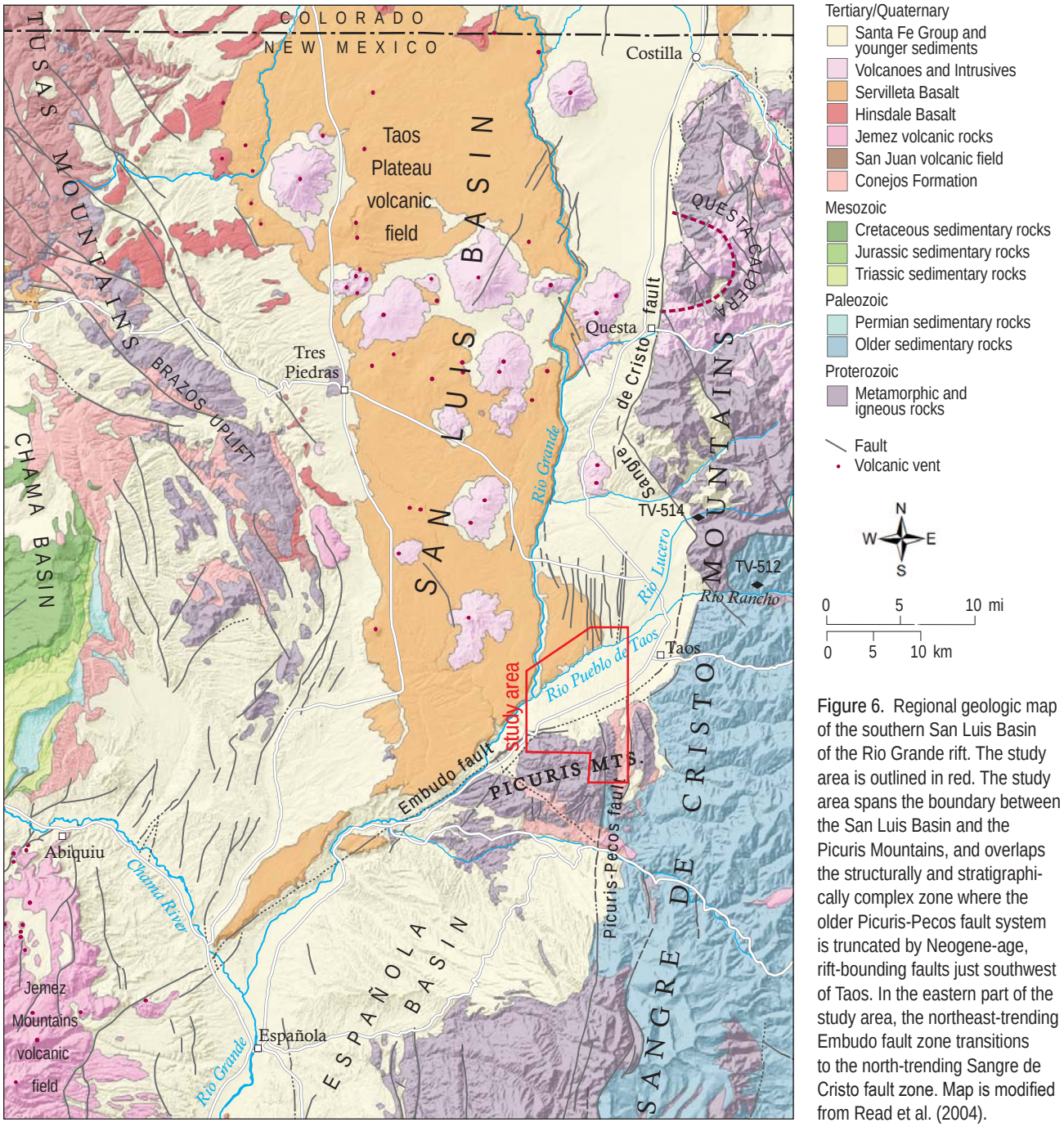

Figure 6. Regional geologic map of the southern San Luis Basin of the Rio Grande rift. The study area is outlined in red. The study area spans the boundary between the San Luis Basin and the Picuris Mountains, and overlaps the structurally and stratigraphically complex zone where the older Picuris-Pecos fault system is truncated by Neogene-age, rift-bounding faults just southwest of Taos. In the eastern part of the study area, the northeast-trending Embudo fault zone transitions to the north-trending Sangre de Cristo fault zone. Map is modified from Read et al. (2004).

Rio Grande gorge

Upon exiting the San Juan Mountains, the Rio Grande turns southward, transects the San Luis Basin, and flows south through successive rift basins toward the Gulf of Mexico. The river follows the topographically lowest part of the rift, carving several spectacular canyons along the way. Beginning in southern Colorado, the Rio Grande has cut a steep-sided basalt canyon known as the Rio Grande gorge. The gorge deepens southward to 850 feet at the Wild Rivers Recreation Area near Questa, and then gradually shallows as the Rio Grande flows through the southern San Luis Basin and into the Española Basin. Several east-side tributaries have cut deep canyons to the Rio Grande, including the Rio Pueblo de Taos, the Rio Hondo, and the Red River.

Picuris Mountains and Sangre de Cristo Mountains

The southern Rocky Mountains of northern New Mexico have experienced a complex geology history that spans 1.7 billion years, including multiple mountain-building events. The rocks of the Taos area contain evidence of all of these events. The Taos area straddles the boundary between Paleoproterozoic and Paleozoic basement rocks of the southern Sangre de Cristo Mountains and Paleo- to Mesoproterozoic and Paleozoic basement rocks of the Picuris Mountains (Fig. 7). The Proterozoic rocks of the northern Picuris Mountains, which underlie much of the watershed in our study area, consist predominantly of quartzite, schist, and slate. The Sangre de Cristo Mountains along the southeastern edge of the study area, including the headwaters of the Rio Grande del Rancho, consist principally of Paleozoic shale, sandstone, limestone, and conglomerate. The transitional zone between the two mountain ranges, including the Rio Grande del Rancho and Miranda canyons, consists of Proterozoic granite, Paleozoic sedimentary rocks, and Tertiary volcaniclastic sedimentary rocks.

Geologic Units

The rocks and deposits exposed in the study area consist of:

1. Surficial deposits of Quaternary age;
2. The Pliocene Servilleta Basalt;
3. Sedimentary units of the Santa Fe Group;
4. Mid-Tertiary sedimentary rocks of the Picuris Formation;
5. Paleozoic sedimentary rocks; and
6. Proterozoic crystalline rocks.

These units are shown on the detailed geologic map (Plate 1), a generalized geologic map and stratigraphic chart (Figs. 7–8; Table 3), and on a series of geologic cross sections (Plate 2). Hydrogeologic cross sections are presented later in this section. Detailed descriptions of all geologic units found in the study area are presented in Appendix 1.

Surficial Deposits

Surficial deposits in the study area provide a means of discerning the locations of faults that have been active in the Quaternary, and to estimate the senses and relative amounts of Quaternary movements (Bauer and Kelson, 2004). The area contains a variety of coalescent alluvial-fan, stream-channel, and terrace deposits that range in age from late Pliocene to Holocene. In the central part of the study area, high alluvial fans derived from the Picuris Mountains interfinger with alluvial terrace deposits along the Rio Grande del Rancho north of Talpa (Plate 1). An ash layer in the oldest alluvial fan on the Picuris piedmont is dated at 1.27 ± 0.02 Ma (Bauer et al., 1997).

Along the major streams, near-surface Quaternary units consist of coarse-grained fluvial sediments deposited by the major streams, and coarse- to fine-grained alluvial-fan sediments derived from smaller, mountain-front drainages. The area contains fluvial and alluvial-fan deposits that range in age from early to middle Pleistocene to recent. Fluvial sediments exist along the Rio Grande del Rancho, Rio Chiquito, Rio Pueblo de Taos, and Rio Fernando valleys. These poorly sorted sands and gravel contain subrounded clasts of quartzite, slate, sandstone, schist, and granite, and are laterally continuous in a down-valley direction (Kelson, 1986). Soils developed on these deposits associated with older, higher stream terraces contain well-developed (stage III to IV) calcic horizons. Younger terraces are associated with lesser amounts of soil development (Kelson, 1986).

Alluvial-fan deposits in the eastern part of the study area are derived mostly from smaller mountain-front drainages developed in Pennsylvanian sandstone and shale. In general, these deposits are coarse-grained sands and gravels near the mountain front, and are finer-grained with distance to the north or west (Bauer and Kelson, 2004). The alluvial-fan deposits likely are laterally discontinuous and moderately heterogeneous. Older fan deposits are associated with well-developed soils (stage III to IV

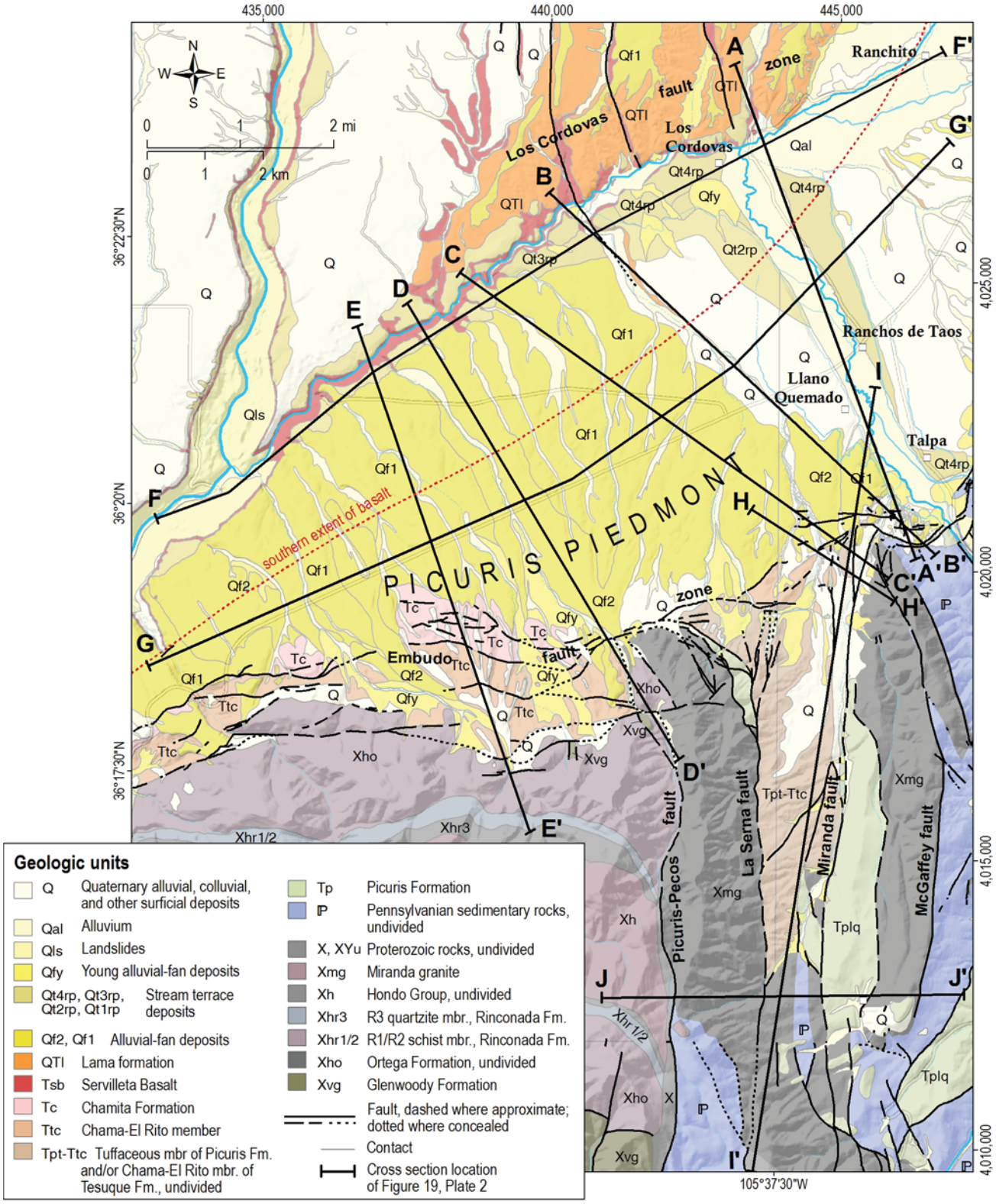

Figure 7. Generalized geologic map of the study area, showing cross section lines. This geologic map is simplified from six 7.5-minute quadrangle maps: Los Cordovas quadrangle (Kelson and Bauer, 2003), Carson quadrangle (Kelson et al., 1998), Taos SW quadrangle (Bauer et al., 1997), Taos quadrangle (Bauer and Kelson, 2001), Penasco quadrangle (Bauer et al., 2005), and Tres Ritos quadrangle (Aby et al., 2007). See Table 3 for geologic unit descriptions. See Plate 1 for the detailed geologic map. The "southern extent of basalt" line represents the approximate southernmost subsurface occurrence of appreciable thickness of Servilleta Basalt, and was interpreted by V.J.S. Grauch and P.W. Bauer from aeromagnetic data and well information.

calcic soils), whereas younger deposits contain moderately developed soils (stage I to II calcic horizons) or lesser-developed soils. The younger fans in many places bury older fan deposits, such that subsurface conditions probably vary considerably across the mountain-front piedmont.

Servilleta Basalt

A single type of volcanic rock volumetrically dominates the Taos Plateau, the olivine tholeiite flood basalts of the Servilleta Basalt. The Rio Grande and Rio Pueblo de Taos gorge walls chiefly consist of thin, near-horizontal layers of this dark gray, pahoehoe, vesicular lava. The basalts were erupted from low-relief shield volcanoes north of the study area, traveling as thin, molten sheets for tens of miles before solidifying. Over 600 feet of basalt were locally stacked up between about 5 and 3 million years ago. These rocks can be seen from any location along the Rio Grande gorge, and in the northwestern part of the study area.

Servilleta Basalt ranges in thickness across the Taos Plateau. Lava flows taper down to zero where they onlap preexisting volcanoes and other highlands. Basalts thin into the study area, and feather out to zero near NM-68. The southern extent of an appreciable thickness of Servilleta Basalt is identified in Figure 7 and is referred to in this report as the "southern extent of basalt" line, also known as the "basalt line." The variable thickness and monolithic nature of the basalt flows make them poor stratigraphic markers that cannot be convincingly correlated in the subsurface using well data alone. These fluid lavas clearly flowed around topographic obstructions, and appear to thicken and thin along paleo-fault scarps in the study area.

Servilleta basalts are extensively fractured, especially by columnar joints that tend to vertically penetrate entire basalt flows (Fig. 9). Many of the columnar fractures are open. Such basalt fracturing formed as each lava flow cooled, thus we expect the buried basalt units to also be extensively fractured and exceedingly permeable in the vertical dimension. In addition, the flow tops are typically characterized by highly vesicular ropy structures that create porous and permeable horizontal zones between flows.

Santa Fe Group basin fill

Borehole data in the San Luis Basin indicate that relatively thin Quaternary deposits are underlain by thick Tertiary sedimentary deposits that are dominated by sand and gravel, with lesser amounts of silt and clay. Although some of the Tertiary sediment that fills the rift basin was deposited by the Rio Grande, most of the clay, silt, sand, gravel, and cobbles were eroded from the nearby mountains during the past 25 million years. The San Luis Basin is surrounded by large alluvial fans (and related deposits) that have slowly advanced from the mountains into the basin. In the Rio Grande rift, these principally Neogene-age deposits are called the Santa Fe Group. Over much of the basin, we can only see the youngest basin fill at the surface. However, glimpses of Santa Fe Group sediments exist along the upper Picuris piedmont, and

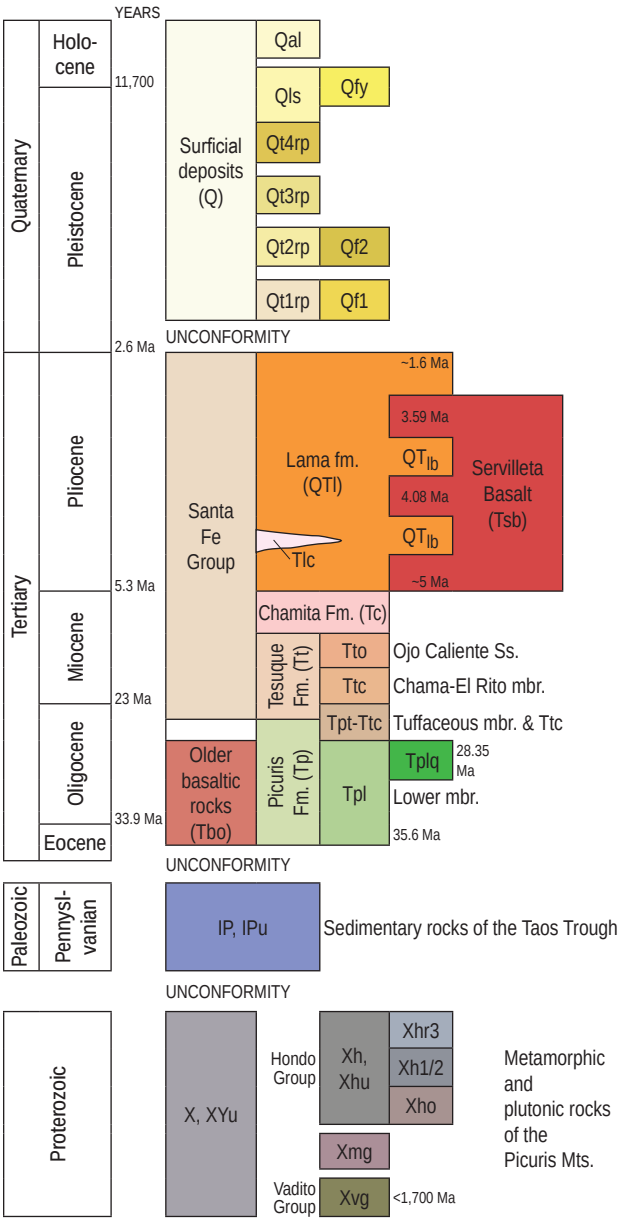

Figure 8. Stratigraphy of the southern Taos Valley, with approximate age on the vertical axis. See Table 3 for geologic unit descriptions.

Table 3. Geologic unit descriptions for Figures 6–8 and Plates 1 and 2, southern Taos Valley.

UNIT	DESCRIPTION
Quaternary alluvial, colluvial, and other surficial deposits (Q)	
Qal	Alluvium-Principally loose silt, silty sand, sand, pebbles, and cobbles, but includes eolian and landslide deposits as well as other surficial deposits.
Qls	Landslides-Poorly sorted rock debris and sand- to boulder-sized debris that was transported downslope in the Rio Grande gorge.
Qfy	Young alluvial-fan deposits-Poorly sorted deposits of silt, sand, pebbles, cobbles and boulders; exists as young, mountain-front fans.
Qt4rp, Qt3rp, Qt2rp, Qt1rp	Stream terrace deposits—Poorly sorted silt, sand, pebbles, and boulders inset in valleys along the Rio Pueblo de Taos and tributaries.
Qf2, Qf1	Alluvial-fan deposits-Poorly sorted silt, sand, pebbles, and boulders that were deposited along the Picuris piedmont.
Pliocene-Quaternary sedimentary deposits of the Santa Fe Group	
QTl	Lama formation-Poorly sorted clay, sand, pebbles, and cobbles with clasts of basalt, quartzite, and other metamorphic and volcanic rock types; commonly stained with black manganese oxide and yellowish-orange iron oxide coatings; oxidized; clasts are typically weathered or grussified; contains distinct discontinuous sandy interbeds.
Tlc	Gray, lacustrine(?) clay layer (1–3 m thick) within the lower Lama fm in the southwestern map area that perches groundwater.
QTlb	Lama formation between Servilleta Basalt layers-Used as a hydrogeologic subdivision only.
Pliocene volcanic rocks	
Tsb	Servilleta Basalt, undivided-Flows of dark-gray tholeiitic basalt characterized by small olivine and tabular plagioclase phenocrysts, diktytaxitic texture, and local vesicle pipes and segregation veins.
Miocene sedimentary deposits of the Santa Fe Group	
Tc	Chamita Formation-Typically rounded to subrounded, pebble- to cobble-size clasts in a sand to silt matrix; dominated by a Proterozoic clast provenance of schist, quartzite, and amphibolite, with lesser volcanic clasts.
Tt	Tesuque Formation-Sand with subordinate gravel, silt, and clay.
Tto	Ojo Caliente Sandstone-Very pale brown, well- to moderately well-sorted, subrounded to rounded, loose to moderately well-indurated eolian sandstone.
Ttc	Chama-El Rito member-Muddy siltstone to silty, very fine to very coarse sandstone interbedded with silty/sandy and sandy pebble conglomerate.
Tpt-Ttc	Tuffaceous member of Picuris Formation and/or Chama-El Rito member of Tesuque Formation, undivided-Tuffaceous and pumiceous silty sandstones and volcaniclastic sandstone and conglomerate that is transitional between the Picuris and Tesuque Formations.
Oligocene-Miocene sedimentary rocks	
Tp	Picuris Formation, undivided-Upper member of tuffaceous and pumiceous silty sandstones and volcaniclastic sandstone and conglomerate; a member of silty sandstone to fine cobble conglomerate and very fine silica-cemented silty to pebbly sandstone which locally contains a basal portion of cobble/boulder conglomerate with Proterozoic clasts; a member of quartzose, silty, fine sand to pebbly, pumiceous sandstone; and a lower member of red, green, and yellow, pebbly/silty sandstone and mudstone containing clasts of quartzite and layers of massive quartzite conglomerate.
Tplq	Llano Quemado Breccia member-Volcanic breccia of angular, light-gray, rhyolite clasts in a red matrix.
Tpl	Lower member-Red, greenish, and yellowish pebbly/silty sandstone and mudstone containing very thick(?) to thin beds and/or lenses and/or isolated clasts of subangular to rounded Proterozoic quartzite and massive quartzite conglomerate.
Tbo	Older basaltic rocks-Unexposed volcanic rocks that predate the Tesuque Formation and may exist within the Picuris Formation.
Paleozoic sedimentary rocks	
IP, IPu	Pennsylvanian sedimentary rocks, undivided-Greenish, reddish, yellowish, buff, tan, black, and brown, sandy to clayey siltstone, mudstone, and shale interbedded with mostly greenish and brownish quartzose, feldspathic, and arkosic, silty to pebbly sandstone and sandy conglomerate, and rare dark limestone.
Proterozoic rocks	
Xmg	Miranda granite-Pink to white, medium-grained, mica-rich, granitic rock with euhedral megacrysts of feldspar.
X, XYu	Proterozoic rocks, undivided-Metamorphic and plutonic rocks of the Picuris Mountains.
Xh, Xhu	Hondo Group, undivided-Schist and quartzite of the Ortega and Rinconada Formations.
Xhr3	R3 quartzite member, Rinconada Formation-Interlayered, crossbedded quartzite and pelitic schist.
Xhr1/2	R1/R2 schist member, Rinconada Formation-Quartz-muscovite-biotite schist and garnet schist.
Xho	Ortega Formation, undivided-Gray to grayish-white, medium- to coarse-grained quartzite.
Xvg	Glenwoody Formation-Feldspathic, quartz-muscovite schist and quartzose schist.

in the Rio Grande gorge just to the west of the study area. From youngest to oldest, the principal subdivisions of the Santa Fe Group in the study area are the Lama formation, the Chamita Formation, and the Tesuque Formation.

Between the Picuris piedmont and Arroyo Hondo, the Servilleta Basalt is interlayered with, and overlain by, sand and gravel deposits of the Lama formation (Bauer et al., 1997) that likely are the distal parts of alluvial fans shed from the Sangre de Cristo Mountains, and/or derived from the ancestral Rio Grande (Kelson, 1986). These highly oxidized and weathered sediments are probably early to middle Pleistocene in age, and appear to have been extensively saturated by a high water table throughout much of the eastern Taos Plateau (Fig. 10). The Lama formation was deposited prior to the development of the Rio Grande gorge (Wells et al., 1987), and reflects alluviation on the plateau prior to regional incision of the gorge and the resulting drop of the water table.

Clay deposits exist locally, especially above Servilleta Basalt in the Los Cordovas fault zone, where they can be several meters thick (Fig. 11). Some of these clays are lacustrine (Bauer and Kelson, 2004b) and likely formed in temporary lakes that formed behind lava dams. The lateral extents of the clays are unknown. A distinctive light gray, sedimentary clay layer is locally exposed in the walls of the Rio Grande

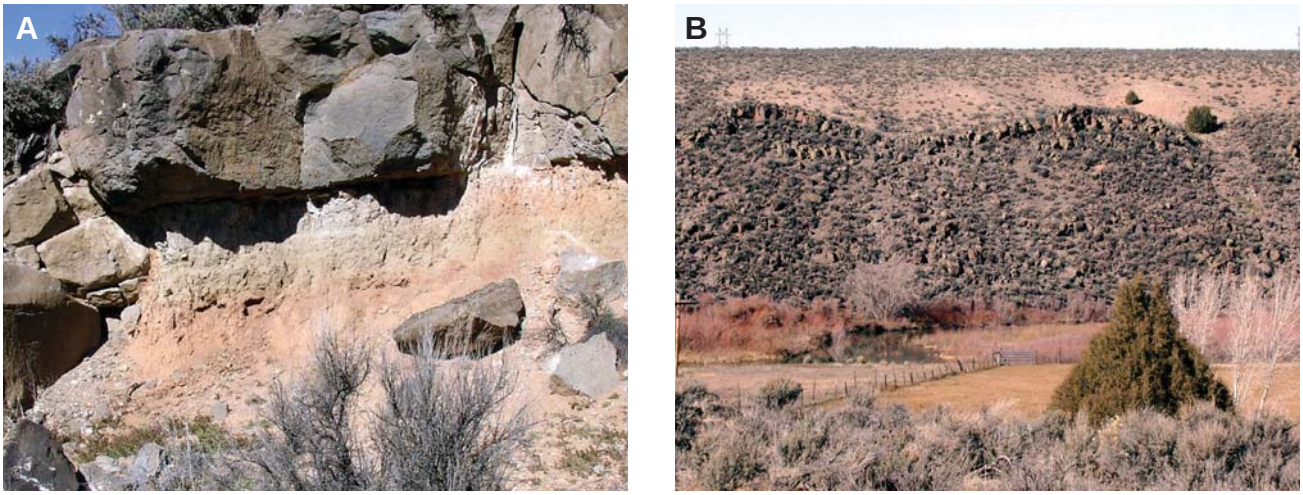

Figure 9. Exposures of Servilleta Basalt in the study area. A—Thin (1 m thick) lava flow exposed in an arroyo just north of the Town of Taos wastewater treatment plant. Note the large number of open fractures in the basalt flow. The basalt flowed over light-colored, sandy to silty, layered sediments of the Lama formation. B—View north of the rocks exposed along the Rio Pueblo de Taos. The river has cut nearly perpendicular to the flow direction of the basalts, exposing the convex tops of highly fractured lava flows. The basalts are overlain by buff-colored, old Rio Pueblo terrace gravels and younger gravel deposits.

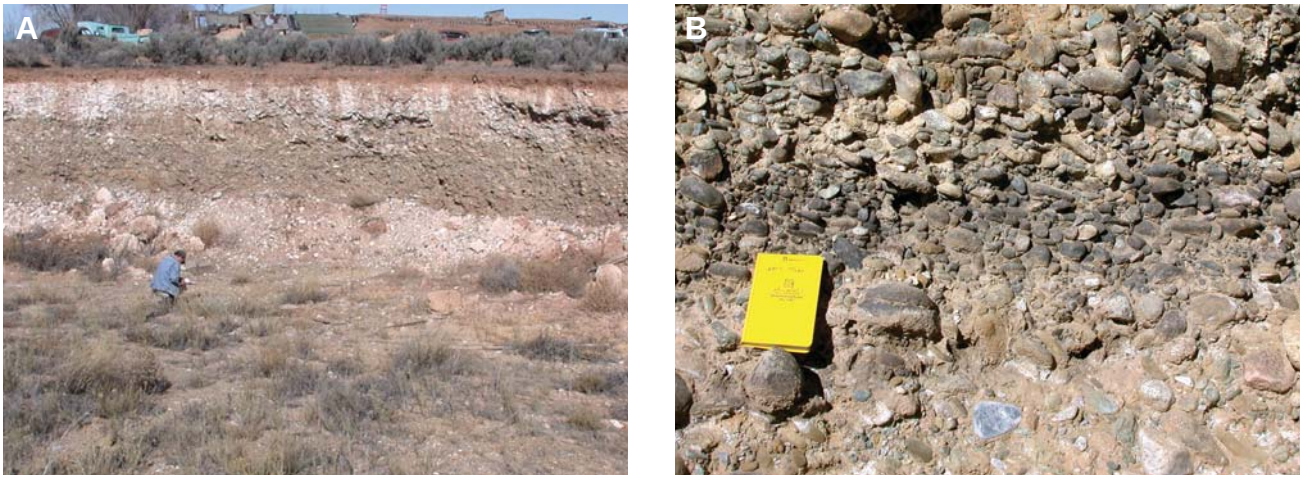

Figure 10. Exposures of the Lama formation in the study area. A—Quarry exposure of Lama formation near the Town of Taos wastewater treatment plant. The brownish conglomerate of the Lama is capped by white carbonate soil profile and a dark brown Quaternary sand and gravel deposit. B—Closeup view of Lama formation showing rounded, oxidized, imbricated cobbles in a sandy to silty matrix.

Figure 11. Arroyo exposure of 4-m-thick, white to yellow, sticky clay in the northern study area. Laboratory analysis has shown that the clay most likely represents a lake deposit, perhaps in the lake that developed behind a basalt flow that dammed the ancestral Rio Pueblo de Taos. Other clay horizons have been encountered in boreholes around the southern Taos Valley area, and probably exist within all of the basin-fill units in the study area.

gorge, just southwest of the study area, downstream from the confluence with the Rio Pueblo de Taos. The clay is composed of very small (20 to 50 microns), well-sorted crystals of quartz and feldspar in a clay matrix that most likely formed in a lake that existed behind a basalt-dammed ancestral Rio Grande. The clay lies within the clastic beds of the Lama formation, above the lowermost Servilleta Basalt, and is estimated to be 1 to 3 m thick. On the north slope of the gorge, between the Taos Junction bridge and the Village of Pilar, the clay is spatially related to a series of small springs and seeps that exist at elevations of approximately 6200 ft. The clay layer extends farther downstream, where it hosts a number of larger springs that emerge from the north gorge wall downstream from Pilar. The known, exposed lateral extent of the layer is a minimum of 17 km (11 mi) in the gorge. In addition, the clay likely extends up the Rio Pueblo de Taos, into the study area, where it is observed in several of the wells used in this study (TV-195, TV-196, TV-198). Two springs within the study area (TS-56 and TS-58), at elevations of approximately 6200 ft, are thought to be perched on the same clay layer. In hydrogeologic cross sections, the clay layer is shown as unit Tlc.

Cuttings from deep exploration boreholes in the Taos area suggest the presence of the Tesuque Formation of the Santa Fe Group in the subsurface. From exposures near Pilar, and westward, and from along the upper Picuris piedmont, a general subsurface stratigraphy has been developed, although the sedimentary layers contain extensive vertical and horizontal compositional and textural variations due to the complex depositional environments found in the rift basin. The mappable members of the Tesuque Formation in the study area are the Chama-El Rito Member and Ojo Caliente Sandstone Member.

Along the western flank of the Picuris Mountains, the oldest Tesuque Formation unit is the Chama-El Rito Member, composed predominantly of volcanic-rich, non-fossiliferous sandstone and conglomerate, with minor mudrock interbeds (Fig. 12). The Chama-El Rito Member represents braided stream deposits on a distal alluvial fan derived from a volcanic terrain to the northeast (Steinpress, 1980). The thickness in the Dixon area is estimated to be 480 m (1,570 ft) (Steinpress, 1980).

The Chama-El Rito Member is conformably below, and interfingers with, the Ojo Caliente Sandstone Member of the Tesuque Formation west of the study area, along Rito Cieneguilla near Pilar (Leininger, 1982; Kelson et al., 1998). The Ojo Caliente is a buff to white, well-sorted eolian sandstone, consisting mostly of fine sand (Fig. 13). Tabular crossbeds are common, with some sets over 4 m in height. Transport was from southwest to northeast (Steinpress, 1980). The Ojo Caliente is not exposed in the study area, but probably exists in the subsurface where it is likely thickly interbedded with Chama-El Rito rocks.

In late Miocene time, high-angle rift faulting produced deep, narrow, fault-bounded basins that filled with kilometers of clastic sediments and volcanic rocks. In the study area, the clastic sediments are named the Chamita Member, and are principally composed of rounded to subrounded, pebble- to cobble-size clasts in a sand to silt matrix (Fig. 14). The thickness of this basin fill is variable and difficult to estimate at any given location. It is also difficult to distinguish in well logs from overlying Lama gravels and from underlying Chama-El Rito gravels. The Chamita Member thickness has been estimated to range from 100 to 230 m (330 to 750 ft) in the Pilar area (Steinpress, 1980).

Picuris Formation

The oldest known Cenozoic unit in the study area is the Picuris Formation, a package of mostly volcaniclastic sedimentary rocks that represents pre-rift and early-rift sedimentation. Baltz (1978) stated that the early shallow rift basins of northern New Mexico

Figure 12. Excellent exposure of the Chama-El Rito member of the Tesuque Formation in a roadcut along NM-68 near the Hondo Canyon of the Picuris Mountains. The interlayered sandstones and conglomerates here are highly tilted, due to the proximity of several major splays of the Embudo fault zone. Several minor faults are visible in the roadcut. *Photo courtesy of Steve Miller.*

Figure 13. The Ojo Caliente Sandstone member of the Tesuque Formation is well exposed along NM-68 near Pilar Mesa. This distinctive dune deposit consists of pale-brown, well-sorted, indurated sandstone that displays large tabular crossbeds. *Photo courtesy of Steve Miller.*

Figure 14. Exposure of the Chamita Formation on the south side of Pilar Mesa. At this location, the unit consists of weakly cemented, pebble- to cobble-sized clasts in a sand to silt matrix, with interlayered beds of fine to coarse sand. *Photo courtesy of Steve Miller.*

were initially infilled by a combination of volcanic eruptions and volcaniclastic alluvial fans with sources in the San Juan volcanic field to the north. Rehder (1986) divided the Picuris Formation into three members: a lower member, the Llano Quemado breccia member, and an upper member, on the basis of 11 scattered exposures north and east of the Picuris Range. Aby et al. (2004) utilized new geochronology, detailed regional mapping, and sedimentological analysis to refine the formation architecture, and their nomenclature is used in this report.

In the Picuris Mountains area, the Picuris Formation consists principally of a variety of volcaniclastic sandstones and conglomerates (Fig. 15), cobble/boulder conglomerates, colorful mudstones, siltstones, and sandstones, and a distinctive basal

Figure 15. Exposure of the Picuris Formation in lower Miranda Canyon, north of Ponce de Leon spring. These flat-lying layers of ash-rich sandstone represent part of the upper unit of the Picuris Formation, named the Tuffaceous member. The unit is overlain by a Quaternary gravel deposit.

quartzite-boulder conglomerate. Based on geologic mapping along the northern Picuris Mountains piedmont, the transition from the upper Picuris Formation to Tesuque Formation is probably continuous, although perhaps punctuated locally by unconformities.

In the Talpa area, the Llano Quemado breccia is a monolithologic volcanic breccia of distinctive, extremely angular, poorly sorted, light-gray, recrystallized rhyolite clasts in a reddish matrix. Rhyolite clasts contain phenocrysts of biotite, sanidine, and quartz. A rhyolite clast yielded an $^{40}Ar/^{39}Ar$ eruptive age of 28.35 ± 0.11 Ma (Aby et al., 2004).

Older Tertiary volcanic rocks

Within the study area, one well (TV-100, RG-83352) penetrates a lava flow that is probably considerably older than the Servilleta Formation. The drillers log lists "basalt" from 840–900 ft, and "fractured basalt" from 900–920 ft. Given that geologic mapping shows the surface unit to be the Chama-El Rito Member of the Tesuque Formation (Miocene), the 80-ft-thick lava flow may be Oligocene in age. Such Oligocene lavas do exist at the surface north of the study area, where they are known as the Conejos Formation (ca. 30–29 Ma) and the Hinsdale Formation (ca. 26 Ma) (Thompson and Machette, 1989; Thompson et al., 1991). These lavas are related to the San Juan volcanic field, which predates the formation of the structural Rio Grande rift.

The Conejos Formation consists of andesite and dacite lava flows, flow breccias, lahar or mudflow breccias, and vent-facies pyroclastic rocks erupted or derived from local sources. The Hinsdale Formation consists of basaltic lava flows, associated breccia, and near-vent pyroclastic deposits (Thompson and Machette, 1989). Even though the Hinsdale Formation rocks are considerably older than the Pliocene rocks of the Taos Plateau volcanic field, the basalt-dominated Hinsdale can be quite similar in appearance to the younger Servilleta Basalt, and where the two formations are contiguous, they could be easily mistaken in lithologic logs from drill holes.

In addition, the magnetic properties on this buried flow are different than the properties of the Servilleta lavas (V.J.S. Grauch, personal communication, 2014).

Paleozoic rocks

Most of the bedrock exposed in the Taos area east of the Rio Grande del Rancho consists of Paleozoic sedimentary strata of Mississippian and Pennsylvanian age. The Mississippian Tererro Formation of the Arroyo Penasco Group contains mudstones, packstones, and crystalline limestone. The limestone contains calcitized evaporites and dolomites. All of the formation has undergone pervasive alteration.

The Arroyo Penasco Group has been extensively fractured, as much of it is a sedimentary breccia that has also been pyritized after fracturing, such that calcite and pyrite were deposited in fractures. Most of the pyrite has been oxidized to hematite and limonite (Ulmer and Laury, 1984). For detailed stratigraphic information on the Mississippian rocks, see Armstrong and Mamet (1979, 1990).

In the Talpa area, the Tererro Formation is present near Ponce de Leon spring (and presumably in the subsurface nearby) where it rests unconformably on the Proterozoic Miranda granite. Pennsylvanian strata exposed from the top of the Mississippian section on Cuchilla del Ojo near Ponce de Leon spring eastward into the Sangre de Cristo Mountains are probably entirely Flechado Formation—a thick sequence of marine, deltaic, and continental sediments equivalent to part of the Madera Group to the south—although a series of large, north-striking faults have repeated and/or deleted parts of the section.

Although only a small portion of the study area contains Paleozoic rocks at the surface, it is likely that some of the area is underlain at depth by these rocks. Baltz and Myers (1999) proposed that the Pennsylvanian Taos trough actually continues northwestward near Taos, and that a thick section of Pennsylvanian rocks could underlie parts of the southern San Luis Basin. However, based on geologic

mapping along the Picuris-Pecos fault system (Bauer et al., 2000), we believe that no significant thickness of Paleozoic strata exist west of the Miranda fault.

Proterozoic rocks

The great variety of Paleoproterozoic and Mesoproterozoic rocks exposed in the Taos Range and Picuris Mountains certainly exist in the subsurface of the San Luis Basin. In general, the Taos Range contains large areas of plutonic and gneissic complexes (including greenstones), whereas the northern Picuris Mountains are composed of metasedimentary rocks (quartzite, schist, phyllite) in fault contact with granite to the east. The eastern granite, known as the Miranda granite, is exposed in the ridges between Arroyo Miranda and Rio Grande del Rancho. For more information on the local Proterozoic rocks, see references cited in Montgomery (1953, 1963), Lipman and Reed (1989), Bauer (1988, 1993), and Bauer and Helper (1994).

Faults of the Southern Taos Valley

Three major fault systems intersect in the study area:

1. Picuris-Pecos fault system;
2. Embudo fault system; and
3. Sangre de Cristo fault system.

Additionally, a 7-km-wide zone of small-displacement, predominantly west-down faults, originally mapped by Lambert (1966) and termed Los Cordovas faults by Machette and Personius (1984), exists along the northern edge of the study area.

The geometries and kinematics of all four of these fault zones have interacted to influence the modern-day hydrogeology of the study area (Bauer and Kelson, 2004b).

Picuris-Pecos fault system

Montgomery (1953) originally mapped the Picuris-Pecos fault in the Picuris Mountains. The fault has been traced for more than 60 km, from the northern Picuris Mountains south of Taos, to near the village of Cañoncito, east of Santa Fe. As summarized by Bauer and Ralser (1995), the Picuris-Pecos fault system appears to have a long history of reactivation, probably from Proterozoic time to the mid-Tertiary time.

In the study area, the Picuris-Pecos fault consists of five major, parallel north-striking fault zones (Figs. 6 and 7, Plate 1). From west to east, they are: Picuris-Pecos, La Serna, Miranda, McGaffey, and Rio Grande del Rancho faults. These faults are collectively referred to as the Picuris-Pecos fault system. Each fault zone consists of high-angle, anastomosing zones of distributed brittle shear in the Proterozoic and Paleozoic rocks. The major faults are located in valleys due to pervasive brittle deformational structures (fractures, fault gouge, fault breccia) that are relatively easily weathered and eroded. Following are short descriptions of each of the five fault zones. More detailed descriptions appear in Bauer et al. (1999).

The Picuris-Pecos fault has experienced enough slip to juxtapose very different Proterozoic rock packages. West of the fault is the Hondo Group, a metasedimentary terrain of quartzite and schist. East of the fault is a distinctive medium-grained, orange-yellow granite (Miranda granite) that is similar in appearance to the granite exposed at Ponce de Leon spring.

Approximately 1.3 km east of the Picuris-Pecos fault is the east-down La Serna fault, which has placed the Miranda granite on the west against the Picuris Formation on the east (Bauer and Kelson, 2004b). The Picuris Formation occupies a graben (Miranda graben) between La Serna fault and the west-down Miranda fault, located about 1.4 km to the east.

The main strand of the Miranda fault is inferred beneath Arroyo Miranda, based on water-well records and the juxtaposition of Picuris Formation and granite. Good exposures in the Talpa/Llano Quemado area, where the Miranda fault zone cuts Picuris Formation, display numerous north-striking, strike-slip faults with map separations measured on the order of meters to hundreds of meters. Importantly, the <18 Ma upper Picuris Formation is cut by high-angle faults with sub-horizontal slickenlines within the Miranda and La Serna fault zones, suggesting that strike-slip faulting overlaps in time with development of the Rio Grande rift.

Approximately 1 km east of the Miranda fault is a set of west-down branching fault splays (the McGaffey fault) located on the bedrock ridge of Cuchilla del Ojo. The McGaffey fault offsets Proterozoic and Paleozoic rocks, but appears to have considerably less throw than adjacent fault zones. Strike-slip slickenlines are common on north-striking, high-angle minor fault planes. Notably, the high-discharge Ponce de Leon thermal springs are located at the intersection of the McGaffey, Miranda, and Embudo faults (Plate 1).

Approximately 1.5 km east of the McGaffey fault is the kilometer-wide, west-down Rio Grande

del Rancho fault zone, a complex of branching faults along, and east of, the Rio Grande del Rancho valley. Most of the main strand of the fault zone is buried in the alluvial valley, but excellent exposures in the valley walls show extensive strike-slip breccia/fracture zones in Pennsylvanian strata. At the northern end of the valley, Pennsylvanian bedding has been rotated into a vertical orientation along a west-down fault that involves the Picuris Formation (Plate 1).

Embudo fault zone

The Embudo fault zone is a left-slip, north-down, oblique fault zone that forms the border between the west-tilted Española Basin and the east-tilted San Luis Basin of the Rio Grande rift (Figs. 6 and 7). The 64-km-long fault links the west-down southern Sangre de Cristo fault with the east-down Pajarito fault, and appears to be a high-angle fault with different senses of vertical separation along strike (Muehlberger, 1979; Leininger, 1982; Machette and Personius, 1984; Kelson et al., 1996, 1997, 2004a; Bauer and Kelson, 2004b).

The 36-km-long northern section, which includes the study area, was mapped in detail by Kelson et al. (1998), Bauer et al. (1997), and Bauer et al. (2000). Notably, the transition from the Embudo fault to the Sangre de Cristo fault is coincident with the Picuris-Pecos fault system. The northern Embudo fault is characterized by left-lateral slip (Muehlberger, 1979; Steinpress, 1980; Leininger, 1982; Kelson et al., 1997, 2004a). Along the northern margin of the Picuris Mountains, the mapped fault zone is over 2 km wide (Bauer et al., 1997), although aeromagnetic data demonstrate that buried, Embudo-style faults exist at least as far north as the Rio Pueblo de Taos (Fig. 8, Plates 1 and 2), thus increasing its minimum width to 8 km (5 mi). The northern Embudo fault shows evidence of displacement possibly as young as late Pleistocene or early Holocene. Muehlberger (1979) and Personius and Machette (1984) noted faulted Pleistocene alluvium in a road cut near the village of Pilar. Detailed mapping along the fault showed additional evidence of late Pleistocene displacement, and identified two localities where young, possibly early Holocene alluvial fans may be faulted.

In Proterozoic bedrock units, the major strands of the Embudo fault are well-developed, high-angle, brittle deformation zones. Some are many tens of meters wide, typically consisting of central zones of intense strain (breccia, fault gouge, closely spaced fractures) flanked by wide zones of fractured rock. Fractures typically are open, with only minor carbonate cementation. Commonly, the massive sandstone and conglomerate beds contain thorough-going fractures, whereas the interlayered, more ductile, shales are unfractured. Tracing the fault zone eastward into the Cañon section of the Sangre de Cristo fault, slickenlines plunge steeper and steeper until they are down dip on the west-dipping Sangre de Cristo fault.

Where the fault is exposed in Tertiary rocks, the bedrock has been reduced to a clay-rich fault gouge that contains a strong tectonic foliation (Fig. 16) that indicates the sense of shearing. Away from the fault plane, the gouge zones grade into altered and fractured bedrock, and then into relatively unstrained country rock. Where the faults cut Quaternary deposits, the alluvium is laced with thin, anastomosing, calcite-filled fracture veins. Alteration zones are common, and gravel clasts are rotated into the foliation plane. However, the overall degree of deformation is considerably less in the Quaternary deposits than in older units.

Sangre de Cristo fault zone

The Sangre de Cristo fault zone is a west-dipping normal fault zone that forms the border between the Sangre de Cristo Mountains on the east and the San Luis Basin on the west. The southern Sangre de Cristo fault within Colorado and New Mexico is divided into five primary sections (Menges, 1988; Machette et al., 1998). From north to south, these are the San Pedro Mesa, Urraca, Questa, Hondo, and Cañon sections (Machette et al., 1998). The southernmost Cañon section strikes about N20°E, and extends south from the Rio Pueblo de Taos to the Rio Grande del Rancho, where it becomes the Embudo fault. Together, the Hondo and Cañon sections of the southern Sangre de Cristo fault border a 30-km-long, 10-km-wide, crescent-shaped re-entrant in the Sangre de Cristo range block, informally referred to as the Taos embayment.

The southernmost Sangre de Cristo fault shows prominent geomorphic evidence of late Quaternary surface rupture, including scarps across alluvial fans of various ages, air-photo lineaments, springs, and alignments of vegetation. Machette and Personius (1984) and Personius and Machette (1984) profiled several scarps along the Cañon section, and suggested a Holocene age for the most-recent movement. Kelson (1986) mapped late Quaternary deposits and some fault strands along this section, and showed faulted late Pleistocene alluvial-fan deposits. Menges (1990) conducted detailed morphometric analyses

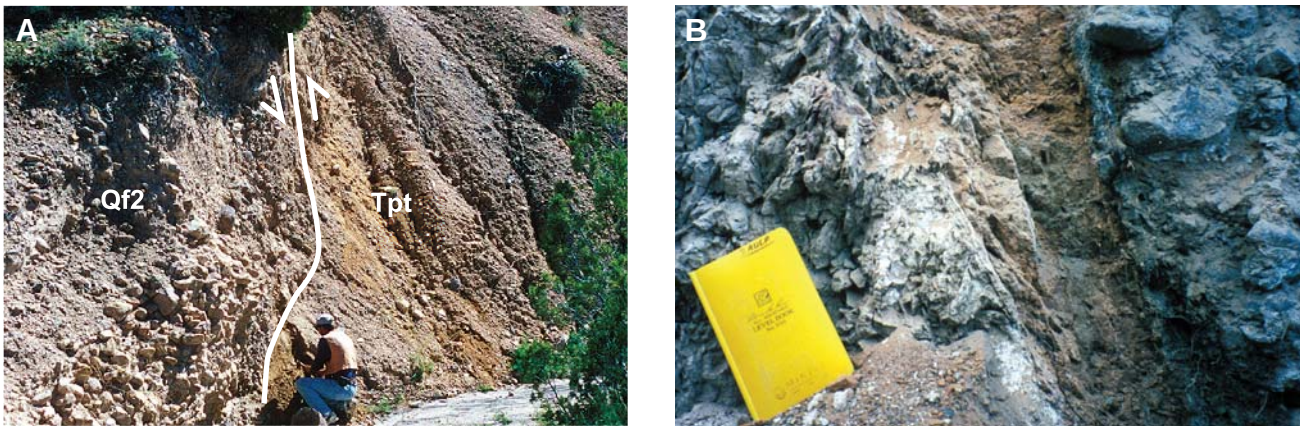

Figure 16. Photos of the Embudo fault zone. A—A rare exposure of a major strand of the Embudo fault zone in an arroyo south of Llano Quemado. This view east, along the fault strike, shows grayish Quaternary gravel (Qf2) on the left down dropped against orange and brown pebbly sandstone of the tuffaceous member of the Picuris Formation. The fault plane dips steeply north, and contains a clay-rich core zone. B—Close up of a near-vertical, clay-cored fault of the Embudo fault zone in Tesuque Formation rocks. This exposure is located in the Rito Cieneguilla drainage, just west of the study area.

of the range front and fault scarps, and suggested the possibility of early Holocene to latest Pleistocene movement along the Cañon section. Recent geologic mapping (Bauer et al., 2000, 2001) and fault trenching (Kelson et al., 2004b) supported these previous age estimates.

Geologic mapping has shown that the southernmost Sangre de Cristo fault zone is a complex system of branching faults that is at least 2 km wide (Bauer and Kelson, 2001). With the exception of the Rio Fernando area, fault scarps in Quaternary deposits are mostly confined to the mountain front where Quaternary deposits are in fault contact with Pennsylvanian rocks. Individual fault planes typically dip steeply west to northwest, with slickenlines plunging moderately to steeply westward.

The transition from strike-slip to dip-slip is gradational, with a prevalence of oblique-slip (plus some strike-slip) faults in the bedrock just southeast of Talpa. In Pennsylvanian rocks near the Rio Grande del Rancho, faults dip between 60–80° northwest with moderately west-plunging slickenlines. North of the Rio Fernando, faults dip between 70–89° westward with generally down-dip slickenlines.

Los Cordovas fault zone

Previous workers described a 5- to 8-km-wide zone of north-striking faults in the Taos plateau (Lambert, 1966; Machette and Personius,1984). The Los Cordovas fault zone consists of perhaps 10 or more individual fault strands that generally are about 10 km long and have fairly regular spacings of 1.0 to 1.5 km. The western margin of the fault zone is roughly coincident with the the Rio Grande gorge. Where separation is greatest, these west-down faults juxtapose piedmont-slope alluvium against older Servilleta Formation basalt.

Machette and Personius (1984) reported that the fault offset is greater than the 15- to 30-m-high erosional scarps that now define the surface expression (Fig. 17), and that faulting may be as old as early Pleistocene, but could be as young as middle Pleistocene. Profiles of stream terraces along the Rio Pueblo de Taos suggest that the faults displace the early to middle Pleistocene piedmont surface, but not a middle Pleistocene terrace (Kelson, 1986; Machette et al., 1998). Geologic mapping suggests that these faults may extend southward from the Rio Pueblo de Taos, and may deform high alluvial-fan deposits on the Picuris piedmont (Bauer and Kelson, 2004b). In addition, the high-resolution aeromagnetic map of the study area may show a buried structural link between the Picuris-Pecos fault system and Los Cordovas faults (V.J.S. Grauch, personal communication, 2003).

An excellent exposure of the eastern fault strand was found just north of the Rio Pueblo in an arroyo that cuts across the fault scarp. In the exposure, Servilleta Basalt and overlying Quaternary fan deposits are faulted on a plane that dips 45° west with down-dip slickenlines and rotated cobbles. Overlying Holocene colluvial gravels are not faulted. A distinctive red to yellow faulted clay horizon rests on the basalt. Laboratory analysis has shown that the clay probably represents a lake deposit that was derived from altered volcanic rocks (G. Austin, personal communication, 2001).

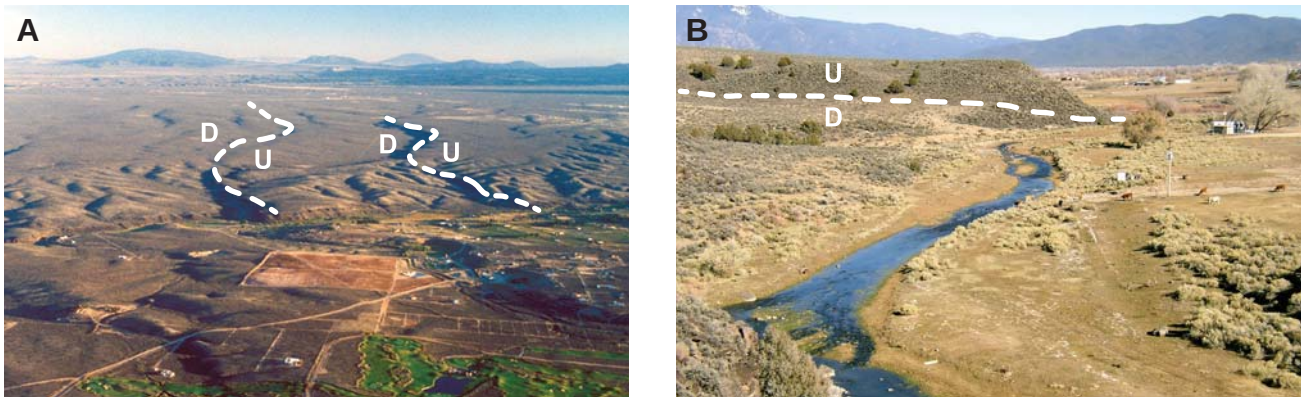

Figure 17. Photos of the Los Cordovas fault zone. A—Aerial view northward of the central part of the southern Taos Valley showing the Taos Country Club, the Town of Taos wastewater treatment plant, and undeveloped Taos Pueblo lands in the middle distance. The Rio Pueblo de Taos flows from right to left against the bluffs in the middle of the photo. Two major splays of the Los Cordovas fault zone (marked in white) have created small drainages that flow into the Rio Pueblo de Taos. These faults presumably continue southward under the river and the young sediments of the Picuris piedmont. B—View east along the Rio Pueblo at the Town of Taos well field (land to the right of the river). A major splay of the Los Cordovas fault zone (marked in white) is buried by rock debris along the base of the ridge in the upper left of the photo. D = down; U = up.

Structural and Subsurface Geology

Taos graben

The Taos graben, first recognized by Cordell (1978) from gravity data, is a major structural feature in the southern San Luis Basin. At the latitude of Taos, the north-south graben is approximately 13 km wide, and locally filled with over 4,500 ft of basin fill. The western edge of the graben is a buried fault zone (the Gorge fault) that is approximately coincident with the Rio Grande gorge (Bauer and Kelson, 2004b).

In 1996, the "Town Yard" exploration well was reported to have encountered Pennsylvanian limestone, shale, and sandstone from a depth of 720 ft to the bottom of the hole at 1020 ft (Drakos et al., 2004). If correct, this would have pinned the eastern structural edge of the Taos graben between that well and the 2,100-ft-deep BOR-3 well, which was drilled about 1 km to the west. This would have required a structural bench with relief of more than 1,400 ft between the two wells. However, recent geophysical analyses (V.J.S. Grauch and B. Drenth, USGS, unpublished data, 2013) and petrographic analysis of well cuttings (D. Koning, personal communication, 2013) concluded that the Town Yard well did not drill into Paleozoic bedrock, but instead was completed in conglomeratic basin-fill rocks, and therefore the eastern edge of the deep, inner graben lies farther to the east.

The Taos graben was mostly formed by the time the lower Servilleta Basalt erupted, approximately 5 million years ago. On the Taos Plateau, the Rio Grande was superposed on the plateau after eruption of the youngest Servilleta basalts (ca. 3 Ma), and began to rapidly entrench upon integration of the river system at approximately 0.5 Ma (Wells et al., 1987). Some of the high-angle faults on the plateau appear to have caused thickening and thinning of volcanic flows across the faults. North of the map area, an exposed example of basalt thinning is the Dunn Bridge fault, where the thickness of the sedimentary interval between the middle and upper basalts varies 17 m (56 ft) across the fault.

Miranda graben

The Miranda graben is formed between two sections of the Picuris-Pecos fault system, the west-down Miranda fault to the east and the east-down La Serna fault to the west. In the study area, the graben is approximately 1.6 km (1.0 mi) wide and is filled with sedimentary rocks of the Picuris Formation that are in fault contact with Proterozoic granites to the east and west. In the Ponce de Leon neighborhood, water wells indicate that about 300 to 400 ft of lower Picuris Formation overlies Proterozoic granite and quartzite. At its northernmost exposure near Ponce de Leon, the graben is transected by numerous segments of the Embudo fault zone. Although the graben certainly exists buried beneath rift-fill sediments to the north of Ponce de Leon, it will be highly segmented and offset by the north-down, left-slip movement along Embudo fault strands. Ponce de Leon spring is located at the east edge of the Miranda graben, where several strands of the Miranda and Embudo faults intersect.

Geometry of buried faults

Because the Picuris-Pecos faults are cut by the Embudo fault, they pre-date the Embudo system and, importantly, most likely exist in the subsurface north of the active Embudo fault. Because the older members of the Picuris Formation are restricted to the structurally low areas within the fault system, Bauer and Kelson (2004b) suggested that the Picuris-Pecos fault zone defined the Eocene to early Miocene grabens, which served as loci for deposition of volcaniclastic sediments of the Picuris Formation that were shed southward from the San Juan volcanic highlands. At least part of the Miranda graben has remained low during the last 25 million years, thus preserving rocks of the Picuris Formation. Therefore, the grabens are generally older than the Embudo fault system, and the graben-bounding faults most likely extend northward into the basin. If so, the Picuris Formation rocks exist on the northern side of the Embudo fault, beneath Santa Fe Group sediments in the study area.

In an evaluation of the three major fault systems of the study area, Bauer and Kelson (2004b) stated: "*In summary, the three major fault systems in the Taos area are more geometrically complex than described in previous literature. The Picuris-Pecos fault is actually only the western strand of an 8-km-wide brittle deformational zone herein named the Picuris-Pecos fault system. The fault system is a repeatedly reactivated crustal flaw that was a locus for south-transported Laramide volcaniclastic sediments from about 35 Ma (Picuris Formation) to 18 Ma (Tesuque Formation), and possibly later. The faults most likely exist in the basement of the basin west of Taos. The Pleistocene Los Cordovas faults may be westward transported, growth-fault remnants of the Picuris-Pecos fault system. The Picuris-Pecos faults may also define the structural boundaries of the Taos graben. The Picuris-Pecos fault system is truncated by the Embudo transfer fault, which merges into the Sangre de Cristo fault. During early extension, prior to development of the Embudo fault, the Picuris-Pecos fault system, and its now-buried northward extension, may have represented the eastern rift margin along with the Questa section of the Sangre de Cristo fault and the Town Yard fault. At some later time (mid- Miocene?), as the Embudo transfer fault developed, the Sangre de Cristo fault jumped eastward to the Cañon and Hondo sections, forming the Taos embayment …*"

These fault relationships are illustrated in the geologic cross sections (Plate 2) and the geologic fault model map (Fig. 18). In the cross sections, the principle elements of the Picuris-Pecos fault system only cut rocks as young as the Picuris Formation, and then shallow into the younger, rift-related Los Cordovas faults. The Embudo fault system cuts both the older rocks affected by the Picuris-Pecos faulting, and the young basin fill, and the faults are consistently north-down into the basin.

Conceptual structural model of the study area

Figure 18 is a simplified geologic map that illustrates our conceptual model for the major fault zones in the study area. For each of the three fault zones (Picuris-Pecos in red; Embudo in black; Los Cordovas in blue), we show their mapped faults, aeromagnetic faults, and conceptual faults. The Picuris-Pecos faults are oldest, and are visualized in the rift basin as being offset in a north-down/left-slip sense by the younger Embudo fault segments. The Picuris-Pecos faults are restricted to the bedrock (Proterozoic, Paleozoic, and the older Picuris Formation). The intersection of these two fault systems therefore divides these older units into complex, fault-bounded polygons. The Embudo fault zone also interacts with the young Los Cordovas faults in some complex manner, especially in areas where the zone fault systems overlap in time. However, these two fault systems will have predominantly divided the basin-fill units (younger Picuris Formation and Santa Fe Group) into complex, fault-bounded polygons. The net result of this complex structural model is a highly heterogenous stratigraphy that has profound effects on the groundwater systems in the study area.

3D patterns of basin-fill units

Although much of the Picuris piedmont is covered by thin alluvial deposits, the underlying Tertiary sedimentary units are well enough exposed to display some general patterns that are the result of the interaction of movement along the Embudo faulting and the primary depositional settings of some of the units. In general, the oldest sedimentary units (Picuris Formation, Chama-El Rito Member) crop out along the mountain front, whereas the younger units (Ojo Caliente Sandstone, Chamita Formation, Lama formation) exist only to the north along the middle to lower parts of the piedmont slope (Plate 1).

Picuris Formation rocks were deposited on pre-rift bedrock (Paleozoic and Proterozoic rocks). Due to movements along the Embudo fault zone, these rocks are now exposed around much of the flank of the Picuris Mountains. In the study area, the Picuris

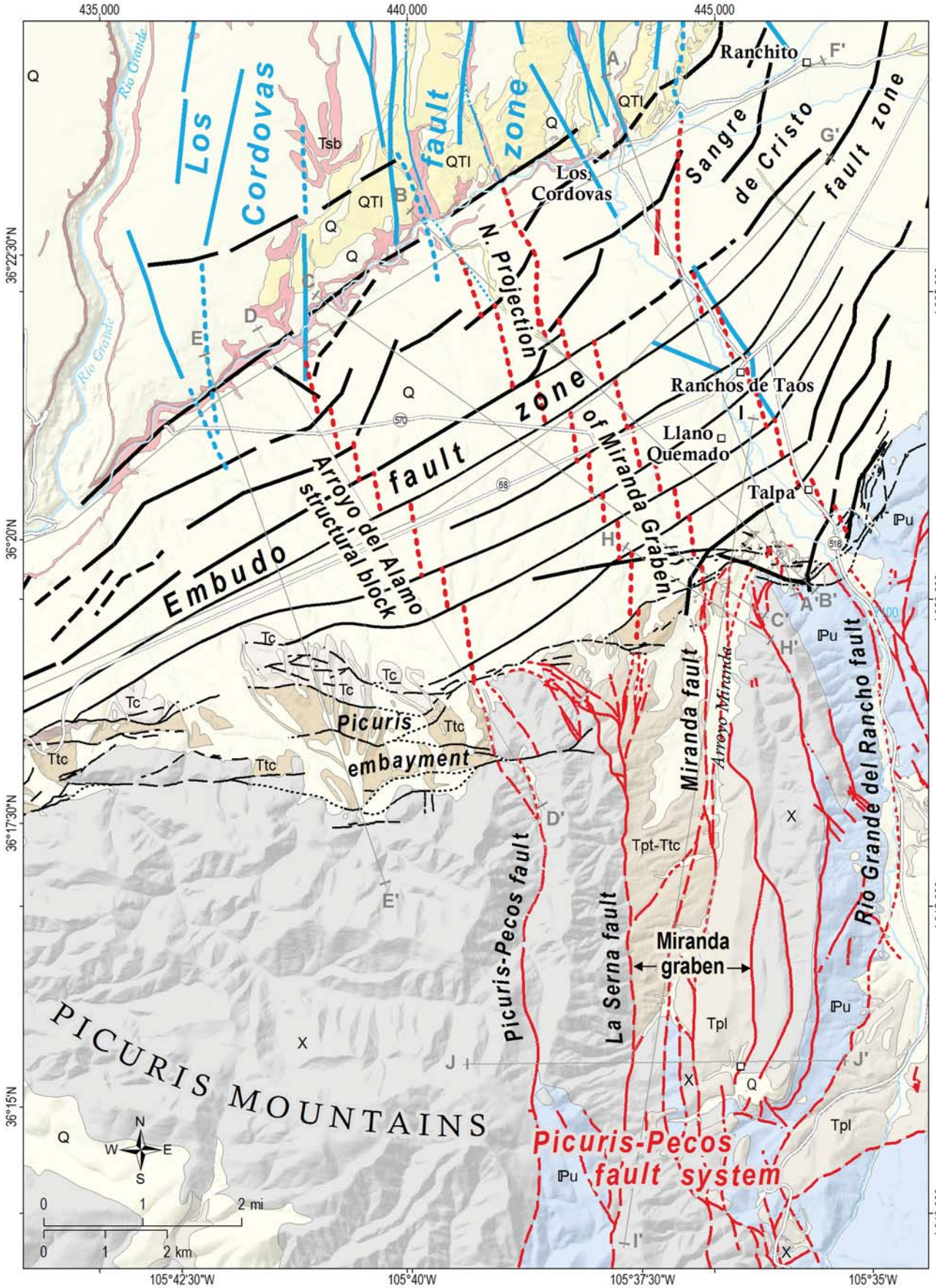
435,000
440,000
445,000
36°22'30"N
36°20'N
36°17'30"N
36°15'N
4,025,000
4,020,000
4,015,000
4,010,000
105°42'30"W
105°40'W
105°37'30"W
105°35'W
Rio Grande
Los Cordovas fault zone
N. projection
Sangre de Cristo fault zone
Embudo fault zone
Arroyo del Alamo structural block
of Miranda Graben
Picuris embayment
Miranda fault
Arroyo Miranda
Rio Grande del Rancho fault
Picuris-Pecos fault
La Serna fault
Miranda graben
Picuris-Pecos fault system
PICURIS MOUNTAINS
Ranchito
Los Cordovas
Ranchos de Taos
Llano Quemado
Talpa
Tsb
QTl
Tpt-Ttc
Tpl
Ttc
Tc
Q
Pu
A
A'
B
B'
C
C'
D
D'
E
E'
F
F'
G
G'
H
H'
I
I'
J
J'
X
N
W
E
S
0
1
2 mi
0
1
2 km

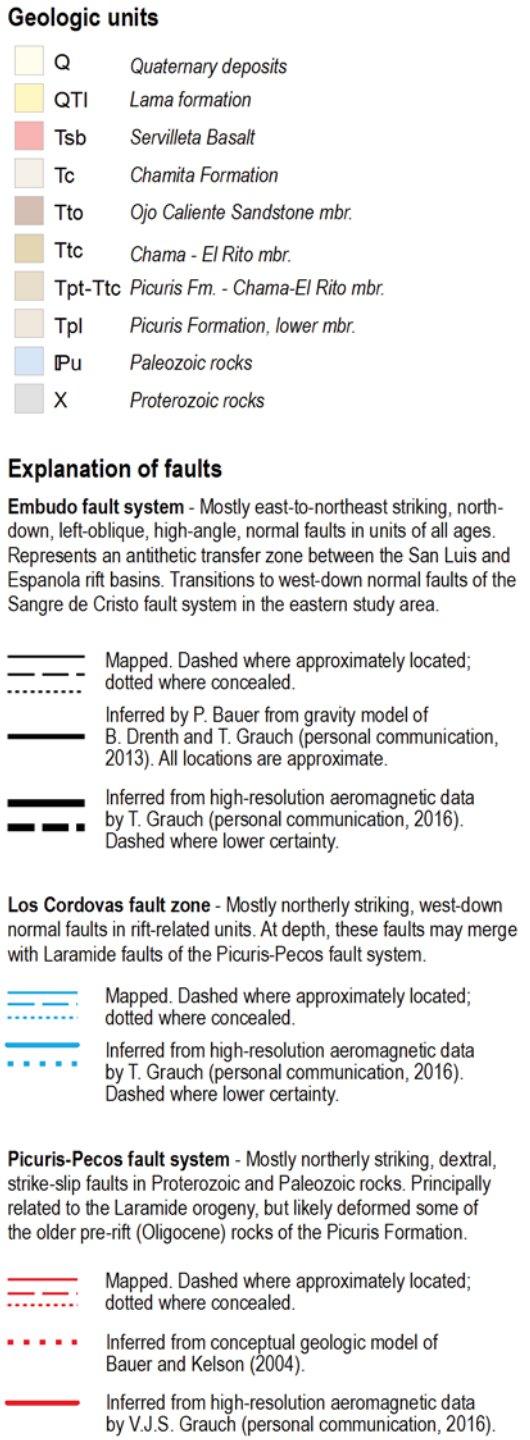

Figure 18. Structural model of the three regional fault systems in the study area. Picuris-Pecos fault system shown in red. Embudo fault zone shown in black. Los Cordovas fault zone shown in blue. Each fault system is coded according to whether the fault segments are mapped, inferred by geophysical methods, or conceptually modeled. See Table 3 for geologic unit descriptions.

Formation is exposed at the surface east of the Picuris-Pecos fault, but not exposed at the surface west of the Picuris-Pecos fault. However, borehole data do indicate that Picuris Formation rocks exist in the subsurface west of the fault. Presumably, the Picuris Formation also extends northward into the rift basin, where it is consecutively dropped down along a series of large-displacement, north-down Embudo faults (Fig. 18; Plate 2).

The Chama-El Rito Member (Ttc) occurs along much the upper Picuris piedmont (Plate 1). Locally, where it has been eroded from the uplifted Picuris Mountains, it may exist as only a thin layer atop the Picuris Formation. Aby et al. (2004) concluded that the uppermost Picuris Formation grades into the overlying Chama-El Rito Member, and therefore the exact location of the contact can be indistinct. Presumably, the Chama-El Rito Member also extends northward into the rift basin, where it is consecutively dropped down along the series of large-displacement, north-down Embudo faults.

In the study area, the Ojo Caliente Sandstone (Tto) is only exposed in the westernmost exposure of the Embudo fault zone, along NM-68 (Plate 1). However, based on borehole analyses, Drakos et al. (2016) concluded that it underlies a significant part of the southern rift basin. In our subsurface model, we show the unit thinning to the south and east as the migrating sand dunes would have begun to encounter the active Embudo and Sangre de Cristo fault zones. Therefore, within the study area, the Ojo Caliente is missing or very thin under the southern and eastern parts of the Picuris piedmont. Additionally, because it is also down dropped northward into the rift basin along medium-displacement faults, significant thicknesses of shallow Ojo Caliente Sandstone are limited to the central zone of the Picuris piedmont.

Based on borehole analysis in the study area, Drakos et al. (2016) defined a stratigraphic unit that is transitional between the eolian sandstone of the Ojo Caliente Member and the conglomeratic sandstones of the Chamita Formation. We have retained that unit as "Tto & Tc" on the cross sections (Plate 2). Its distribution in the study area is similar to that of the Ojo Caliente Sandstone.

The Chamita Formation (Tc) is not exposed in the study area, although excellent exposures exist on the south side of Pilar Mesa, just west of the study area. The Chamita was locally derived from the Picuris and Sangre de Cristo Mountains, and exists in the shallow subsurface throughout the study area, except where it has been eroded from the upper Picuris piedmont. Although the Chamita is dropped

down into the rift basin by Embudo faults, the fault offsets are typically less than 200 feet, and so Chamita deposits likely underlie much of the study area at shallow levels.

The Lama formation was derived mainly from the Sangre de Cristo Mountains to the east, and it now exists at or near the surface over much of the northeastern part of the study area. In the stratigraphic model shown in Plate 2, approximately half way up the Picuris piedmont, the Lama formation merges into equivalent uppermost Chamita Formation alluvial fans that prograded northward from the Picuris Mountains. The location of the contact between the Lama and Chamita is approximate, and certainly represents an interfingering of the two deposits over considerable distances and in complex ways.

Southern extent of basalt

Aeromagnetic and borehole analysis make it possible to accurately define the extent of Servilleta Basalt in the subsurface of the study area. The surface projection of this zone is shown on the geologic map as the line labeled "southern extent of basalt" (Fig. 6). In the geologic cross sections (Plate 2), the basalt flows terminate southward on a major, buried splay of the Embudo fault. The coincidence of the fault and the lava flow terminations can be placed with high confidence due to the interpretations of the high-resolution aeromagnetic data by V.J.S. Grauch of the U.S. Geological Survey (Grauch et al., 2015). In general, the number of basalt-flow packages, and their thicknesses, decrease southward as they approach this fault splay. Most likely, Embudo fault scarps created topographic barriers to the prograding lava flows during Pliocene time.

In the Los Cordovas area, near the confluence of the Rio Pueblo de Taos and Rio Grande del Rancho, there exists a ~1-km-wide domain where the basalt flows show a wide range of abrupt thickness changes, including areas where the Servilleta ranges from zero to several hundred feet thick over short distances. The controls on basalt thicknesses in this area are unknown, but probably involve some combination of fault scarp dams, other paleotopography, and later erosion of basalts.

The Picuris embayment

In the central study area, just west of the Picuris-Pecos fault, the contact between the basin-fill units and the Proterozoic rocks along the north flank of the Picuris Mountains delineate an indentation, herein named the "Picuris embayment" (Fig. 18, Plate 1). The embayment is about 3 km across (east-west) and 1 km deep (north-south), and is filled with rocks of the Chama-El Rito Member, which either onlap the basement rocks, or are faulted against them, or both. Several mappable splays of the Embudo fault zone cross the area, and the strata of the Chama-El Rito are tilted at least up to 45°, indicating that the basin-fill rocks have been strongly affected by the faults. A combination of movement along the Picuris-Pecos fault (and perhaps other unidentified north-striking faults along the western edge of the embayment) and younger movement along the Embudo fault segments was likely responsible for the development of the embayment.

The sole water well (TV-100) identified in the embayment was drilled through basin-fill sediments until encountering "quartz" (interpreted as at, or just above, Proterozoic bedrock) at 920 ft depth. As interpreted in cross sections D-D' and E-E' (Plate 2), the Picuris embayment is a zone in which the older basin-fill units (Tp and Ttc) are inset into the flank of the Picuris Mountains on a shallow basement bench.

The conceptual fault model of the area shows the Picuris-Pecos fault continuing northward under the Picuris piedmont, and linking up with a major, buried segment of the Los Cordovas fault zone near the Rio Pueblo de Taos (Fig. 18). Because the Picuris-Pecos fault is older than the Embudo fault zone, the fault model also shows multiple zones of segmentation of the buried Picuris-Pecos fault as it crosses each strand of the Embudo fault zone. In this conceptual model, the section of the Picuris-Pecos fault that is buried under the Picuris piedmont has caused major offset of the Proterozoic rocks, and only moderate offset of the basin-fill rocks as it merges upward with the buried Los Cordovas fault.

The area of the Picuris piedmont that is bordered by the Picuris embayment to the south, the Picuris-Pecos/Los Cordovas fault trace to the east, and the Rio Pueblo de Taos to the north, is herein referred to as the "Arroyo del Alamo structural block" (Fig. 18). This fault-bounded block displays some unique hydrogeologic conditions that are thought to be the result of the characteristics of the faulted basin-fill deposits.

The projection of the Picuris-Pecos/Los Cordovas fault to the Rio Pueblo de Taos also corresponds with a major river nickpoint. Above the fault intersection, the river gradient is low (36 ft/mi) and the channel is broad. Below the fault intersection, the gradient is high (151 ft/mi), and the river has carved a steep

canyon through the basalts to its confluence with the Rio Grande. Our preferred working hypothesis is that the buried fault is a steeply dipping normal fault, and the footwall block of upper Servilleta Basalt has created the nickpoint.

Hydrogeologic Cross Sections

Many observations and interpretations of the Southern Taos Valley groundwater flow system were made from an analysis of geologic cross sections, well data, and water-level data. Based on an analysis of lithologic logs from water well records (Table 1), and the geologic map and cross sections (Plates 1 and 2), we developed eight detailed hydrogeologic cross sections that depict the subsurface distribution of geologic and hydrostratigraphic units, faults, well data, and hydrologic features and characteristics including rivers, streams, springs, acequias, and depth to groundwater (Fig. 19). These cross sections illustrate the distribution, location, and extent of aquifers in the context of both the geologic framework and surface water features. Integrating geologic and hydrologic

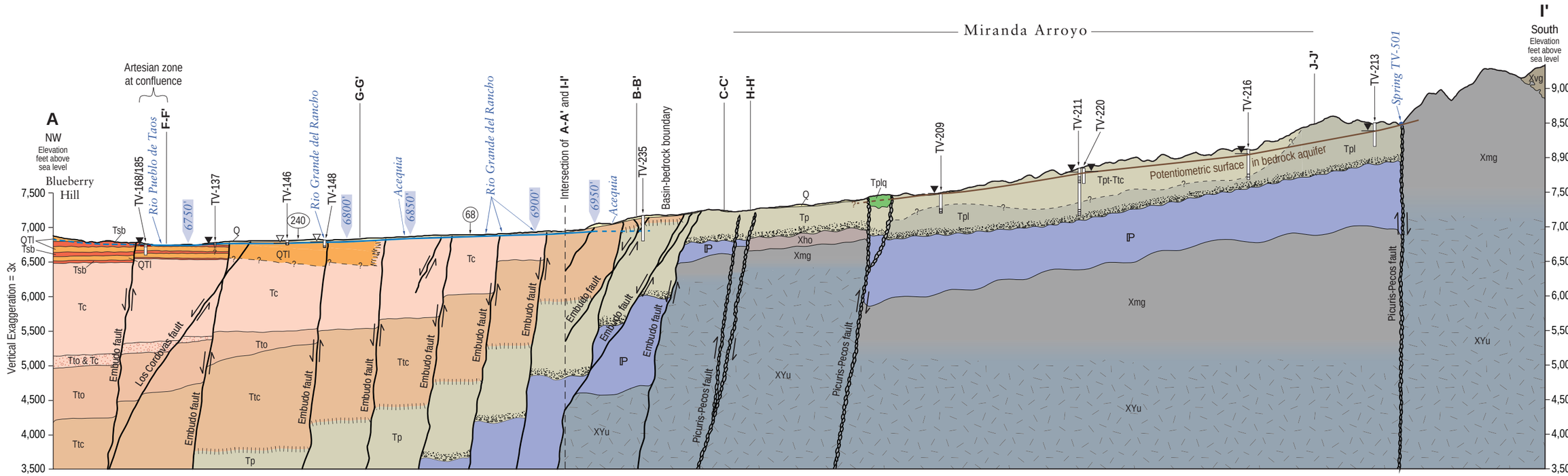

Figure 19. Seven hydrogeologic cross sections depict subsurface views of hydrostratigraphic units, wells, and the water-table surface for perched and regional systems in the basin and bedrock aquifers. These cross sections are derived from the geologic cross sections shown on Plate 2. They have been scaled down to fit on these pages, are vertically exaggerated by 3 times, and only go as deep as the deepest water well. See Tables 1 and 2 for well and spring information; Table 3 for geologic unit descriptions; and Tables 5 and 6 for water-level data.

Geologic Units

Q	*Quaternary deposits, undivided*
QTl	*Lama formation*
Tsb	*Servilleta Basalt*
Tcc	*Chamita Formation*
Tc	*Chamita Formation*
Tto	*Ojo Caliente Sandstone*
Ttc	*Chama-El Rito member*
Tplq	*Llano Quemado Breccia member*
Tbo	*Older basaltic rocks*
Tp	*Picuris Formation*
IP	*Pennsylvanian sedimentary rocks*
Xmg	*Miranda granite*
XYu	*Proterozoic rocks*
Xh	*Hondo Group*
Xhr3	*R3 quartzite member,*
Xhr1/2	*R1/R2 schist member*
Xho	*Ortega Formation*
Xvg	*Glenwoody Formation-Feldspathic*

Fault – Arrows show sense of vertical movement

Gradational contact

Well Key

TV-276 NMBG database name *(Table 1 and Figure 5)*

Well head, elevation

Volcanic intervals *(Tsb from well record)*

Measured water level

Driller's static water level

Screened interval

Aquifer Symbols

Water table surface in basin aquifer

Certain

Approximate

Zone of perched groundwater

Bedrock aquifer

6850' Water table elevation

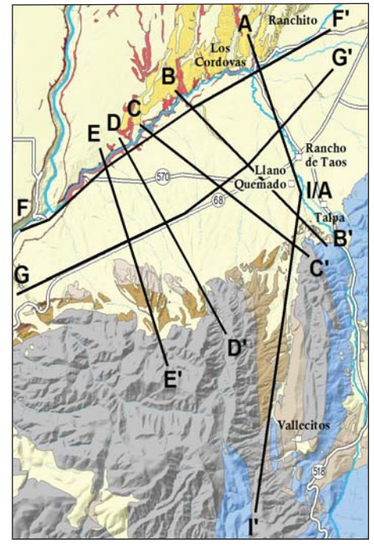

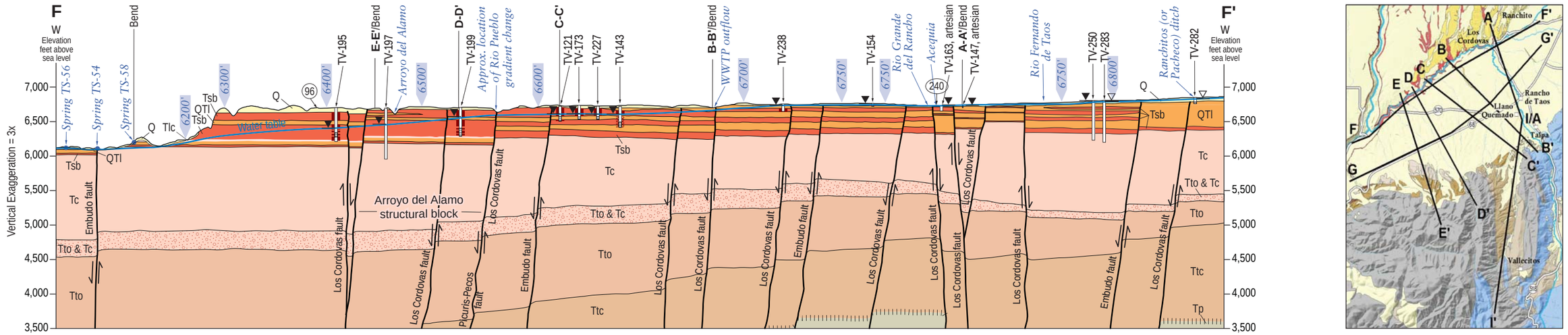

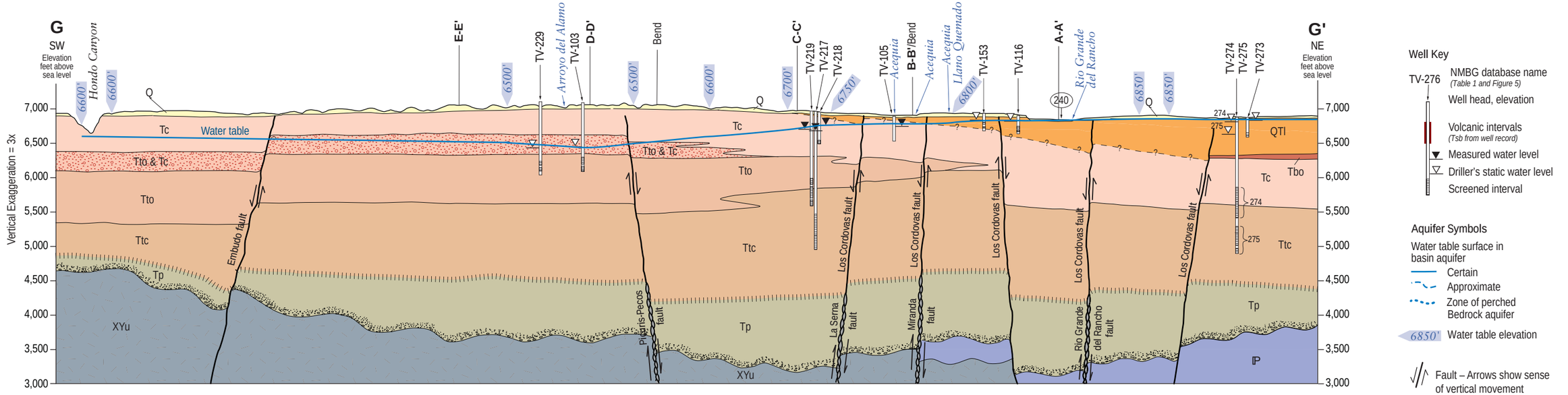

Geologic Units

Q	*Quaternary deposits, undivided*	Ttc	*Chama-El Rito member*	XYu	*Proterozoic rocks*
QTl	*Lama formation*	Tplq	*Llano Quemado Breccia member*	Xh	*Hondo Group*
Tsb	*Servilleta Basalt*	Tbo	*Older basaltic rocks*	Xhr3	*R3 quartzite member,*
Tcc	*Chamita Formation*	Tp	*Picuris Formation*	Xhr1/2	*R1/R2 schist member*
Tc	*Chamita Formation*	IP	*Pennsylvanian sedimentary rocks*	Xho	*Ortega Formation*
Tto	*Ojo Caliente Sandstone*	Xmg	*Miranda granite*	Xvg	*Glenwoody Formation-Feldspathic*

Figure 19. Seven hydrogeologic cross sections.—Continued

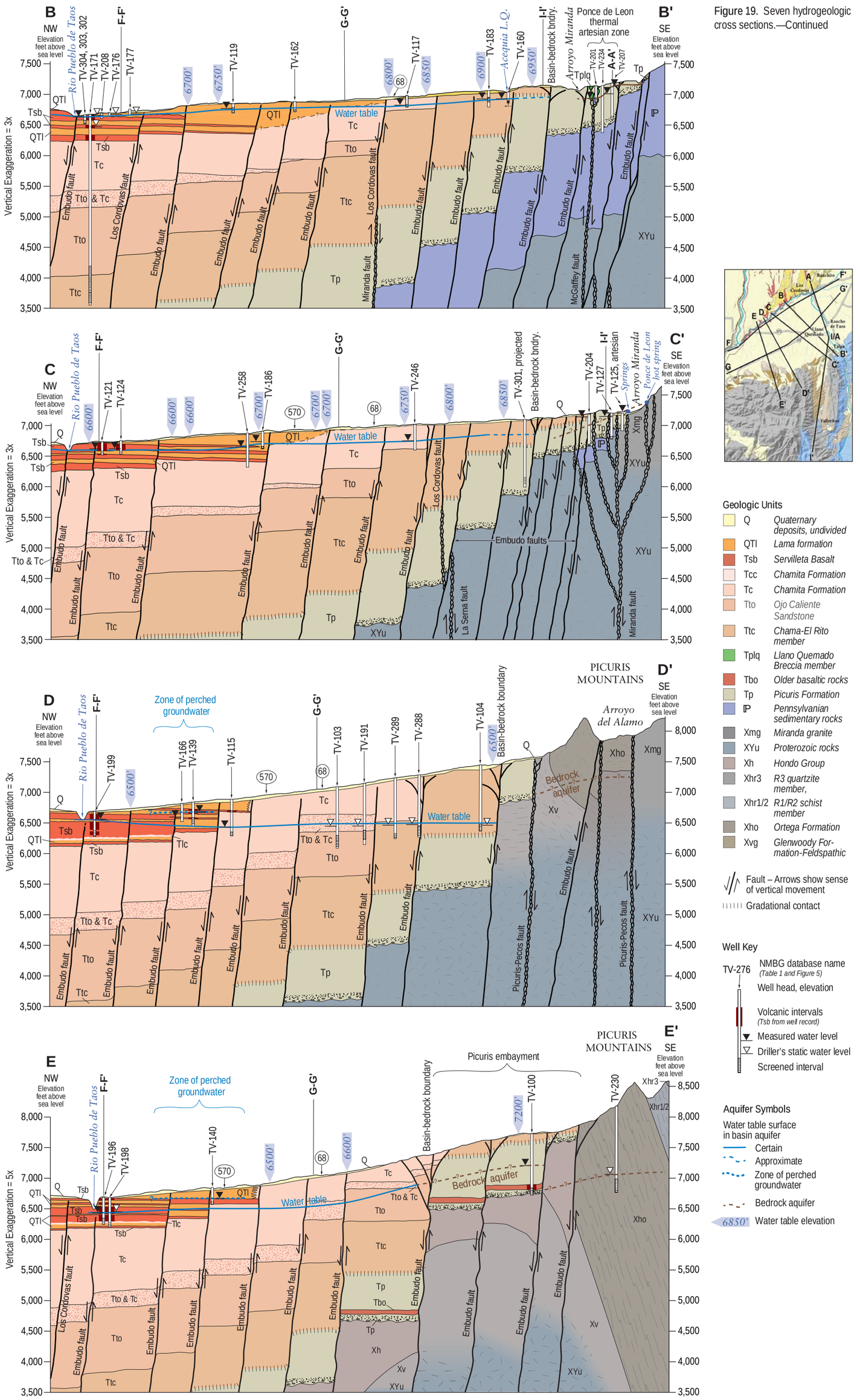

Figure 19. Seven hydrogeologic cross sections.—Continued

Geologic Units

	Q	*Quaternary deposits, undivided*
	QTl	*Lama formation*
	Tsb	*Servilleta Basalt*
	Tcc	*Chamita Formation*
	Tc	*Chamita Formation*
	Tto	*Ojo Caliente Sandstone*
	Ttc	*Chama-El Rito member*
	Tplq	*Llano Quemado Breccia member*
	Tbo	*Older basaltic rocks*
	Tp	*Picuris Formation*
	IP	*Pennsylvanian sedimentary rocks*
	Xmg	*Miranda granite*
	XYu	*Proterozoic rocks*
	Xh	*Hondo Group*
	Xhr3	*R3 quartzite member,*
	Xhr1/2	*R1/R2 schist member*
	Xho	*Ortega Formation*
	Xvg	*Glenwoody Formation-Feldspathic*

Fault – Arrows show sense of vertical movement

Gradational contact

Well Key

TV-276 NMBG database name *(Table 1 and Figure 5)*

Well head, elevation

Volcanic intervals *(Tsb from well record)*

Measured water level

Driller's static water level

Screened interval

Aquifer Symbols

Water table surface in basin aquifer

Certain

Approximate

Zone of perched groundwater

Bedrock aquifer

6850' Water table elevation

information on the cross sections provides insight regarding the distribution of aquifers and geologic controls on groundwater flow.

Summary of Geologic Investigations

1. **Complex geologic setting**—The study area is located in the southeast corner of the San Luis Basin of the Rio Grande rift, and includes stratigraphic and structural elements of the rift, the Taos Plateau volcanic field, and the southern Rocky Mountains. These elements combine to create an extremely complex geologic setting with a great diversity of rock types and ages that is overprinted by a long history of tectonism and volcanism.
2. **Diverse stratigraphy**—The study area contains rocks and deposits that range in age from Meso-proterozoic (1.7 billion years old) to Recent. Proterozoic crystalline rocks and Paleozoic sedimentary rocks are exposed in the Picuris and Sangre de Cristo Mountains, and presumably also exist buried within the rift basin. The oldest Tertiary sedimentary rocks (Picuris Formation) represent pre-rift to early-rift deposition, and are found in Laramide grabens (Miranda and Rio Grande del Rancho grabens) and buried in the rift basin. The youngest Tertiary sedimentary rocks (Santa Fe Group) are found only in the rift basin, where they were deposited in a complex three-dimensional package that is up to about 5,000 ft thick. The only volcanic rocks exposed in the area are packages of thin basaltic lava flows (Servilleta Basalt) that flowed into the study area from the northwest. The youngest units in the study area are unconsolidated, thin alluvial and colluvial sheets of surficial deposits that cover much of the rift basin.
3. **Clay deposits**—Sedimentary clay deposits appear to be fairly common in the basin-fill sediments. Analyses of several clays suggest that they can be laterally extensive and may have formed in temporary shallow lakes that formed behind lava flow dams. A 2-m-thick clay in the western study area is clearly related to a number of perched seeps and springs that exist on the canyon walls of the Rio Grande gorge.
4. **Intersecting fault zones**—Three major systems of faults intersect in the southern Taos Valley. The oldest, the Picuris-Pecos fault system, consists of multiple, north-striking, high-angle, strike-slip faults that offset rocks as young as the Picuris Formation in the eastern Picuris Mountains. The Sangre de Cristo and Embudo fault zones flank the edge of the Rio Grande rift, and have dropped down rocks of all ages into the rift basin. Both of these rift-flanking fault systems are considerably wider than their mapped exposures, with zones at least several kilometers wide buried beneath the piedmont slopes that surround the basin. A fourth fault zone, the Los Cordovas fault zone, consists of several small-displacement, west-down, normal faults in the northern study area. All of these fault systems consist of geometrically complex fault planes that branch, merge, curve, and terminate in three dimensions. Out of necessity, our geologic cross sections are intentionally simplified in order to be able to show the general geometries and kinematics of the major faults.
5. **Miranda graben**—The Miranda graben of the Picuris-Pecos fault system is formed between the west-down Miranda fault and the east-down La Serna fault. In the study area, it is filled with sedimentary strata of the Picuris Formation that overlie crystalline basement rocks. The graben is truncated by the Embudo fault system, but certainly exists in the subsurface of the rift basin where it presumably is progressively offset by each of the north-down, left-oblique Embudo fault segments.
6. **Ponce de Leon spring**—Ponce de Leon hot spring is located at the intersection of several fault splays along the eastern edge of the Miranda graben. Other thermal springs in the region (Manby spring, Black Rock spring, unnamed spring near Taos Junction bridge) are also located on faults.
7. **Geologic model for faults**—The four fault systems in the study area overlap in various ways in time and space. Our geologic model states that the Picuris-Pecos fault system exists in the basement rocks (Picuris Formation and older units) of the rift, where it is progressively down dropped and offset to the west by each Embudo fault segment between the Picuris Mountains and the Rio Pueblo de Taos. In this model, the Miranda graben therefore exists in the subsurface as a series of offset basement blocks between the Ponce de Leon neighborhood and the Town of Taos well field. In the study area, the Embudo faults are pervasive structures between the Picuris Mountains and the Rio Pueblo de Taos, affecting all geologic units that are older than the Quaternary surficial deposits. The Los Cordovas faults are thought to represent the Late Tertiary

to Quaternary reactivation of the old and deeply buried Picuris-Pecos faults. If so, then the Los Cordovas may extend southward under the Picuris piedmont, where they form growth faults as they merge downward into the Picuris-Pecos faults. If the Los Cordovas and Picuris-Pecos faults are interconnected in this way, they would be likely to facilitate upward flow of deep fluids into shallow aquifer zones.

8. **Fault-generated permeability—**Common exposures of Picuris-Pecos and Embudo faults in some bedrock units (Proterozoic rocks, Paleozoic sandstones and carbonates) show severe fracturing and brecciation of the rocks, producing high-permeability zones in the rocks. In contrast, rare exposures of faults in the basin-fill units (Santa Fe Group, other than Ojo Caliente Sandstone) show clay-filled damage zones that would likely decrease lateral permeabilities across high-angle faults, and create water-bearing domains and compartments in the basin-fill aquifers.
9. **Fault stratigraphy—**The exceptionally high density of cross-cutting faults in the study area has severely disrupted the stratigraphy of the Picuris Formation and the Santa Fe Group. The Picuris Formation exists at the surface in the Miranda and Rio Grande del Rancho grabens, and locally along the top of the Picuris piedmont. In the subsurface, it deepens rapidly from the mountain front into the rift basin. In a similar manner, the Tesuque and Chamita Formations are shallowly exposed close to the mountain front, but are down dropped into the basin along the Embudo faults. The Ojo Caliente Sandstone of the Tesuque Formation appears to be thickest in the northwestern study area, and thins toward the south and the east. In the study area, the Lama formation thins westward and southward. The Servilleta Basalt is generally thickest to the north and northwest, thins under the Picuris piedmont, and terminates along an exceptionally linear, major, buried strand of the Embudo fault zone. We therefore conclude that these lava flows were spatially and temporally related to Embudo fault activity.
10. **Model for Paleozoic strata—**Our geologic model shows a thick section of Paleozoic rocks to the east, with a general thinning trend westward until the section is truncated by the Miranda fault. In this model, no Paleozoic strata exist in the rift basin west of the projection of the Miranda fault northward to the Rio Pueblo de Taos.
11. **Picuris embayment—**The Picuris embayment is an indentation along the Picuris Mountains range front in the central part of the study area, just west of the Picuris-Pecos fault and Arroyo del Alamo. The embayment is filled with Tesuque Formation rocks that overlie basement units. The area between the Picuris embayment to the south, the projection of the Picuris-Pecos fault to the east, and the Rio Pueblo de Taos to the north is herein called the Arroyo del Alamo structural block. The northeast corner of this structural block corresponds with a segment of the Los Cordovas fault zone, and an abrupt gradient change on the Rio Pueblo de Taos. The gradient change is interpreted as a river knickpoint that was created by the offset of the uppermost Servilleta Basalt layer by a west-down Los Cordovas fault. The geology of the Arroyo del Alamo structural block has created a unique, complex hydrogeologic setting that combines a hydrogeologic window in the Picuris embayment, with shallow Ojo Caliente Sandstone, and a clay layer in the lower Rio Pueblo area.

Using a water level probe to measure the level of water in an open well on the Picuris piedmont. *Photo by Paul Bauer.*

IV. HYDROGEOLOGIC SYSTEMS OF THE SOUTHERN TAOS VALLEY

Hydrostratigraphic Units

The distribution of hydrostratigraphic units is best understood through examination of the geologic maps and stratigraphic chart (Figs. 6–8, Plate 1), a shallow groundwater domain map (Fig. 20), and seven hydrogeologic cross sections (Fig. 19). The hydrostratigraphy of the southern Taos Valley can be divided into two zones—the Santa Fe Group basin fill and the Pennsylvanian/Proterozoic bedrock—separated by transitional strata of the Tertiary Picuris Formation. Five hydrostratigraphic units exist within the Santa Fe Group in the southern Taos Valley: 1) alluvial deposits of the Lama formation (QTl); 2) Servilleta Basalt and thinly interlayered sediments of the Lama formation (Tsb and QTlb); 3) alluvial deposits of the Chamita Formation (Tc) that lie below the oldest Servilleta Basalt; 4) the eolian Ojo Caliente Sandstone Member of the Tesuque Formation (Tto); and 5) the sedimentary deposits of the Chama-El Rito Member of the Tesuque Formation (Ttc). These hydrostratigraphic units and their associated aquifers are summarized in the following sections.

Santa Fe Group basin fill

Santa Fe Group sediments comprise the major alluvial aquifer in the Taos area. A significant range in thicknesses of basin-fill units exists throughout the southern Taos Valley. Some contacts between units are gradational and/or the units interfinger in complex ways, both laterally and vertically. Despite these variabilities, the spatial distribution of Santa Fe Group hydrostratigraphic units at or near the land surface, and hence in shallow basin-fill wells, manifests a regular pattern as northeast-trending bands that become progressively older from north to south (Fig. 20). The youngest units in the basin (Pliocene age QTl and Tsb) are exposed near the Rio Pueblo; upper Miocene Chamita Formation (Tc) exists in the center of the study area; and lower Miocene deposits of the Tesuque Formation (Ttc and Tto) lie nearest their source in the Picuris Mountains. Servilleta Basalt progressively thins to the south and east and pinches out near or along the basalt line ("southern extent of basalt" in Figures 7 and 20).

Lama formation (QTl), Servilleta Basalt (Tsb) and Chamita Formation (Tc)—Shallow regional groundwater throughout the southern Taos Valley occurs primarily within the Lama formation alluvial deposits, the Servilleta Basalt, Tertiary basin-fill sediments of the Chamita Formation, and locally within the Tesuque Formation. This shallow aquifer, which we call the "Picuris piedmont aquifer" or the "piedmont aquifer", stretches from the basin-bedrock boundary to the Rio Pueblo and generally exists under unconfined conditions.

In the northern portion of the Picuris piedmont, north of the basalt line, the majority of domestic wells draw water, individually or collectively, from the Lama formation, the underlying Servilleta Basalt, and thin layers of Lama formation sediments between the basalt flows. Clay deposits above and between Servilleta Basalt flows in the Los Cordovas fault zone can perch water above, or vertically partition groundwater within, the Picuris piedmont aquifer. A few wells in the northern Arroyo del Alamo structural block penetrate the oldest basalt layer and draw groundwater from the underlying Chamita Formation alluvial sediments (wells TV-115, TV-149, and TV-188) or Chamita sediments and the lowermost Servilleta basalt (TV-263). South of the basalt line, Chamita deposits also provide water to shallow wells in and adjacent to the Rio Grande del Rancho valley. Wells in the Lama formation and Servilleta Basalt are shallowest in the floodplains of the upper Rio Pueblo and Rio Grande del Rancho (40–50 feet in depth, with a 10- to 50-foot-deep water table) and deepest along the incised lower Rio Pueblo canyon (400–480 feet in depth, with a 250- to 285-foot-deep water table). The highly variable thickness of Servilleta Basalt and interlayered sediments, the presence of an extensive clay layer above the oldest Servilleta basalt (unit Tlc in Figure 19), and incision of the Rio Pueblo

produce a dramatic range in depth to water of about 50 to 480 feet north of the basalt line. This clay layer is spatially related to small springs and seeps exposed on the canyon walls of the Rio Grande to the southwest (TS-58 and TS-56, Figure 19, cross sections F-F'). A small zone of perched groundwater is localized in Lama formation sediments above the deepest basalt, southwest of the golf course. Data compiled from drilling records indicate average well yields of about 20 gallons per minute (gpm) in the Lama formation, 11 gpm in Servilleta Basalt, and 20 gpm in the Chamita Formation. Where fracturing is noted in the Servilleta Basalt, well yields increase to an average of 35 gpm. See Tables 1 and 4 for information on well depth, water-bearing formation, depth to water, and well yield.

Tesuque Formation Ojo Caliente Sandstone (Tto) and Chama-El Rito (Ttc) Members—Regional groundwater beneath the southern Taos Valley exists at both shallow and deep horizons within the Ojo Caliente Sandstone (a well-sorted, fine-grained eolian sandstone) and the Chama-El Rito (a volcanic-rich sandstone and conglomerate) Members of the Tesuque Formation. Significant thicknesses of Ojo Caliente are limited to the central zone of the Picuris piedmont, near the Arroyo del Alamo structural block. The Ojo Caliente Sandstone is a unique eolian deposit that possesses different sedimentary and hydrologic characteristics than adjacent alluvial deposits in the Chama El Rito Member and Chamita Formation. As dune sand, its deposition is not limited by topography (dune sands can be deposited up-slope on the flanks of highlands), its sediments are better sorted, and thus the deposits retain a relatively higher porosity and permeability.

Both the Ojo Caliente and the Chama-El Rito generally form productive water-bearing zones that yield the first viable water supplies between NM-68 and the basin-bedrock hydrologic boundary. The most notable examples are: 1) the Tierra Blanca neighborhood in the Arroyo del Alamo structural block; 2) the Picuris piedmont near Camino de Golondrina and Selph Road; and 3) the Rio Grande del Rancho valley south of Llano Quemado. In the Arroyo del Alamo area, the shallow aquifer is exceptionally deep, but apparently is still under unconfined or semi-confined conditions. In the Tierra Blanca

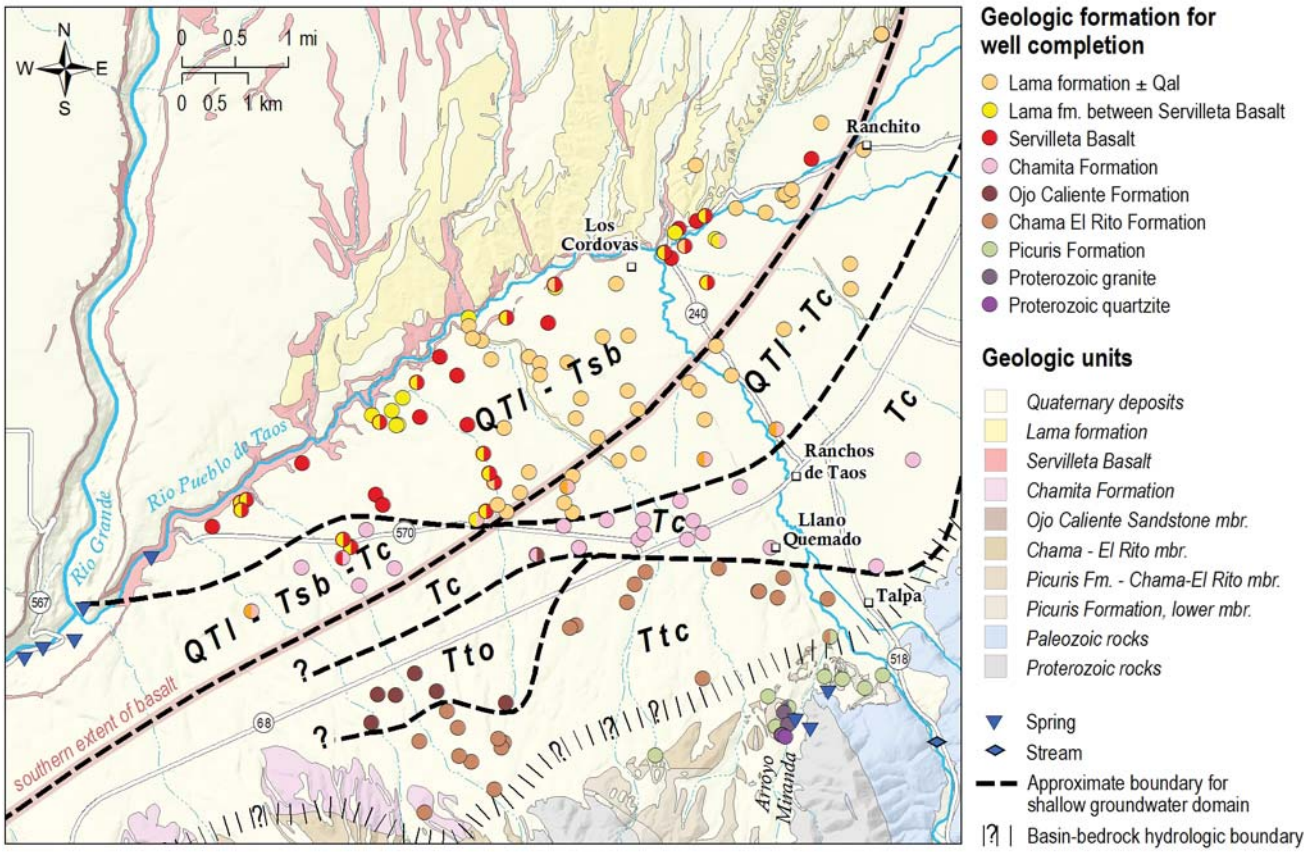

Figure 20. Map of groundwater domains in the Picuris piedmont aquifer. The domains depict the distribution of hydrostratigraphic units defined using lithologic data from well logs and geologic mapping. See Table 1 for well information and water-bearing formation.

Table 4. Summary statistics for well yields in various geologic units (in gallons per minute, gpm). See Table 1 for well data and Table 3 for geologic unit descriptions.

Site ID	QTl	QTlb	Tsb	Tsb (f)	QTl-Tsb	Tc	Tto	Ttc	Tp	Tpl	IP	Xmg	Xmg (f)	Xho	Xho (f)
Minimum	10	15	5	25	12	5	25	8	1	23	20	0.5	60	10	30
Maximum	50	40	15	50	53	45	100	200	15	50	20	6.5	60	25	45
Average	19	22	11	35	23	20	54	31	6	33	20	3	60	18	38
Number	30	8	8	3	12	19	8	24	6	3	2	3	1	2	2

f–fractured

neighborhood, well depths range from 1,000–1,120 feet in the Ojo Caliente near NM-68, to 950–1,290 feet in the Chama-El Rito near the mountains. The water table in the Ojo Caliente lies 550 to 700 feet below the surface and even deeper (760 to 1,050 feet) in the Chama-El Rito (Table 1). In contrast, shallow wells in the Chama-El Rito Member near the Rio Grande del Rancho are 120–250 feet total depth, with a depth to water less than 140 feet. The Ojo Caliente Sandstone is the most productive part of the Santa Fe Group aquifer. Based on data compiled from drilling records, the Ojo Caliente has an average well yield of 54 gpm. The average yield in Chama-El Rito wells is 31 gpm (Table 4).

A deep confined alluvial aquifer also exists in the Ojo Caliente Sandstone and the Chama-El Rito north of NM-68, where the units are faulted down into the basin to progressively greater depths (Fig. 19, cross sections A-A' through E-E'). Knowledge of this deep aquifer is limited to geologic, hydrologic and geochemical information gathered from three production or test wells and four exploration wells, which are clustered west and east of the Rio Grande del Rancho and include: 1) the UNM Taos well (TV-152), the RP-2500 well (TV-170), the RP-3200 well (TV-171), the RP-2000 piezometer (TV-302, TV-303, TV-304), and the BOR-1 (TV-219, TV-217) exploration well, all located on the Picuris piedmont west of the Rio Grande del Rancho and south of the Rio Pueblo; and 2) exploration wells BOR-2 (TV-274, TV-275) and K2 (TV-291 through TV-298) located farther east and north. Another domestic test well (TV-301) is located high on the Picuris piedmont, about 1.4 miles southwest of the village of Llano Quemado. See Fig. 5 and Table 1 for well locations and information.

North of NM-68, west of Rio Grande del Rancho, and south of the Rio Pueblo, the wells (UNM Taos, RP-2500, RP-3200, and RP-2000) are completed in both the Ojo Caliente Sandstone and the Chama-El Rito Members. At locations closer to the mountain front, east of Rio Grande del Rancho, and northeast of the confluence, the Ojo Caliente Sandstone is absent, and deep wells are completed in Chamita and Chama-El Rito sediments. In well TV-301, the shallowest productive water-bearing zone is encountered in volcanic-rich Chama-El Rito sediments, possibly interlayered with Picuris Formation, at a depth of over 1,000 feet. Recorded yields in these deep, long-screened wells are as much as 100 gpm in a thin Ojo Caliente Sandstone and 200 gpm in Chama-El Rito sediments (Table 1).

Effects of faults on groundwater in the Santa Fe Group aquifer—The complex network of intersecting fault zones in the study area (Fig. 18) affects both the shallow and deep zones of the Santa Fe Group aquifer in the southern Taos Valley. The area bounded by the Picuris Mountains, the Rio Grande del Rancho, the Rio Pueblo, and the Rio Grande contains three major overlapping fault zones—specifically the Picuris-Pecos and Embudo fault zones and the Los Cordovas faults—and possibly the most structurally complex alluvial aquifer in New Mexico. In the Española Basin to the south, Grauch et al. (2009) hypothesized that such basement-piercing faults may serve as partial flow barriers, compartmentalize aquifers, or possibly control upwelling of deep groundwater from fractured basement. Similar intrabasin and basin-boundary structures have been shown to have a major effect on groundwater flow, heat flow, and water chemistry in other basins of the Rio Grande rift (Johnson et al., 2013; Witcher et al., 2004). Our evaluation of hydrologic and geochemical data in this and following sections supports a similar model for the southern Taos Valley.

Pennsylvanian–Proterozoic bedrock

Although several bedrock units of Pennsylvanian and Proterozoic age exist along the front of the Picuris Mountains, only three appear to have hydrologic significance for the southern Taos Valley. These are: 1) Pennsylvanian sedimentary rocks (IP); 2) Proterozoic Miranda granite (Xmg); and 3) Proterozoic Ortega Formation quartzite (Xho). The Picuris Formation is the oldest alluvial deposit in the basin, but hydrologically we consider the formation to be part of the bedrock hydrostratigraphic zone.

Picuris Formation (Tp)—The Picuris Formation represents the earliest alluvial deposition of sediments in the basin. This diverse package of sediments includes interlayered volcanic-sourced sandstones, conglomerates, cobble/boulder conglomerates, mudstones and siltstones, and a distinctive basal quartzite-boulder conglomerate. Everywhere in the basin, Picuris volcaniclastic sediments underlie and interfinger with Chama-El Rito alluvial deposits, and unconformably overlie either Pennsylvanian strata or Proterozoic crystalline rocks (Plate 2). Surface exposures of Picuris Formation sediments are only visible at the base of the Picuris Mountains along the first major basin-bounding faults (where they typically display significant fault damage) and in Miranda Canyon.

Few wells are completed in the Picuris Formation. Of the 20 such wells visited during this study, most are exploration wells in Miranda Canyon. Others are located on the west side of the community of Ponce de Leon and in the lower elevations of the Picuris Mountains. The wells range from 31 to 1,000 feet in depth. Several wells show poor yields or have been damaged by collapsed casings, and two were abandoned or undeveloped dry holes. Viable wells generally yield less than 5 gpm, but as little as 1 gpm (Tables 1 and 4). Significantly higher well yields of 23 to 50 gpm are documented in three wells with thin sand and gravel layers or a boulder conglomerate commonly encountered at the base of the formation. In the Ponce de Leon area, water from the Picuris Formation is typically warm and of poor quality.

Pennsylvanian and Proterozoic bedrock (Pu, Xmg, Xho)—At the mouth of the Rio Grande del Rancho canyon south of Talpa, Pennsylvanian sedimentary rocks that underlie the Picuris Formation west of the river yield water from intensely faulted and fractured sandstone and limestone layers. Two productive wells sited in these units record well yields of 20 gpm (TV-201 and TV-270, Tables 1and 4), but the water quality is poor. Most of the unfractured non-carbonate Pennsylvanian rocks in the Taos area are likely to have low permeability and porosity, low water production potential, and poor water quality.

Two Proterozoic bedrock units in the Picuris Mountains, the Miranda granite (Xmg) and the Ortega Formation quartzite (Xho), can provide significant volumes of water where these hard, crystalline rocks are strongly fractured. Such deformation is concentrated along the major north-south faults of the Picuris-Pecos fault zone and the northeast-trending faults of the Embudo fault zone at the base of the Picuris Mountains and across the Picuris piedmont; and particularly where faults of these two systems intersect (Figs. 7, 18 and 19). The two most probable areas of intense fracturing of Proterozoic rock in the study area are: 1) Ponce de Leon where the Miranda and southern Embudo faults intersect and deform the Miranda granite and Ortega Formation quartzite; and 2) the Picuris embayment where the Picuris-Pecos and Embudo faults intersect in the Ortega Formation quartzite. Eight wells were catalogued in these two areas during this study. Where rock fractures were noted on drill logs, wells yields were exceptionally high, 30–60 gpm (Tables 1 and 4). Where no fracturing was noted, well yields decreased to 0.5–25 gpm. Unfractured crystalline rocks have essentially zero porosity and do not yield water to wells.

Basin-bedrock hydrologic boundary and hydrogeologic windows

There is little evidence that groundwater moves freely from mountain bedrock aquifers, through the Picuris Formation, and into the shallow Santa Fe Group aquifer. A zone of reduced permeability at the base of the Picuris Mountains, associated with Embudo faulting in the basin fill and thick intervals of mudstone and siltstone in the Picuris Formation, appears to create a broad barrier to the direct movement of groundwater from the mountain block into the basin. Thus, we have defined a hydrologic discontinuity or groundwater barrier between bedrock and basin aquifers located along the trace of the southernmost strand of the basin-bounding Embudo fault zone (Figs. 7, 18, 19, 20). On the high Picuris piedmont west of Talpa, well data further constrain the hydrologic discontinuity near the edge of the basin beyond the southernmost, viable well in the basin-fill aquifer (Fig. 19, cross sections C-C' and D-D', wells TV-301 and TV-104; Fig. 20).

We also believe that areas of intensely fractured Proterozoic bedrock locally facilitate groundwater movement between bedrock and basin aquifers through hydrogeologic windows that connect water-bearing zones in fractured bedrock with those in Chama-El Rito alluvial sediments, Ojo Caliente Sandstone, and/or coarse intervals in the Picuris Formation, such as the basal conglomerate. One such locality is the Picuris embayment and adjoining Arroyo del Alamo structural block where fractured Ortega quartzite is adjacent to the Chama El Rito and Ojo Caliente Sandstone Members of the Tesuque Formation (Fig. 19, cross sections D-D' and E-E'). A second possible window located in the Ponce de Leon area is hydrologically more complex. At this

location surface movement of thermal, mineralized groundwater from Ponce de Leon spring clearly crosses the basin-bedrock boundary along Arroyo Miranda and infiltrates into Quaternary and Tertiary basin fill. Surface flow and infiltration of this deeply sourced water would mask the presence of subsurface groundwater that might also cross the boundary. Geochemical data, presented later in this report, addresses this question.

Picuris Piedmont Aquifer

A groundwater map of the Picuris piedmont aquifer, shown in Figure 21, provides basic information for understanding this complex groundwater system (see Table 5 for basin water-level data). Groundwater enters the study area from the large mountain watersheds to the east, southeast and south (Fig. 4). The water-table surface grades to the Rio Pueblo and the Rio Grande as elevations drop from 6,950 feet at the mouth of Miranda Canyon to under 6,100 feet near Taos Junction. Groundwater flow direction is generally westward toward the lower Rio Pueblo canyon, but varies locally where the groundwater surface is affected by stream interactions, stream incision, and changes in aquifer properties. Colored arrows in Figure 21B illustrate general groundwater flow direction beneath the Picuris piedmont (green arrows) and discharge to the Rio Grande del Rancho (purple arrows), the upper Rio Pueblo (orange arrows), and the lower Rio Pueblo (brown arrows). Converging flow lines delineate zones of groundwater discharge to streams. The groundwater map demonstrates that the lower Rio Pueblo, not the Rio Grande, is the primary discharge zone for the piedmont aquifer and exerts substantial control over groundwater movement. Incision of the Rio Pueblo downstream of the structurally-controlled nickpoint (which marks the change from a low-gradient meandering stream to a high-gradient stream in an incised canyon) lowers the interconnected water table and allows the stream to capture groundwater from most of the Picuris piedmont (Fig. 21, Fig. 19 cross section G-G'). The map also shows a small zone of artesian water levels near along the upper Rio Pueblo between Ranchito and the confluence with the Rio Grande del Rancho (referred to as the Ranchito artesian zone, Fig. 21).

There is no evidence of significant groundwater in shallow Chama-El Rito sediments (above 1,000 feet in depth) near the mountain front between Miranda Canyon and the Picuris-Pecos fault at the eastern boundary of Tierra Blanca. Unlike the Sangre de Cristo Mountains to the east, the Picuris Mountains contain no large, high-elevation watersheds with perennial streamflow. Indeed, this reach of the mountain front simply lacks a watershed (Fig. 4). Neither do geologic conditions exist to facilitate the subsurface movement of groundwater from the mountains into the piedmont aquifer. Thus, there is no significant source of mountain front recharge to replenish the Picuris piedmont aquifer along this part of its southern boundary. Two domestic test wells in the area resulted in one 860-foot dry hole in the Picuris Formation (TV-206), and a 1,100-foot well in the Chama-El Rito Member with first significant water below 1,000 feet (TV-301). This reach of the basin-bedrock hydrologic boundary is marked on Figure 21B as a "zone of no recharge". Water-table contours near this zone are oriented perpendicular to the mountain front. Based on geologic conditions, the authors further believe that the mountain front west of the Picuris embayment to Arroyo Hondo may also be a zone of no recharge.

In the Picuris embayment and Arroyo del Alamo structural block west of the Picuris-Pecos fault, conditions do exist to support both surface and subsurface movement of groundwater from the mountains into the piedmont aquifer. This hydrogeologic window funnels groundwater from fractured zones in the Ortega quartzite (TV-100) into thick, high-yield, basin-fill sediments (the Chama-El Rito and Ojo Caliente Sandstone Members) that extend at least to the center of the piedmont near NM-68. This very productive aquifer zone corresponds to a large depression in the water-table, which indicates it also gains groundwater from the adjacent aquifer to the east and west (Fig. 21A).

Perched groundwater

Groundwater elevations range considerably where the Picuris piedmont aquifer consists of basalts and interlayered sand, gravel, and clay. North of the basalt line where shallow wells draw groundwater from the Lama formation and layers of Servilleta Basalt, clay layers above and between basalt flows can perch water above, or vertically partition groundwater within, the Picuris piedmont aquifer. One such area of perched groundwater is located at the western end of the study area, near county road 570, where wells drilled in the basalts and sediments define a shallow water-table that lies more than 200 feet above groundwater in the underlying Chamita Formation. Lowering of the regional water table and down-faulting of basalts and sediments near the

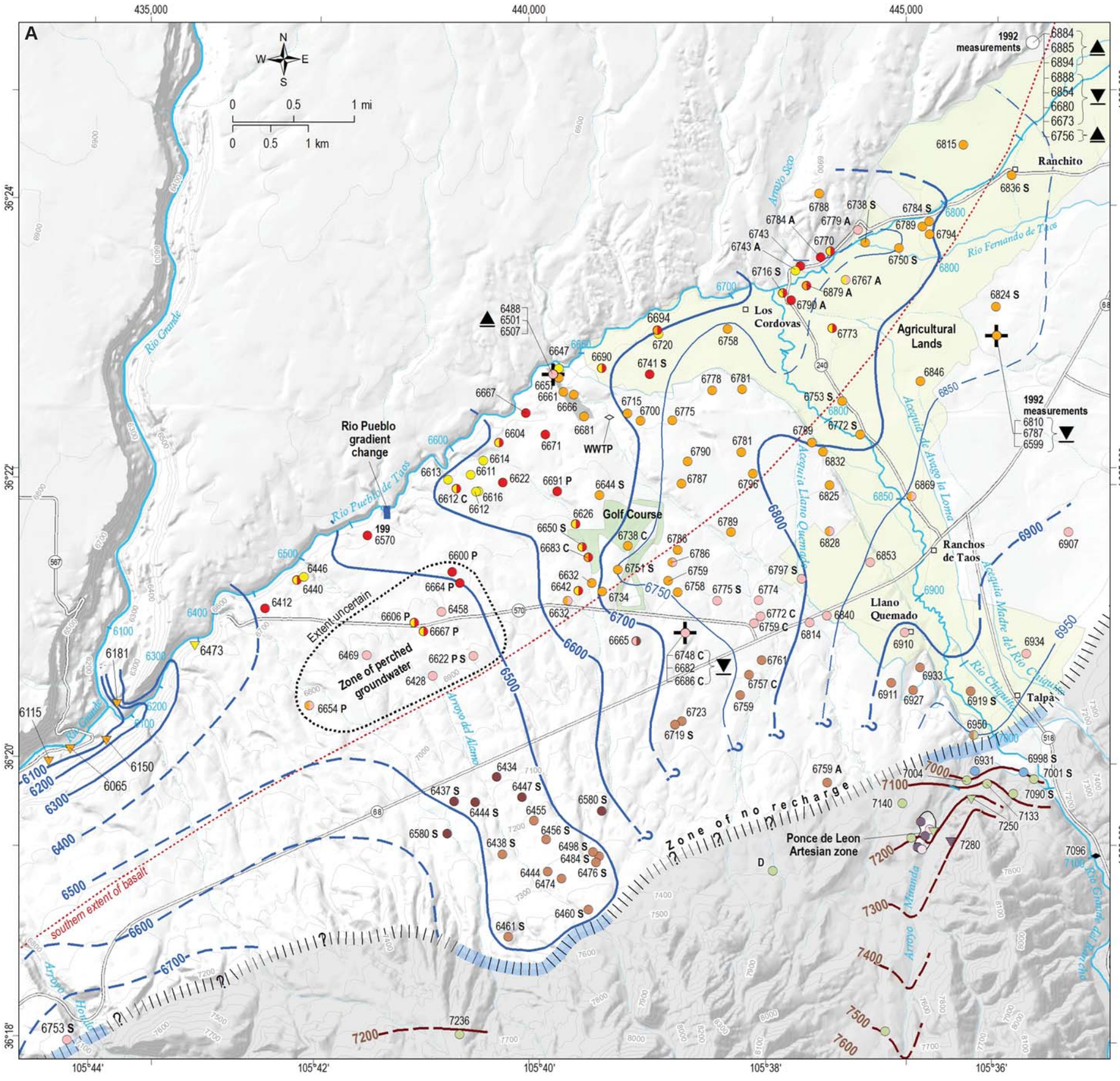

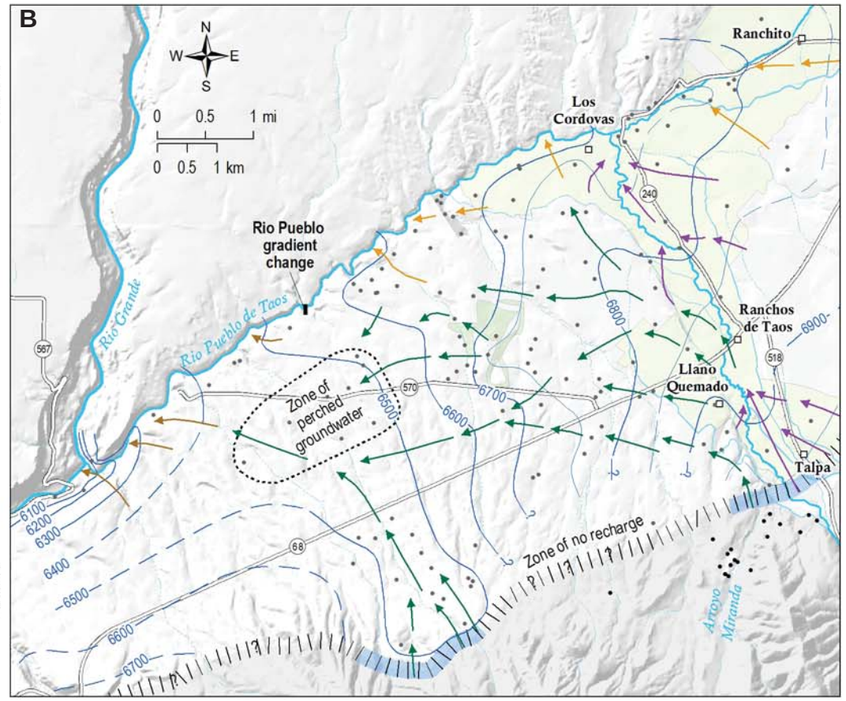

Data

- 6874 Control well or spring with water-level elevation
- A Artesian water level at or above land surface
- P Perched water level above regional aquifer
- S Driller's static water level
- D Dry well
- Depth-specific groundwater levels
- Effluent
- Stream
- Downward gradient
- Upward gradient

Geologic formation for well completion

- Lama formation ± Qal
- Lama fm. between Servilleta Basalt
- Servilleta Basalt
- Chamita Formation
- Chama El Rito Formation
- Ojo Caliente Formation
- Picuris Formation
- Pennsylvanian
- Proterozoic granite
- Proterozoic quartzite

Water-level elevation contour

Basin
- 100-ft contour interval, dashed where poorly constrained
- 50-ft contour interval

Bedrock (Figure 22)
- 100-ft contour interval dashed where poorly constrained

Horizontal groundwater flow direction

- Picuris piedmont
- Rio Grande del Rancho
- Upper Rio Pueblo
- Lower Rio Pueblo

Map Symbol

- 6700 Perennial stream channel elevation (feet asl)
- Topographic contour interval 100 feet
- ? Basin–Bedrock hydrologic discontinuity w/ hydrogeologic window in blue
- Irrigated lands derived from National Geospatial Data Asset (NGDA), National Agriculture Imagery Program (NAIP), Planned Acquisition Map 2009

Figure 21. Groundwater maps of the Picuris piedmont aquifer in the southern Taos Valley. A—Map of the unconfined water-table surface and related well control. The map was constructed from groundwater levels measured in spring 2011 and 2012, historic levels from existing sources, and spring elevations in the Rio Grande gorge (Table 5). Depth-specific water levels from four piezometer nests show vertical gradients between the shallow Picuris piedmont aquifer and the deep confined aquifer. B—Map showing groundwater flow lines.

Table 5. Water-level data for the Picuris piedmont aquifer (Fig. 21).—Continued

Site ID	Site type	Aquifer type	Water-level code	Date measured	Water depth (ft bls)	Water depth elevation (ft asl)	Data Source	Water depth elevation (ft asl)
TV-101	control	U	S	9/26/69	400.00	6753	Drilling record	7235
TV-102	well	U		4/9/2012	326.22	6723	NMBGMR	6753
TV-103	control	M		4/4/07	652.00	6434	Glorieta Geoscience, Inc., 2007b	6723
TV-104	control	U	S	10/7/97	980.00	6460	Drilling record	6434
TV-105	well	U		4/10/2012	155.82	6774	NMBGMR	6460
TV-106	control	U		6/3/96	878	6474	Turner Environmental Consultants, 1996	6774
TV-107	control	U		8/20/82	868.70	6444	Turner Environmental Consultants, 1996	6474
TV-108	well	U		4/9/2012	118.4	6613	NMBGMR	6444
TV-109	control	P	P S	9/13/86	290.00	6622	Drilling record	6613
TV-110	well	UF		4/9/2012	138.35	6622	NMBGMR	6622
TV-111	well	U		4/9/12	90.24	6853	NMBGMR	6622
TV-112	well	U		4/10/12	212.72	6761	NMBGMR	6853
TV-115	well	U		4/9/2012	455.46	6428	NMBGMR	6761
TV-116	control	Sc		5/29/08	72.98	6825	MJDarrconsult, Inc., 2008	6428
TV-117	well	U		3/13/11	145.48	6814	NMBGMR	6825
TV-118	well	U		4/10/2012	137.34	6840	NMBGMR	6814
TV-119	well	U		4/9/12	65.34	6787	NMBGMR	6840
TV-120	well	U		4/10/12	86.09	6933	NMBGMR	6787
TV-121	well	U	C	3/14/2012	119.99	6612	NMBGMR	6933
TV-122	well	U		4/10/2012	96.16	6786	NMBGMR	6612
TV-123	well	U		4/9/2012	135.34	6616	NMBGMR	6786
TV-124	well	U		4/9/2012	137.09	6612	NMBGMR	6616
TV-135	well	U		4/9/2012	29.21	6846	NMBGMR	6612
TV-136	well	U		4/10/2012	12.80	6720	NMBGMR	6846
TV-137	well	U		4/9/2012	8.64	6773	NMBGMR	6720
TV-138	well	U		4/10/12	36.19	6694	NMBGMR	6773
TV-139	well	P	P	4/9/2012	173.22	6667	NMBGMR	6694
TV-140	well	P	P	4/9/2012	190.99	6654	NMBGMR	6667
TV-142	well	U		4/9/2012	17.49	6869	NMBGMR	6654
TV-143	well	UF		4/9/2012	121.54	6604	NMBGMR	6869
TV-144	well	U		4/9/12	121.69	6788	NMBGMR	6604
TV-145	control	U	S	6/1/84	25.00	6738	Drilling record	6788
TV-146	control	U	S	5/26/05	52.85	6753	Drilling record	6738
TV-147	well	A	A	3/14/11	-140.00	6879	NMBGMR	6753
TV-148	control	U	S	9/12/10	40.00	6772	Drilling record	6879
TV-149	well	C		8/3/11	374.31	6469	NMBGMR	6772
TV-150	well	U		4/9/12	11.30	6794	NMBGMR	6469
TV-151	control	U	S	8/7/94	131.00	6738	Drilling record	6794
TV-152	well	C		4/9/2012	303.64	6665	NMBGMR	6738
TV-153	control	U		3/20/01	104.90	6828	Glorieta Geoscience, Inc., 2001	6665
TV-154	well	UF		4/9/2012	2.58	6758	NMBGMR	6828
TV-155	well	U		4/10/12	59.03	6690	NMBGMR	6758
TV-156	well	U	C	3/14/2012	175.18	6759	NMBGMR	6690
TV-157	well	U	C	3/14/2012	153.14	6772	NMBGMR	6759
TV-158	control	U	S	5/10/00	139.35	6751	Drilling record	6772
TV-159	well	PF	P	3/15/11	187.69	6600	NMBGMR	6751
TV-160	well	U		4/10/2012	108.86	6927	NMBGMR	6600
TV-161	well	U		4/9/12	76.22	6796	NMBGMR	6927
TV-162	well	U		4/9/2012	98.52	6789	NMBGMR	6796
TV-163	well	A	A	3/15/11	-59.00	6790	NMBGMR	6789
TV-164	well	UF		4/10/2012	18.64	6667	NMBGMR	6790

Table 5. Continued

Site ID	Site type	Aquifer type	Water-level code	Date measured	Water depth (ft bls)	Water depth elevation (ft asl)	Data Source	Water depth elevation (ft asl)
TV-165	well	UF		4/10/12	61.44	6671	NMBGMR	6667
TV-166	well	P	P	4/9/12	217.61	6606	NMBGMR	6671
TV-167	well	U	C	4/9/2012	242.32	6757	NMBGMR	6606
TV-168	well	U		4/9/2012	15.32	6743	NMBGMR	6757
TV-169	well	A	A	3/15/11	-1.00	6784	NMBGMR	6743
TV-173	well	U		4/9/12	121.44	6611	NMBGMR	6784
TV-174	well	U		4/9/12	14.70	6647	NMBGMR	6611
TV-176	control	U		12/9/10	19.90	6666	Town of Taos, written comm.	6647
TV-177	well	UF		4/9/2012	72.37	6681	NMBGMR	6666
TV-178	well	U		4/9/12	12.65	6657	NMBGMR	6681
TV-179	well	U		4/9/2012	60.88	6790	NMBGMR	6657
TV-180	well	Sc		4/9/12	271.68	6632	NMBGMR	6790
TV-181	well	U		4/9/2012	58.83	6789	NMBGMR	6632
TV-182	well	Sc		4/10/12	97.68	6910	NMBGMR	6789
TV-183	well	U		4/10/2012	146.36	6911	NMBGMR	6910
TV-185	well	A	A	4/9/2012	1.70	6743	NMBGMR	6911
TV-186	well	Sc		4/9/12	167.36	6734	NMBGMR	6743
TV-187	well	U		4/9/2012	25.08	6781	NMBGMR	6734
TV-188	well	U		4/9/2012	344.00	6458	NMBGMR	6781
TV-189	well	U	P	12/13/12	113.23	6691	NMBGMR	6458
TV-191	control	Sc	S	7/30/09	698.50	6447	Drilling record	6691
TV-192	well	Sc	C	3/14/2012	158.02	6683	NMBGMR	6447
TV-193	well	Sc		4/10/12	149.87	6758	NMBGMR	6683
TV-194	well	U		4/9/12	33.81	6778	NMBGMR	6758
TV-195	well	UF		4/9/2012	286.97	6412	NMBGMR	6778
TV-196	well	UF		3/14/2012	252.67	6440	NMBGMR	6412
TV-197	well	U		4/9/12	212.85	6446	NMBGMR	6440
TV-199	well	UF		4/9/2012	127.61	6570	NMBGMR	6446
TV-200	well	U		4/9/2012	74.11	6781	NMBGMR	6570
TV-208	well	U		4/9/12	26.80	6661	NMBGMR	6781
TV-218	well	U	C	3/14/12	210.80	6748	NMBGMR	6661
TV-219	well	M		2/8/12	265.80	6682	NMBGMR	6748
TV-217	well	M	C	3/14/12	273.43	6686	NMBGMR	6682
TV-223	well	U		4/11/12	20.30	6775	NMBGMR	6686
TV-224	well	U		4/10/2012	56.85	6715	NMBGMR	6775
TV-226	well	U		4/10/12	8.08	6832	NMBGMR	6715
TV-227	well	U		4/9/12	104.81	6614	NMBGMR	6832
TV-228	well	U		4/9/12	82.37	6700	NMBGMR	6614
TV-229	control	M	S	5/14/96	666.78	6437	Drilling record	6700
TV-231	well	PF	P	10/14/11	133.84	6664	NMBGMR	6437
TV-233	well	U		4/10/12	245.21	6642	NMBGMR	6664
TV-235	well	U		3/10/2012	72.44	6950	NMBGMR	6642
TV-237	control	Sc	S	12/23/97	1047.00	6461	Drilling record	6950
TV-238	control	U	S	8/23/97	10.00	6741	Drilling record	6461
TV-239	control	U	S	2/5/00	105.00	6786	Drilling record	6741
TV-240	well	C		6/12/12	31.50	6770	NMBGMR	6786
TV-241	control	U	S	9/10/00	845.00	6484	Drilling record	6770
TV-244	control	Sc	S	3/2/04	154.00	6797	Drilling record	6484
TV-246	well	U		6/19/12	262.91	6759	NMBGMR	6797
TV-249	well	U		10/13/12	13.60	6815	NMBGMR	6759
TV-250	well	U		6/12/12	9.01	6789	NMBGMR	6815

Table 5. Continued

Site ID	Site type	Aquifer type	Water-level code	Date measured	Water depth (ft bls)	Water depth elevation (ft asl)	Data Source	Water depth elevation (ft asl)
TV-252	control	Sc	S	10/21/02	873.00	6476	Drilling record	6789
TV-253	control	U	S	8/24/00	556.75	6580	Drilling record	6476
TV-254	well	U		6/28/12	125.68	6759	NMBGMR	6580
TV-255	control	UF	S	8/17/02	180.00	6650	Drilling record	6759
TV-256	well	U		6/28/12	177.18	6626	NMBGMR	6650
TV-257	control	U	S	10/8/04	140.00	6775	Drilling record	6626
TV-258	well	U		7/11/12	232.32	6632	NMBGMR	6775
TV-260	control	U	S	8/8/03	200.00	6644	Drilling record	6632
TV-264	control	U	S	9/18/02	50.00	6919	Drilling record	6644
TV-266	control	U	S	5/9/96	23.09	6824	Drilling record	6919
TV-267	well	U		1/11/13	119.80	6907	NMBGMR	6824
TV-268	well	U		1/11/13	145.18	6934	NMBGMR	6907
TV-273	control	C		6/3/08	63.89	6807	Glorieta Geoscience, Inc., 2002	6934
TV-274	control	C		6/3/08	86.68	6783	Glorieta Geoscience, Inc., 2002	6807
TV-275	control	M		6/3/08	236.56	6633	Glorieta Geoscience, Inc., 2002	6783
TV-276	control	C	A	5/5/10	-13.39	6767	Drilling record	6633
TV-277	control	U	S	3/29/03	766.00	6438	Drilling record	6767
TV-278	control	U	S	1/18/03	666.00	6444	Drilling record	6438
TV-280	control	UF	S	11/17/00	10.00	6716	Drilling record	6444
TV-281	well	C	A S	11/26/12	27.00	6750	Drilling record	6716
TV-282	control	U	S	10/5/93	10	6836	Drilling record	6750
TV-283	control	U	S	6/16/97	20	6784	Drilling record	6836
TV-285	control	U	S	6/14/96	670	6580	Drilling record	6784
TV-286	control	U	S	9/25/03	833	6498	Drilling record	6580
TV-287	control	U	S	6/12/07	340	6719	Drilling record	6498
TV-288	control	U	S	7/24/09	801	6456	Drilling record	6719
TV-289	control	Sc		8/3/09	762	6455	Drilling record	6456
TV-290	control	A	A	1/1/05	-4	6779	Glorieta Geoscience, Inc., written comm.	6455
TV-291	control	U		8/1/92	34.00	6884	Sorrel and Banet, 1993	6779
TV-292	control	C		8/1/92	164.75	6756	Sorrel and Banet, 1993	6884
TV-293	control	C		8/1/92	247.13	6673	Sorrel and Banet, 1993	6756
TV-294	control	C		8/1/92	239.81	6680	Sorrel and Banet, 1993	6673
TV-295	control	Sc		8/1/92	66.48	6854	Sorrel and Banet, 1993	6680
TV-296	control	Sc		8/1/92	32.37	6888	Sorrel and Banet, 1993	6854
TV-297	control	U		8/1/92	26.68	6894	Sorrel and Banet, 1993	6888
TV-298	control	U		8/1/92	34.84	6885	Sorrel and Banet, 1993	6894
TV-301	well	C	A	9/30/15	375.00	6759	NMBGMR	6885
TV-302	well	Sc		5/31/01	175.66	6488	Drakos et al., 2016	6759
TV-303	well	Sc		5/31/01	163.44	6501	Drakos et al., 2016	6488
TV-304	well	Sc		5/31/01	156.52	6507	Drakos et al., 2016	6501
TS-54	spring	M			0.00	6065		6507
TS-55	spring	P			0.00	6473		6065
TS-56	spring	U			0.00	6115		6473
TS-58	spring	U			0.00	6150		6115
TV-511	spring	U			0.00	6181		6150
TV-511	spring	U			0.00	6181		6181

bls—below land surface; asl—above sea level

Aquifer type: C—confined; U—unconfined; M—confined multiple aquifers; P—perched; F—fractured; Sc—semiconfined; A—artesian;
Water-level code: S—static water level from driller's record; P—perched aquifer; C—continuous measurements; A—artesian aquifer

Rio Pueblo confluence may locally strand and disconnect shallow groundwater in the basalts and sediments over deeper water-bearing zones in the Chamita Formation. Extensive withdrawals from the zone of perched groundwater should be avoided. The approximate extent of this perched groundwater is shown in Figure 21 and cross sections D-D', E-E' and F-F' in Figure 19.

Deep confined basin-fill aquifer

A deep, confined alluvial aquifer exists north of NM-68, where the Ojo Caliente Sandstone and the Chama-El Rito Members of the Tesuque Formation are faulted down into the basin to progressively greater depths (Fig. 19, cross sections A-A' through E-E'). Groundwater at these depths (1,000 to 3,200 feet) occurs under semi-confined to confined conditions created when relatively low permeability strata bound the water-bearing zones and contain the stored groundwater under pressures greater than atmospheric pressure. As a result, water levels in wells completed in the deep confined aquifer rise hundreds of feet above the top of the aquifer, typically to within 100–375 feet of land surface. In nested piezometers at BOR-1 and BOR-2 (Figs. 5 and 21, TV-273, TV-274, TV-275), where water levels can be measured at multiple depths in the aquifer, the vertical difference in water pressure creates a downward hydraulic gradient, indicating that conditions support the downward movement of water. In RP-2000 adjacent to the Rio Pueblo (Figs. 5 and 21, TV-302, TV-303, TV-304), the hydraulic gradient is vertically upward.

Miranda Canyon Bedrock Aquifers

A simplified groundwater map of Miranda Canyon and Ponce de Leon, shown in Figure 22, was developed from water-level measurements taken in 2011–2012, spring elevations, and measurements from unpublished reports and records (see Table 6 for water-level data). Miranda Canyon is a small dry watershed with no perennial surface water except for small seeps and springs. Groundwater in the canyon exists in discontinuous layers of coarse sediments in the Picuris Formation and in fracture zones in the Miranda granite, under confined or flowing artesian conditions. Test wells installed in 2005 generally revealed low yields. In at least two instances, well casings collapsed under the pressure of thick saturated clays in the Picuris Formation. Repeat water-level measurements taken over 18 months, in nine wells, for this study, exhibited negligible change during the measurement period or compared to 2005 levels. Based on the geologic conditions in the canyon and the hydrologic data collected, it is the opinion of the authors that there is not a viable water supply in Miranda Canyon to support development.

Miranda Canyon and Ponce de Leon are situated within the Miranda graben, an area bounded by the La Serna and Miranda faults. Severely deformed and fractured bedrock near the faults allows deep circulation and heating of meteoric water. The result is a small-scale hydrothermal system that recharges in upper Miranda Canyon near the top of the Picuris Mountains and discharges at Ponce de Leon. In this report, the system is referred to as the Ponce de Leon hydrothermal system. Based on the structural model (Fig. 18), we infer that the Miranda graben and its bounding faults also facilitate movement of thermal waters across the basin-bedrock boundary in the deep subsurface, and allow upward leakage of thermal water from basement rocks directly into basin-fill aquifers. Geochemical data collected during the study and discussed later in the report addresses this premise.

The community of Ponce de Leon at the bottom of the canyon relies on an artesian water supply from a small number of domestic wells tapping fractured zones in the Miranda granite or coarse layers in the Picuris Formation. Artesian waters are warm with a moderate to high dissolved mineral content. The high-discharge Ponce de Leon thermal springs, measured roughly at 66 gallons per minute, are located just east of the community at the intersection of the McGaffey, Miranda, and Embudo faults (Plate 1). Spring discharge flows into Miranda Creek and joins the Rio Grande del Rancho southwest of Talpa.

Groundwater Fluctuations

Water levels in most shallow, unconfined aquifers follow a natural, seasonal fluctuation, typically rising and falling in response to changes in precipitation, stream recharge, and evapotranspiration. The magnitude of seasonal fluctuations in water levels can also vary from year to year, or over multi-year cycles, in response to varying climatic conditions. Changes in groundwater recharge and storage caused by climate variability commonly occur over years to decades and groundwater levels generally have a delayed response to the cumulative effects of long-term drought (Taylor and Alley, 2001).

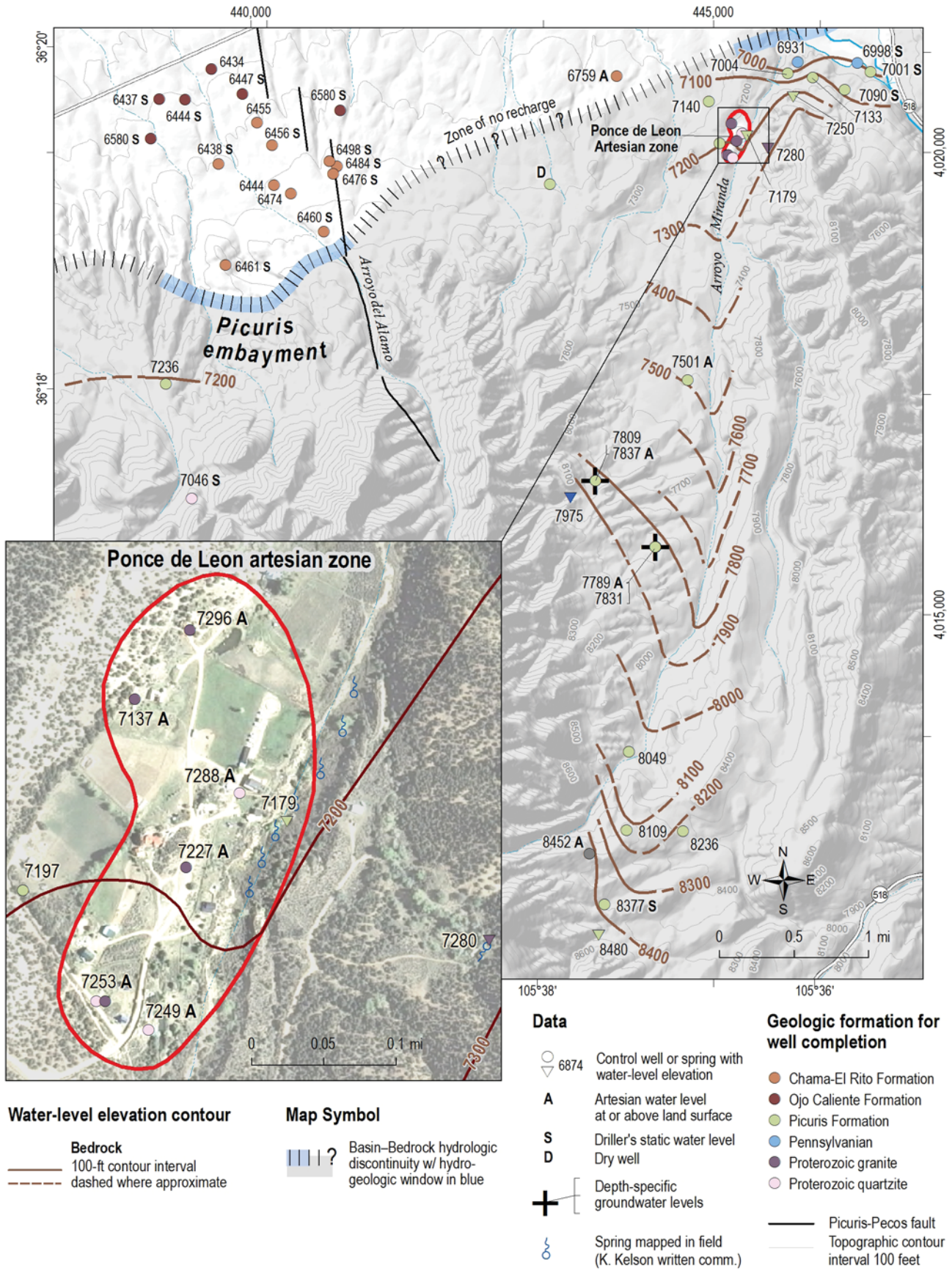

Figure 22. Simplified groundwater map of Miranda Canyon bedrock aquifers. Water-level data are presented in Table 6.

Table 6. Water-level data for the bedrock aquifer in Miranda Canyon (Fig. 22).

Site ID	Surface elevation (ft asl)	Site type	Aquifer type*	Water-level code	Date measured	Water depth (ft bls)	Water depth elevation (ft asl)	Data Source
TV-125	7214	well	FA	A	3/13/11	-74.00	7288	NMBGMR
TV-126	7204	well	FA	A	4/9/11	-92.00	7296	NMBGMR
TV-127	7205	well	FA	A	4/10/12	69.21	7137	NMBGMR
TV-128	7242	well	M		4/10/2012	44.74	7197	NMBGMR
TV-129	7227	well	FA	A	4/9/11	0.00	7227	NMBGMR
TV-132	7252	well	FA	A	4/9/11	0.00	7253	NMBGMR
TV-133	7252	well	FA	A	4/9/11	0.00	7253	NMBGMR
TV-134	7248	well	FA	A	4/9/11	0.00	7249	NMBGMR
TV-201	7134	well	C		4/10/12	203.12	6931	NMBGMR
TV-205	7182	well	U		4/10/2012	42.47	7140	NMBGMR
TV-206	7296	control	D	D	4/21/10	>860	<6436	NMBGMR
TV-207	7178	well	C		4/10/2012	44.50	7133	NMBGMR
TV-209	7500	well	A	A	4/22/11	-1.00	7501	NMBGMR
TV-210	7853	well	A	A	3/10/12	15.51	7838	NMBGMR
TV-211	7840	well	A	A	4/22/11	50.83	7789	NMBGMR
TV-212	8365	well	C		4/22/11	128.66	8236	NMBGMR
TV-213	8492	control	C	S	10/24/05	114.60	8377	Drilling record
TV-214	8531	control	C		9/12/05	422.20	8109	John Shomaker & Assoc., Inc., 2008
TV-215	8666	control	FA	A	9/8/05	214.01	8452	John Shomaker & Assoc., Inc., 2008
TV-216	8120	well	C		3/10/2012	71.32	8049	NMBGMR
TV-221	7840	well	U		3/10/2012	9.09	7831	NMBGMR
TV-222	7853	well	C		11/9/12	43.89	7809	NMBGMR
TV-234	7139	well	C		3/10/2012	135.21	7004	NMBGMR
TV-265	7061	control	U	S		53.00	7001	TSWCD, written comm.
TV-269	7150	control	U	S	11/16/89	60.00	7090	Drilling record
TV-270	7058	control	C	S	11/25/97	60.00	6998	Drilling record
TV-501	8480	spring					8480	
TV-502	7975	spring					7975	
TV-503	7280	spring					7280	
TV-504	7179	spring					7179	
TV-509	7250	spring					7250	

bls—below land surface; asl—above sea level; TSWCD—Taos Soil and Water Conservation District;
Aquifer type: F—fractured; A—artesian; M—confined multiple aquifers; C—confined; U—unconfined; D—dry
Water-level code: A—artesian aquifer; D—dry; S—static water level from driller's record

Fluctuations in groundwater levels reflect the continuous balance between recharge to, storage in, and discharge from an aquifer. Changes in groundwater recharge or discharge over time result in fluctuations of the water-table surface that are documented by repeatedly measuring groundwater levels at the same locations. In the southern Taos Valley, we studied seasonal, annual, and short-term changes in water levels in the shallow Picuris piedmont aquifer. Results are shown on Figures 23–25, in Tables 7 and 8, and are discussed below.

Seasonal water-level fluctuations

Seasonal groundwater fluctuations were first evaluated using repeat water-level measurements in 29 shallow wells between winter and summer seasons of 2011 and 2012.The dominant seasonal trend shows high summer groundwater levels (early June 2012) and low winter levels (December 2012) along the Rio Grande del Rancho and the Rio Pueblo within acequia-irrigated agricultural lands (Fig. 23). Water levels rose between December 2011 and June 2012

by +0.66 to +11.59 feet, followed by a decline of -1.10 to –16.78 feet in December 2012 (Table 7, wells TV-135, TV-136, TV-137, TV-142, TV-168, TV-181, TV-185, TV-187, TV-200). Large seasonal variations in water level characterized by a rise in late spring to early summer demonstrate an interconnection between the shallow aquifer and streams, acequias and irrigation that generate aquifer recharge. Hydrographs of multiyear water-level changes provide a more detailed view of seasonal fluctuations and are discussed further below.

A persistent decline in water levels ranging from -0.47 to -2.52 feet, which overrode seasonal fluctuations, occurred in wells clustered near the intersection of county road 570 and NM-68 (TV-122, TV-156, TV-157, and TV-162). This declining trend is more evident in, and better defined by, short-term year-to-year fluctuations and hydrographs, which are discussed below. All other wells had negligible seasonal water-level fluctuations of less than ±0.4 feet.

Annual and short-term water-level fluctuations

Water-level records covering months to years are important for monitoring the effects of: 1) natural variability in precipitation and recharge; and 2) trends in groundwater storage and depletion (Taylor and Alley, 2001; Konikow, 2015). Annual changes in the water table in the southern Taos Valley were evaluated by comparing water levels from 54 shallow wells measured in 2011with repeat measurements in the same wells during a similar period in 2012. Results show a widespread annual drop in water levels throughout the northern portion of the study area (Fig. 24A, Table 8). Water levels declined in most wells (83%), with large drops of over one foot clustered south of Los Cordovas. Annual declines ranged from -0.04 to -2.6 feet overall and averaged -0.7 feet (fluctuations less than about ±0.4 feet are considered negligible). Because short-term local to regional water-table declines may be caused by natural

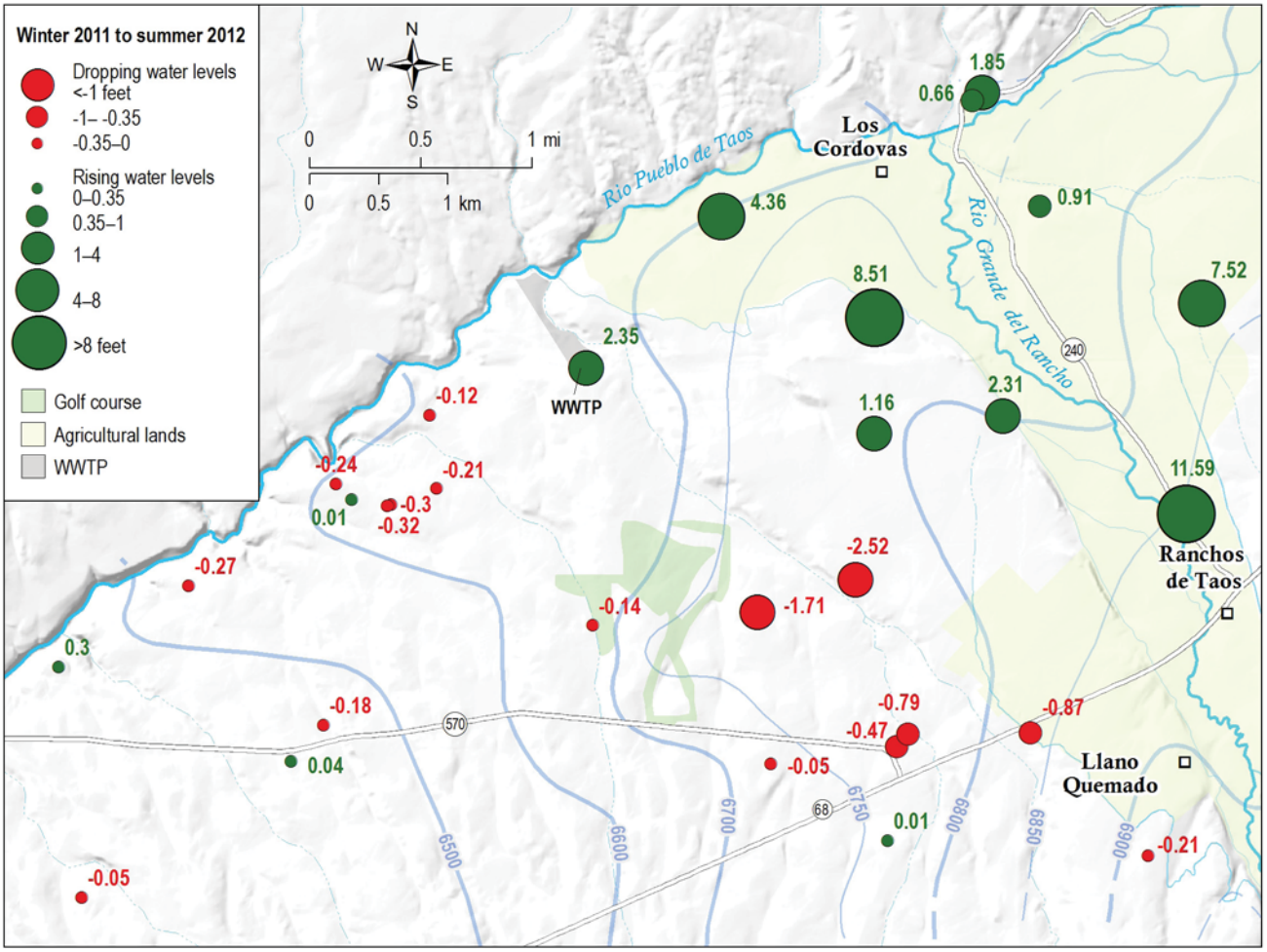

Figure 23. Seasonal changes in groundwater levels in the Picuris piedmont aquifer from winter 2011 to summer 2012. Water-level data are shown in Table 7.

Table 7. Data for seasonal changes in groundwater levels, winter 2011 to summer 2012, in the Picuris piedmont aquifer (Fig. 23).

	WINTER 2011		SUMMER 2012			WINTER 2012		
Site ID	Date measured	Depth to water (ft bls)	Date measured	Depth to water (ft bls)	Change in depth (ft) winter–summer	Date measured	Depth to water (ft bls)	Change in depth (ft) summer–winter
TV-108	12/14/2011	118.43	6/5/2012	118.67	-0.24	12/12/2012	118.75	-0.08
TV-110	12/14/2011	138.27	6/5/2012	138.48	-0.21	12/12/2012	138.53	-0.05
TV-118	12/15/2011	134.94	6/5/2012	135.81	-0.87	12/13/2012	135.46	0.35
TV-121	12/16/2011	120.00	6/6/2012	119.99	0.01	11/30/2012	120.28	-0.29
TV-122	12/15/2011	95.24	6/5/2012	96.95	-1.71	12/13/2012	97.11	-0.16
TV-123	12/13/2011	135.22	6/5/2012	135.52	-0.30	12/15/2012	135.49	0.03
TV-124	12/13/2011	136.98	6/5/2012	137.30	-0.32	12/15/2012	137.24	0.06
TV-135	12/13/2011	32.94	6/6/2012	25.42	7.52	12/13/2012	35.49	-10.07
TV-136	12/13/2011	13.99	6/6/2012	9.63	4.36	12/13/2012	14.12	-4.49
TV-137	12/13/2011	8.95	6/6/2012	8.04	0.91	12/13/2012	9.61	-1.57
TV-139	12/12/2011	173.18	6/5/2012	173.14	0.04	12/14/2012	173.01	0.13
TV-140	12/13/2011	190.87	6/6/2012	190.92	-0.05	12/12/2012	190.88	0.04
TV-142	12/13/2011	24.69	6/6/2012	13.10	11.59	12/13/2012	29.88	-16.78
TV-143	12/14/2011	121.45	6/5/2012	121.57	-0.12	12/12/2012	121.73	-0.16
TV-156	12/14/2011	174.57	6/5/2012	175.04	-0.47	11/30/2012	175.35	-0.31
TV-157	12/14/2011	152.65	6/5/2012	153.44	-0.79	11/30/2012	153.94	-0.50
TV-162	12/13/2011	96.88	6/5/2012	99.40	-2.52	12/13/2012	100.70	-1.30
TV-167	12/16/2011	242.21	6/5/2012	242.20	0.01	11/30/2012	242.33	-0.13
TV-168	12/13/2011	17.40	6/5/2012	15.55	1.85	12/12/2012	16.65	-1.10
TV-177	12/14/2011	72.53	6/5/2012	70.18	2.35	12/17/2012	72.71	-2.53
TV-181	12/13/2011	60.91	6/6/2012	58.60	2.31	12/13/2012	61.55	-2.95
TV-183	12/14/2011	146.02	6/5/2012	146.23	-0.21	12/13/2012	146.26	-0.03
TV-185	12/13/2011	6.12	6/5/2012	5.46	0.66	12/12/2012	5.26	0.20
TV-187	12/13/2011	30.01	6/5/2012	21.50	8.51	12/13/2012	31.30	-9.80
TV-188	12/12/2011	343.86	6/5/2012	344.04	-0.18	12/14/2012	343.66	0.38
TV-192	12/16/2011	158.05	6/5/2012	158.19	-0.14	11/30/2012	158.28	-0.09
TV-196	12/16/2011	252.78	6/6/2012	252.48	0.30	11/30/2012	252.57	-0.09
TV-199	12/13/2011	127.66	6/4/2012	127.93	-0.27	12/14/2012	127.79	0.14
TV-200	12/13/2011	73.78	6/5/2012	72.62	1.16	12/13/2012	75.86	-3.24
TV-218	12/15/2011	212.29	6/5/2012	212.34	-0.05	11/30/2012	212.75	-0.41

bls—below land surface

variability in precipitation and recharge over months to years (Konikow, 2015), thirteen of the wells were remeasured in October 2015 in the area of observed 2012 declines to reassess the annual trend. Results indicate that in all but two wells the annual declining trend persisted, with four-year declines being double or triple the 2012 observations (Fig. 24B, Table 8). Within the zone of declining water levels identified in Figure 24A, the total water-level drop between March-April 2011 and October 2015 ranged from -1.19 to -6.28 feet. The zone of decline lies within a fault-bounded area that coincides with the northern projection of the Miranda graben. The Los Cordovas faults that correspond with the La Serna and Miranda basement faults (Fig. 18), and the northern projection of the graben, are likely barriers or partial barriers to horizontal groundwater flow, focus and intensify the effects of pumping, and contribute to the severe water-level declines.

Water-level changes and hydrographs

Changes in groundwater levels reflect the movement of water through the aquifer in response to recharge and discharge, both natural and human-related. Interactions between the shallow aquifer and streams, acequias, irrigation, surface-water ponding, wet and dry climate cycles, and groundwater pumping generate fluctuations in the water-table surface. Deep-aquifer hydraulic pressures are far removed from surface processes, but are highly sensitive to deep withdrawals of groundwater. To better understand the hydromechanics of the Picuris piedmont aquifer we examined hydrographs (graphs that show the

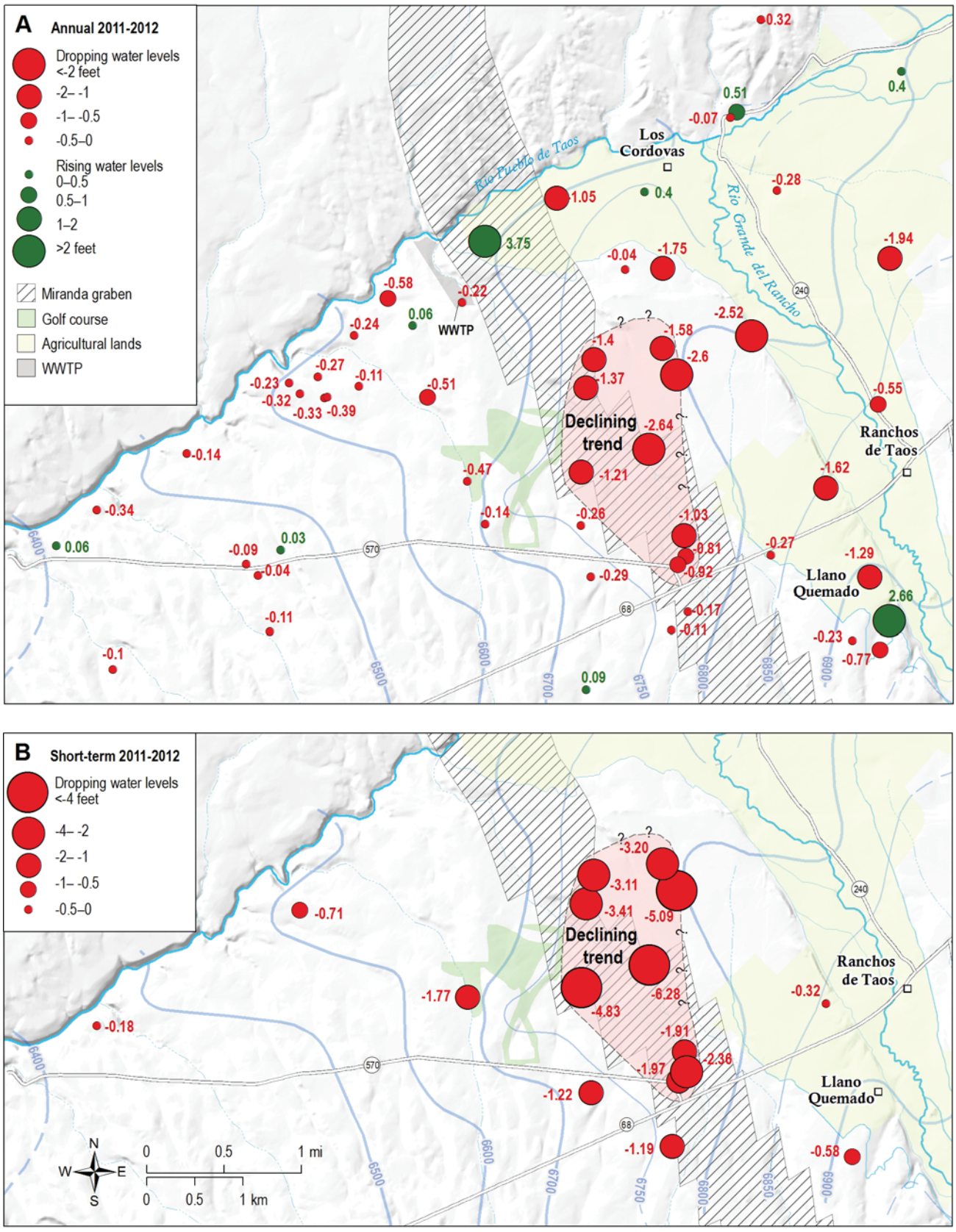

Figure 24. Changes in groundwater levels in the Picuris piedmont aquifer. A—Annual changes from 2011 to 2012. B—Short-term changes from 2011 to 2014–2015. A zone of progressive water-level decline was identified in a cluster of wells south of Los Cordovas. The Miranda graben (from Fig. 18) and the water-table surface (from Fig. 21) are shown in the background. Water-level data are located in Table 8 and Appendix 2.

Table 8. Data for annual and short-term changes in groundwater levels in the Picuris piedmont aquifer (see Figs. 24A-B and 25).

		FIRST WATER LEVEL MEASUREMENT			ANNUAL CHANGE, FIGURE 24A (SPRING 2011 TO SPRING 2012)				SHORT-TERM CHANGE FIGURE 24B (2011 TO 2014– 2015)			
Site ID	Aquifer zone	Date measured	Water depth (ft bls)	Water depth elevation (ft asl)	Date measured	Water depth (ft bls)	Water depth elevation (ft asl)	Delta WL1	3rdDate	DTW3	3rdWL Elev	Delta WL2 [wl1 - wl3]
TV-102	Ttc	3/12/2011	326.15	6722.97	2/9/12	326.06	6723.06	0.09				
TV-105	Tc	3/12/2011	154.79	6774.78	4/10/2012	155.82	6773.75	-1.03	10/6/15	156.7	6772.87	-1.91
TV-108	QTlb	3/13/2011	118.42	6612.62	2/8/12	118.65	6612.39	-0.23				
TV-110	Tsb	3/13/2011	138.37	6621.94	2/8/12	138.48	6621.83	-0.11				
TV-111	Tc	3/13/2011	88.62	6854.52	4/9/2012	90.24	6852.90	-1.62	10/6/15	88.94	6854.20	-0.32
TV-112	Ttc	3/13/2011	212.55	6761.42	4/10/2012	212.72	6761.25	-0.17				
TV-115	Tc	3/13/2011	455.17	6427.81	2/9/12	455.28	6427.70	-0.11				
TV-118	Tc	3/13/2011	135.18	6842.49	2/8/12	135.45	6842.22	-0.27				
TV-119	QTl	3/13/2011	63.97	6788.25	4/9/2012	65.34	6786.88	-1.37	10/7/15	67.38	6784.84	-3.41
TV-120	Ttc	3/13/2011	88.75	6930.77	4/10/2012	86.09	6933.43	2.66				
TV-121	QTlb, Tsb	3/13/2011	119.67	6611.83	3/14/12	119.99	6611.51	-0.32	12/8/14	120.38	6611.12	-0.71
TV-122	QTl	3/13/2011	94.27	6787.83	2/7/12	95.48	6786.60	-1.21	10/6/15	99.10	6783.00	-4.83
TV-123	QTlb	3/13/2011	135.03	6616.77	2/8/12	135.42	6616.38	-0.39				
TV-124	QTlb	3/13/2011	136.85	6611.86	2/8/12	137.18	6611.53	-0.33				
TV-135	QTl	3/14/2011	32.46	6842.64	2/9/12	34.40	6840.70	-1.94				
TV-136	QTlb	3/14/2011	13.58	6719.29	2/9/12	14.63	6718.24	-1.05				
TV-137	QTlb, Tsb	3/14/2011	8.42	6773.03	2/9/12	8.70	6772.75	-0.28				
TV-139	QTlb, Tsb	3/14/2011	173.20	6666.59	2/7/12	173.24	6666.55	-0.04				
TV-140	QTl, Tc	3/14/2011	190.96	6653.72	2/8/12	191.06	6653.62	-0.10				
TV-142	QTl, Tc	3/14/2011	27.12	6859.32	2/9/12	27.67	6858.77	-0.55				
TV-143	QTlb, Tsb	3/14/2011	121.39	6604.53	2/8/12	121.63	6604.29	-0.24				
TV-144	QTl	3/14/2011	121.37	6788.24	4/9/2012	121.69	6787.92	-0.32				
TV-150	QTl	3/14/2011	11.70	6793.92	4/9/2012	11.30	6794.32	0.40				
TV-154	QTl	3/15/2011	11.37	6748.84	2/9/12	12.27	6747.94	0.40				
TV-155	QTlb, Tsb	3/15/2011	62.78	6685.94	4/10/2012	59.03	6689.69	3.75				
TV-156	Tc	3/15/2011	174.26	6759.59	3/14/12	175.18	6758.67	-0.92	10/6/15	176.23	6757.62	-1.97
TV-157	Tc	3/15/2011	152.33	6773.03	3/14/12	153.14	6772.22	-0.81	8/26/15	154.69	6770.67	-2.36
TV-160	Ttc	3/15/2011	109.16	6926.92	2/7/12	109.93	6926.15	-0.77				
TV-161	QTl	3/15/2011	73.62	6798.49	4/9/2012	76.22	6795.89	-2.60	10/6/15	78.71	6793.40	-5.09
TV-162	QTl	3/15/11	95.02	6792.26	2/8/12	97.66	6786.58	-2.64	10/7/15	101.30	6785.98	-6.28
TV-164	Tsb	12/14/11	18.26	6666.51	12/12/2012	18.84	6666.65	-0.58				
TV-165	Tsb	3/15/2011	61.50	6670.87	4/10/2012	61.44	6670.93	0.06				
TV-166	QTlb, Tsb	3/15/2011	217.52	6605.66	4/9/2012	217.61	6605.57	-0.09				
TV-167	Ttc	3/15/2011	242.03	6757.62	3/14/12	242.14	6756.51	-0.11	10/6/15	243.22	6756.43	-1.19
TV-168	Tsb	3/15/2011	17.85	6740.89	2/8/12	17.34	6741.40	0.51				
TV-173	QTlb	3/15/2011	121.17	6611.04	4/9/2012	121.44	6610.77	-0.27				
TV-177	QTl	3/15/2011	72.51	6680.73	2/8/12	72.73	6680.51	-0.22				
TV-179	QTl	3/16/2011	59.48	6790.90	4/9/2012	60.88	6789.50	-1.40	10/6/15	62.59	6787.79	-3.11
TV-181	QTl	3/16/2011	59.72	6787.82	2/9/12	62.24	6785.30	-2.52				
TV-182	Tc	3/16/2011	96.39	6911.73	4/10/2012	97.68	6910.44	-1.29	10/7/15	96.35	6911.77	0.04
TV-183	Ttc	3/16/2011	145.65	6911.37	2/7/12	145.88	6911.14	-0.23	10/6/15	146.23	6910.79	-0.58
TV-185	QTlb	3/16/2011	6.07	6738.99	2/8/12	6.14	6738.92	-0.07				
TV-186	QTL	3/16/2011	167.22	6733.80	4/9/2012	167.36	6733.66	-0.14				
TV-187	QTL	3/16/2011	29.91	6776.22	2/8/12	31.66	6774.47	-1.75				
TV-188	Tc	3/16/2011	343.93	6457.85	2/9/12	343.90	6457.88	0.03				
TV-189	Tsb	4/9/11	112.68	6691.38	2/8/12	113.19	6690.87	-0.51				
TV-192	QTl, Tsb	4/20/11	157.55	6683.71	3/14/12	158.02	6683.24	-0.47	9/5/13	159.32	6681.94	-1.77
TV-193	QTL	4/21/2011	149.61	6758.64	4/10/2012	149.87	6758.38	-0.26				
TV-194	QTL	4/21/2011	33.77	6777.79	4/9/2012	33.81	6777.75	-0.04				
TV-195	Tsb	4/21/2011	287.03	6411.62	4/9/2012	286.97	6411.68	0.06				
TV-196	QTlb, Tsb	4/21/2011	252.33	6440.21	3/14/12	252.67	6439.87	-0.34	3/3/14	252.51	6440.03	-0.18
TV-199	Tsb	4/21/2011	127.59	6570.39	2/7/12	127.73	6570.25	-0.14				
TV-200	QTL	4/21/2011	72.53	6782.66	4/9/12	74.11	6781.08	-1.58	10/6/15	75.73	6779.46	-3.20
TV-218	Tc	6/2/11	212.05	6747.00	6/5/12	212.34	6746.71	-0.29	9/6/13	213.27	6745.78	-1.22

bls—below land surface; asl—above sea level

Aquifer type: C–confined; U–unconfined; M–confined multiple aquifers; P–perched; F–fractured; Sc–semiconfined; A–artesian;
Water-level code: S–static water level from driller's record; P–perched aquifer; C–continuous measurements; A–artesian aquifer

change in groundwater levels over time) from wells that we measured bimonthly and with continuous water-level recorders from March 2011 to December 2012, and in some cases as late as October 2015. These records show four distinct water-level trends: 1) seasonal fluctuations related to recharge from streams, acequias, and flood irrigation adjacent to the Rio Grande del Rancho and upper Rio Pueblo; 2) seasonal fluctuations related to stream-aquifer interactions near the lower Rio Pueblo; 3) progressive water-level declines south of Los Cordovas; and 4) static water levels with no significant change. Each water-level trend is discussed below and shown in Figure 25. Supplemental hydrographs and data are located in Appendix 2.

Recharge from streams and acequias—The cycle of snowmelt and stream runoff, acequia diversions, and flood irrigation in the southern Taos Valley begins each year in late spring and ends in early fall. Seasonal fluctuations in the surface-water system generate a similar pattern in shallow groundwater levels that is simultaneous or lags in time behind peak discharge, depending on how closely linked the aquifer is with the surface water system. Wells that demonstrate stream- and acequia-connected recharge are located near the Rio Grande del Rancho, the upper Rio Pueblo de Taos, or an associated acequia (Fig. 25 and Appendix 2.1). Shallow wells less than 125 feet depth that are close to a stream or acequia show rapid water-level fluctuations greater than six feet (TV-135, TV-142, TV-154, TV-160 and TV-187). Wells greater than 120 feet depth, located further from the recharge source, generally show more gradual water-level fluctuations of less than six feet that may display a slight time lag (TV-118, TV-136, TV-137, TV-181, TV-183 and TV-185).

Stream-aquifer interactions—Seasonal or more erratic changes in stream stage in the lower Rio Pueblo can generate similar low-amplitude changes in groundwater level in wells adjacent to the Rio Pueblo canyon. A good example is illustrated by the continuous groundwater hydrograph for well TV-121, sited about 900 feet south-southeast of the Rio Pueblo in the Servilleta Basalt and interlayered sediments (Fig. 25). The TV-121 hydrograph captures the shape of a stream hydrograph, with spring peaks in May-June 2014 and 2015 and diminished or absent spring peaks in the preceding drought years of 2012 and 2013. The maximum seasonal change recorded from September 2014 to June 2015 was 2.05 feet. Supplemental groundwater hydrographs with bimonthly measurements (Appendix 2.2) show less regular fluctuations with lower amplitudes of about 0.5 to 0.8 feet.

Water-level declines—A zone of declining groundwater levels was identified in a cluster of wells between Los Cordovas and NM-68, within the northern projection of the Miranda graben (Figs. 24A, B). In the center of the zone of decline, water levels dropped by 1.4 to 2.6 feet from 2011 to 2012. Similar annual declines are commonly associated with severe drought, but when a number of active wells are concentrated in a small area it is unclear whether the decline is linked to drought or to local groundwater withdrawal. To further evaluate the water-level declines wells in and around the decline zone were remeasured in October 2015. Results varied and showed that water levels: 1) continued to decline at a reduced rate even though the drought diminished in late 2013 and a wet climate prevailed through fall of 2015 (wells TV-122 and TV-162); 2) remained stable at the December 2012 level (wells TV-179, TV-200 and TV-156); or 3) recovered slightly in late 2014 then remained stable (TV-157). Over the three- to four-year period from 2011 to 2014–2015, water levels in the center of the decline dropped by 3.1 to 6.3 feet and wells beyond the zone to the south and west (TV-167, TV-218, and TV-192) declined by 1.2 to 1.8 feet, suggesting a possible expansion of the decline zone (Figs. 24B and 25, Appendix 2.3). It is possible that water-level declines were initially linked to drought, but the aquifer failed to recover in following years. The zone of decline lies within a fault-bounded area that coincides with the northern projection of the Miranda graben. The Los Cordovas faults that correspond with the La Serna and Miranda basement faults (Fig.18), and the northern projection of the graben, are likely barriers or partial barriers to horizontal groundwater flow, focus and intensify the effects of pumping, and contribute to the severe water-level declines.

Static trend—Wells located far from sources of recharge or significant groundwater pumping tend to show minimal water-level changes over time. One area where measurements were taken—the lower Rio Pueblo neighborhood west of the golf course—showed no significant change in water levels. In wells completed in the Lama formation above and between Servilleta basalt flows and the Chamita Formation beneath the basalts, water levels were essentially static. Water-level fluctuations in these units are

Figure 25. Groundwater hydrographs for select wells in the southern Taos Valley illustrate four trends in water-level changes: 1) seasonal fluctuations near streams in irrigated lands; 2) seasonal fluctuations near the lower Rio Pueblo; 3) progressive decline; and 4) no change. Hydrographs with continuous daily measurements (TV-121, TV-157, TV-192) display water levels as a three-day moving mean. Supplemental hydrographs and groundwater data are located in Appendix 2. bls—below land surface.

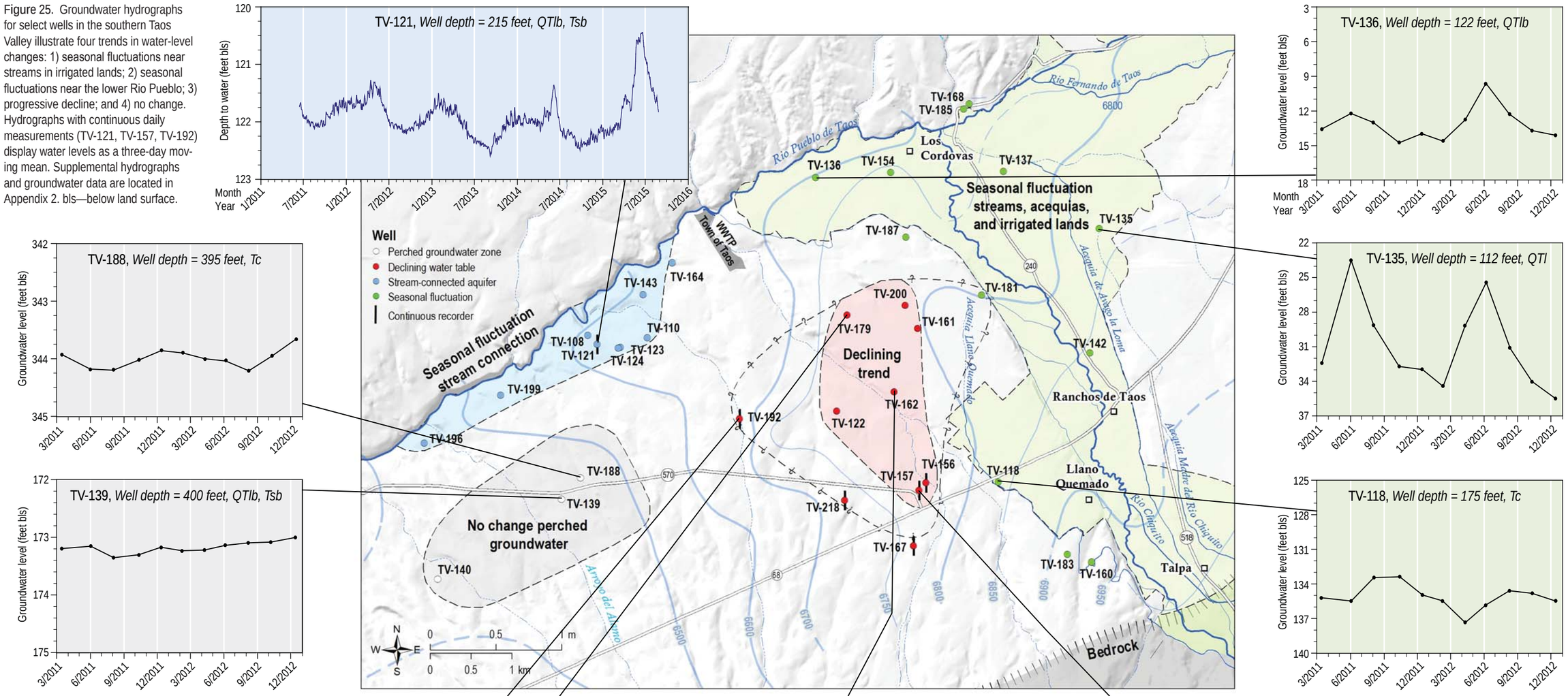

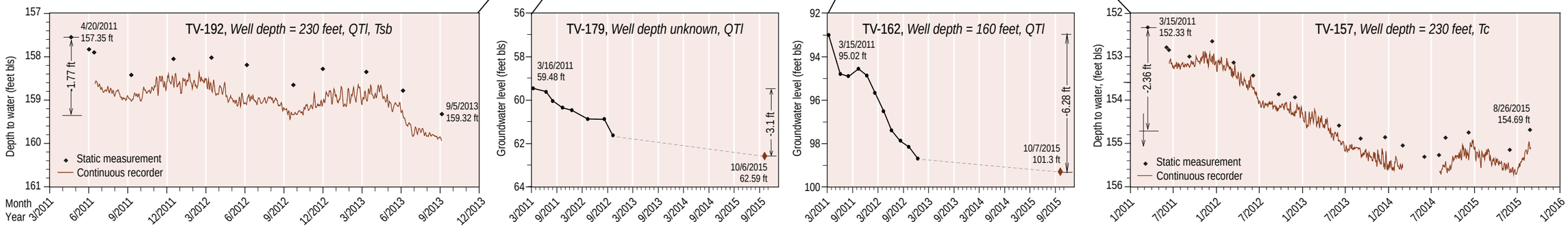

within about ±0.4 feet and are considered to be negligible. A hydrograph for well TV-140 located in the zone of perched water is representative of a static trend (Appendix 2.4).

Drought versus depletion

There are several potential reasons for the local water-table declines south of Los Cordovas, including: 1) drought conditions that prevailed statewide from 2008 through 2014 (Chermak et al., 2015); 2) local groundwater pumping that may have intensified because of drought conditions; or 3) a combination of drought and overexploitation of groundwater resources. Geologic barriers to groundwater movement such as faults in unconsolidated basin fill and low permeability strata often intensify local water-table drawdown; such barriers are known to exist in the Los Cordovas area (unpublished consultant report, Glorieta Geoscience, Inc.). In order to unequivocally demonstrate an anthropogenic link to declining water tables, one must establish a long-term trend of depletion over periods of multiple decades and climate cycles (Konikow, 2015). This level of observation and documentation has not been achieved for the southern Taos Valley, so the cause of declining water levels is not certain. However because the declines are substantial, are well defined within a small dense monitoring network, and persisted beyond the end of drought conditions, it is likely that local groundwater pumping is contributing to the water-table decline. Consequently, the area of aquifer decline south of Los Cordovas should receive continued annual or biannual monitoring. Where early recognition of overdevelopment leads to comprehensive monitoring (and the results indicate continued declines are a direct consequence of depletion) then the public awareness and knowledge can more effectively move communities, local government, and water-resource administrators to mitigate the depletion.

Summary of Hydrogeologic Systems

Information on the hydrostratigraphy, well yields, faults that create hydrologic boundaries and windows, water levels, and groundwater fluctuations and declines advances our understanding of the aquifers in the southern Taos Valley. The significant characteristics of the area's groundwater hydrology relevant to water planning and conservation are summarized here.

1. **Hydrostratigraphy (aquifer zones)—**The hydrostratigraphy of the study area is divided into alluvial sediments and basalt flows of the Santa Fe Group basin fill and Pennsylvanian/Proterozoic bedrock, separated by sediments of the Picuris Formation. The Picuris piedmont aquifer is in the Santa Fe Group and includes five hydrostratigraphic units: 1) Lama formation (QTl); 2) Servilleta Basalt and thinly interlayered sediments of the Lama formation (Tsb and QTlb); 3) Chamita Formation (Tc),which lies below the oldest Servilleta Basalt; 4) Ojo Caliente Sandstone (Tto); and 5) Chama-El Rito (Ttc). In the shallow aquifer these units form a regular pattern of northeast-trending bands (Fig. 20). The Lama formation and Servilleta Basalt lie near the Rio Pueblo; the Chamita Formation is in the center of the study area; and the Ojo Caliente and Chama-El Rito lie nearest to the Picuris Mountains. These hydrostratigraphic units are used to designate water-bearing zones yielding water to wells, are included with data tables for water levels, chemistry and water yields, and provide support for hydrologic interpretations.
2. **Picuris piedmont aquifer—**The Picuris piedmont aquifer is the shallowest unconfined aquifer that lies between the Picuris Mountains and the Rio Pueblo. In the northern piedmont, north of the basalt line, domestic wells draw water from Lama sediments, the underlying basalt flows and thin layers of sediment between the basalts, and the Chamita Formation underlying the oldest basalt. Locally, clay deposits between the basalt flows perch or vertically partition groundwater. In the southern piedmont, south of the basalt line, domestic wells draw water from the Chamita Formation, the Ojo Caliente and Chama-El Rito. In the Arroyo del Alamo area, the shallow aquifer is exceptionally deep, but still generally unconfined. In the Tierra Blanca neighborhood between NM-68 and the mountains, well depths range from 1,000–1,120 feet in the Ojo Caliente (550 700 feet to water) and 950–1,290 feet in the Chama-El Rito (760–1,050 feet to water). Average well yields are about 20 gpm in the Lama formation, 11 gpm in Servilleta Basalt, 20 gpm in the Chamita Formation, 54 gpm in the Ojo Caliente Sandstone, and 31 gpm in the Chama-El Rito. The Ojo Caliente Sandstone is the most productive unit in the piedmont aquifer. Where the Servilleta Basalt is fractured by faulting, well yields increase to 35 gpm.

3. **Deep confined aquifer**—A deep confined aquifer also exists in the Ojo Caliente and the Chama-El Rito north of NM-68, where the units are faulted down to progressively greater depths in the basin (Fig. 19). Near the mountain front and east of the Rio Grande del Rancho, the Ojo Caliente is absent, and deep wells are completed in Chamita and Chama-El Rito sediments. Knowledge of the deep aquifer is limited to a few production and exploration wells clustered west and east of the Rio Grande del Rancho. Water levels in deep confined wells rise hundreds of feet above the top of the aquifer, typically to within 100–375 feet of land surface. In nested piezometers at BOR-1 and BOR-2 (Fig. 21, TV-273, TV-274, TV-275), water levels indicate a downward vertical gradient of water. In RP-2000 adjacent to the Rio Pueblo (Fig. 21, TV-302, TV-303, TV-304), the hydraulic gradient is upward. Well yields in these deep, long-screened wells are 100 gpm in thin Ojo Caliente and 200 gpm in Chama-El Rito (Table 1). The deep aquifer is a target for future water development.
4. **Fault zones and groundwater**—A complex network of intersecting fault zones affects both the Picuris piedmont and deep confined aquifers. Where crystalline basement rocks underlying the alluvial aquifer are intensely faulted and fractured by the Picuris-Pecos and Embudo fault systems, they act as conduits for upward movement of water into the overlying alluvium. Where the Picuris-Pecos faults extend upwards into the basin fill (to merge with the Los Cordovas rift faults) and intersect the Embudo faults, they typically reduce permeability and create barriers or partial barriers to lateral groundwater flow. In the piedmont and deep confined aquifers, the intersecting faults will likely: 1) create fault-bounded compartments that hamper movement of groundwater through the aquifer and into wells; and 2) localize upward movement of potentially large volumes of water from fractured basement.
5. **Bedrock aquifers**—Bedrock aquifers exist in Pennsylvanian sedimentary rocks (IP) and Proterozoic Miranda granite (Xmg) and Ortega quartzite (Xho) in the Picuris Mountains. The volcanic-rich sediments of the Picuris Formation, at the base of the mountains and in Miranda Canyon, often generate poor well yields (less than 5 gpm and as little as 1 gpm), damage or collapse well casings, or result in dry holes. However, thin coarse layers of sand, gravel or boulder conglomerates locally encountered at the base of the formation have recorded well yields of 23 to 50 gpm. Where Pennsylvanian sandstone and limestone layers are intensely faulted and fractured south of Talpa, they produce well yields of 20 gpm, but have poor water quality. Proterozoic granite and quartzite produce 30–60 gpm where they are faulted and fractured, particularly by intersecting faults at Ponce de Leon and in the Picuris embayment. Where no fracturing is noted, well yields decrease to 0.5–25 gpm. Tables 1 and 4; Figs. 7, 18 and 19.
6. **Basin-bedrock boundary**—A hydrologic discontinuity (or groundwater barrier) that impedes flow between bedrock and basin aquifers (labeled "basin-bedrock boundary" on maps) is created at the base of the mountains by Embudo faulting in thick Picuris Formation mudstone and siltstone. Hydrogeologic windows in the basin-bedrock boundary connect water-bearing zones in intensely fractured bedrock with coarse sediments in the Chama-El Rito, Ojo Caliente, and/or Picuris Formation. These fracture zones allow groundwater to cross the basin-bedrock boundary at: 1) the Picuris embayment and Arroyo del Alamo structural block; and 2) the Ponce de Leon area in the bottom of Miranda Canyon.
7. **Groundwater flow in the Picuris piedmont aquifer**—Groundwater enters the Picuris piedmont aquifer primarily from the large mountain watersheds to the east, southeast, and south (Fig. 4) and from the Rio Grande del Rancho. Groundwater flow direction is generally westward toward the lower Rio Pueblo canyon and the Rio Grande near the confluence. The groundwater map (Fig. 21) shows that the lower Rio Pueblo, not the Rio Grande, is the primary discharge zone for the piedmont aquifer and exerts substantial control over groundwater movement. The mountain front between Miranda Canyon and the Picuris-Pecos fault at the eastern boundary of Tierra Blanca lacks a large, high-elevation perennial watershed and geologic conditions do not support subsurface flow into the piedmont aquifer. Thus, there are no significant shallow groundwater sources (above 1,000 feet in depth) in this zone. The mountain front west of the Picuris embayment to Arroyo Hondo may also be a zone of no recharge.
8. **Perched groundwater**—North of the basalt line near County Road 570, clay layers between

basalt flows create a zone of perched groundwater that lies more than 200 feet above the water table in the underlying Chamita Formation (Fig. 19, cross section E-E'). Extensive pumping from this perched zone should be avoided.

9. **Miranda Canyon**—Miranda Canyon is a small dry watershed with no perennial surface water. Groundwater is limited to discontinuous sedimentary layers and fracture zones in the granite, and is confined or artesian. It is the opinion of the authors that there is not a viable water supply in Miranda Canyon to support development.

10. **Ponce de Leon hot springs**—The Ponce de Leon thermal springs, located at the intersection of the McGaffey, Miranda, and Embudo faults, discharge about 66 gpm (Plate 1). Spring discharge flows into Miranda Creek and joins the Rio Grande del Rancho southwest of Talpa. Hydrothermal water circulates through fractured bedrock and into the Picuris piedmont aquifer across the basin-bedrock boundary.

11. **Water-level changes**—Bimonthly and continuous groundwater-level measurements in the Picuris piedmont aquifer show three trends: 1) seasonal fluctuations; 2) progressive water-level declines south of Los Cordovas; and 3) static levels with no significant change. The dominant seasonal trend (winter to summer) shows high summer levels (early June 2012) and low winter levels (December 2012) along the Rio Grande del Rancho and the upper Rio Pueblo within acequia-irrigated agricultural lands (Fig. 23), which demonstrate stream- and acequia-connected recharge. Changes in stream stage in the lower Rio Pueblo generate similar low-amplitude changes in groundwater level in adjacent wells in Servilleta Basalt. Water-levels are essentially static (±0.4 feet) in areas far from sources of recharge or significant pumping, specifically the lower Rio Pueblo neighborhood west of the golf course, in the Lama formation above basalt flows, and in the Chamita Formation beneath the basalts.

12. **Zone of water-level decline**—A zone of progressive water-level declines is identified between Los Cordovas and NM-68, within the northern projection of the Miranda graben (Figs. 24A, B). In the center of the zone, water levels dropped by 1.4 to 2.6 feet from 2011 to 2012. When remeasured in October 2015, most levels had continued in decline at a reduced rate even though drought conditions had diminished and a wet climate was restored, or levels remained stable at the December 2012 level. Over the three- to four-year period from 2011 to 2014–2015, water levels in the center of the decline dropped by 3.1 to 6.3 feet. Initially the declines may have been linked to drought, but the aquifer failed to recover in following years and continued in decline. The zone of decline lies within a fault-bounded area that coincides with the northern projection of the Miranda graben. Faulting related to the graben likely creates barriers or partial barriers to horizontal groundwater flow, focuses and intensifies the effects of pumping, and contributes to the water-level declines. When remeasured in October 2015, most levels had continued in decline at a reduced rate even though drought conditions had diminished and a wet climate was restored, or levels remained stable at the December 2012 level. Over the three- to four-year period from 2011 to 2014–2015, water levels in the center of the decline dropped by 3.1 to 6.3 feet. Possibly the water-level declines were initially linked to drought, but the aquifer failed to recover in following years and continued in decline due to localized groundwater withdrawals and fault compartmentalization of the aquifer.

View northeast down Arroyo Miranda, with the Sangre de Cristo Mountains on the skyline. The arroyo contains a perennial flow of warm stream water below Ponce de Leon spring. In the summer of 2011, spring discharge was measured at about 108 gpm (0.24 cfs) in this area. The layered rocks forming the arroyo walls are clay-rich, volcaniclastic sediments of the lower Picuris Formation, which are typically poor aquifer units. *Photo by Paul Bauer.*

V. THERMAL AND CHEMICAL CHARACTERISTICS OF GROUNDWATER

In this chapter we describe several thermal and chemical characteristics of groundwater in the southern Taos Valley that help determine the water's source, flow path, recharge, mixing, and residence time. The objective is to differentiate the different types of groundwater and their origins, including: 1) shallow groundwater that originated from surface sources—precipitation and stream flow—during recent times; 2) deep groundwater that originated from surface sources but has changed chemically while circulating deep within the subsurface; and 3) groundwater originating from deep within the earth and flowing upward into the shallow aquifer along bedrock faults.

The groundwater constituents evaluated include: groundwater discharge temperature, dissolved solid content (TDS), calcium (Ca), sodium (Na), bicarbonate/carbonate (HCO_3/CO_3), sulfate (SO_4), chloride (Cl), fluoride (F), and naturally occurring radio isotopes used to determine the age or residence time of water in the aquifer. Results of these analyses are discussed below. Concentrations of the chemical constituents measured in well water, springs, and streams are presented in Tables 9 and 10, and in Appendix 3.

Thermal Conditions

Groundwater temperature can help identify aquifer zones affected by recent recharge, upflow of deep thermal water, and intermixing of shallow and deep sources. Local and regional variations in groundwater temperatures are primarily caused by differences in depth of circulation and the local thermal gradient (Mazor, 2004). Shallow groundwater with circulation depths of about 100 meters (328 feet) or less represents recent recharge and is typically close to the local mean surface temperature (Mazor, 2004). Groundwater temperatures significantly above the mean surface temperature indicate either a long aquifer residence time with circulation to great depth, or upflow of deep geothermal waters into the rift-basin aquifers. We use temperature measurements of groundwater from wells and springs to establish temperature patterns in southern Taos Valley aquifers and identify thermally anomalous wells.

The local mean annual surface temperature for the Taos area is 8.4°C (47.1°F). Groundwater temperatures measured in the study area range from 11 to 35°C (52 to 95°F) (Fig. 26, Table 9). The highest temperatures (>23°C) occur in wells and hot springs in the Ponce de Leon artesian zone, and in three wells in the deep confined aquifer at depths of 1,100 to 3,200 feet. Cool groundwater (<15°C) is detected in shallow wells less than 450 feet in depth near the Rio Grande del Rancho and the upper Rio Pueblo de Taos, and in the perched groundwater zone southwest of the Taos golf course (TV-139, TV-140). Warm groundwater (15–20°C) occurs across the high Picuris piedmont, from the Tierra Blanca neighborhood to the golf course, at well depths of 240 to 1,400 feet. Hot and cold springs are found in close proximity in Ponce de Leon (TV-503, TV-504). Two warm springs discharge on the southeast wall of the Rio Grande gorge below Taos Junction (TS-54, TS-56), and one cold spring discharges from high on the canyon wall above the lower Rio Pueblo de Taos (TS-55).

Generally, groundwater temperatures in the Picuris piedmont aquifer strongly correlate with aquifer depth, indicating that the local geothermal gradient controls groundwater temperature (Fig. 27). However, several wells in the Picuris piedmont aquifer with depths between 50 and 2,000 feet have groundwater temperatures outside the 95% confidence interval for the temperature-depth regression, indicating the temperatures are higher than expected from the well depth and geothermal gradient alone (wells TV-168, 186, 188, 192, 198, 201, 217, 218, and 301 noted in Figs. 26 and 27). These wells are located near the projected traces of the Picuris-Pecos faults, the Miranda graben, and the lower Rio Pueblo geophysical faults (Fig. 26). The results suggest that upflow of deep geothermal waters along the major bedrock faults and at fault intersections may produce the anomalously high temperatures in the Picuris piedmont aquifer. Deep thermal waters may also locally impact water quality with high solute contents

Table 9. Data for field parameters, general chemistry, and major ions in well, spring, stream and waste waters (Figs. 26–37). Sample sites are shown on Figure 5. Units are in mg/L unless otherwise noted.—Continued

						GENERAL CHEMISTRY				MAJOR IONS								
	Site ID	Site type	Sample date	Aquifer zone	Well depth (ft bls)	Field pH*	Temperature (°C)	TDS	Water type	Ca	Na	Ca:Na ratio	HCO_3	CO_3	SO_4	Cl	F	Ion balance (% difference)
SHALLOW PICURIS PIEDMONT AQUIFER	TV-102A	GW	1/10/13	Ttc	460	7.6	15.7	322	Ca-Na-HCO_3-SO_4	65	27	2.8	206	0	62	21	0.9	-0.78
	TV-103C	GW	4/5/07	Tto	1000	8.2*	nr	240	Na-Ca-HCO_3-SO_4	22	41	0.6	117	1.2	42	12	0.8	-1.68
	TV-104B	GW	12/1/05	Ttc	1080	7.8*	na	345	Ca-Na-HCO_3-SO_4	47	31	1.7	170	0	80	10	1.0	0.18
	TV-106A	GW	7/27/11	Ttc	972	8.1	18.4	206	Ca-Mg-Na-HCO_3	28	13	2.5	125	0	24	3.2	0.8	-0.37
	TV-107C	GW	9/1/82	Ttc	955	7.2*	nr	199	Ca-Na-HCO_3-SO_4	40	37	1.2	125	0	50	7.4	0.8	4.31
	TV-108A	GW	8/15/11	QTlb	185	7.7	13.4	370	Ca-Mg-HCO_3-SO_4	75	25	3.4	175	0	110	23	0.5	1.75
	TV-115A	GW	8/15/11	Tc	600	7.5	17.0	292	Ca-Na-HCO_3-SO_4	59	27	2.5	190	0	52	17	0.9	1.09
	TV-116C	GW	5/30/08	QTl	260	7.6*	nr	500		130	33	4.5	330	0	nr	18	0.7	
	TV-118A	GW	8/16/11	Tc	175	7.3	13.2	369	Ca-Na-HCO_3	63	55	1.3	310	0	55	4.2	1.1	-0.75
	TV-121C	GW	12/11/97	QTlb, Tsb	215	7.2*	nr	346	Ca-Na-HCO_3-SO_4	76	29	3.0	175	0	106	24	0.6	2.71
	TV-135A	GW	8/16/11	QTl	112	7.5	12.1	413	Ca-Na-HCO_3-SO_4	88	40	2.5	320	0	71	5.3	0.5	3.35
	TV-136A	GW	8/17/11	QTlb	122	7.2	11.2	790	Ca-Mg-SO_4-HCO_3	175	35	5.7	355	0	310	18	1.3	0.82
	TV-139A	GW	7/25/12	QTlb, Tsb	400	7.3	13.5	336	Ca-HCO_3-SO_4	70	22	3.7	181	0	83	22	0.5	-0.47
	TV-140A	GW	6/6/12	QTl, Tc	260	7.6	13.8	290	Ca-HCO_3-SO_4	59	20	3.4	150	0	69	20	0.3	0.72
	TV-142A	GW	8/16/11	QTl, Tc	65	7.3	13.1	456	Ca-HCO_3	115	24	5.5	400	0	54	10	0.7	-0.01
	TV-143C	GW	4/7/09	QTlb, Tsb	300	7.1*	nr	343	Ca-Mg-HCO_3-SO_4	76	28	3.1	160	0	120	22	<0.5	-1.54
	TV-153C	GW	3/20/01	QTl, Tc	245	7.6*	13.0	494	Ca-Na-HCO_3-SO_4	92	76	1.4	400	0	100	7	1.9	-1.23
	TV-160C	GW	6/15/89	Ttc	125	7.7*	nr	305	Ca-HCO_3-SO_4	80	19	4.8	254	0	64	<10	nr	2.79
	TV-162A	GW	1/10/13	QTl	160	7.6	11.7	459	Na-Ca-HCO_3	45	117	0.4	369	0	74	3.4	1.4	0.50
	TV-168A	GW	8/17/11	Tsb	50	7.6	14.1	256	Ca-Na-HCO_3-SO_4	41	29	1.6	140	0	61	14	0.2	-1.04
	TV-179A	GW	8/17/11	QTl	180	7.3	12.9	512	Ca-HCO_3-SO_4	130	28	5.3	380	0	115	9	0.5	-0.99
	TV-181A	GW	8/18/11	QTl	150	7.4	12.1	475	Ca-HCO_3-SO_4	115	33	4.0	355	0	84	23	0.4	0.65
	TV-184A	GW	5/22/12	Ttc	255	7.2	11.8	321	Ca-Na-HCO_3	70	31	2.6	250	0	51	6.5	2.6	0.45
	TV-185A	GW	8/17/11	QTlb	180	7.6	13.2	176	Ca-Na-HCO_3	31	18	2.0	130	0	22	7.5	0.3	-1.92
	TV-186A	GW	5/22/12	QTl	280	7.5	15.4	295	Ca-Na-HCO_3-SO_4	65	24	3.1	215	0	50	12	0.8	0.45
	TV-188A	GW	8/18/11	Tc	395	7.9	16.5	205	Na-Ca-HCO_3-SO_4	24	41	0.7	135	0	34	9	1.4	0.00
	TV-191A	GW	4/20/11	Tto	1002	7.8	19.6	254	Ca-Na-HCO_3-SO_4	36	25	1.7	125	0	43	19	1.0	-1.70
	TV-192C	GW	3/20/89	QTlb, Tsb	240	7.5	18.4	270	Ca-HCO_3-SO_4	78	20	4.4	151	0	82	27	0.8	-1.86
	TV-194A	GW	1/10/13	QTl	100	7.6	11.6	460	Ca-HCO_3-SO_4	113	30	4.3	308	0	111	13	0.6	1.02
	TV-198A	GW	8/15/11	QTlb, Tsb	480	8.2	16.8	176	Na-Ca-HCO_3-SO_4	20	36	0.6	115	0	29	6.9	1.2	-0.01
	TV-229C	GW	5/3/96	Tto	1070	7.7*	nr	189	Na-Ca-HCO_3-SO_4	15	54	0.3	101	0	59	16	0.9	-4.42
	TV-232A	GW	8/18/11	QTl	120	7.4	12.2	592	Ca-HCO_3-SO_4	125	45	3.2	275	0	205	26	0.7	0.95
	TV-235A	GW	7/23/12	Ttc	220	7.1	13.4	505	Na-HCO_3-SO_4-Cl	28	143	0.2	173	0	120	67	15	-0.15
	TV-237B	GW	9/18/02	Ttc	1290	7.8*	na	260	Ca-Mg-HCO_3	41	14	3.4	190	0	13	12	0.5	-1.08
	TV-238B	GW	9/18/02	Tsb	105	7.3*	na	390	Ca-Na-HCO_3-SO_4	80	32	2.9	280	0	75	13	0.9	-0.64
	TV-239B	GW	9/18/02	QTl	300	7.4*	na	410	Ca-HCO_3-SO_4	95	21	5.2	191	0	120	31	0.3	-0.34
	TV-240B	GW	9/18/02	QTlb, Tsb	200	8.3*	na	110	Ca-Na-HCO_3	17	18	1.1	83	0	8.7	3.0	0.2	1.25
	TV-243B	GW	9/18/02	Tc	138	7.4*	na	470	Na-Ca-HCO_3	70	85	0.9	405	0	63	7.4	0.8	0.74
	TV-244B	GW	12/12/05	Tc	320	8.0*	na	544	Ca-Na-HCO_3-SO_4	105	55	2.2	245	0	190	30	1.2	-2.30
	TV-245B	GW	12/12/05	Ttc	120	7.7*	na	409	Ca-Na-HCO_3-SO_4	79	43	2.1	230	0	104	25	1.0	-2.21
	TV-246B	GW	12/13/05	Ttc	400	7.7*	na	326	Ca-Na-HCO_3-SO_4	63	27	2.7	215	0	55	26	0.7	-2.55
	TV-247B	GW	9/18/02	QTl	60	7.4*	na	360	Ca-HCO_3	85	25	3.9	309	0	50	7.6	0.3	0.62
	TV-248B	GW	6/8/05	QTlb	180	8.0*	na	232	Ca-Na-HCO_3	38	36	1.2	195	0	33	2.0	0.4	-2.17
	TV-249B	GW	3/9/05	QTl	130	7.6*	na	160	Ca-Na-HCO_3	30	12	2.9	115	0	22	3.6	0.2	1.30
	TV-250B	GW	3/9/05	QTl	60	7.8*	na	342	Ca-HCO_3	80	24	3.8	285	0	50	7.7	0.2	0.02
	TV-251B	GW	3/9/05	Tsb	280	7.8*	na	207	Ca-HCO_3	47	14	3.9	195	0	15	3.2	0.1	-0.05
	TV-252B	GW	12/1/05	Ttc	1190	7.9*	na	285	Ca-Na-HCO_3-SO_4	41	18	2.6	145	0	51	15	1.0	-1.94
	TV-253B	GW	12/29/05	Tto	1048	8.5*	na	220	Na-HCO_3	11	51	0.2	125	0	28	11	1.0	-1.24
	TV-254B	GW	12/20/05	QTl	210	8.0*	na	386	Ca-HCO_3-SO_4	88	24	4.2	195	0	98	31	0.4	0.00
	TV-255B	GW	12/20/05	QTlb, Tsb	286	8.0*	na	347	Ca-HCO_3-SO_4	79	20	4.5	190	0	82	26	0.4	-0.53
	TV-256B	GW	12/20/05	QTlb, Tsb	260	7.7*	na	478	Ca-HCO_3-SO_4	115	24	5.5	265	0	125	33	<0.5	-0.14
	TV-257B	GW	12/20/05	Tc	280	7.8*	na	393	Ca-HCO_3-SO_4	85	29	3.4	205	0	91	38	0.6	-0.59
	TV-258B	GW	12/20/05	QTl	na	7.9*	na	287	Ca-Na-HCO_3-SO_4	61	23	3.0	200	0	50	14	0.7	-0.67
	TV-259B	GW	12/20/05	Tc	na	7.7*	na	316	Ca-HCO_3-SO_4	65	22	3.4	185	0	63	26	0.5	-2.47
	TV-260B	GW	12/20/05	QTl	275	7.8*	na	331	Ca-HCO_3-SO_4	67	23	3.3	200	0	81	20	0.6	-2.44
	TV-261B	GW	12/20/05	QTl	140	8.0*	na	522	Ca-Na-HCO_3-SO_4	82	91	1.0	350	0	130	11	0.9	0.09
	TV-262B	GW	12/20/05	QTl	200	8.0*	na	496	Na-Ca-HCO_3	77	90	1.0	425	0	76	4.4	0.9	-0.81

Table 9. Continued

	Site ID	Site type	Sample date	Aquifer zone	Well depth (ft bls)	GENERAL CHEMISTRY: Field pH*	Temperature (°C)	TDS	Water type	MAJOR IONS: Ca	Na	Ca:Na ratio	HCO_3	CO_3	SO_4	Cl	F	Ion balance (% difference)
PICURIS PIEDMONT AQUIFER	TV-263B	GW	12/23/05	Tsb, Tc	700	7.7*	na	293	Ca-HCO_3-SO_4	59	19	3.6	165	0	63	19	0.5	-0.89
	TV-264B	GW	3/31/05	Ttc	210	7.4*	na	313	Ca-HCO_3	85	8.2	12	305	0	36	3.2	0.4	-2.70
	TV-265B	GW	5/7/05	Qal, Tp	72	7.4*	na	322	Ca-HCO_3	88	9.4	11	295	0	46	5.4	0.1	-2.58
	TV-266A	GW	1/11/13	QTl	75	7.6	12.0	473	Ca-HCO_3-SO_4	107	26	4.8	279	0	109	37	0.3	0.31
	TV-267A	GW	1/11/13	Tc	182	7.7	11.8	409	Ca-Na-HCO_3-SO_4	77	51	1.7	305	0	91	3.5	0.3	-0.61
	TV-268A	GW	1/11/13	Tc	215	7.5	10.8	355	Ca-HCO_3	79	25	3.7	304	0	42	11	0.4	-0.47
	TV-273C	GW	5/9/00	QTl	291	7.9*	15.5	230	Ca-Na-HCO_3	51	26	2.3	210	0	36	6	0.3	0.37
	TV-297A	GW	10/1/92	QTlb, Tsb	348	9.9*	nr	86	Na-Ca-HCO_3	7.9	22	0.4	57	5	<5	1.8	0.5	2.37
	TS-055A	SP	4/24/07	QTlb	na	8.3	9.9	na		na	na	na	na	na	na	na	na	
	TV-512AB	PS	2/11/08		na	7.1	na	223	Ca-HCO_3	58	7.6	8.8	205	0	29	6	0.1	-1.25
	TV-513C	PS	5/27/14		na	8.2	10.4	73	Ca-Mg-HCO_3	18	2.4	8.5	62	0	7.5	<1	<0.1	4.51
	TV-514C	PS	5/27/14		na	8.3	9.3	52	Ca-HCO_3	12	1.8	7.9	42	0	4.5	<1	0.1	2.91
SUMMARY STATISTICS FOR SHALLOW PICURIS PIEDMONT AQUIFER																		
					min	7.1	10.8	86		7.9	8.2	0.22	57	0	8.7	1.8	0.1	-4.42
					max	8.3	19.6	790		175	143	12	425	5	310	67	15	4.3
					median	7.6	13.2	336		70	27	3	200	0	63	13	1	-0.36
BEDROCK AQUIFERS	TV-100A	GW	7/27/11	Tpl	1000	7.4	16.7	270	Ca-HCO_3	55	11	5.7	225	0	11	3	0.6	-0.79
	TV-125A	GW	8/16/11	Xhu	280	9.0	21.9	526	Na-Cl-SO_4	5.8	170	0.04	45	6.2	140	105	19	-0.45
	TV-126A	GW	8/16/11	Tp, Xmg	420	9.0	26.2	534	Na-Cl-SO_4	6.4	170	0.04	53	9.9	140	105	20	-2.16
	TV-127A	GW	8/16/11	Xmg	400	7.9	24.3	1888	Na-SO_4-Cl	63	570	0.1	205	0	715	415	4.4	-3.49
	TV-128A	GW	8/16/11	Tp	500	8.0	28.5	775	Na-Cl-SO_4	13	290	0.1	145	0	145	225	8	4.27
	TV-132B	GW	3/31/05	Xhu	400	9.0*	na	518	Na-Cl-SO_4	6.1	165	0.04	36	0	140	110	20	-1.09
	TV-201A	GW	7/23/12	/Pu	260	9.1	15.2	872	Na-SO_4-Cl-HCO_3	2.1	312	0.01	221	21	252	133	1.1	1.04
	TV-207B	GW	5/7/05	Tpl	598	8.6*	na	852	Na-HCO_3-SO_4	2.2	335	0.01	620	20	180	8	2.6	0.95
	TV-209A	GW	8/16/11	Tp	295	9.2	25.9	282	Na-HCO_3	1.3	100	0.01	190	22	17	7	3.7	-1.96
	TV-214C	GW	9/13/05	Tp	580	8.1*	nr	224	Ca-HCO_3	50	7.5	7.7	154	0	4.1	2.3	<0.05	9.17
	TV-216A	GW	4/22/11	Tp	420	6.8	11.4	160	Ca-Mg-HCO_3	18	8.1	2.5	99	0	3.2	2.5	0.6	-1.69
	TV-230A	GW	7/27/11	Xhu	1400	7.1	16.5	48	Ca-HCO_3	8.0	1.9	4.8	35	0	2.3	2.2	0.1	-5.12
	TV-503A	SP	8/15/11	Xmg	na	8.6	34.9	492	Na-SO_4-Cl	10	150	0.1	80	0	125	89	16	-0.76
	TV-504A	SP	8/16/11	Qal, Tp	na	7.2	12.7	694	Na-Ca-HCO_3-Cl-SO_4	94	130	0.8	245	0	160	120	5.6	0.04
SUMMARY STATISTICS FOR BEDROCK AQUIFER																		
					min	6.8	11.4	48		1.3	1.9	0.01	35	0	2.3	2.2	0.1	-5.12
					max	9.2	34.9	1888		94	570	8	620	22	715	415	20	9.17
					median	9.0	21.9	522		9	158	0.1	150	0	140	97	4.4	-0.15
DEEP CONFINED AQUIFERS	TV-152A	GW	7/25/12	Tc, Tto	1200		20.1	189	Na-HCO_3-SO_4	2.6	61	0.05	88	10	31	10	0.7	1.03
	TV-170A	GW	5/11/11	Tto	2527		28.0	223	Na-CO_3-HCO_3-SO_4	1.4	70	0.02	56	30	44	12	1.8	-1.96
	TV-171A	GW	4/28/11	Tto, Ttc	3180		34.5	255	Na-HCO_3-SO_4-CO_3	1.5	91	0.02	79	33	58	16	1.8	-1.64
	TV-217A1	GW	5/23/12	Ttc	1575		na	190	Na-CO_3-HCO_3	0.7	72	0.01	70	40	14	15	0.6	-1.38
	TV-217A2	GW	5/23/12	Ttc	1785		na	186	Na-CO_3-HCO_3	0.6	72	0.01	66	45	9.3	15	0.6	-1.34
	TV-217A3	GW	5/23/12	Ttc	2003		na	191	Na-CO_3-HCO_3	0.6	73	0.01	74	40	12	15	0.6	-1.36
	TV-217C	GW	2001	Ttc	1968		28 †	na	na	na	na	na	na	na	na	na	na	na
	TV-219A	GW	5/22/12	Tto, Ttc	1400		16.6	201	Na-HCO_3-SO_4	2.1	69	0.03	90	15	31	16	0.4	0.29
	TV-274C	GW	5/31/00	Tc, Ttc	1480		20.4	260	Na-HCO_3-CO_3	5.3	70	0.1	98	29	30	7	0.8	-1.68
	TV-275C	GW	6/15/00	Ttc	2020		24.8	280	Na-SO_4	1.9	100	0.02	32	26	104	16	5.8	1.78
	TV-292A	GW	9/23/92	Ttc	1942		nr	262	Na-SO_4-Cl	10	76	0.2	33	23	81	29	6.3	1.17
	TV-293A	GW	9/29/92	Tc	1117		nr	180	Na-CO_3-SO_4	7.0	49	0.2	8	46	58	7	2.3	1.82
	TV-301A	GW	10/9/15	Ttc	1185		30.5	313	Na-HCO_3-SO_4	7.1	95	0.1	163	9	67	7.5	4.0	-2.36
	TS-054A	SP	4/23/07	Tc	na		18.6	303	Na-HCO_3	13	89	0.2	270	0	20	2.2	1.3	-2.82
	TS-056A	SP	4/24/07	Tc	na		15.7	258	Ca-Na-HCO_3	36	33	1.3	140	0	71	4.2	0.4	-1.59
SUMMARY STATISTICS FOR DEEP CONFINED AQUIFERS																		
					min		15.7	180		0.6	33	0.01	8	0	9.3	2.2	0.4	-2.82
					max		34.5	313		36	100	0.2	270	46	104	29	6.3	1.82
					median		20.4	239		2	72	0.04	77	28	38	14	1.1	
U.S. E.P.A. DRINKING WATER STANDARDS																		
							TDS=500 s		Na=20 h	SO_4=250 s					Cl=250 s		F=4 e	

GW—groundwater;
SP—spring;
PS—perennial stream;
bls—below land surface;
*—indicates lab pH if field pH was not analyzed;
nr—not reported;
na—not analyzed;
†—temperature from geophysical log (Reiter, 2004);

—parameter not calculated; s—secondary drinking water regulation, nonenforceable guideline regarding cosmetic or aesthetic effects; h—USEPA health advisory of acceptable drinking water level for a substance based on health effects information; e—maximum contaminant level (MCL), an enforceable standard for the highest level of a contaminant allowed in drinking water

Table 10. Data for trace elements in well and spring waters. Sample sites are shown on Figure 5.—Continued

					TRACE ELEMENTS (mg/L)										
	Sample ID	Site type	Aquifer zone	Well depth (ft bls)	As	Ba	Cr	Cu	Ni	Pb	SiO_2	Sr	U	V	Zn
SHALLOW PICURIS PIEDMONT AQUIFER	TV-102A	GW	Ttc	460	0.0006	0.075	0.0006	0.0008	0.001	<0.0005	27.1	0.496	0.0056	0.0025	0.0067
	TV-103C	GW	Tto	1000	0.002	<0.02	<0.006	<0.006	<0.01	<0.005	na	na	0.0036	na	0.24
	TV-104B	GW	Ttc	1080	0.004	0.05	0.005	0.001	0.001	0.003	71	0.31	0.009	0.009	1.4
	TV-106A	GW	Ttc	972	0.0017	0.099	0.0028	<0.0005	0.0005	<0.0005	64	0.26	0.003	0.0067	0.038
	TV-108A	GW	QTlb	185	<0.0005	0.032	0.001	<0.0005	0.0009	<0.0005	25	0.43	0.0032	0.0031	0.0012
	TV-115A	GW	Tc	600	0.0005	0.055	0.0013	0.0008	0.0007	<0.0005	29	0.41	0.0052	0.0034	0.0011
	TV-116C	GW	QTl	260	<0.001	0.082	<0.006	<0.006	<0.01	0.0072	na	na	0.009	na	<0.02
	TV-118A	GW	Tc	175	0.0008	0.052	0.0009	0.0011	0.0008	<0.0005	23	0.35	0.0057	0.0023	0.059
	TV-121C	GW	QTlb, Tsb	215	<0.005	0.04	<0.01	<0.01	na	<0.005	na	na	na	na	<0.02
	TV-135A	GW	QTl	112	<0.0005	0.043	<0.0005	<0.0005	0.0011	<0.0005	19	0.6	0.0095	0.0006	0.0086
	TV-136A	GW	QTlb	122	<0.0005	0.019	<0.0005	0.0087	0.0025	<0.0005	35	1.1	0.018	0.002	0.027
	TV-139A	GW	QTlb, Tsb	400	0.0009	0.099	0.0014	0.0005	0.0011	<0.0005	27.3	0.477	0.003	0.0029	0.0092
	TV-140A	GW	QTl, Tc	260	0.0012	0.087	0.0021	<0.0005	0.0009	<0.0005	28	0.4	<0.0005	<0.0005	0.0008
	TV-142A	GW	QTl, Tc	65	<0.0005	0.086	<0.0005	0.0015	0.0015	<0.0005	21	0.62	0.0056	0.0006	0.0046
	TV-143C	GW	QTlb, Tsb	300	<0.005	<0.3	<0.01	0.008	<0.02	<0.002	29	na	na	na	0.045
	TV-153C	GW	QTl, Tc	245	<0.003	0.027	<0.02	<0.01	<0.02	<0.002	na	na	na	na	<0.01
	TV-162A	GW	QTl	160	0.001	0.036	0.0005	0.0011	0.0007	<0.0005	16.7	0.256	0.0054	0.002	0.0037
	TV-168A	GW	Tsb	50	<0.0005	0.026	0.0018	0.0031	0.0007	<0.0005	28	0.27	0.004	0.0035	0.025
	TV-179A	GW	QTl	180	<0.0005	0.058	<0.0005	0.0012	0.0018	<0.0005	18	0.52	0.0089	0.0006	0.0017
	TV-181A	GW	QTl	150	<0.0005	0.091	<0.0005	0.0008	0.0016	<0.0005	16	0.53	0.006	0.0006	0.0015
	TV-184A	GW	Ttc	255	<0.0005	0.055	0.0009	0.0006	0.0008	<0.0005	20	0.38	0.0025	0.0013	0.0034
	TV-185A	GW	QTlb	180	0.0008	0.022	0.0033	<0.0005	0.0005	<0.0005	24	0.23	0.0021	0.0051	0.018
	TV-186A	GW	QTl	280	<0.0005	0.08	0.0013	0.0018	0.0008	<0.0005	23	0.41	0.0024	0.0018	0.017
	TV-188A	GW	Tc	395	0.0008	0.04	0.0007	0.0006	<0.0005	<0.0005	22	0.26	0.0019	0.0034	0.0006
	TV-191A	GW	Tto	1002	0.0022	0.009	0.0019	<0.0005	0.0006	<0.0005	58	0.26	0.0067	0.0084	0.2
	TV-192C	GW	QTlb, Tsb	240	<0.001	na	na	<0.05	<0.01	<0.005	na	na	na	na	0.12
	TV-194A	GW	QTl	100	<0.0005	0.075	0.0007	0.001	0.0017	<0.0005	14.2	0.442	0.0066	0.0006	0.0273
	TV-198A	GW	QTlb, Tsb	480	0.0009	0.022	0.0025	<0.0005	<0.0005	<0.0005	20	0.26	0.0016	0.0039	0.0012
	TV-218A	GW	Tc	460	<0.005	1.5	<0.005	0.0075	0.019	0.059	1.1	3.6	<0.005	<0.005	1.2
	TV-229C	GW	Tto	1070	<0.06	<0.01	<0.02	0.1	<0.04	<0.0001	na	na	na	<0.003	0.1
	TV-232A	GW	QTl	120	0.0005	0.026	<0.0005	0.0008	0.0017	<0.0005	20	0.53	0.011	0.001	0.0063
	TV-235A	GW	Ttc	220	0.0044	0.028	0.0007	0.0005	0.0023	<0.0005	33.8	0.231	<0.0005	0.002	0.0282
	TV-237B	GW	Ttc	1290	0.002	0.155	0.007	0.005	<0.001	<0.001	64	0.39	0.003	0.011	1.03
	TV-238B	GW	Tsb	105	<0.001	0.036	0.001	0.002	<0.001	<0.001	20	0.427	0.004	<0.001	0.022
	TV-239B	GW	QTl	300	<0.001	0.066	0.002	0.002	<0.001	<0.001	25	0.545	0.03	0.002	0.036
	TV-240B	GW	QTlb, Tsb	200	<0.001	0.021	0.009	<0.001	<0.001	<0.001	19	0.116	0.001	0.008	0.01
	TV-243B	GW	Tc	138	<0.001	0.484	0.002	0.032	<0.001	<0.001	23	0.529	0.016	0.002	0.418
	TV-244B	GW	Tc	320	0.001	0.035	0.003	0.004	0.001	<0.001	17	0.54	0.005	0.002	0.006
	TV-245B	GW	Ttc	120	0.001	0.16	0.002	0.004	<0.001	<0.001	24	0.36	0.007	0.003	0.033
	TV-246B	GW	Ttc	400	0.002	0.093	0.001	0.014	0.001	0.001	31	0.5	0.008	0.005	0.02
	TV-247B	GW	QTl	60	<0.001	0.08	0.013	<0.001	<0.001	<0.001	20	0.44	0.02	0.006	<0.001
	TV-248B	GW	QTlb	180	0.001	0.065	0.002	0.004	<0.001	<0.001	18	0.37	<0.004	0.005	0.002
	TV-249B	GW	QTl	130	<0.001	0.028	0.001	0.003	<0.001	<0.001	26	0.18	0.002	0.002	0.002
	TV-250B	GW	QTl	60	<0.001	0.091	0.001	0.002	0.001	<0.001	19	0.43	0.03	0.003	0.075
	TV-251B	GW	Tsb	280	<0.001	0.037	0.001	0.013	<0.001	<0.001	20	0.22	0.005	0.002	0.001
	TV-252B	GW	Ttc	1190	0.003	0.073	0.002	0.001	<0.001	<0.001	71	0.49	0.011	0.002	1.9
	TV-253B	GW	Tto	1048	0.004	0.002	0.002	0.005	0.001	<0.001	51	0.038	0.004	0.014	0.25
	TV-254B	GW	QTl	210	0.001	0.073	0.001	0.002	0.001	<0.001	25	0.54	0.004	0.002	0.02
	TV-255B	GW	QTlb, Tsb	286	0.001	0.12	0.001	0.006	0.001	<0.001	24	0.44	0.004	0.002	0.053
	TV-256B	GW	QTlb, Tsb	260	<0.001	0.05	0.001	0.005	0.001	0.001	20	0.47	0.008	0.001	0.055
	TV-257B	GW	Tc	280	0.001	0.059	0.001	0.01	0.001	0.001	23	0.49	0.004	0.002	0.14
	TV-258B	GW	QTl		0.001	0.1	0.001	0.018	<0.001	<0.001	25	0.42	0.003	0.002	0.006
	TV-259B	GW	Tc		0.001	0.12	0.002	0.003	0.001	<0.001	29	0.51	0.004	0.003	0.023
	TV-260B	GW	QTl	275	<0.001	0.076	0.002	0.004	0.001	<0.001	20	0.37	0.004	0.004	0.014
	TV-261B	GW	QTl	140	<0.001	0.028	0.004	0.003	0.001	<0.001	15	0.35	0.009	0.002	0.017
	TV-262B	GW	QTl	200	<0.001	0.049	0.001	0.006	0.001	<0.001	16	0.33	0.007	0.001	0.061
	TV-263B	GW	Tsb, Tc	700	0.001	0.097	0.002	0.019	0.001	0.001	32	0.39	0.003	0.003	0.034

Table 10. Continued

	Sample ID	Site type	Aquifer zone	Well depth (ft bls)	TRACE ELEMENTS (mg/L) As	Ba	Cr	Cu	Ni	Pb	SiO_2	Sr	U	V	Zn
	TV-264B	GW	Ttc	210	<0.001	0.041	0.002	0.13	0.001	0.007	14	0.44	0.001	0.001	0.15
	TV-265B	GW	Qal, Tp	72	<0.001	0.094	<0.001	0.039	0.001	<0.001	9.4	0.47	0.001	<0.001	0.031
	TV-266A	GW	QTl	75	<0.0005	0.114	0.0008	0.001	0.0017	<0.0005	24.1	0.546	0.0042	0.0008	0.0011
	TV-267A	GW	Tc	182	<0.0005	0.059	0.0008	0.002	0.0012	<0.0005	14.4	0.402	0.0021	0.0006	0.003
	TV-268A	GW	Tc	215	<0.0005	0.065	0.0005	0.0017	0.0013	<0.0005	13.7	0.412	0.0012	<0.0005	0.0021
	TV-273C	GW	QTl	291	<0.005	0.05	<0.01	<0.01	<0.01	<0.005	na	na	<0.005	na	0.058
	TV-295A	GW	Tsb	672	<0.005	<0.5	<0.02	<0.02	na	<0.002	na	na	na	na	na
	TV-296A	GW	QTlb	508	<0.005	<0.5	0.03	<0.05	na	<0.005	na	na	na	na	na
	TV-297A	GW	QTlb, Tsb	348	<0.005	<0.05	<0.02	<0.02	na	na	na	na	na	na	na
	TV-512AB	PS			<0.001	0.046	<0.001	<0.001	0.001	<0.001	8.8	0.34	<0.001	<0.001	<0.001
	TV-513C	PS			<0.0005	0.023	<0.0005	0.0017	0.0008	<0.0005	8.25	0.066	<0.0005	0.0005	0.0029
	TV-514C	PS			<0.0005	0.020	<0.0005	0.0015	<0.0005	<0.0005	8.12	0.056	0.0006	0.0005	0.0046
	SUMMARY STATISTICS FOR SHALLOW PICURIS PIEDMONT AQUIFER														
				min	0.0005	0.002	0.0005	0.0005	0.0005	0.0010	1.1	0.038	0.0010	0.0006	0.0006
				max	0.004	1.5	0.03	0.13	0.019	0.059	71	3.6	0.03	0.014	1.9
				median	0.001	0.059	0.001	0.003	0.001	0.002	23	0.42	0.004	0.002	0.022
BEDROCK AQUIFERS	TV-100A	GW	Tpl	1000	0.0018	0.09	0.0023	<0.0005	0.0009	<0.0005	63	0.32	0.0013	0.0073	0.69
	TV-125A	GW	Xhu	280	0.0024	0.021	<0.0005	0.0006	<0.0005	<0.0005	54	0.13	<0.0005	<0.0005	<0.0005
	TV-126A	GW	Tp, Xmg	420	0.0025	0.014	<0.0005	<0.0005	<0.0005	<0.0005	52	0.17	<0.0005	<0.0005	<0.0005
	TV-127A	GW	Xmg	400	0.0022	0.028	<0.0005	0.0008	0.0008	<0.0005	5.8	0.96	0.0015	<0.0005	0.0012
	TV-128A	GW	Tp	500	0.0035	0.066	<0.0005	0.008	<0.0005	<0.0005	18	0.23	0.016	0.0017	0.019
	TV-132B	GW	Xhu	400	0.003	0.007	<0.001	0.006	<0.001	0.001	54	0.24	<0.001	<0.001	0.005
	TV-201A	GW	/Pu	260	0.0052	0.011	<0.0025	<0.0025	<0.0025	<0.0025	36	0.06	0.0078	<0.0025	<0.0025
	TV-207B	GW	Tpl	598	<0.001	0.026	0.003	<0.001	<0.001	<0.001	11	0.1	<0.001	0.001	0.001
	TV-209A	GW	Tp	295	0.0045	0.007	<0.0005	<0.0005	<0.0005	<0.0005	36	0.021	<0.0005	<0.0005	<0.0005
	TV-216A	GW	Tp	420	0.0011	0.13	0.0017	<0.0005	<0.0005	<0.0005	68	0.1	<0.0032	0.0028	0.021
	TV-230A	GW	Xhu	1400	<0.0005	0.008	0.0005	<0.0005	0.0029	<0.0005	10	0.06	<0.0005	<0.0005	1.4
	TV-503A	SP	Xmg	na	0.0046	0.001	<0.0005	<0.0005	<0.0005	<0.0005	56	0.2	0.0008	<0.0005	0.0006
	TV-504A	SP	Qal, Tp	na	0.0015	0.24	<0.0005	0.0018	0.0014	<0.0005	46	0.54	0.0036	0.0028	0.011
	SUMMARY STATISTICS FOR BEDROCK AQUIFERS														
				min	0.0011	0.001	0.0005	0.0006	0.0008	0.001	5.8	0.021	0.0008	0.001	0.0006
				max	0.0052	0.24	0.003	0.008	0.0029	0.001	68	0.96	0.016	0.007	1.4
				median	0.003	0.021	0.002	0.002	0.0012	0.001	46	0.17	0.003	0.003	0.011
DEEP CONFINED AQUIFERS	TV-152A	GW	Tc, Tto	1200	0.021	0.002	0.0005	<0.0005	<0.0005	<0.0005	28.9	0.011	<0.0005	0.0417	0.0287
	TV-170A	GW	Tto	2527	0.016	<0.001	0.0024	0.0007	<0.0005	0.0005	35	0.015	<0.0005	0.083	0.024
	TV-171A	GW	Tto, Ttc	3180	0.023	0.007	0.0011	0.0019	0.0026	0.0012	29	0.015	0.0005	0.078	0.0063
	TV-217A1	GW	Ttc	1575	0.016	<0.001	<0.0005	0.0005	<0.0005	<0.0005	12	0.0045	<0.0005	0.025	0.0065
	TV-217A2	GW	Ttc	1785	0.012	<0.001	<0.0005	<0.0005	<0.0005	<0.0005	9.1	0.0038	<0.0005	0.016	0.0057
	TV-217A3	GW	Ttc	2003	0.015	<0.001	<0.0005	<0.0005	<0.0005	<0.0005	12	0.0038	<0.0005	0.036	0.003
	TV-219A	GW	Tto, Ttc	1400	0.0073	0.0006	0.0068	<0.0005	<0.0005	<0.0005	21	0.012	<0.0005	0.031	0.0031
	TV-274C	GW	Tc, Ttc	1480	0.017	0.03	<0.01	0.002	<0.01	0.024	na	na	<0.005	na	<0.025
	TV-275C	GW	Ttc	2020	0.016	<0.01	<0.01	<0.01	<0.01	<0.005	na	na	<0.001	na	<0.025
	TV-292A	GW	Ttc	1942	0.0033	0.05	0.0014	<0.004	na	na	na	na	na	na	na
	TV-293A	GW	Tc	1117	0.0059	0.05	0.0013	<0.004	na	na	na	na	na	na	na
	TV-301	GW	Ttc	1185	0.0234	0.071	0.0013	0.0011	0.0008	0.0006	43.5	0.143	0.0017	0.0177	0.0143
	TS-054A	SP	Tc		0.005	0.01	0.007	0.008	<0.001	<0.001	34	0.23	0.004	0.029	<0.001
	TS-056A	SP	Tc		0.002	0.024	0.004	0.005	0.001	<0.001	31	0.34	0.004	0.007	0.001
	SUMMARY STATISTICS FOR DEEP CONFINED AQUIFER														
				min	0.002	0.0006	0.0005	0.0005	0.0008	0.0005	9.1	0.0038	0.0005	0.007	0.001
				max	0.0234	0.071	0.007	0.008	0.0026	0.024	43.5	0.34	0.004	0.083	0.0287
				median	0.0155	0.024	0.0014	0.0019	0.001	0.0009	28.95	0.0135	0.00285	0.03	0.0063
	U.S. E.P.A. DRINKING WATER STANDARDS														
					As	Ba	Cr	Cu		Pb			U		
					0.01 e	2 e	0.1 e	1.3 t		0.015 t			0.03 e		

GW—groundwater;
SP—spring;
PS—perennial stream;
bls—below land surface;
na—not analyzed;
—element equals or exceeds quality standard;
—element is elevated, but meets quality standard;
e—maximum contaminant level (MCL), an enforceable standard for the highest level of a contaminant allowed in drinking water; t—action level at the tap

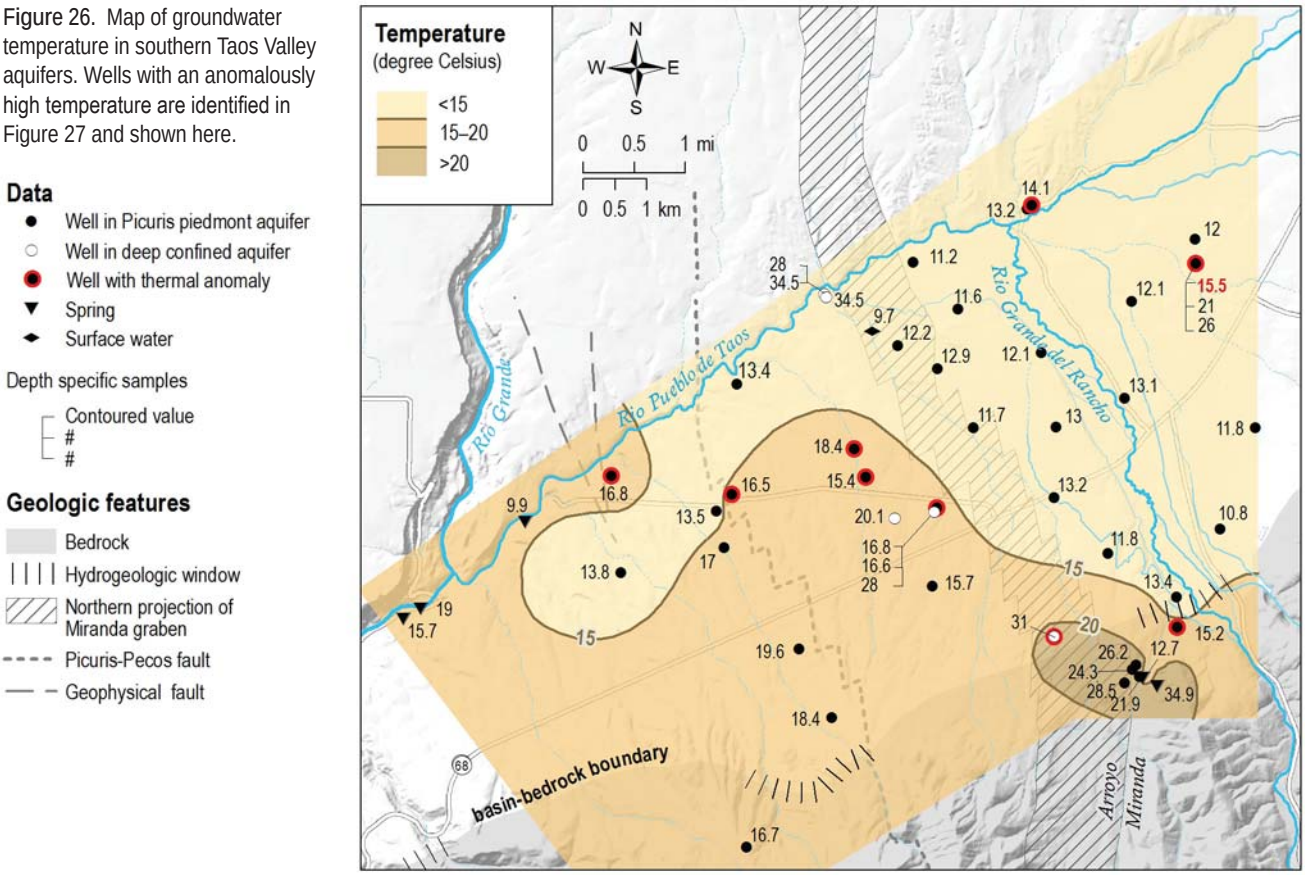

Figure 26. Map of groundwater temperature in southern Taos Valley aquifers. Wells with an anomalously high temperature are identified in Figure 27 and shown here.

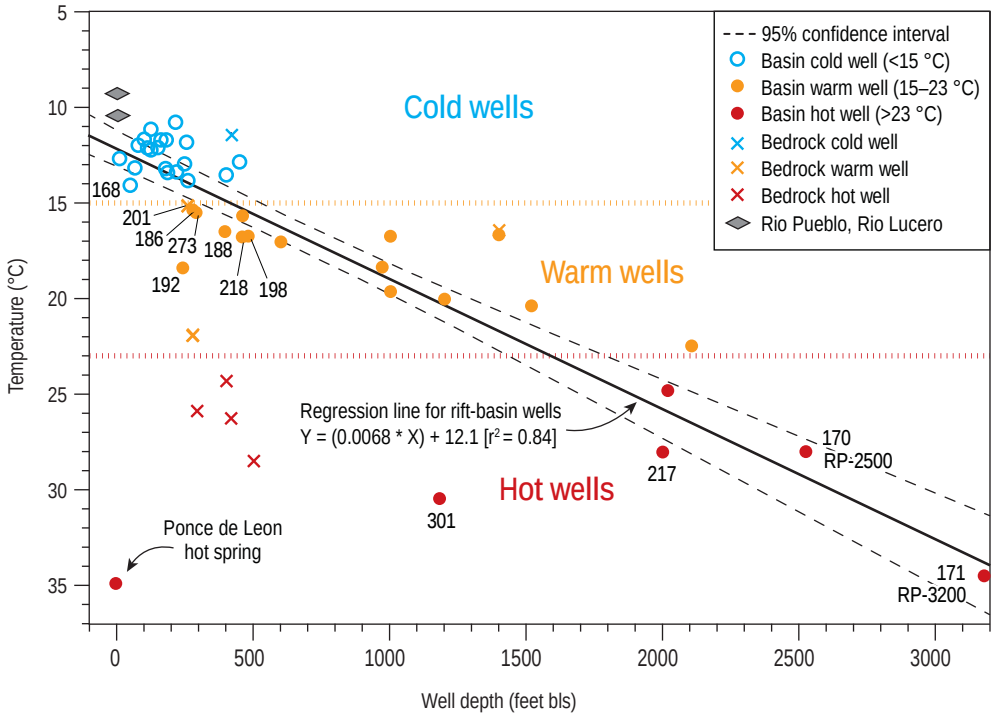

Figure 27. Plot and linear regression of groundwater temperature versus well depth in the Picuris piedmont and deep confined aquifers. Wells plotting below the lower 95% confidence interval have higher temperatures than expected from the local geothermal gradient. Data from bedrock aquifers, including Ponce de Leon are also shown. The discharge temperature for TV-218 was taken from a geophysical log by Reiter (2004).

and elevated concentrations of undesirable or regulated constituents. This issue is addressed in the following evaluation of the chemical characteristics of groundwater.

Chemical Characteristics

Major ions and water type

The major inorganic elements found in groundwater of the southern Taos Valley are calcium, sodium, bicarbonate/carbonate, sulfate, and chloride. Magnesium and potassium are negligible. Major cations (a positively charged dissolved particle) and anions (a negatively charged dissolved particle) combine to form distinct water types. A variety of major water types occur in Taos Valley aquifers, including calcium-bicarbonate (Ca-HCO_3), sodium-sulfate with some chloride (Na-SO_4 ± Cl), and mixtures of these two end members (Fig. 28, Table 9).

Calcium-bicarbonate water is found in the Picuris piedmont aquifer near the Rio Grande del Rancho and upper Rio Pueblo and in both basin and bedrock aquifers in upper Arroyo del Alamo and the Picuris embayment. In shallow aquifers, this water type is most commonly sourced from precipitation and stream recharge, but the dissolution of limestone can also be a source. Groundwater from the Ponce de Leon hydrothermal system is Na-Cl-SO_4 and Na-SO_4-Cl, whereas water from upper Miranda Canyon is HCO_3 water with various amounts of Ca, Na, and Mg. Groundwater in the deep confined aquifer west of the Rio Grande del Rancho consists of Na with some combination of HCO_3, CO_3, and SO_4. East of the Rio Grande del Rancho, deep confined groundwater is partially or totally a Na-SO_4-Cl water type similar to the Ponce de Leon artesian system. In the shallow Picuris piedmont aquifer, groundwater falls into three basic water types with calcium or sodium cations combined with bicarbonate, sulfate, and/or chloride anions (Fig. 28, Table 9).

This simple evaluation indicates that shallow groundwater in the Picuris piedmont aquifer likely represents the intermixing of multiple sources—stream and arroyo recharge, inflow of artesian discharge from the Ponce de Leon hydrothermal system, inflow of shallow bedrock groundwater through the Picuris embayment hydrogeologic window, and

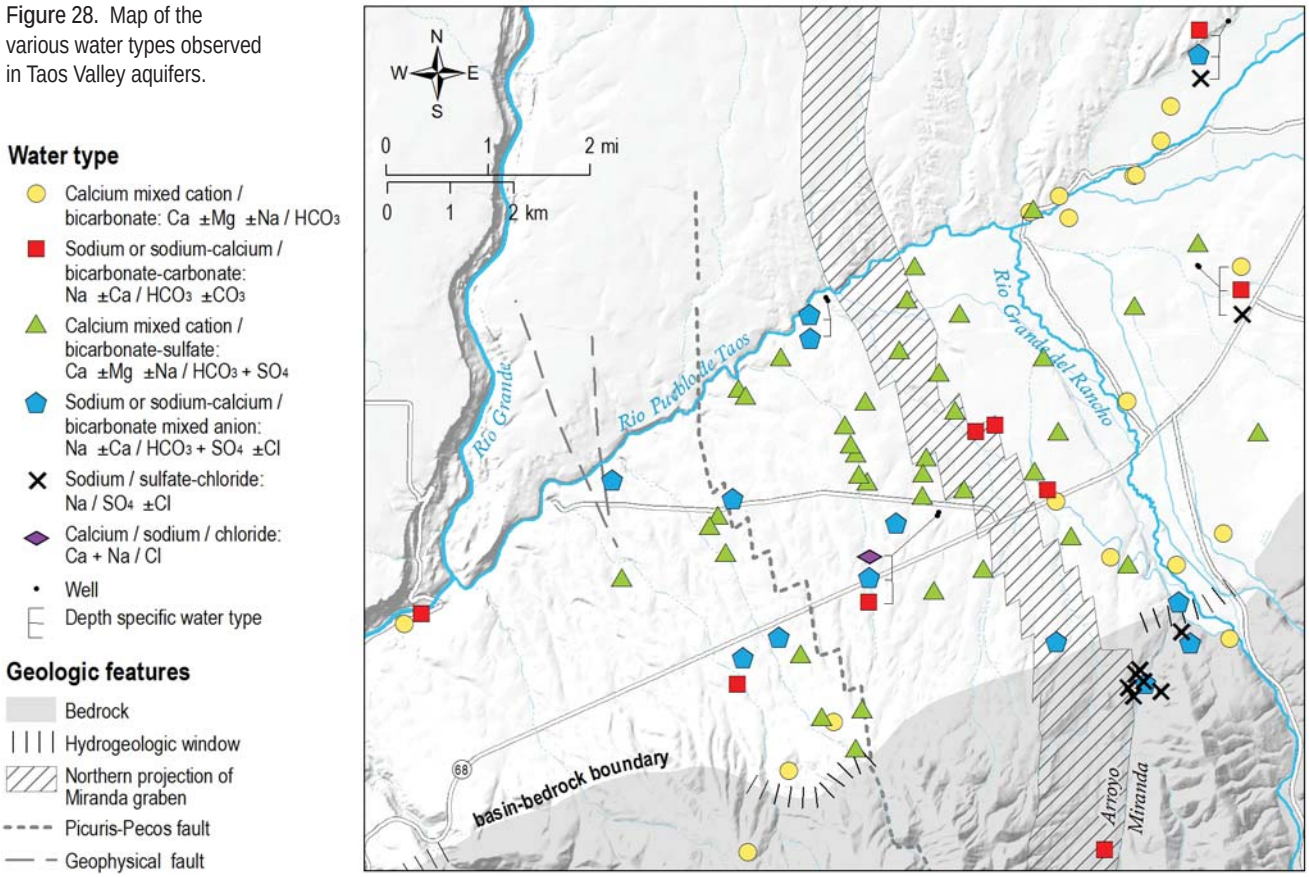

Figure 28. Map of the various water types observed in Taos Valley aquifers.

vertical upflow of deeply sourced thermal waters along faults or at fault intersections.

To further investigate groundwater sources and intermixing, we examine distribution maps of major ions and Piper diagrams that show cation and anion percentages and ion trends. Chemistry data from shallow wells between the mountain front and the Rio Pueblo, including Ponce de Leon and upper Arroyo del Alamo, are used to construct concentration maps of the dissolved solids content and the major ions Ca/Na, HCO_3, SO_4, and Cl for the shallow basin and bedrock aquifers (Figs. 29–33). Chemistry results from surface water and wells in the deep confined aquifer were not used to create the concentration maps, but are shown on the figures. Ion chemistry and summary statistics for each aquifer are presented in Table 9. The observed patterns and some hydrologic implications are discussed.

Dissolved solid content—Concentrations of dissolved solids, called TDS, range from 86–790 mg/L in the Picuris piedmont aquifer (Fig. 29, Table 9). High TDS values (400–600 mg/L) are clustered in the northern Rio Grande del Rancho valley and westward toward the Taos golf course, but both higher and lower values are scattered throughout the area, for example: 790 mg/L TDS in a 122-foot deep well (TV-136) and 390 mg/L TDS in an adjacent 105-foot deep well (TV-238) (Fig. 29, Table 9). An intriguing and unusual trend in the distribution of TDS in the basin-fill aquifers is that TDS does not increase with depth, and concentrations in the deep confined aquifer (180–313 mg/L) are lower than or comparable to those in the shallow Picuris piedmont aquifer. Bedrock aquifers exhibit an extreme range in TDS, with the highest concentrations found in the hydrothermal waters at Ponce de Leon (492–1,888 mg/L) and the lowest from a well in quartzite bedrock in the upper Arroyo del Alamo watershed (48 mg/L, TV-230).

Calcium and sodium—Calcium concentrations range from 2.6 to 175 mg/L, and sodium ranges from 8.2 to 143 mg/L (Table 9). The distribution of calcium and sodium is illustrated as a calcium-to-sodium ratio (Fig. 30), where values greater than 1 indicate calcium dominance and values less than 1 indicate sodium dominance. Shallow groundwater in the Picuris piedmont aquifer is generally Ca-rich, as are stream waters from the Rio Grande del Rancho (TV-512), Rio Pueblo (TV-513) and Rio Lucero (TV-514). The

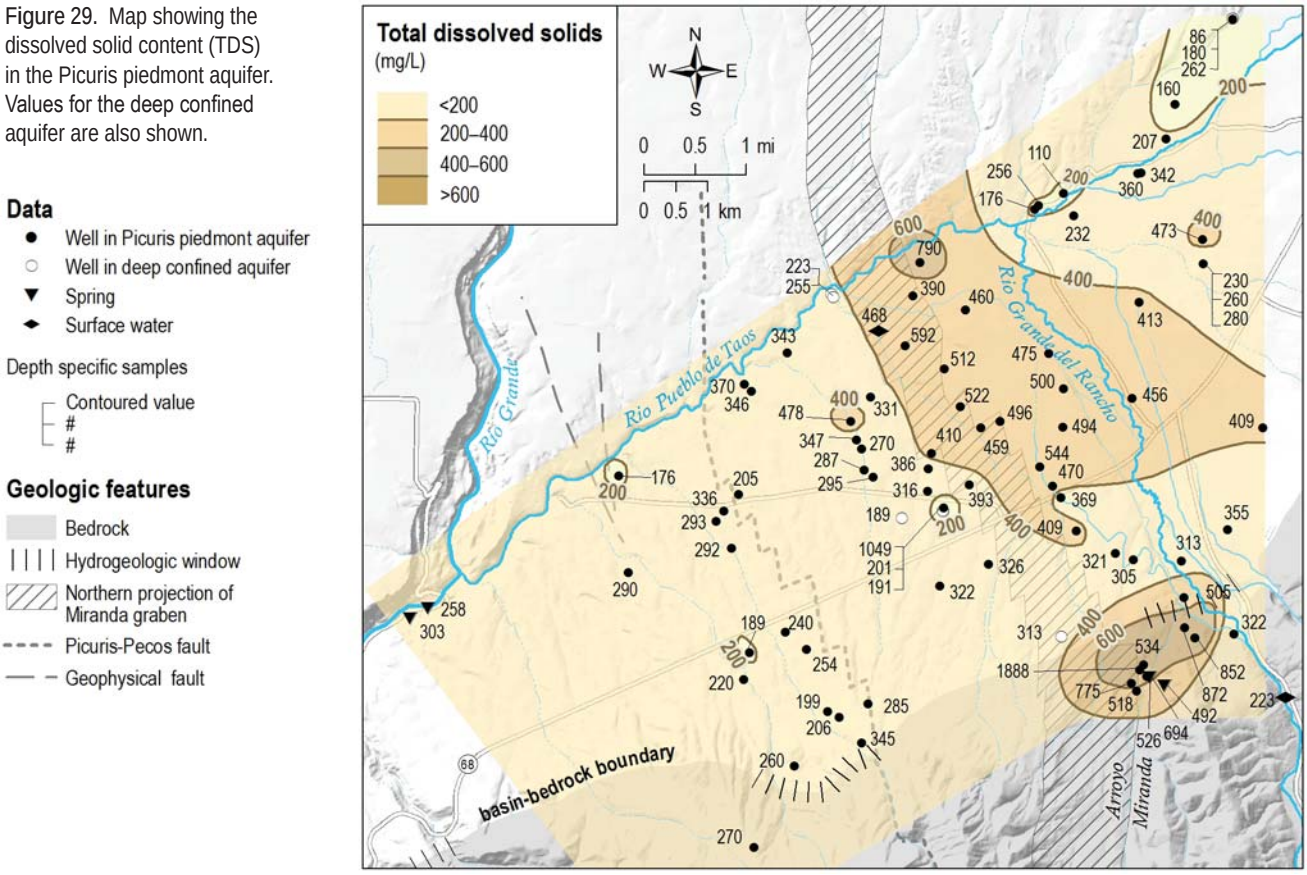

Figure 29. Map showing the dissolved solid content (TDS) in the Picuris piedmont aquifer. Values for the deep confined aquifer are also shown.

highest relative calcium concentrations in groundwater (Ca/Na ratio >3) are found near the Rio Grande del Rancho and the Rio Pueblo. Shallow Ca-rich zones typically indicate the influence of groundwater recharge and flow unaffected by clay-rich sediments. Sodium-rich waters (Ca/Na ratio <1) are limited to solitary wells or well clusters scattered throughout the study area, specifically: the Tierra Blanca neighborhood at NM-68 (TV-103, TV-229, TV-253), the National Guard facilities (TV-218), an area between Los Cordovas and NM-68 (TV-162, TV-261, TV-262, TV-243), a single well near the lower Rio Pueblo (TV-198), and a Rio Grande gorge spring (TS-54). Ponce de Leon hydrothermal water and a basin-margin well near Ponce de Leon (TV-235) have the highest sodium concentrations. Sodium dominates groundwater in the deep confined aquifer (Ca/Na ratio of 0.2 or less), although concentrations of both sodium and dissolved solids are remarkably low. The origins of excess sodium will be discussed further in this section.

Bicarbonate and carbonate—The anion content of groundwater in the southern Taos valley falls into three groups: 1) bicarbonate (HCO_3) or carbonate/bicarbonate (CO_3/HCO_3); 2) a combination of HCO_3, sulfate (SO_4), and chloride (Cl); and 3) a distinctive mixture of strictly SO_4 and Cl. Bicarbonate is the principal anion in groundwater throughout the Picuris piedmont aquifer, where concentrations range from 57 to 425 mg/L with a median of 200 mg/L (Fig. 31; Table 9). The highest HCO_3 values (>200 mg/L) are clustered between Talpa and Los Cordovas, throughout the Rio Grande del Rancho valley. Bicarbonate water is also prevalent in the bedrock aquifers of upper Miranda Canyon and the southern Picuris embayment, but is a minor component in the Ponce de Leon hydrothermal system. Groundwater in the deep confined aquifer is a mixture of HCO_3, CO_3, and SO_4.

The carbonate balance, or carbonate equilibrium, is one of the primary and most complex natural chemical reactions in groundwater that controls water chemistry. It dictates the relative concentrations of the dissolved carbonates (HCO_3^- and CO_3^{2-}) in groundwater, which vary with the pH, temperature, and the amount of carbon dioxide dissolved in the water. When considering the carbonate balance, there are two distinct cases: 1) systems open to the atmosphere, which include carbon dioxide, such as the unconfined Picuris piedmont aquifer; and 2) systems

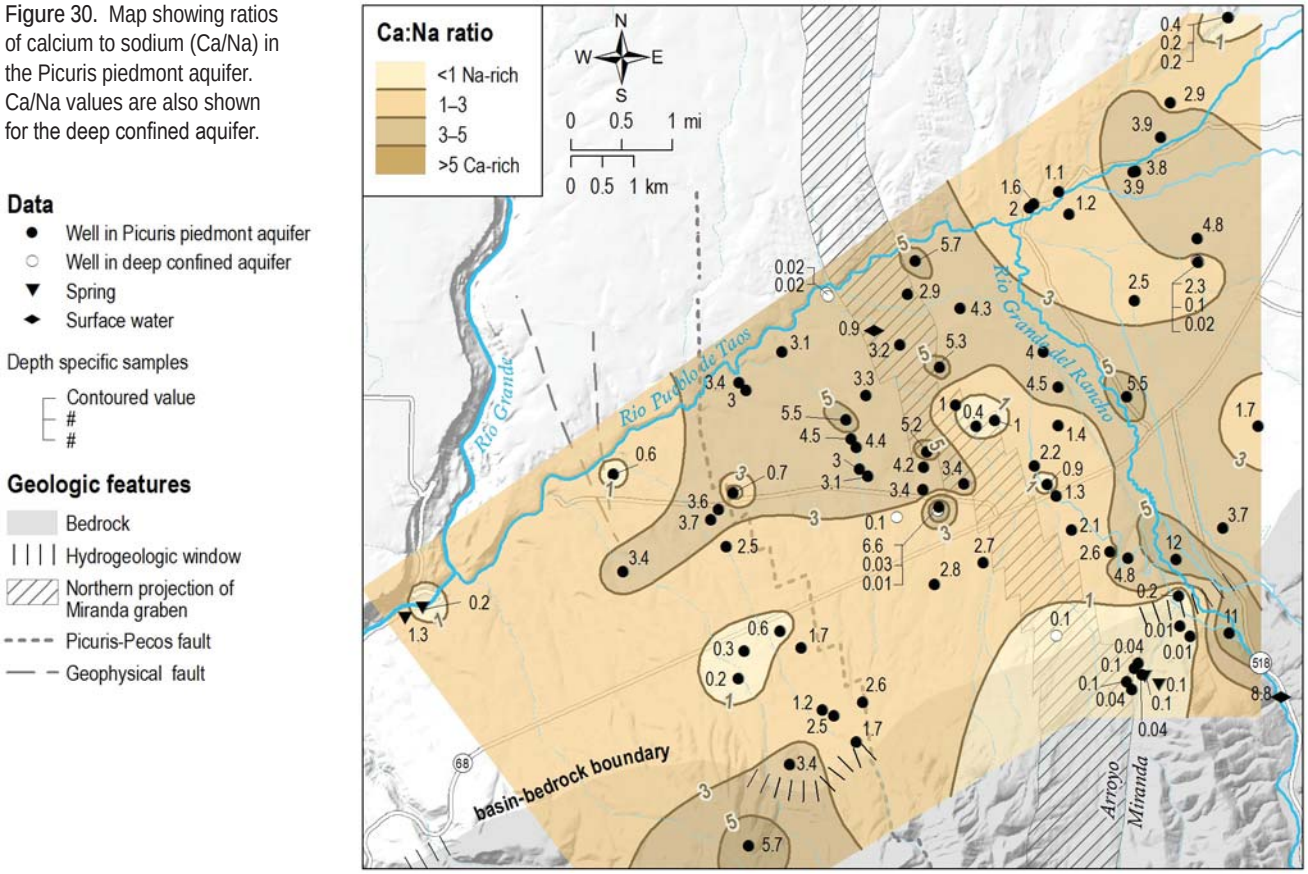

Figure 30. Map showing ratios of calcium to sodium (Ca/Na) in the Picuris piedmont aquifer. Ca/Na values are also shown for the deep confined aquifer.

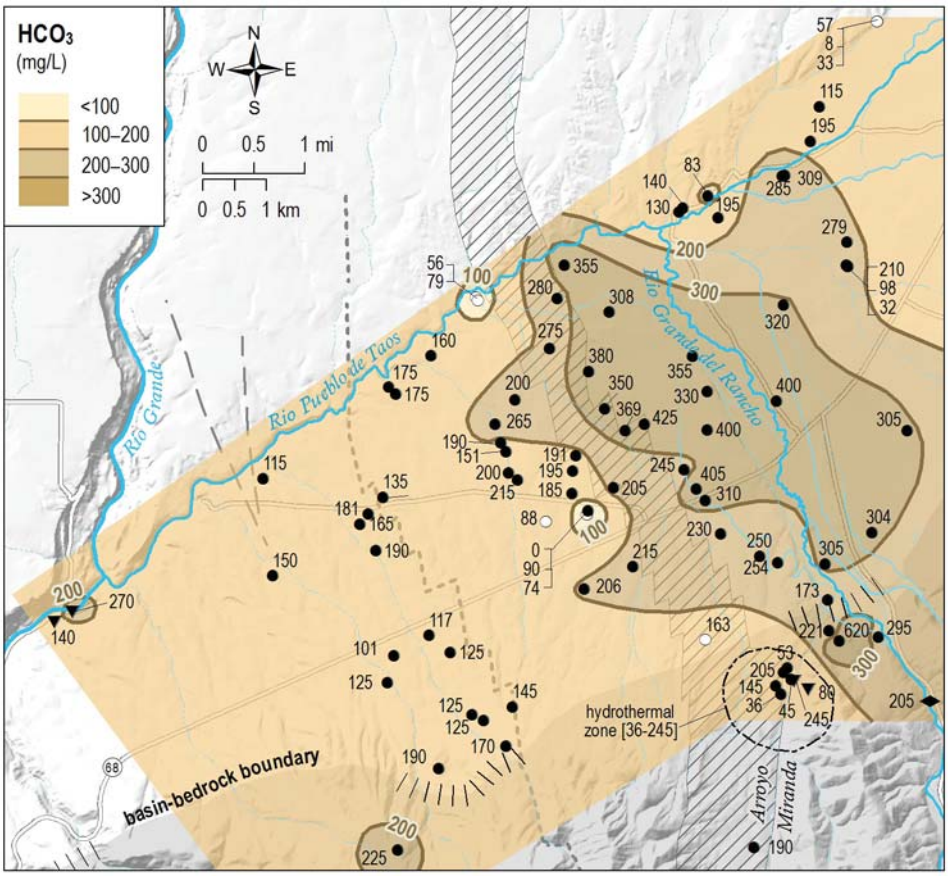

Figure 31. Map showing bicarbonate (HCO_3) in the Picuris piedmont aquifer. HCO_3 values are also shown for the deep confined aquifer.

closed to the atmosphere, such as the deep confined aquifer. At a pH of 10.3, the HCO_3^- and CO_3^{2-} contents are equal. At a pH greater than 10.3, CO_3^{2-} is predominant whereas HCO_3^- is more abundant at pH less than 10.3. In the Picuris piedmont aquifer the pH is fairly uniform between 7.1 and 8.3. In the bedrock aquifers pH ranges from 6.8 to 9.2, and in the deep confined aquifer, 7.9 to 10.1 (Table 9). Carbonate equilibrium is discussed in a following section on mineral precipitation.

Sulfate and chloride—Sulfate and chloride are fairly significant components of groundwater throughout the Picuris piedmont aquifer, where sulfate concentrations range from 9 to 310 mg/L and chloride ranges from 2 to 67 mg/L (Figs. 32 and 33; Table 9). Sulfate concentrations over 40 mg/L and chloride concentrations over 10 mg/L affect much of the area. The two anions also display very similar spatial patterns, with the highest concentrations appearing in the Ponce de Leon hydrothermal system (140 to 715 mg/L SO_4 and 105 to 415 mg/L Cl). Surface flow down Miranda Creek carries thermal Na-SO_4-Cl waters into the shallow Picuris piedmont aquifer where they were detected in a shallow basin-fill well (TV-235 next to the stream). The Ponce de Leon thermal waters also appear to generate plumes of SO_4 and Cl in the aquifer that extend northwest from Ponce de Leon toward the Rio Pueblo and the Town of Taos well field, on a trend that overlaps with the northern projection of the Miranda graben (Figs. 32 and 33). Low concentrations appear in the bedrock aquifers of upper Miranda Canyon and the Picuris embayment (2–17 mg/L SO_4 and 2–7 mg/L Cl). In the deep confined aquifer, SO_4 and Cl concentrations are relatively low (9–104 mg/L SO_4 and 2–29 mg/L Cl), although sulfate is the predominant anion in deep wells east of the Rio Grande del Rancho and secondary in deep wells west of the Rio Grande. High chloride occurs in only one deep well at the northeast corner of the study area (TV-292).

Piper diagrams and ion plots—Quantitative plots of the proportions of major cations and anions in water are shown on Piper diagrams. The Piper plots in Figures 34–36 illustrate water type and major ion chemistry for the three aquifers of the southern Taos Valley and compliment the spatial figures of ion distribution (Figs. 30–33). The important conclusions that can be derived from multiple analyses plotted

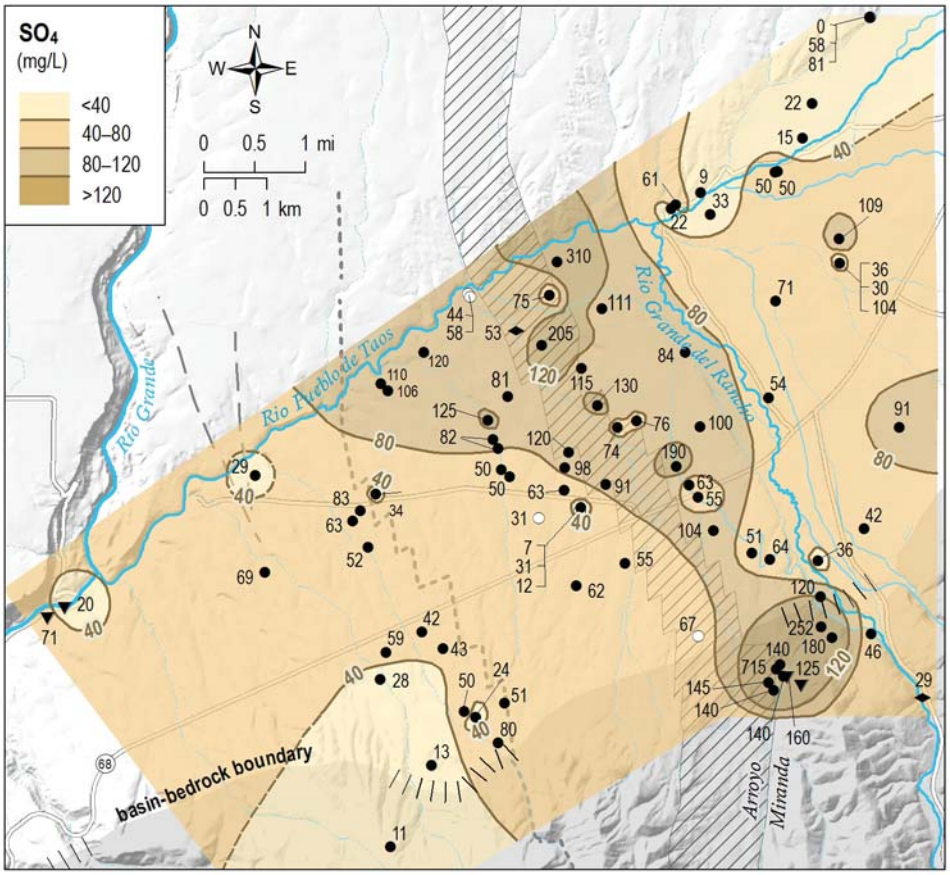

Figure 32. Map showing the distribution of sulfate (SO_4) in the Picuris piedmont aquifer. SO_4 values are also shown for the deep confined aquifer.

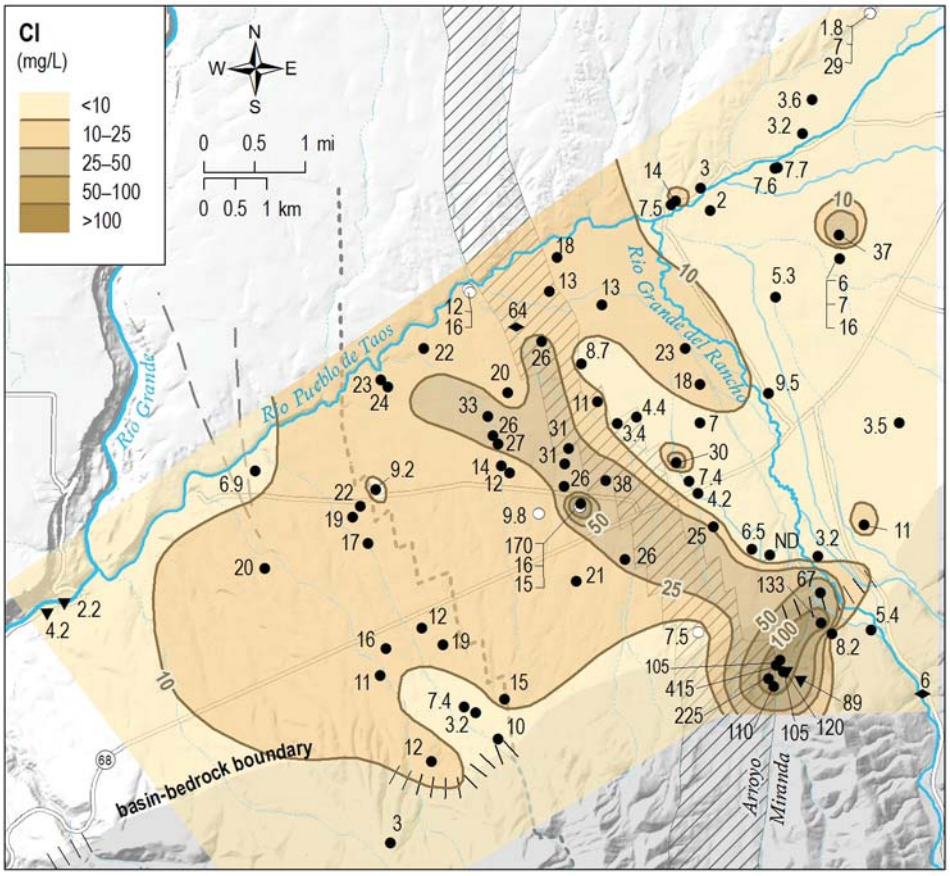

Figure 33. Map showing the distribution of chloride (Cl) in the Picuris piedmont aquifer. Cl values are also shown for the deep confined aquifer.

on a Piper diagram include: 1) water type; 2) ion exchange; 3) mixing of different sources and types of water; and 4) mineral precipitation or dissolution. These Piper diagrams show that complex chemical interactions involving multiple processes—ion exchange, mixing, and mineral precipitation and dissolution—affect the chemical characteristics of groundwater in all three aquifers. The Piper diagrams and ion distribution maps also advance our understanding of how groundwater moves through and between these remarkably complex hydrologic systems.

Bedrock aquifers—The Piper diagram for the bedrock aquifers shows three primary water types. In order of decreasing aquifer elevation, these include: 1) cold Ca-HCO_3 water from upper Miranda Canyon and the Picuris embayment; 2) Na-HCO_3 hydrothermal water from the Picuris Formation in lower Miranda Canyon; and 3) Na-Cl-SO_4 and Na-SO_4-Cl water from the Ponce de Leon hydrothermal system (Fig. 34). Two water samples from the Picuris Formation and Pennsylvanian rocks below Ponce de Leon have added SO_4 (TV-207) and SO_4-Cl (TV-201) and plot between hydrothermal waters from Ponce de Leon and lower Miranda Canyon. The two samples might represent mixtures of hydrothermal waters discharging in lower Miranda Canyon and at Ponce de Leon, as implied by the potential mixing lines in Figure 34. The proportions of end members mixed in well TV-201 below Ponce de Leon are estimated to be 28–34% from lower Miranda Canyon and 66–72% from Ponce de Leon. However, because the mixing lines do not exhibit the same proportions or trends throughout the Piper diagram, more

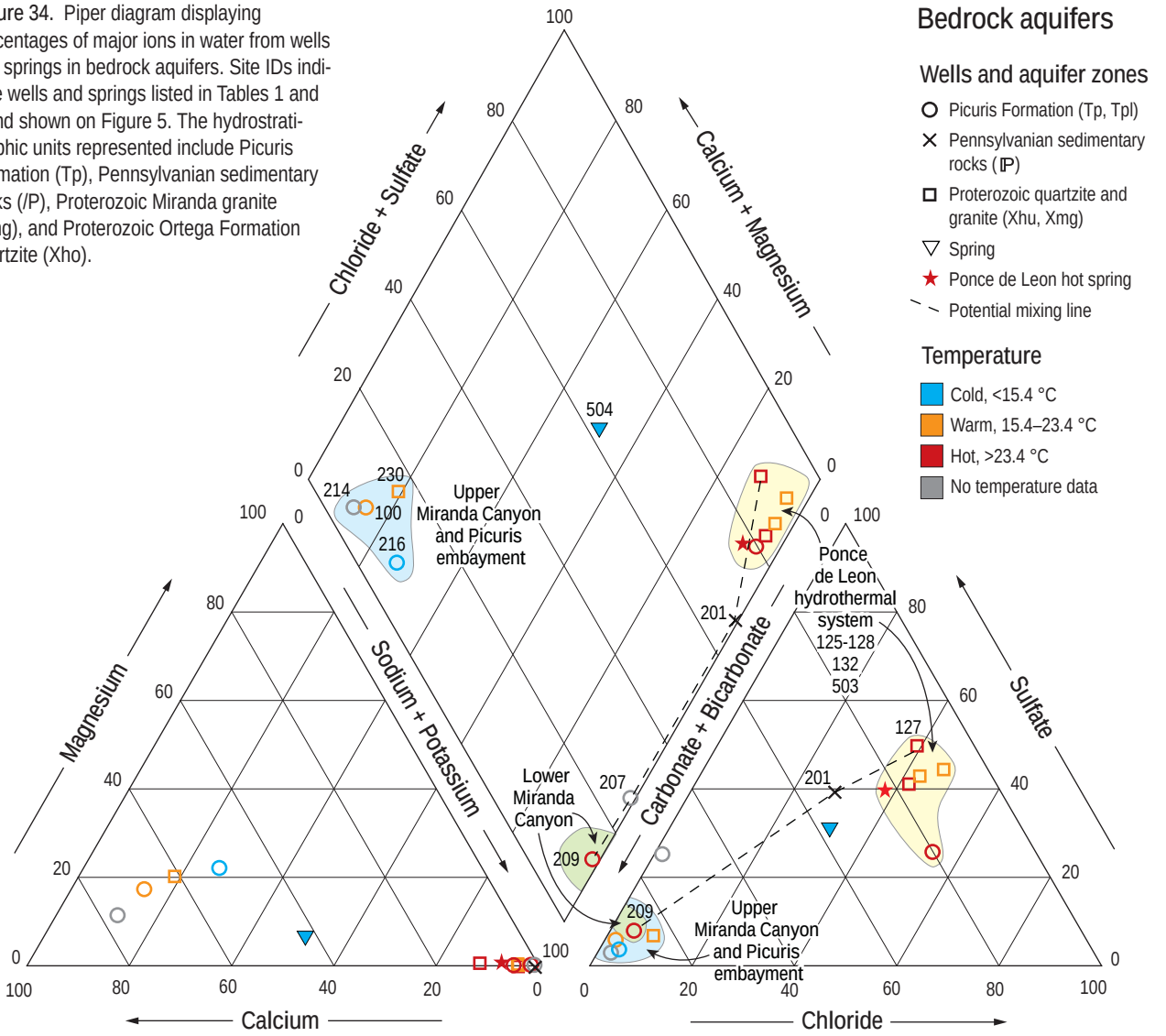

Figure 34. Piper diagram displaying percentages of major ions in water from wells and springs in bedrock aquifers. Site IDs indicate wells and springs listed in Tables 1 and 2 and shown on Figure 5. The hydrostratigraphic units represented include Picuris Formation (Tp), Pennsylvanian sedimentary rocks (/P), Proterozoic Miranda granite (Xmg), and Proterozoic Ortega Formation quartzite (Xho).

complex interactions than simple mixing are indicated, including mixing more than two water sources and mineral solution and precipitation.

Picuris piedmont aquifer—The Piper diagram for the Picuris piedmont aquifer shows one primary water type, Ca-HCO_3, from streams and a few adjacent shallow wells (TV-142, TV-247, TV-250, TV-251, TV-264, TV-265, TV-268) (Fig. 35, left corner of the diamond). This water type is typical of precipitation and recharge from streams and arroyos. The majority of groundwater samples from the piedmont aquifer contain added sodium, sulfate and chloride in small to large amounts. Wells showing the highest Na and SO_4 are situated near the northern projections of Picuris-Pecos bedrock faults (Fig. 18). These include: 1) TV-103, TV-229 and TV-253 in the Tierra Blanca neighborhood at NM-68, near the projected Picuris Pecos bedrock fault and the Embudo fault; 2) TV-198, near the lower Rio Pueblo geophysical fault; 3) TV-188, north of county road 570 near the projected Picuris-Pecos bedrock fault; and 4) TV-162, near the northern projection of the Miranda graben bounding faults. Well TV-235, a 220-foot-deep well situated near Miranda Creek at the Ponce de Leon hydrogeologic window, has the highest Cl level and chemical characteristics similar to the hydrothermal waters. The elevated SO_4 and Cl stem from inflow of hydrothermal waters through the Ponce de Leon hydrogeologic window and upward migration along the Picuris-Pecos basement faults into the Santa Fe Group aquifers.

Deep confined aquifer—The Piper diagram for the deep confined aquifer shows that all wells in the deep aquifer have an ion chemistry intermediate

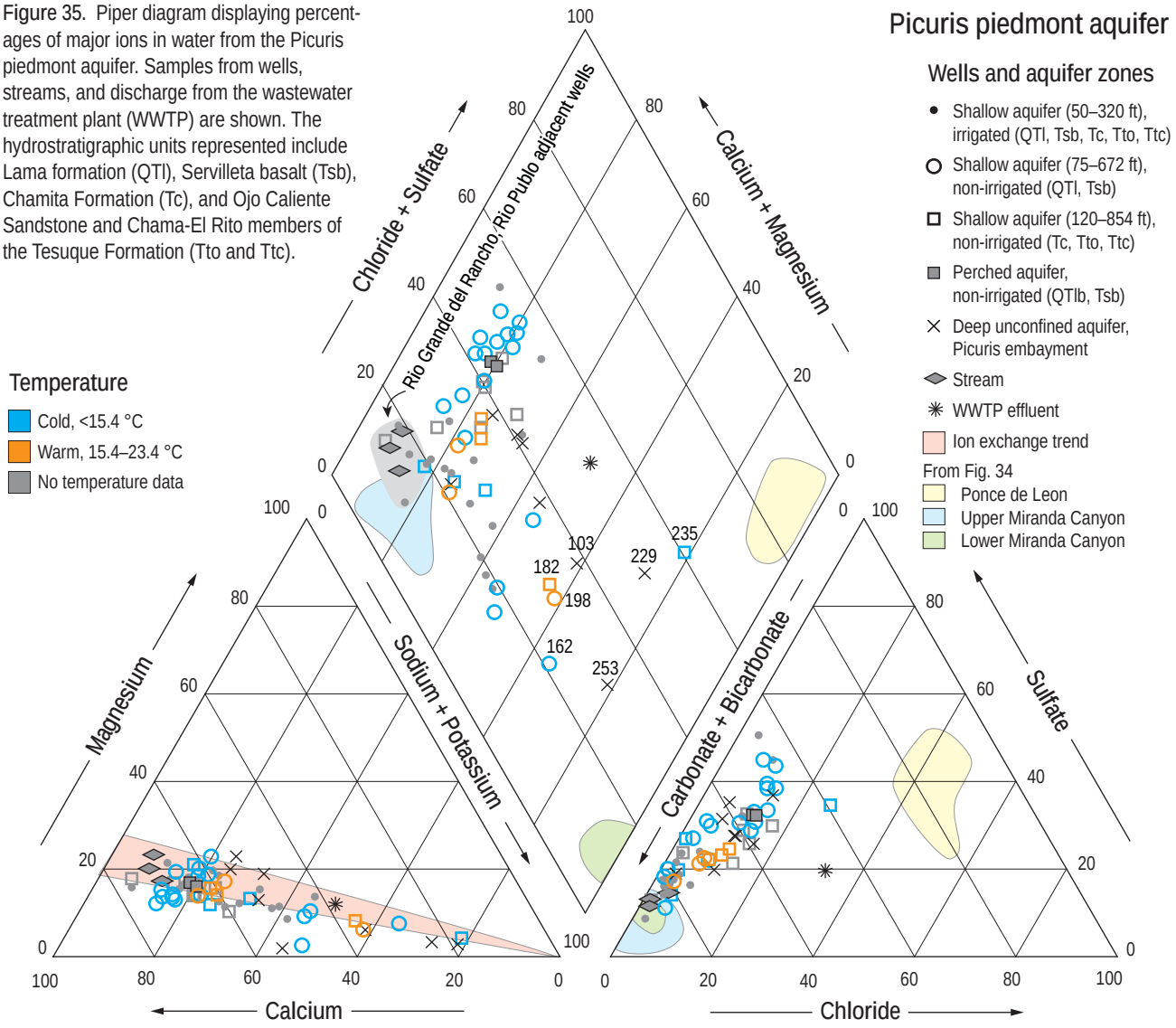

Figure 35. Piper diagram displaying percentages of major ions in water from the Picuris piedmont aquifer. Samples from wells, streams, and discharge from the wastewater treatment plant (WWTP) are shown. The hydrostratigraphic units represented include Lama formation (QTl), Servilleta basalt (Tsb), Chamita Formation (Tc), and Ojo Caliente Sandstone and Chama-El Rito members of the Tesuque Formation (Tto and Ttc).

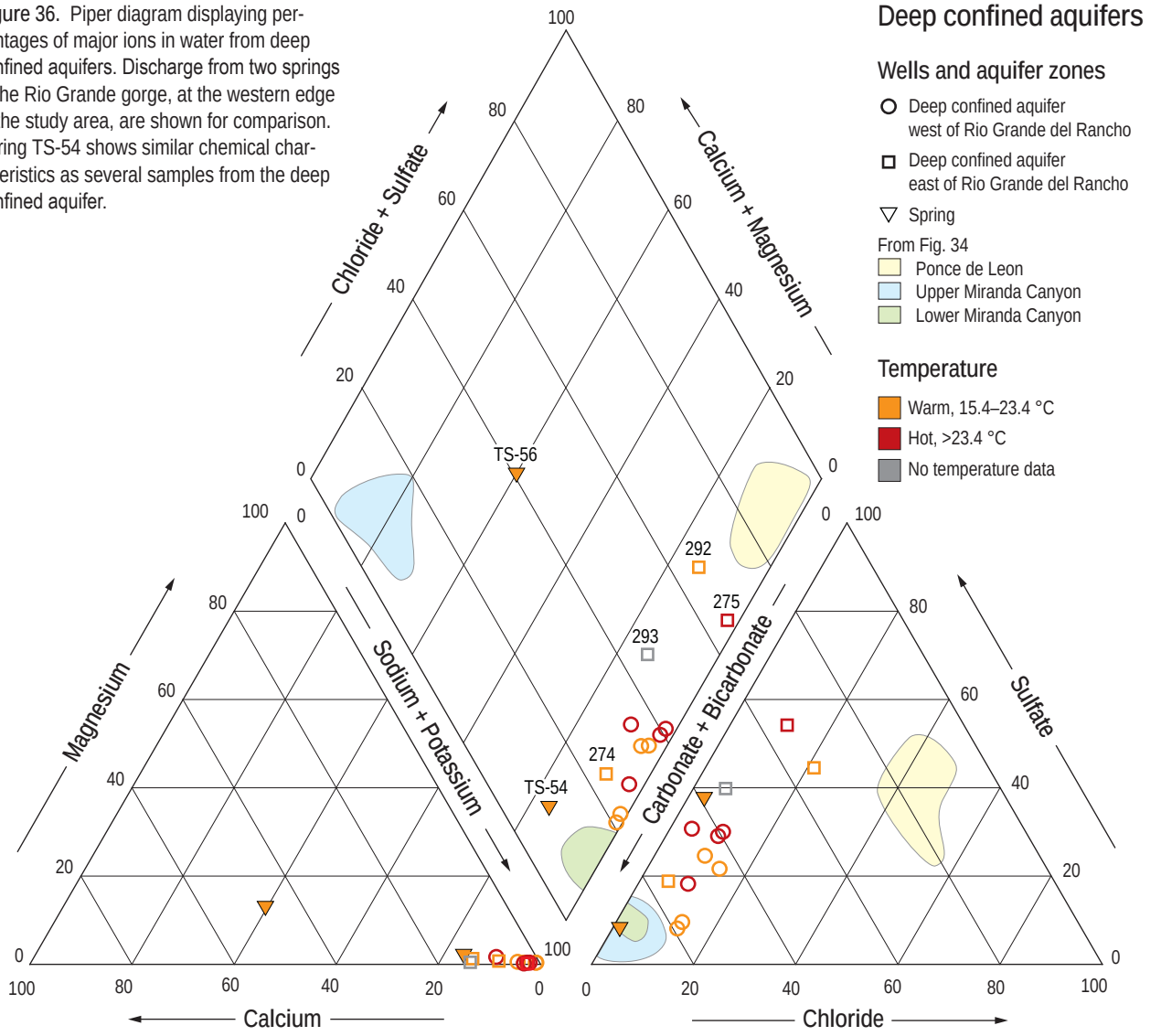

Figure 36. Piper diagram displaying percentages of major ions in water from deep confined aquifers. Discharge from two springs in the Rio Grande gorge, at the western edge of the study area, are shown for comparison. Spring TS-54 shows similar chemical characteristics as several samples from the deep confined aquifer.

between waters of the Ponce de Leon hydrothermal system (Na-SO_4-Cl) and shallow groundwater in lower Miranda Canyon (Na-HCO_3) (Fig. 36). Similar to examples from the bedrock aquifers discussed above, these intermediate ion compositions indicate that the deep confined aquifer is affected by mixing of hydrothermal water from deep upflow along Picuris-Pecos bedrock faults and possibly through the Ponce de Leon hydrogeologic window. East of the Miranda bedrock fault, upward migrating thermal waters pass through Pennsylvanian carbonate and evaporite rocks before entering the deep confined aquifer. These highly soluble rocks contain Ca, CO_3, Na, Cl and SO_4 that can further affect shallow water chemistry and may explain higher Cl concentrations in deep aquifers east of the Rio Grande del Rancho. Spring discharge from TS-54 in the Rio Grande gorge shows similar chemical characteristics as several samples from the deep confined aquifer.

Explaining sodium excess and water sources—The Piper diagram for the Picuris piedmont aquifer (Fig. 35) shows a trend in the cation (left) triangle between Ca-HCO_3 and Ca-Mg-HCO_3 waters and $NaHCO_3$ waters, which often represents the replacement of Ca and Mg in solution by Na with no change in anion content, known as cation exchange. The gray band depicts the region of the Piper diagram in which Ca-type waters (for example, surface waters of the Rio Grande del Rancho and adjacent shallow groundwater) evolving to Na as a result of cation exchange will plot. Many waters from the Picuris piedmont aquifer fall within the cation-exchange region, including shallow groundwater within both irrigated and

non-irrigated lands, perched groundwater, and deep unconfined groundwater in the Picuris embayment. Sodium enrichment in these samples might result from cation exchange where there is no addition of SO_4 or Cl. However, several samples from all aquifer zones except perched groundwater fall outside of the cation-exchange region and most samples have added SO_4 and Cl, suggesting that the source of sodium enrichment in the Picuris piedmont aquifer results from some process other than cation exchange. Based on chemical trends and the hydrogeologic conceptual model, the most compelling explanations are: 1) mixing of Na-SO_4-Cl thermal waters from the Ponce de Leon hydrothermal system with shallow stream-connected groundwater; 2) upflow of deeply circulating, Na-SO_4-Cl thermal waters along the Picuris-Pecos bedrock faults directly into Santa Fe Group aquifers; and 3) dissolution of Pennsylvanian carbonate rocks by thermal waters during fault-controlled upflow. The dissolution of carbonate and evaporite rocks by upward-migrating hydrothermal waters can explain the more exotic water chemistry encountered east of the Rio Grande del Rancho in the Karavas #2 exploration well (TV-292 through 297) and BOR #2 exploration well (TV-273 through 275) and west of the Rio Grande del Rancho in the UNM, BOR #1, and National Guard wells (TV-152, 217, 218, 219) (see Figs. 28, 30–36; Table 9; and Appendix 3).

Minor ions, trace elements and mineral saturation

Fluoride—In the Picuris piedmont aquifer, fluoride ranges from 0.1 to 15 mg/L, but is typically less than 1 mg/L (Fig. 37). The highest concentrations in the area appear in the Ponce de Leon hydrothermal system (4.4 to 20 mg/L). The highest level detected in the shallow aquifer (15 mg/L) was measured in a shallow basin-fill well next to Miranda Creek (TV-235), which carries discharge from the Ponce de Leon hot spring. The fluoride plume from thermal water appears to travel into the basin as far as Llano Quemado. Several wells with low concentrations (0.8 to 1.4 mg/L) lie west and northwest of Llano Quemado, along the eastern boundary of the Miranda graben. Fluoride levels above the maximum contaminant level (MCL) of 4 mg/L have also been reported in the deep confined aquifer east of the Rio Grande del Rancho valley (TV-292 and TV-275) and on the Picuris piedmont northwest of Ponce de Leon (TV-301).

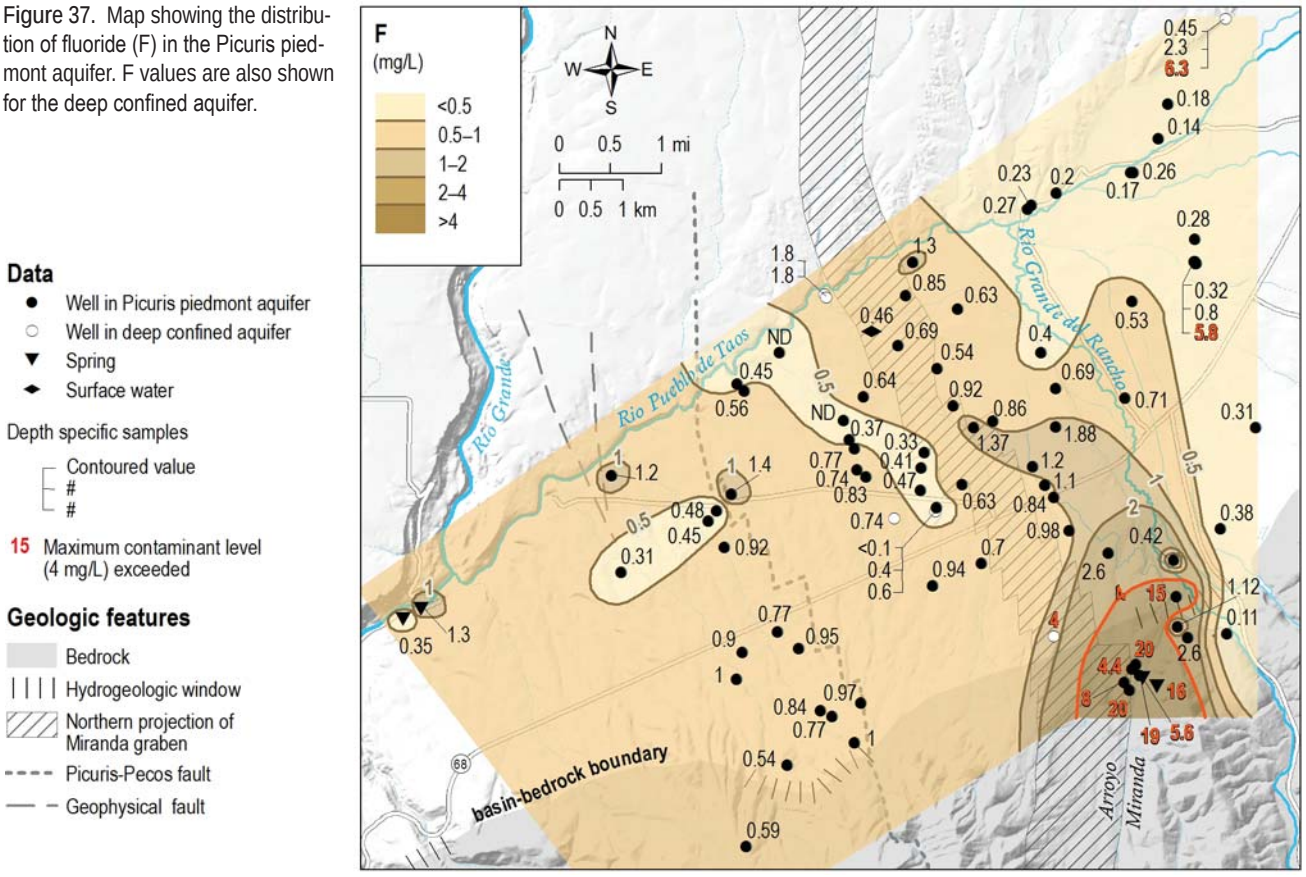

Figure 37. Map showing the distribution of fluoride (F) in the Picuris piedmont aquifer. F values are also shown for the deep confined aquifer.

Fluoride is brought into groundwater by leaching from minerals in the rocks. Fluoride equilibrium with the mineral fluorite (CaF2) controls its concentration in groundwater (Appelo and Postma, 2007). This means that water with a high natural Ca concentration will generally contain low fluoride, whereas groundwater with a low Ca concentration (hence a high Na concentration) will be rich in fluoride. High fluoride is often associated with thermal waters having both high sodium and high pH (Hem, 1992). This is true for the southern Taos Valley where high fluoride concentrations exist in calcium-poor, sodium-rich Ponce de Leon thermal waters and concentrations are reduced downstream by mixing with Ca-rich water from stream recharge in the Rio Grande del Rancho Valley (Fig. 37).

***Trace elements*—**Several trace elements were detected in the aquifers of the southern Taos Valley but few occur at levels of concern. Data show that three elements were detected in groundwater of the Picuris piedmont or deep confined aquifer at levels above the MCL or a health advisory for drinking water (Table 10). These are arsenic (As, MCL 0.01 mg/L), lead (Pb, action level 0.015 mg/L), and uranium (U, MCL 0.03 mg/L). In the Picuris piedmont aquifer, 0.059 mg/L lead was detected at TV-218 (the BOR-1 observation well), and U was detected in two domestic wells, TV-239 and TV-250, at levels equivalent to the MCL. Several trace elements were also detected in many or most wells in the piedmont aquifer at low to moderate levels below the MCL (see Table 10), including: arsenic (As), barium (Ba), chromium (Cr), copper (Cu), nickel (Ni), strontium (Sr), uranium (U), vanadium (V), and zinc (Zn). The highest concentrations of copper, uranium, vanadium and zinc are observed in the Picuris embayment and the Miranda graben, and to a lesser extent in the Ranchito artesian zone (Fig. 21) along the upper Rio Pueblo between Ranchito and its confluence with the Rio Grande del Rancho. The prevalence of such a large number of trace elements at moderate levels, over a large scale, is remarkable, and suggests that upward migration of hydrothermal waters along the Picuris-Pecos basement faults and into the Picuris piedmont aquifer has a significant negative impact on the water quality.

In the deep confined aquifer, arsenic was reported at levels above the MCL in 7 of 10 wells, including Town of Taos production and exploration wells (TV-170, TV-171), the UNM well (TV-152), the BOR-1 exploration well (TV-217), the BOR-2 exploration wells (TV-274, TV-275), and a mutual domestic exploration well (TV-301). Lead was also reported in BOR-2 (TV-274) above the MCL. No trace elements were detected in bedrock aquifers, including Ponce de Leon thermal waters, above water standards.

Groundwater Residence Time

The "age" or residence time of groundwater is evaluated using radiocarbon (^{14}C) dating of dissolved inorganic carbon and the tritium (^{3}H) content of water. ^{14}C is used to detect groundwater with a residence time of several 100s to many 1,000s of years. The presence of ^{3}H in water indicates recharge within the last 50 years. By measuring both the ^{14}C activity and ^{3}H content in groundwater we can estimate how long groundwater has resided in the aquifer and detect whether the water represents a mixture of surface and deep sources. In some geologic settings, chemical interactions between dissolved carbonate and carbonate- or organic-rich sediments in the aquifer can dilute the amount of ^{14}C measured in a water sample, and provide an anomalously old age. No corrections for geochemical effects were completed for this study and results are reported as an "apparent radiocarbon age," which presumes that no hydro-geochemical effects have altered the ^{14}C content.

In summary, the youngest groundwater (^{3}H contents greater than or equal to 2 TU) is found: 1) throughout the valleys and irrigated lands adjacent to the Rio Grande del Rancho and the Rio Pueblo de Taos; 2) in bedrock aquifers in the mid to upper Picuris Mountains; and 3) in the cold spring at the head of Miranda Creek in Ponce de Leon (TV-504). Groundwater with the longest residence time (18,850 to 26,440 RCYBP) is found in: 1) thermal artesian wells in the Proterozoic granite and quartzite in Ponce de Leon (TV-125 and TV-126); 2) spring discharge of deep groundwater on the eastern wall of the Rio Grande (TS-54); and 3) the deep confined aquifer (TV-152, TV-170, and TV-171). See Figure 38 and Table 11.

Assessing the ^{3}H results from both groundwater and surface water, and weighing the combined ^{3}H and ^{14}C results, is informative. Stream-connected groundwater in the Picuris piedmont aquifer has ^{3}H contents of 6.7 to 8.8 TU and ^{14}C ages of 0 to 760 years, while stream waters from the Rio Grande del Rancho and the Rio Pueblo have tritium contents of 8.4 and 6.6 TU, respectively. The ^{3}H values indicate that most shallow groundwater in the valleys and irrigated lands has a residence time of less than 3.5 years,

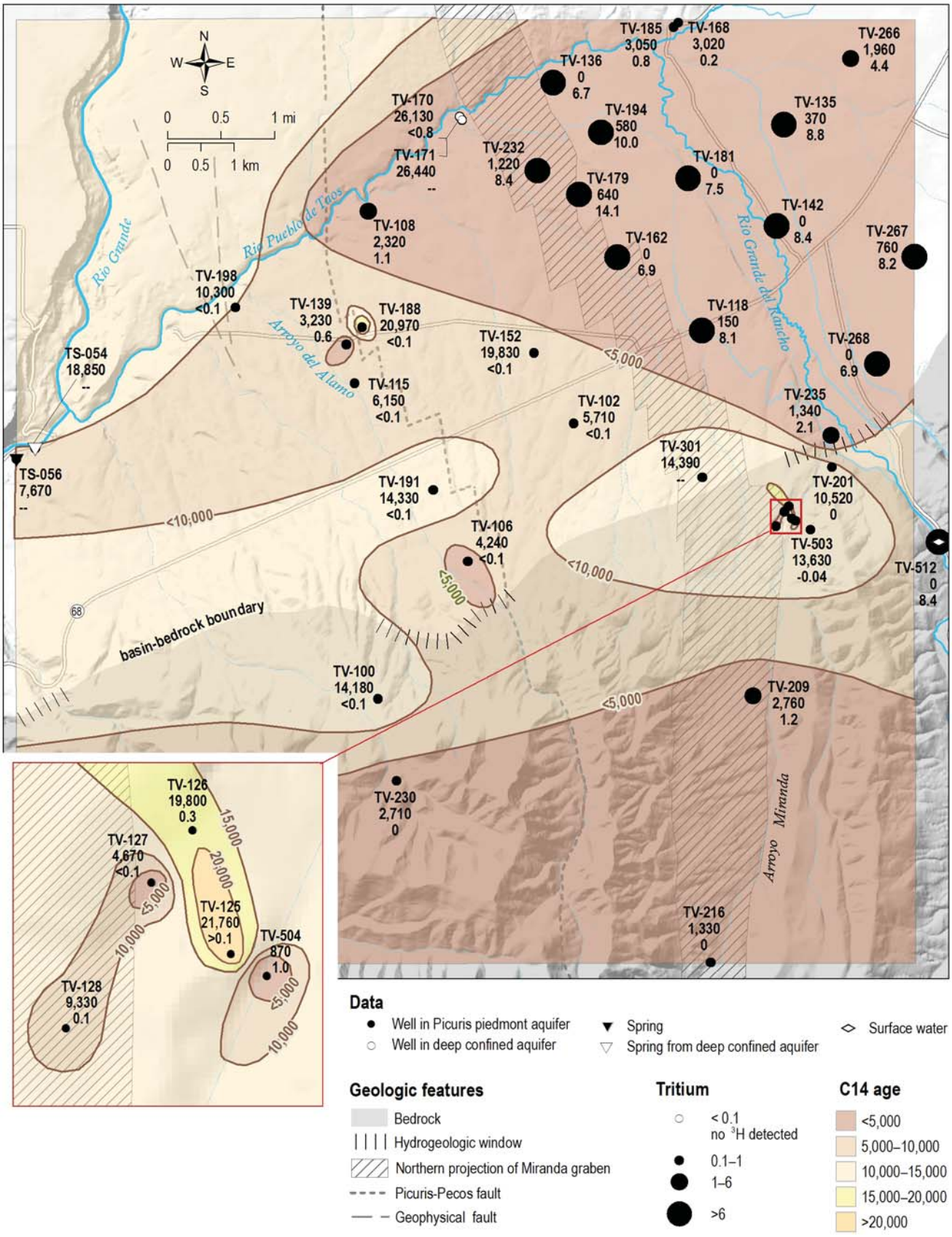

Figure 38. Map showing the apparent ^{14}C age (RCYBP) and tritium content (^{3}H in tritium units, TU) in the Picuris piedmont aquifer. Values are also shown for the deep confined aquifer.

Table 11. Radiocarbon and tritium data showing groundwater residence time in Taos Valley aquifers (see Fig. 38).

Site ID	Site type	Well depth	^{3}H (TU)*	δ^{13}C (‰)	^{14}C activity (pmC)	^{14}C apparent age (RCYBP)	^{14}C age standard error (±RCYBP)
TV-100	GW	1000	0.03	-12.8	17.1	14,180	60
TV-102	GW	460	0.02	-13.9	49.1	5,710	30
TV-106	GW	972	0.05	-13.8	59.0	4,240	30
TV-108	GW	185	1.07	-10.1	74.9	2,320	30
TV-115	GW	600	0.01	-11.7	46.5	6,150	40
TV-118	GW	175	8.05	-14	98.2	150	30
TV-125	GW	280	0.02	-13.8	6.7	21,760	90
TV-126	GW	420	0.34	-10.7	8.5	19,800	80
TV-127	GW	400	0.07	-9.8	55.9	4,670	30
TV-128	GW	500	0.11	-11	31.3	9,330	40
TV-135	GW	112	8.78	-12.4	95.5	370	30
TV-136	GW	122	6.73	-13.1	101.6	0	0.4 pmc
TV-139	GW	400	0.61	-12.1	66.9	3,230	30
TV-142	GW	65	8.35	-13	107.1	0	0.3 pmc
TV-152	GW	1200	0.05	-13.7	8.5	19,830	70
TV-162	GW	160	6.91	-14.4	108.6	0	0.3 pmc
TV-168	GW	50	0.18	-13.3	68.7	3,020	30
TV-170	GW	2527	<0.8	-12.4	3.9	26,130	140
TV-171	GW	3180	--	-10.9	3.7	26,440	140
TV-179	GW	180	14.1	-11.5	92.3	640	30
TV-181	GW	150	7.49	-13	103.6	0	0.3 pmc
TV-185	GW	180	0.79	-15.2	68.4	3,050	30
TV-188	GW	395	0.03	-11.8	7.4	20,970	90
TV-191	GW	1002	0.03	-12.4	16.8	14,330	70
TV-194	GW	100	10	-12.3	93.0	580	30
TV-198	GW	480	0.07	-12.9	27.7	10,300	40
TV-201	GW	260	0	-21.2	27.0	10,520	40
TV-209	GW	295	1.2	-11	70.9	2,760	30
TV-216	GW	420	0	-12.5	84.7	1,330	30
TV-230	GW	1400	0	-17.9	71.4	2,710	30
TV-232	GW	120	8.35	-10.1	85.9	1,220	30
TV-235	GW	220	2.09	-18.1	84.6	1,340	30
TV-266	GW	75	4.39	-11.7	78.4	1,960	30
TV-267	GW	182	8.21	-12.5	91.0	760	30
TV-268	GW	215	6.94	-13.3	106.2	0	0.3 pmc
TV-301	GW	1185	--	-11.1	16.7	14,390	--
TV-503	SP		0	-11.7	18.3	13,630	100
TV-504	SP		0.99	-16.2	89.7	870	50
TS-054	SP		--	-8.37	9.6	18,850	50
TS-056	SP		--	-11.4	38.5	7,670	30
TV-512	PS		8.37	--	--	--	--
TV-513	PS		6.61	--	--	--	--
TV-514	PS		8.02	--	--	--	--
			SUMMARY STATISTICS FOR GROUNDWATER				
		MIN	0	-21.2	3.72	0	
		MAX	14.1	-8.4	108.56	26,440	
		MEAN	0.6	-12.5	67.7	3,140	

GW—groundwater; SP—spring; PS—perennial spring; S—Stream; TS-512—Rio Grande del Rancho; TS-513—Rio Pueblo; TS-514—Rio Lucero; ‰—per mil (parts per thousand); TU—tritum units; * Standard analytical error for ^{3}H in all samples is 0.09 TU. Results less than 0.1 TU are effectively below the method detection limit and are shown as <0.1 TU; pmC—percent modern carbon; RCYBP = radiocarbon years before present (1950), Cambridge half-life 5,730 ±40 yr;

and in some cases has been replenished by streams and irrigation within a single year (TV-142, TV-135, TV-136, and TV-232). Wells far from streams that have a stream-equivalent (or slightly lower) tritium content and ^{14}C ages of a few hundred years indicate minor mixing with older groundwater. Shallow groundwater in the Ranchito artesian zone (TV-168, TV-185) and in well TV-108 near the lower Rio Pueblo has older ^{14}C ages (2,320 to 3,050 RCYBP) and low ^{3}H contents (0.2 to 1.1 TU), indicating a mixture of older groundwater and stream water.

Groundwater in the Picuris piedmont aquifer, outside of stream valleys, shows a wide range of ^{14}C ages, from 3,230 to 20,970 RCYBP, with ^{3}H undetected. This indicates a mixture of old groundwater with different flow paths and sources of recharge. The results also show some noteworthy spatial patterns and trends:

1. Most wells with depths of 1,000 feet or more sampled in the Picuris piedmont aquifer and lower Picuris Formation south of NM-68 have ^{14}C ages of over 14,000 RCYBP. The exceptions are well TV-106, near the mountain front adjacent to the ephemeral channel of the Arroyo del Alamo, and the shallow well TV-102 in the center of the piedmont. The relatively young ^{14}C age in TV-106 is consistent with active groundwater movement through the Picuris embayment hydrogeologic window, and possibly channel recharge through Arroyo del Alamo.
2. The oldest and youngest waters observed on the piedmont are from two wells along County Road 110 that are adjacent to each other and to the Picuris Pecos fault. TV-139, a 400-foot well completed in the Servilleta basalts and interlayered Lama formation, draws water from the perched groundwater zone and has a ^{14}C age of 3,230 RCYBP. A nearby 395-foot well completed in Chamita Formation sediments below the oldest basalt (TV-188) has a ^{14}C age of 20,970 RCYBP.

Apparent ^{14}C ages for samples from the Picuris piedmont aquifer range from 0 to 20,970 RCYBP and ^{3}H content ranges from 0 to 14.1 tritium units. The oldest waters are from artesian wells drilled into basement rocks (Miranda granite and Ortega quartzite) in the Ponce de Leon hydrothermal system (TV-126 and TV-127). The youngest water is from a cold spring that discharges at the head of perennial flow in Miranda Creek (TV-504). Groundwater from wells in upper Miranda Canyon and a small watershed to the west range from 1,330 to 2,760 RCYBP.

Mineral Solution, Precipitation and Disequilibrium

Minerals dissolve in natural water. A variety of rock materials underlies the Picuris piedmont and deep confined aquifers, including: crystalline granite and metamorphic bedrock, Paleozoic carbonates, evaporites, and organic rich shales, and Tertiary volcanic-rich sediments. Upward migrating thermal water can easily dissolve carbonate, evaporite and volcanic minerals from the Paleozoic and Tertiary sediments and transfer them to the overlying aquifers. As conditions change, the same or other minerals can precipitate and accumulate in pipes, streams, lakes, or aquifers. This is significant for the southern Taos Valley because the concentrations of some metal ions in water—calcium (Ca^{2+}), magnesium (Mg^{2+}), zinc (Zn^{2+}), among others—is controlled by the amount of dissolved carbonate (CO_3), and the solubility of the metal carbonates present in the different aquifers. Because of the diverse physical and chemical conditions in the southern Taos Valley aquifers, precipitation and dissolution reactions may be a significant consideration during groundwater development, particularly from the deep confined aquifer when mixing of deep and shallow waters occurs.

The minerals of concern in this setting are the metal carbonates, which occur as solids ($MeCO_3(s)$) or dissolved in water (Me^{2+} and CO_3^{2-}). Common examples of metal carbonates that could occur in the aquifers of the southern Taos Valley are: $CaCO_3$ (calcium carbonate, the mineral calcite), $SrCO_3$ (strontium carbonate), and $ZnCO_3$ (zinc carbonate, the mineral smithsonite). Whether the metal carbonate occurs in a solid or dissolved state depends on physical and chemical conditions, including concentration of the metal, pH, temperature, and pressure. The conditions that favor a solid or dissolved state are reflected in a factor called the saturation index (SI). We used the geochemical model PHREEQC to calculate the state of saturation of the groundwater sampled in the study area with respect to calcite, aragonite, and dolomite (three calcium-containing carbonate minerals). The results are shown in Table 12, where positive values (highlighted) indicate the water is "oversaturated" and conditions exist for precipitation of solid calcium carbonate from the water. Negative values indicate the water is undersaturated and can dissolve carbonate minerals. Most samples in the Picuris piedmont and deep confined aquifers are oversaturated with respect to calcite. A

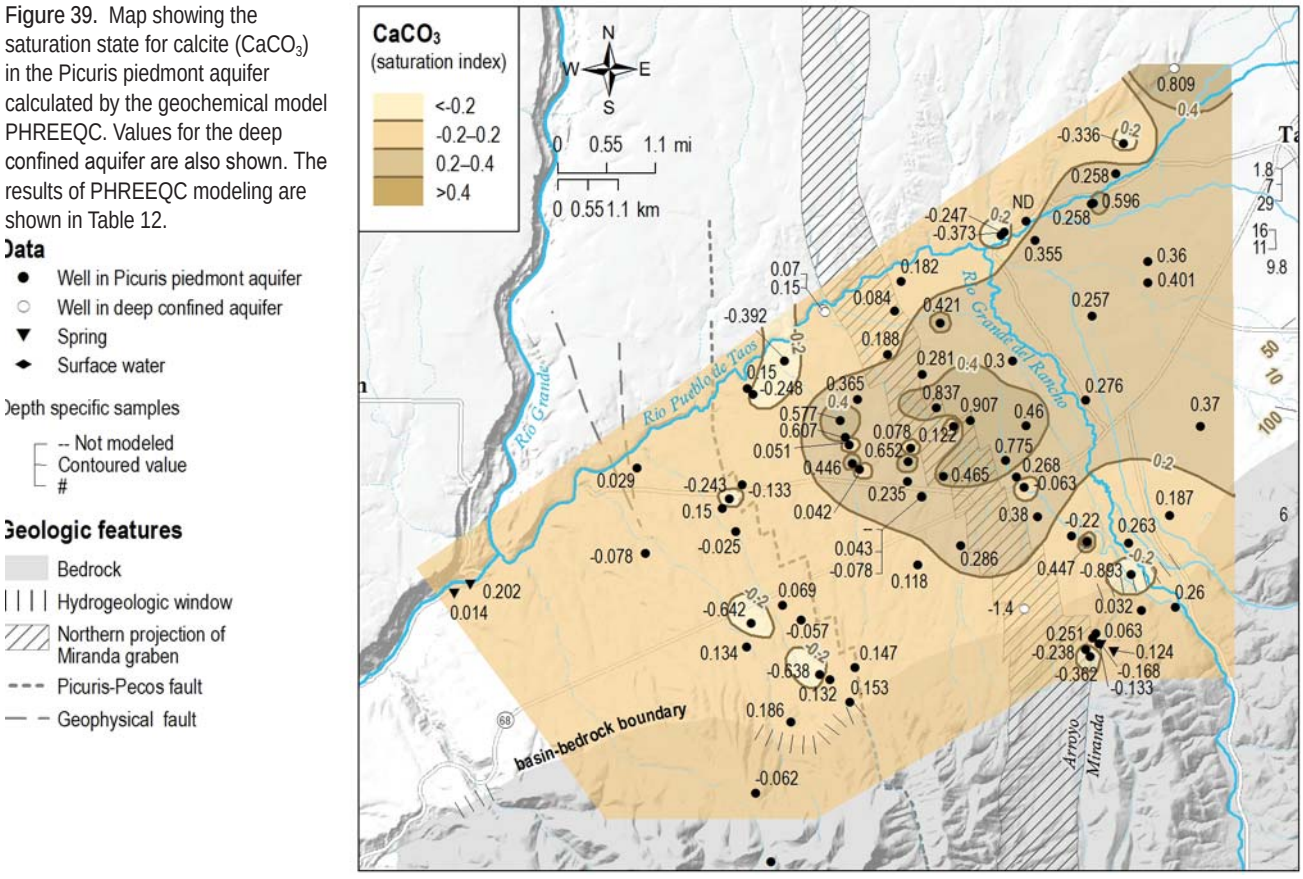

Figure 39. Map showing the saturation state for calcite ($CaCO_3$) in the Picuris piedmont aquifer calculated by the geochemical model PHREEQC. Values for the deep confined aquifer are also shown. The results of PHREEQC modeling are shown in Table 12.

Table 12. Saturation states for carbonate minerals in Taos Valley aquifers calculated by the geochemical model PHREEQC (see Fig. 39).—Continued

												SATURATION INDEX (SI)		
	Sample ID	Water bearing formation	Well depth (ft bls)	Field pH*	Temperature (°C)	Water type	Ca	Na	HCO_3	CO_3	Calcite $CaCO_3$	Aragonite $CaCO_3$	Dolomite $CaMg(CO_3)_2$
SHALLOW PICURIS PIEDMONT AQUIFER	TV-102A	Ttc	460	7.6	15.7	Ca-Na-HCO_3-SO_4	65	27	206	0	0.1176	-0.0331	-0.3528
	TV-103C	Tto	1000	8.2*	nr	Na-Ca-HCO_3-SO_4	22	41	117	1.2	0.0694	-0.078	-0.5581
	TV-104B	Ttc	1080	7.8*	na	Ca-Na-HCO_3-SO_4	47	31	170	0	0.1532	0.0058	-0.0416
	TV-106A	Ttc	972	8.1	18.4	Ca-Mg-Na-HCO_3	28	13	125	0	0.1315	-0.0171	-0.0542
	TV-107C	Ttc	955	7.2*	nr	Ca-Na-HCO_3-SO_4	40	37	125	0	-0.6384	-0.7858	-2.662
	TV-108A	QTlb	185	7.7	13.4	Ca-Mg-HCO_3-SO_4	75	25	175	0	0.1498	-0.0027	-0.2166
	TV-115A	Tc	600	7.5	17.0	Ca-Na-HCO_3-SO_4	59	27	190	0	-0.0253	-0.175	-0.6625
	TV-118A	Tc	175	7.3	13.2	Ca-Na-HCO_3	63	55	310	0	-0.0631	-0.2157	-0.8036
	TV-121C	QTlb, Tsb	215	7.2*	nr	Ca-Na-HCO_3-SO_4	76	29	175	0	-0.2477	-0.3952	-0.9364
	TV-135A	QTl	112	7.5	12.1	Ca-Na-HCO_3-SO_4	88	40	320	0	0.2573	0.1038	-0.039
	TV-136A	QTlb	122	7.2	11.2	Ca-Mg-SO_4-HCO_3	175	35	355	0	0.1824	0.0282	-0.1998
	TV-139A	QTlb, Tsb	400	7.3	13.5	Ca-HCO_3-SO_4	70	22	181	0	-0.2425	-0.3948	-1.1003
	TV-140A	QTl, Tc	260	7.6	13.8	Ca-HCO_3-SO_4	59	20	150	0	-0.0782	-0.2303	-0.7836
	TV-142A	QTl, Tc	65	7.3	13.1	Ca-HCO_3	115	24	400	0	0.2763	0.1236	-0.1005
	TV-143C	QTlb, Tsb	300	7.1*	nr	Ca-Mg-HCO_3-SO_4	76	28	160	0	-0.3916	-0.539	-1.119
	TV-153C	QTl, Tc	245	7.6*	13.0	Ca-Na-HCO_3-SO_4	92	76	400	0	0.46	0.3072	0.2106
	TV-160C	Ttc	125	7.7*	nr	Ca-HCO_3-SO_4	80	19	254	0	0.4472	0.2998	0.3552
	TV-162A	QTl	160	7.6	11.7	Na-Ca-HCO_3	45	117	369	0	0.1221	-0.0317	-0.3892
	TV-168A	Tsb	50	7.6	14.1	Ca-Na-HCO_3-SO_4	41	29	140	0	-0.2468	-0.3987	-1.044
	TV-179A	QTl	180	7.3	12.9	Ca-HCO_3-SO_4	130	28	380	0	0.2811	0.1283	-0.2642
	TV-181A	QTl	150	7.4	12.1	Ca-HCO_3-SO_4	115	33	355	0	0.3	0.1466	-0.0966
	TV-184A	Ttc	255	7.2	11.8	Ca-Na-HCO_3	70	31	250	0	-0.2198	-0.3735	-1.2235
	TV-185A	QTlb	180	7.6	13.2	Ca-Na-HCO_3	31	18	130	0	-0.3727	-0.5253	-1.4573
	TV-186A	QTl	280	7.5	15.4	Ca-Na-HCO_3-SO_4	65	24	215	0	0.0419	-0.109	-0.5855
	TV-188A	Tc	395	7.9	16.5	Na-Ca-HCO_3-SO_4	24	41	135	0	-0.1333	-0.2833	-0.8968
	TV-191A	Tto	1002	7.8	19.6	Ca-Na-HCO_3-SO_4	36	25	125	0	-0.0574	-0.2051	-0.6694
	TV-192C	QTlb, Tsb	240	7.5	18.4	Ca-HCO_3-SO_4	78	20	151	0	0.0507	-0.098	
	TV-194A	QTl	100	7.6	11.6	Ca-HCO_3-SO_4	113	30	308	0	0.4207	0.2668	0.0646
	TV-198A	QTlb, Tsb	480	8.2	16.8	Na-Ca-HCO_3-SO_4	20	36	115	0	0.0286	-0.1213	-0.6854
	TV-229C	Tto	1070	7.7*	nr	Na-Ca-HCO_3-SO_4	15	54	101	0	-0.6417	-0.7891	-2.0698
	TV-232A	QTl	120	7.4	12.2	Ca-HCO_3-SO_4	125	45	275	0	0.188	0.0346	-0.2562
	TV-235A	Ttc	220	7.1	13.4	Na-HCO_3-SO_4-Cl	28	143	173	0	-0.8929	-1.0453	-2.4505
	TV-237B	Ttc	1290	7.8*	na	Ca-Mg-HCO_3	41	14	190	0	0.1858	0.0384	0.085
	TV-238B	Tsb	105	7.3*	na	Ca-Na-HCO_3-SO_4	80	32	280	0	0.0836	-0.0638	-0.4527
	TV-239B	QTl	300	7.4*	na	Ca-HCO_3-SO_4	95	21	191	0	0.0777	-0.0697	-0.4983
	TV-240B	QTlb, Tsb	200	8.3*	na	Ca-Na-HCO_3	17	18	83	0	-0.0002	-0.1476	-1.2135
	TV-243B	Tc	138	7.4*	na	Na-Ca-HCO_3	70	85	405	0	0.2681	0.1207	0.1218
	TV-244B	Tc	320	8.0*	na	Ca-Na-HCO_3-SO_4	105	55	245	0	0.7749	0.6274	0.8908
	TV-245B	Ttc	120	7.7*	na	Ca-Na-HCO_3-SO_4	79	43	230	0	0.3804	0.233	0.0599
	TV-246B	Ttc	400	7.7*	na	Ca-Na-HCO_3-SO_4	63	27	215	0	0.286	0.1385	0.0565
	TV-247B	QTl	60	7.4*	na	Ca-HCO_3	85	25	309	0	0.2579	0.1104	-0.0152
	TV-248B	QTlb	180	8.0*	na	Ca-Na-HCO_3	38	36	195	0	0.355	0.2076	0.0173
	TV-249B	QTl	130	7.6*	na	Ca-Na-HCO_3	30	12	115	0	-0.3359	-0.4833	-1.0802
	TV-250B	QTl	60	7.8*	na	Ca-HCO_3	80	24	285	0	0.5957	0.4483	0.653
	TV-251B	Tsb	280	7.8*	na	Ca-HCO_3	47	14	195	0	0.2584	0.1109	0.0328
	TV-252B	Ttc	1190	7.9*	na	Ca-Na-HCO_3-SO_4	41	18	145	0	0.1472	-0.0002	-0.081
	TV-253B	Tto	1048	8.5*	na	Na-HCO_3	11	51	125	0	0.134	-0.0134	-0.4869

Table 12. Continued

	Sample ID	Water bearing formation	Well depth (ft bls)	Field pH*	Temperature (°C)	Water type	Ca	Na	HCO_3	CO_3	SATURATION INDEX (SI) Calcite $CaCO_3$	Aragonite $CaCO_3$	Dolomite $CaMg(CO_3)_2$
	TV-254B	QTl	210	8.0*	na	Ca-HCO_3-SO_4	88	24	195	0	0.6522	0.5048	0.6443
	TV-255B	QTlb, Tsb	286	8.0*	na	Ca-HCO_3-SO_4	79	20	190	0	0.6069	0.4595	0.5919
	TV-256B	QTlb, Tsb	260	7.7*	na	Ca-HCO_3-SO_4	115	24	265	0	0.5769	0.4295	0.5531
	TV-257B	Tc	280	7.8*	na	Ca-HCO_3-SO_4	85	29	205	0	0.4651	0.3176	0.3258
	TV-258B	QTl	na	7.9*	na	Ca-Na-HCO_3-SO_4	61	23	200	0	0.4463	0.2989	0.3001
	TV-259B	Tc	na	7.7*	na	Ca-HCO_3-SO_4	65	22	185	0	0.2353	0.0879	-0.1242
	TV-260B	QTl	275	7.8*	na	Ca-HCO_3-SO_4	67	23	200	0	0.3645	0.2171	0.2656
	TV-261B	QTl	140	8.0*	na	Ca-Na-HCO_3-SO_4	82	91	350	0	0.8369	0.6894	1.0453
	TV-262B	QTl	200	8.0*	na	Na-Ca-HCO_3	77	90	425	0	0.9071	0.7597	1.2565
	TV-263B	Tsb, Tc	700	7.7*	na	Ca-HCO_3-SO_4	59	19	165	0	0.1502	0.0028	-0.2186
	TV-264B	Ttc	210	7.4*	na	Ca-HCO_3	85	8.2	305	0	0.2629	0.1155	-0.0398
	TV-265B	Qal, Tp	72	7.4*	na	Ca-HCO_3	88	9.4	295	0	0.2598	0.1124	-0.0989
	TV-266A	QTl	75	7.6	12.0	Ca-HCO_3-SO_4	107	26	279	0	0.3596	0.206	0.1272
	TV-267A	Tc	182	7.7	11.8	Ca-Na-HCO_3-SO_4	77	51	305	0	0.3702	0.2165	0.0674
	TV-268A	Tc	215	7.5	10.8	Ca-HCO_3	79	25	304	0	0.1872	0.0327	-0.1767
	TV-273C	QTl	291	7.9*	15.5	Ca-Na-HCO_3	51	26	210	0	0.4006	0.2531	0.3432
	TV-297A	QTlb, Tsb	348	9.9*	nr	Na-Ca-HCO_3	7.9	22	57	5	0.8094	0.6619	0.0766
BEDROCK AQUIFERS	TV-100A	Tpl	1000	7.4	16.7	Ca-HCO_3	55	11	225	0	-0.062	-0.2118	-0.7044
	TV-125A	Xhu	280	9.0	21.9	Na-Cl-SO_4	5.8	170	45	6.2	-0.1329	-0.2789	-2.0338
	TV-126A	Tp, Xmg	420	9.0	26.2	Na-Cl-SO_4	6.4	170	53	9.9	0.0629	-0.08	-1.4359
	TV-127A	Xmg	400	7.9	24.3	Na-SO_4-Cl	63	570	205	0	0.2514	0.1072	-0.5541
	TV-128A	Tp	500	8.0	28.5	Na-Cl-SO_4	13	290	145	0	-0.2375	-0.3788	-2.0987
	TV-132B	Xhu	400	9.0*	na	Na-Cl-SO_4	6.1	165	36	0	-0.3615	-0.5089	-1.54
	TV-207B	Tpl	260	8.6*	na	Na-HCO_3-SO_4	2.2	335	620	20	0.0318	-0.1157	-0.2789
	TV-230A	Xhu	598	7.1	16.5	Ca-HCO_3	8.0	1.9	35	0	-1.9004	-2.0505	-4.2699
	TV-503A	Xmg	295	8.6	34.9	Na-SO_4-Cl	10	150	80	0	0.1235	-0.0133	-0.5524
	TV-504A	Qal, Tp	420	7.2	12.7	Na-Ca-HCO_3-Cl-SO_4	94	130	245	0	-0.1683	-0.3213	-1.1916
DEEP CONFINED AQUIFERS	TV-152A	Tc, Tto	1200	9.2	20.1	Na-HCO_3-SO_4	2.6	61	88	10	0.0601	-0.0872	-1.5972
	TV-170A	Tto	2527	9.5	28.0	Na-CO_3-HCO_3-SO_4	1.4	70	56	30	0.0697	-0.0719	-1.198
	TV-171A	Tto, Ttc	3180	9.4	34.5	Na-HCO_3-SO_4-CO_3	1.5	91	79	33	0.1497	0.0126	-1.0019
	TV-217A1	Ttc	1575	9.9	na	Na-CO_3-HCO_3	0.7	72	70	40	0.0247	-0.1238	-1.1036
	TV-217A2	Ttc	1785	10	na	Na-CO_3-HCO_3	0.6	72	66	45	0.1694	0.0278	-0.3495
	TV-217A3	Ttc	2003	9.9	na	Na-CO_3-HCO_3	0.6	73	74	40	-0.0778	-0.2249	-1.157
	TV-219A	Tto, Ttc	1400	9.3	16.6	Na-HCO_3-SO_4	2.1	69	90	15	0.0431	-0.1069	-1.5849
	TV-274C	Tc, Ttc	1480	9.7	20.4	Na-HCO_3-CO_3	5.3	70	98	29	0.5742	0.4268	0.0351
	TV-275C	Ttc	2020	9.6	24.8	Na-SO_4	1.9	100	32	26	-0.08	-0.2274	-1.1459
	TV-292A	Ttc	1942	9.6	nr	Na-SO_4-Cl	10	76	33	23	0.7487	0.602	0.5066
	TV-293A	Tc	1117	10.1	nr	Na-CO_3-SO_4	7.0	49	8	46	0.9308	0.7834	0.0391
	TV-301A	Ttc	1185	8.5	30.5	Na-HCO_3-SO_4	7.1	95	163	9	-1.4173	-1.5647	-3.6177
	TS-054A	Tc		8.2	18.6	Na-HCO_3	13	89	270	0	0.2024	0.0539	-0.2959
	TS-056A	Tc		7.9	15.7	Ca-Na-HCO_3	36	33	140	0	0.0141	-0.1366	-0.516

bls—below land surface; t—action level at the tap; na—not analyzed; ▭—sample is supersaturated with the noted mineral

map of calcite saturation state (Fig. 39) shows that oversaturated conditions extend from the eastern boundary of the study area to west of the municipal golf course, with the highest SI values observed near the Miranda graben.

Examples of mineral precipitation—The saturation state of calcium and other metal carbonates is a relevant and significant consideration when developing the carbonate-rich groundwater in Taos Valley aquifers. Two incidents of the precipitation of a mineral(s) from groundwater standing in a well are known to the authors and described here.

1. In May 2011, during testing of the Town of Taos well RP-3200 (TV-171), an obstruction was unexpectedly encountered in the well during pump installation by the consulting geologists. This was surprising as a sampling pump had been temporarily installed the previous week. The blockage occurred at a depth of about 1,880 feet in the 3,180-foot casing and prevented testing and development of the well. A down-hole camera was acquired and lowered into the well to investigate the obstruction. The camera captured the active growth of a solid mineral rapidly precipitating around a casing break where groundwater was pouring into the well. A photo frame from the film, taken at a depth of 1,892.0 feet (Fig. 40), depicts a small portion of the mineral growth. Flakes of the unidentified mineral actively appearing in the water are visible in the photo frame as bright, reflective patches. No samples of the water or the mineral were retrieved and its composition is unknown. The mineral blockage extended from at least 1,882 to 1,894 feet inside the well casing.
2. During the course of measuring water levels in the inactive well on the UNM Taos campus (TV-152) in 2011, the authors and hydrological field staff from NMBGMR repeatedly encountered small white flakes floating in the well water and coating the steel tape. Samples of the material were taken and analyzed at NMBGMR by electron microprobe in December 2011 to quantify the chemical content. The results showed that the material consisted almost entirely of zinc, with very minor amounts of silicon, calcium, iron, and sulfur (N. Dunbar, written communication). Based on the physical and chemical setting of the well (which is similar to that for RP-3200) and the laboratory analyses, we believe the mineral is zinc carbonate ($ZnCO_3$), known as smithsonite. Zinc carbonate, one of the metal carbonates discussed above, is soluble in systems closed to carbon dioxide, in this case the deep confined aquifer, but will readily precipitate out of solution when the water is opened to the atmosphere. Although the mineral precipitate from RP-3200 was not analyzed, it is quite possibly $ZnCO_3$.

Figure 40. Photograph of a mineral precipitate and crystal growth taken from a down-hole camera at 1,892 feet in the well casing of the RP-3200 test well (unpublished video frame, May 5, 2011). Based on the chemistry of groundwater and mineral precipitates in nearby wells, the material is believed to be zinc carbonate ($ZnCO_3$).

Summary of Water Chemistry and Age Investigations

Our interpretations of the thermal, chemical, and age characteristics of groundwater in the three aquifers of the southern Taos Valley illustrate aspects of the regional hydrology that are important to the sustainable development and management of the region's water resources. These data help determine the groundwater's source or sources, flow path, recharge, residence time, and chemical stability. The most significant thermal and chemical characteristics, and groundwater flow interpretations, are summarized here.

1. **Thermal characteristics**—Several wells in the Picuris piedmont aquifer with depths between 50 and 2,000 feet have groundwater temperatures higher than expected based on well depth and geothermal gradient (Figs. 26 and 27). These high-temperature wells are located near prominent structural features related to the three regional fault systems (Fig. 18). The spatial correlation between elevated groundwater temperature and major structures indicates upflow

of deep geothermal waters along the Picuris-Pecos faults, the Miranda graben, and at fault intersections produces the anomalously high temperatures in the Picuris piedmont aquifer.

2. **Structural controls for upflow of hydrothermal water**—Distribution maps of groundwater temperature (Fig. 26), total dissolved ion content (TDS) (Fig. 29), and the major cations and anions (Figs. 30–33) indicate that the highest values, in some cases extremely anomalous values, coincide with the Picuris-Pecos faults, the Miranda graben, and the lower Rio Pueblo geophysical faults (see also Fig. 18, the regional fault and structure model). The spatial correlation between high temperature and ion content, and the major fault structures indicates the two are related. Upflow of deep hydrothermal waters through the fracture zones of major bedrock faults, particularly at fault intersections and in the Miranda graben, produce anomalously high water temperatures and elevate the mineral content in overlying parts of the Picuris piedmont aquifer.
3. **Identifying groundwater sources**—Unique ion chemistry and water type, identified in quantitative plots called Piper diagrams, differentiate groundwater sources in the three southern Taos Valley aquifers. Figures 34 and 35 show the major water types for the bedrock and Picuris piedmont aquifers: 1) calcium-bicarbonate ($Ca\text{-}HCO_3$) water, which originates from stream and arroyo recharge and is characteristic of shallow stream-connected aquifers, upper watersheds, and the Picuris embayment; 2) sodium-sulfate water with some chloride ($Na\text{-}SO_4 \pm Cl$) from the Ponce de Leon hydrothermal system; 3) sodium-bicarbonate ($Na\text{-}HCO_3$) thermal water from lower Miranda Canyon; and 4) intermediate mixtures of these end members. The bedrock aquifer diagram (Fig. 34) indicates more complex interactions than simple mixing, including mixing of more than two water sources, and mineral solution and precipitation. The Piper diagram for the piedmont aquifer (Fig. 35) shows that most groundwater sampled contains significant levels of sodium, sulfate, and chloride and represents mixtures of surface water and deep hydrothermal sources.
4. **Inflow of hydrothermal water to the Picuris piedmont aquifer**—The widespread presence of Na, SO_4, and Cl in the piedmont aquifer (Figs. 30, 32, 33) supports our hydrogeologic model of upward migration of hydrothermal water along bedrock faults, with direct discharge into the piedmont aquifer, and dispersion throughout. In addition, the high SO_4 and Cl levels in groundwater near Miranda Creek indicate that channel infiltration of hydrothermal waters from the Ponce de Leon hot springs also recharges the Picuris piedmont aquifer, affecting shallow groundwater quality as far as the Rio Grande del Rancho. Plumes of SO_4 and Cl that extend far to the northwest of Ponce de Leon, and overlap the Miranda graben, stem from: 1) inflow of hydrothermal water through the Ponce de Leon hydrogeologic window; and/or 2) upward migration of hydrothermal water along the Picuris-Pecos basement faults.
5. **Deep confined aquifer**—The Piper diagram for the deep confined aquifer (Fig. 35) shows that deep groundwater is a mixture of hydrothermal waters from the Ponce de Leon system. The chemical end members of the hydrothermal system are represented by water at Ponce de Leon ($Na\text{-}SO_4\text{-}Cl$) and from lower Miranda Canyon ($Na\text{-}HCO_3$) (Fig. 36). Deep confined groundwater derives primarily, perhaps entirely, from hydrothermal waters with deep circulation through, and upflow along, the network of Picuris-Pecos bedrock faults. Upward migrating thermal waters pass through severely damaged, highly soluble, Pennsylvanian carbonates and evaporites, and volcanic-rich Picuris Formation sediments, before entering the deep confined aquifer. These rocks contain Ca, CO_3, Na, Cl and SO_4, or are laden with trace elements, that alter water chemistry in overlying aquifers.
6. **Fluoride**—High concentrations of fluoride (F^-) in the Picuris piedmont aquifer (up to 15 mg/L) originate from the Ponce de Leon hydrothermal system (4.4 to 20 mg/L). A fluoride plume with concentrations above 4 mg/L (the USEPA maximum contaminant level (MCL)) extends from the Ponce de Leon hot spring, down the Miranda Creek valley, to the Rio Grande del Rancho, and concentrations above 1 mg/L extend beyond Llano Quemado (Fig. 37). Fluoride levels at or above the MCL of 4 mg/L have been reported in the deep confined aquifer east of the Rio Grande del Rancho valley (TV-292 and TV-275). Fluoride concentrations in groundwater are controlled by equilibrium with the mineral fluorite (CaF_2). The addition of calcium to fluoride-rich water, using gypsum (a common calcium-rich mineral) for example, is a conventional water treatment to remove or reduce F^-. Concentrations of F^- downstream of Ponce de Leon are reduced naturally by mixing

with Ca-rich water from stream recharge along the Rio Grande del Rancho Valley (Fig. 37).

7. **Trace elements**—Lead and uranium were detected in the Picuris piedmont aquifer, and arsenic and lead in the deep confined aquifer, at levels above an MCL or health advisory (Table 10). Several trace elements were detected in many wells throughout the piedmont aquifer at levels below the MCL, including: arsenic (As), barium (Ba), chromium (Cr), copper (Cu), nickel (Ni), strontium (Sr), uranium (U), vanadium (V), and zinc (Zn) (Table 10). The highest concentrations of copper, uranium, vanadium and zinc are observed in the Picuris embayment, the Miranda graben, and the Ranchito artesian zone. The prevalence of this variety of trace elements at moderate levels, over a large scale, is remarkable and consistent with our hydrogeologic model. The chemical data generally indicate that upward migration of mineralized hydrothermal waters along the Picuris-Pecos basement faults has a significant impact on the water quality in the Picuris piedmont aquifer.

7. **Groundwater age**—Groundwater in south Taos Valley aquifers ranges in age from 1 or 2 years to over 26,000 years. Stream-connected groundwater in the Picuris piedmont aquifer (valleys and irrigated lands) has a residence time of less than 3.5 years, and in some cases has been replenished by streams and irrigation within a single year. Groundwater outside of stream valleys shows a wide range of ^{14}C ages, from 3,230 to 20,970 RCYBP (radiocarbon years before present). The oldest groundwater in the Picuris piedmont aquifer (sampled near Picuris-Pecos bedrock faults and the Miranda graben) is 20,000 to 21,000 RCYBP, and is similar in age to hydrothermal waters at Ponce de Leon. The oldest groundwater in the basin, sampled from the RP-3200 and RP-2500 wells in the deep confined aquifer, has a residence time of about 26,000 RCYBP.

8. **Mineral equilibria**—Upward migrating thermal water dissolves carbonate, evaporite and volcanic minerals from deep geologic horizons and transfers them to overlying aquifers. As conditions change in shallow aquifers or at the surface, the same or other minerals can precipitate and accumulate in pipes, streams, lakes, or aquifers. Concentrations of some metal ions in water—calcium (Ca^{2+}), magnesium (Mg^{2+}), zinc (Zn^{2+}), among others—is controlled by the amount of dissolved carbonate (CO_3), and the solubility of the metal carbonates present. Because of the diverse physical and chemical conditions in the southern Taos Valley aquifers, precipitation and dissolution reactions should be a consideration during future development of the deep confined aquifer if mixing of deep and shallow waters occurs. Two examples of the precipitation of a mineral likely to be zinc carbonate ($ZnCO_3$) are known—one in a well on the UNM Taos campus (TV-152) and a second from a casing break in the RP-3200 well. Both cases involve mixing of groundwater from the deep confined aquifer and overlying zones. The area where the Picuris piedmont aquifer is most vulnerable to metal carbonate precipitation extends from the eastern boundary of the study area westward beyond the municipal golf course (Fig. 39).

VI. SUMMARY AND CONCLUSIONS

The southern Taos Valley is located along the edge of the Rio Grande rift, and contains a great diversity of rock types and ages (from 1.7 billion years to Recent) that are overprinted by a long history of faulting and volcanism. This exceptionally complex geologic setting translates into an exceptionally complex groundwater network that includes three distinct aquifers. This study provides the first comprehensive depiction of the three interconnected aquifers and the multifaceted hydrogeologic system of the southern Taos Valley.

The key to deciphering the groundwater network is development of a geologic model capable of depicting the complexities of the local stratigraphy combined with the local structural geology. Our approach to this problem is to integrate state-of-the-art geologic mapping with the latest subsurface information and high-resolution geophysics to create a network of intersecting geologic cross sections of the study area, which become the foundation of the hydrogeologic model. The model is then tested and expanded by integrating hydrologic and geochemical data and analyses from the three aquifers. The results of this process, the hydrogeologic model, and our significant findings and conclusions are discussed in this chapter.

Geologic Model

Within the study area, four major fault systems overlap in various ways in time and space. The Picuris-Pecos fault system is exposed in the Picuris Mountains, and also exists in the buried basement rocks of the rift. The Los Cordovas faults represent the Late Tertiary to Quaternary reactivation of the old and deeply buried Picuris-Pecos faults, and as such, likely extend southward under the Picuris piedmont where they exist as growth faults that merge downward with the Picuris-Pecos structures. The Neogene Embudo fault zone affects all geologic units that are older than the Quaternary surficial deposits, and progressively down drops rocks and older structures into the basin between the Picuris Mountains and the Rio Pueblo de Taos. Collectively, these fault zones represent an enormously complex interconnected and intersecting network of faults and fractures that extend from deep in the bedrock into the shallowest aquifer zones. The surface expression of this fault model is shown in Figure 18.

The exceptionally high density of cross-cutting faults in the study area has severely disrupted the stratigraphy of the Picuris Formation and the Santa Fe Group. The Picuris Formation exists at the surface locally in bedrock valleys, and at the base of the Picuris Mountains along the top of the piedmont. In the subsurface, it deepens rapidly from the mountain front into the rift basin where it forms the transitional strata between Santa Fe Group alluvial fill and the underlying Pennsylvanian/Proterozoic bedrock. In a similar manner, the Tesuque and Chamita Formations are shallowly exposed close to the mountain front, but are down dropped into the basin along the Embudo faults. The Ojo Caliente Sandstone of the Tesuque Formation, which comprises a productive aquifer zone in the Picuris piedmont aquifer, is thickest in the northwestern study area, and thins to the south and the east. Within the study area, the Lama formation pinches out westward and southward. The Servilleta Basalt is generally thickest to the north and northwest, thins under the Picuris piedmont, and terminates near NM-68. The youngest sedimentary units of the Santa Fe Group and related lava flows are found only in the rift basin, where they were deposited in a complex three-dimensional package that is up to about 5,000 ft thick. The three-dimensional architecture of the study area is displayed in the series of intersecting geologic and derivative hydrogeologic cross sections shown in Figure 19.

Picuris Piedmont Aquifer

The Picuris piedmont aquifer is the shallow, unconfined, basin-fill aquifer that lies between the Picuris Mountains and the Rio Pueblo. The aquifer zones (composed of the Lama formation, Servilleta Basalt, Chamita Formation, Ojo Caliente Sandstone, and the Chama-El Rito Member) form a regular pattern of northeast-trending bands, shown in Figure 20, that step down into the basin along the Embudo fault zone. The most productive zones of the piedmont

aquifer are the Ojo Caliente Sandstone and fractured Servilleta Basalt. Average well yields are about 20 gpm in the Lama formation, 11 gpm in Servilleta Basalt (35 gpm for fractured basalt), 20 gpm in the Chamita Formation, 54 gpm in the Ojo Caliente Sandstone, and 31 gpm in the Chama-El Rito.

Groundwater enters the Picuris piedmont aquifer from the large mountain watersheds to the east, southeast, and south. Groundwater flow direction is generally westward toward the lower Rio Pueblo de Taos canyon. The lower Rio Pueblo de Taos, not the Rio Grande, is the primary discharge zone for the piedmont aquifer, and exerts substantial control over groundwater movement.

Sedimentary clay deposits, some of which appear to be laterally extensive, are common in the basin-fill sediments. Clay layers between basalt flows can perch and vertically partition groundwater. In the western study area near County Road 570, clay layers between basalt flows create a zone of perched groundwater that lies more than 200 feet above the regional water table. The same clay is associated with perched seeps and springs on the canyon walls of the Rio Grande gorge. Extensive pumping from such perched zones is completely unsustainable and should be avoided.

Deep Confined Aquifer

A deep confined aquifer also exists north of NM-68, where the Ojo Caliente and Chama-El Rito units are faulted down to progressively greater depths. Knowledge of this deep aquifer is limited to information gathered from seven production and test wells in two areas west and east of the Rio Grande del Rancho. West of Rio Grande del Rancho, between NM-68 and the Rio Pueblo, deep confined wells (UNM Taos, RP-2500, RP-3200, and RP-2000) draw water from the Ojo Caliente Sandstone and the Chama-El Rito at depths of 1,400–3,200 feet. South of NM-68 and closer to the mountain front the shallowest productive aquifer zone is encountered in the deep confined aquifer at a depth of over 1,000 feet. Water levels rise hundreds of feet above the top of the aquifer, typically to within 100–375 feet of land surface. East of the Rio Grande del Rancho, water levels in nested piezometers indicate a slight downward vertical gradient. Near the Rio Pueblo de Taos the hydraulic gradient is upward. Well yields are about 100 gpm in thin Ojo Caliente Sandstone and 200 gpm in Chama-El Rito. The deep confined aquifer has been targeted for future water development. Minimal confined aquifer storage, fault-related flow barriers, aquifer compartmentalization, and upward leakage of poor quality groundwater from bedrock faults are limitations for the development of deep confined aquifers in the southern Taos Valley.

Bedrock Aquifers

Small localized aquifers exist in fault-generated fracture zones in crystalline and sedimentary bedrock in the Picuris Mountains. These aquifers can have high well yields, but aquifer storage is limited. Faulted and fractured Proterozoic granite and quartzite produce 30–60 gpm. Pennsylvanian sandstone and limestone layers yield about 20 gpm, but have poor water quality. Without fracturing, well yields drop as low as 0.5 gpm. The Ponce de Leon thermal springs, located at the intersection of several faults, discharge about 66 gpm of poor quality water into Miranda Creek.

A groundwater barrier, created by faulting at the base of the mountains, generally impedes groundwater flow between bedrock and basin aquifers. Hydrogeologic windows in this basin-bedrock boundary can connect water-bearing fractured zones in bedrock with coarse sediments in the Tesuque and Picuris Formations, allowing groundwater to cross the basin-bedrock boundary. Two areas with hydrogeologic windows are: 1) the Picuris embayment and Arroyo del Alamo structural block; and 2) the Ponce de Leon area in the bottom of Miranda Canyon. There are no significant shallow groundwater sources (above 1,000 feet in depth) along the mountain front between Miranda Canyon and the Picuris-Pecos fault at the eastern boundary of Tierra Blanca. The mountain front west of the Picuris embayment to Arroyo Hondo may also be a zone of no recharge.

Miranda Canyon Hydrogeology

The Miranda graben, a fault-bounded structure in the Picuris Mountains, forms Miranda Canyon. The graben and the canyon are filled with sedimentary strata of the Picuris Formation that overlie crystalline basement rocks. The graben is truncated by the Embudo fault system, but exists in the subsurface of the rift basin where it is progressively offset by each of the north-down, left-oblique Embudo fault segments. Miranda Canyon is a small dry watershed with no perennial surface water. In the canyon, groundwater is limited to discontinuous coarse layers in the Picuris Formation and fracture zones in the granite. There is no viable water supply in Miranda Canyon to support development.

Aquifer Interconnection and Compartments

Common exposures of Picuris-Pecos and Embudo faults in some bedrock units show severe fracturing, producing high-permeability zones in the rocks that focus groundwater movement. In contrast, rare exposures of faults in the basin-fill units display clay-filled damage zones that decrease lateral permeability across high-angle faults, and create compartments in the basin-fill aquifers.

The complex network of intersecting faults in the study area affects both the Picuris piedmont and deep confined aquifers. Zones of highly faulted and fractured basement rocks act as conduits for upward movement of water into the overlying alluvial aquifer. Where the Picuris-Pecos/Los Cordovas faults intersect the Embudo faults in basin-fill units, they tend to reduce permeability and create barriers or partial barriers to lateral groundwater flow. In the piedmont and deep confined aquifers, the intersecting fault systems create fault-bounded compartments that hamper movement of groundwater through the aquifer and into wells, while focusing upward movement of potentially large volumes of water from fractured basement.

Groundwater Trends

Bimonthly and continuous groundwater-level measurements in the Picuris piedmont aquifer show three trends: 1) Seasonal fluctuations; 2) Progressive water-level declines south of Los Cordovas; and 3) Static levels with no significant change. Groundwater fluctuations and trends are illustrated in a series of hydrographs in Figure 25.

Seasonal water-level fluctuations affect areas adjacent to streams. In acequia-irrigated agricultural lands along the Rio Grande del Rancho and the upper Rio Pueblo de Taos, groundwater levels are high in the summer and low in the winter, demonstrating the significance of stream- and acequia-connected recharge. In the lower Rio Pueblo de Taos, changes in stream stage generate similar low-amplitude groundwater-level changes in adjacent wells in the Servilleta Basalt.

In the area between Los Cordovas and NM-68 groundwater levels are in progressive decline. Between 2011 and 2012, levels dropped by 1.4 to 2.6 feet, possibly in response to severe drought. By October 2015, most levels had continued to drop even though drought conditions had diminished and a wet climate was restored. From 2011 to 2014–2015, water levels at the center of the decline dropped by 3.1 to 6.3 feet. Initially the declines may have been linked to drought, but the aquifer failed to recover in the following years and continued to decline. The zone of decline lies within a fault-bounded area that coincides with the northern projection of the Miranda graben. Faulting related to the graben likely creates barriers or partial barriers to horizontal groundwater flow in the Picuris piedmont aquifer that focus and intensify the effects of pumping, therefore contributing to the water-level declines. Significant water-level declines in parts of the Picuris piedmont aquifer are expected to continue as pumping exceeds recharge.

In areas far from sources of recharge or significant pumping, specifically the lower Rio Pueblo neighborhood west of the golf course, in the Lama formation above basalt flows, and in the Chamita Formation beneath the basalts, water-levels are essentially static (±0.4 feet).

Groundwater Chemistry and Age

The thermal, chemical, and age characteristics of groundwater in the three aquifers of the southern Taos Valley indicate a hydrologically and chemically complex regional flow system affected by upflow of mineralized hydrothermal water into basin-fill aquifers via bedrock faults. Unique ion chemistry and water type differentiate groundwater sources in the three southern Taos Valley aquifers. The major water sources for the Picuris piedmont aquifers include: 1) calcium-bicarbonate ($Ca\text{-}HCO_3$) water that originates from stream and arroyo recharge; 2) sodium-sulfate-chloride water ($Na\text{-}SO_4 \pm Cl$) from the Ponce de Leon hydrothermal system; and 3) sodium-bicarbonate ($Na\text{-}HCO_3$) thermal water from lower Miranda Canyon. Most groundwater sampled from the Picuris piedmont aquifer contains significant levels of sodium, sulfate, and chloride, indicating a mixture of surface water and deep hydrothermal sources. High groundwater temperatures and sodium-sulfate-chloride content coincide with major fault structures, particularly the Picuris-Pecos faults, the Miranda graben, and the lower Rio Pueblo geophysical faults, and the Miranda Creek valley between Ponce de Leon and the Rio Grande del Rancho. Plumes of SO_4 and Cl extend northwest of Ponce de Leon and overlap the Miranda graben. The spatial distribution of elevated temperature, SO_4 and Cl indicates the input of hydrothermal waters via Miranda Creek, the Ponce de Leon hydrogeologic window, and the Picuris-Pecos basement faults. This hydrogeologic model is illustrated in Figure 41.

Upward migrating thermal water dissolves carbonate, evaporite and volcanic minerals from Pennsylvanian strata and Picuris Formation sediments and transfers them to overlying aquifers. These rocks contain Ca, CO_3, Na, Cl, SO_4 and trace elements that affect water chemistry in the overlying deep confined and piedmont aquifers. Hydrothermal water from the Ponce de Leon hot springs contains high levels of fluoride (4.4 to 20 mg/L) that impact the Picuris piedmont aquifer beyond Llano Quemado and the deep confined aquifer near the mountain front. The array of trace elements detected at low to moderate levels (below the MCL) in wells throughout the piedmont aquifer—arsenic, barium, chromium, copper, nickel, strontium, uranium, vanadium, and zinc—are likely leached by thermal fluids from volcanic-rich sediments present in the Picuris Formation. Lead and uranium are present in the Picuris piedmont aquifer and arsenic and lead in the deep confined aquifer at levels above an MCL or health advisory.

Because of the diverse physical and chemical conditions in the southern Taos Valley aquifers, mineral precipitation and dissolution reactions should be a significant consideration during groundwater development, particularly from the deep confined aquifer if mixing of deep and shallow waters occurs. The dissolved concentration of metal ions such as calcium (Ca^{2+}), magnesium (Mg^{2+}) and zinc (Zn^{2+}) is controlled by the amount of dissolved carbonate (CO_3), and the solubility of metal carbonates in the aquifer material. Precipitation of the mineral zinc carbonate ($ZnCO_3$) in the UNM Taos well and the RP-3200 well demonstrate that mixing of groundwater from the deep confined aquifer and overlying zones is an issue of concern that deserves consideration and careful planning. The area where the Picuris piedmont aquifer is most vulnerable to metal carbonate precipitation is shown in Figure 39 and extends from the eastern boundary of the study area westward beyond the municipal golf course.

Groundwater in south Taos Valley aquifers ranges in age from 1 or 2 years to over 26,000 years. Stream-connected groundwater in shallow wells (valleys and irrigated lands) has a residence time of less than 3.5 years, and in some cases has been replenished by streams and irrigation within a single year. Outside of stream valleys, groundwater shows a wide range of ^{14}C ages, from 3,230 to 20,970 RCYBP (radiocarbon years before present). The oldest groundwater in the Picuris piedmont aquifer (sampled near Picuris-Pecos bedrock faults and the Miranda graben) is 20,000 to 21,000 RCYBP, and is similar in age to hydrothermal waters at Ponce de Leon. The oldest groundwater in the basin, detected in the RP-3200 and RP-2500 wells in the deep confined aquifer, has a residence time of about 26,000 RCYBP.

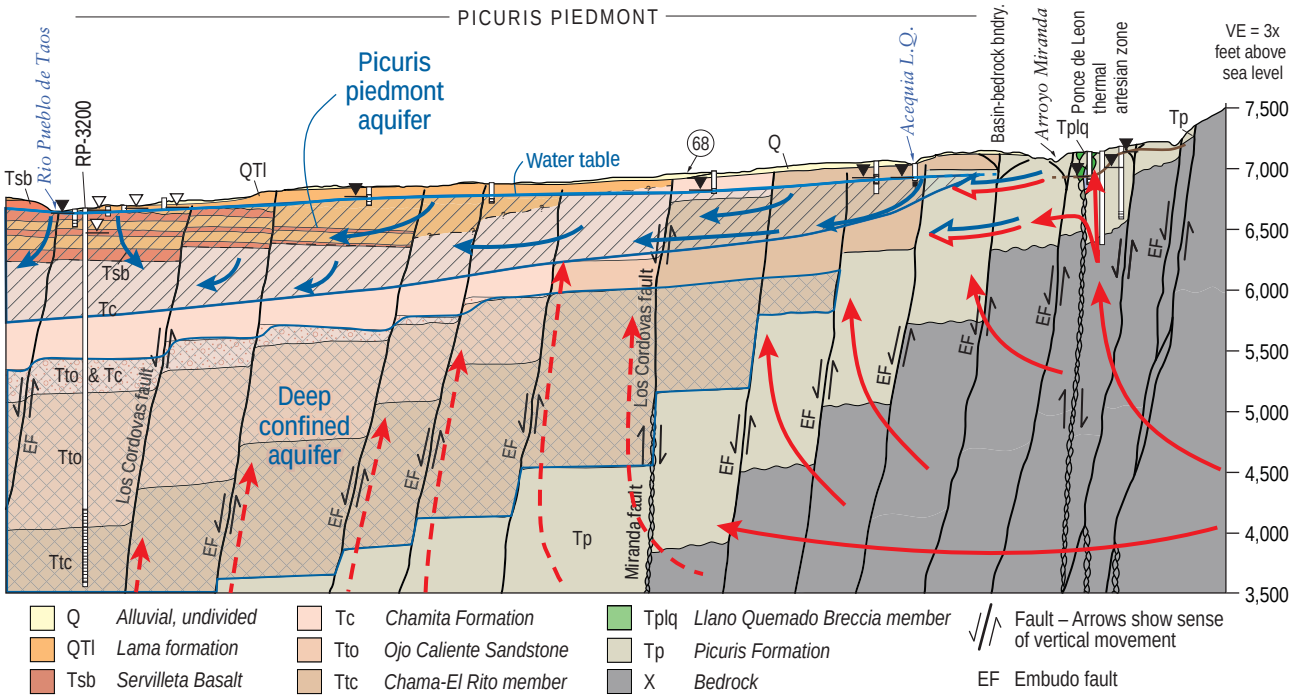

Figure 41. A hydrogeologic conceptual model of the southern Taos Valley regional groundwater flow system showing the Picuris piedmont and deep confined aquifers and the Ponce de Leon hydrothermal system.

VII. RECOMMENDATIONS

A) Water Resource Management

1. Beware of the potential consequences of mixing deep water with shallow water.
2. Water-level monitoring priorities: (1) The decline zone northwest of Llano Quemado and east of the golf course; (2) Aquifer-scale monitoring of the entire southern Taos Valley, particularly around the pumping areas. The geologic setting creates aquifer compartments that are prone to excessive drawdowns.
3. Beware of development in no-water zones, such as the high piedmont west from Talpa to the Picuris-Pecos fault at the eastern boundary of Tierra Blanca.
4. Consider water-quality maps developed in this study when siting public supply wells.
5. Nurture acequia irrigation, which helps recharge the shallow aquifer over a large area beyond the stream channel, and holds water locally in shallow aquifer/stream systems. Irrigation also simulates the natural pre-development stream system and enhances the local hydrologic cycle.

B) Future Work (science and infrastructure)

1. Geochemical modeling of the various waters, to better understand the mineral equilibria.
2. Other parts of Taos County, such as the zone from the southern Taos Valley area to Arroyo Hondo, can benefit from expanded hydrogeologic studies.
3. Seek partnerships and collaborations with state and federal sources to install regional piezometers for water-level monitoring of deep and shallow zones.
4. Make sure complete data (water levels and geochemistry) are gathered from all new test and exploration wells, and data are made public, and are applied to new studies.

PROJECT STAFF & ACKNOWLEDGMENTS

New Mexico Bureau of Geology and Mineral Resources - Project Personnel

Peggy S. Johnson, Principal Hydrogeologist
Data collection, compilation, analysis, and interpretation; technical report

Paul W. Bauer, Principal Geologist, paul.bauer@nmt.edu
Project management; data collection, compilation, and interpretation; technical report

Brigitte Felix, Report Production Coordinator, GIS Specialist, brigitte.felix@nmt.edu
GIS analysis; cartography, figures and tables; report design, layout and production editing; data collection

Support Personnel

Trevor Kludt, Hydrogeologic Lab Associate, tkludt@nmt.edu
Data collection

Mark Mansell, GIS Specialist, mmansell@nmbg.nmt.edu
GIS; cartography

Kylian Robinson, Research Assistant,
Data collection

Stacy Timmons, Aquifer Mapping Program Manager, stacy.timmons@nmt.edu
Analytical geochemistry coordination, data collection

Cathryn Pokorny, Hydrogeological Lab Technician, Kitty.Pokorny@nmt.edu
Data base

Cathie Eisen, Hydrology Field Technician,
Data collection

Bonnie Frey, Geochemist, Chemistry Lab Manager, bfrey@nmbg.nmt.edu
Geochemical sample analysis

The funding for this project was made possible through the perseverance and persuasive efforts of Ron Gardiner of Questa. We thank Adam Baker (former Taos County Manager) for arranging the principal funding for this study. The Taos County commissioners were highly supportive of the project, especially former commissioner Andrew Chavez of Ranchos de Taos. Trudy and Ed Healy provided a grant to Peggy Johnson from the Healy Foundation for an overlapping study of the Rio Grande gorge springs and for the time to complete this technical report.

Paul Drakos, Jim Riesterer, and Megan Hodgins (Glorieta Geoscience, Inc.) were exceptionally helpful by providing information on the wells and hydrogeology of the area.

Peter Vigil, Tony Benson, and Ron Gervason of the Taos Soil & Water Conservation District provided locations of some inventoried water wells in the study area.

Tien Grauch and Benjamin Drenth (USGS, Denver) provided critical geophysical insights that greatly improved the geologic cross sections. Ren Thompson (USGS, Denver) shared his expertise on the geology of the Taos Plateau volcanic field. Maryanne Wasiolek (Hydroscience Associates, Inc.) provided information on the exploratory water wells in Miranda Canyon. Michael Darr kindly shared his knowledge of the subsurface hydrogeologic conditions of the Llano Quemado area. Stan Love (NASA) assisted with geological, hydrological, and geophysical data collection. Steve Miller (New Wave Rafting) provided several fine photos.

We are greatly appreciative of the many people who helped us with land and well access, and who provided unpublished information on water wells; including Alex Abeyta (Abeyta Engineering, Inc.), Roy Cunnyngham, Mauro Bettini (Stakeout Restaurant), Bruce McClymond, Greg Hiner (The Trust for Public Land), Mark Cowan (Mark Cowan and Associates), Vishu Magee (Archetype Design), Amos Torres (Town of Taos), Rudy Baca (UNM Taos), Larry Brooks (Brooks, Pearsall, and Zantow, LLC), Gil Vigil (Vigil's Welding & Well Drilling), Ernie Atencio (Taos Land Trust), and Iris Foster. We are sincerely grateful to all of the friendly inhabitants of the Ponce de Leon area for inviting us into their homes, especially Glenda Gloss, Frank and Jonell Wilson, Brian and Jen Young, Marcy Piersol, and Steve Jackman.

We thank UNM-Taos students (under the supervision of Tony Benson) Kylian Robinson, Kathryn Gillen, Jesse Harrison, and Clyde Moya who worked with us to locate water wells.

Finally, we are greatly appreciative to the many land owners who graciously allowed us access to their wells for water level measurements and sampling.

REFERENCES

Aby, S.B., Bauer, P.W., and Kelson, K.I., 2004, The Picuris Formation: A late Eocene to Miocene sedimentary sequence in northern New Mexico; *in* Brister, B.S., Bauer, P.W., Read, A.S., and Lueth, V. W. (eds), Geology of the Taos Region: New Mexico Geological Society, Guidebook 55, pp. 335–350.

Aby, S.B., Hallet, B., and Bauer, P.W., 2007, Geologic map of the Tres Ritos quadrangle, Taos County, New Mexico: New Mexico Bureau of Geology and Mineral Resources, Open-file Geologic Map OF-GM 145, scale 1:24,000.

Appelt, R.M., 1998, $^{40}Ar/^{39}Ar$ geochronology and volcanic evolution of the Taos Plateau volcanic field, northern New Mexico and southern Colorado: Unpublished M.S. thesis, New Mexico Tech, Socorro, 58 pp.

Armstrong, A.K., and Mamet, B.L., 1979, The Mississippian system of north-central New Mexico; *in* Ingersoll, R.V.; Woodward, L.A., James, H.L. (eds.), Santa Fe Country: New Mexico Geological Society, Guidebook 30, pp. 201–207.

Armstrong, A.K., and Mamet, B.L., 1990, Stratigraphy, facies, and paleotectonics of the Mississippian system, Sangre de Cristo Mountains, New Mexico and Colorado and adjacent areas; *in* Bauer, P.W.; Lucas, S.G., Mawer, C.K., and McIntosh, W.C. (eds.), Tectonic Development of the Southern Sangre de Cristo Mountains, New Mexico: New Mexico Geological Society, Guidebook 41, pp. 241–249.

Baltz, E. H., 1978, Resume of Rio Grande depression in north-central New Mexico; *in* J.W. Hawley (ed.), Guidebook to Rio Grande rift in New Mexico and Colorado: New Mexico Bureau of Geology and Mineral Resources, Circular 163, pp. 21–228.

Baltz, E.H. and Myers, D.A., 1999, Stratigraphic framework of upper Paleozoic rocks, southeastern Sangre de Cristo Mountains, New Mexico, with a section on speculations and implications for regional interpretation of Ancestral Rocky Mountains paleotectonics: New Mexico Bureau of Geology and Mineral Resources, Memoir 48, 272 pp.

Bankey, V., Grauch, V.J.S., Drenth, B.J., and Geophex, Inc., 2006, Digital data from the Santa Fe East and Questa-San Luis helicopter magnetic surveys in Santa Fe and Taos Counties, NM, and Costilla County, Colorado: U.S. Geological Survey, Open-file Report 2006–1170, 4 pp. with maps; online only at http://pubs.usgs.gov/of/2006/1170/.

Bauer, P.W., 1988, Precambrian geology of the Picuris Range, north-central New Mexico: Ph.D. dissertation, New Mexico Bureau of Geology and Mineral Resources, Open-file Report OF-325, 260 pp.

Bauer, P.W., 1993, Proterozoic tectonic evolution of the Picuris Mountains, northern New Mexico: Journal of Geology, v. 101, pp. 483–500.

Bauer, P.W., and Helper, M., 1994, Geology of the Trampas 7.5-minute quadrangle, Taos County, New Mexico: New Mexico Bureau of Mines and Mineral Resources, Geologic Map GM-71, scale 1:24,000.

Bauer, P.W., and Kelson, K.I., 2001, Geologic map of the Taos 7.5-minute quadrangle, Taos County, New Mexico: New Mexico Bureau of Geology and Mineral Resources, Open-file Geologic Map OF-GM 43, scale 1:24,000.

Bauer, P.W., and Kelson, K.I., 2004a, Rift extension and fault slip rates in the southern San Luis Basin, New Mexico; *in* Brister, B.S., Bauer, P.W., Read, A.S., and Lueth, V.W. (eds), Geology of the Taos Region: New Mexico Geological Society, Guidebook 55, pp. 172–180.

Bauer, P.W., and Kelson, K.I., 2004b, Cenozoic structural development of the Taos area, New Mexico; *in* Brister, B. S., Bauer, P. W., Read, A. S., and Lueth, V. W. (eds), Geology of the Taos Region: New Mexico Geological Society, Guidebook 55, pp. 129–146.

Bauer, P.W., and Kelson, K.I., 2004c, Fault geometry and Cenozoic kinematic history of the southeastern San Luis Basin near Taos, New Mexico: New Mexico Bureau of Geology and Mineral Resources, Bulletin 160, pp. 70–95.

Bauer, P.W., and Ralser, S., 1995, The Picuris-Pecos fault–repeatedly reactivated, from Proterozoic(?) to Neogene; *in* Bauer, P.W., Kues, B.S., Dunbar, N.W., Karlstrom, K.E.; Harrison, B., (eds.), Geology of the Santa Fe Region: New Mexico Geological Society, Guidebook 46, pp. 111–115.

Bauer, P.W., Kelson, K.I., and Aby, S.B., 1997, Geology of the Taos SW 7.5-minute quadrangle, Taos County, New Mexico: New Mexico Bureau of Geology and Mineral Resources, Open-file Geologic Map OF-GM 12, scale 1:24,000.

Bauer, P.W., Johnson, P.S., and Kelson, K.I., 1999, Geology and hydrogeology of the southern Taos Valley, Taos County, New Mexico: Technical report for the New Mexico Office of the State Engineer: New Mexico Bureau of Geology and Mineral Resources, Open-file Report 501, 80 pp., with 4 oversize plates.

Bauer, P.W., Kelson, K.I., Aby, S.B., Lyman, J., Heynekamp, M., and McCraw, D., 2000, Geologic map of the Ranchos de Taos 7.5-minute quadrangle, Taos County, New Mexico: New Mexico Bureau of Geology and Mineral Resources, Open-file Geologic Map OF-GM 33, scale 1:24,000.

Bauer, P.W., Kelson, K.I., and Aby, S.B., 2005, Geologic map of the Peñasco 7.5-minute quadrangle, Taos County, New Mexico: New Mexico Bureau of Geology and Mineral Resources, Open-file Geologic Map OF-GM 62, scale 1:24,000.

Bauer, P.W., Johnson, P.S., and Timmons, S., 2007, Springs of the Rio Grande Gorge, Taos County, New Mexico: Inventory, Data Report, and Preliminary Geochemistry: New Mexico Bureau of Geology and Mineral Resources, Open-file Report 506, 20 pp., plus appendices and oversize plate.

Bauer, P.W., Kelson, K.I., Aby, S.B., and Mansell, M. M., in prep., Geologic map of the Picuris Mountains region, Taos County, New Mexico: New Mexico Bureau of Geology & Mineral Resources, Open-file Geologic Map, scale 1:24,000.

Benson, A.L., 2004, Groundwater geology of Taos County; *in* Brister, B.S., Bauer, P.W., Read, A.S., and Lueth, V.W. (eds), Geology of the Taos Region: New Mexico Geological Society, Guidebook 55, pp. 420–432.

Brassington, R., 2007, Field Hydrogeology: John Wiley & Sons, Ltd., West Sussex, 264 p.

Brister, B.S., Bauer, P.W., Read, A.S., and Lueth, V. W., (eds.), 2004, Geology of the Taos Region: New Mexico Geological Society, Guidebook 55, 448 pp.

Bryan, K., 1938, Geology and groundwater conditions of the Rio Grande depression in Colorado and New Mexico, in Regional Planning, Part 6, The Rio Grande Joint Investigation in the Upper Rio Grande: U.S. National Resources Commission, pp. 197–225.

Burck, P., Barroll, P., Core, A., and Rappuhn, D., 2004, Taos regional groundwater flow model; *in* Brister, B.S., Bauer, P.W., Read, A.S., and Lueth, V.W. (eds.), Geology of the Taos Region: New Mexico Geological Society, Guidebook 55, pp. 433–439.

Chapin, C.E. and Cather, S.M., 1994, Tectonic setting of the axial basins of the northern and central Rio Grande rift, *in* Keller, G.R. and Cather, S.M. (eds.), Basins of the Rio Grande rift: Structure, stratigraphy and tectonic setting: Geological Society of America, Special Paper 291, pp. 5–25.

Chapin, R.S, 1981, Geology of the Fort Burgwin Ridge, Taos County, New Mexico: Unpublished M.S. thesis, University of Texas, Austin, 151 pp.

Chermak, J., Gutzler, D.S., Johnson, P., King, J.P. and Reynis, L., 2015, New Mexico Universities Working Group on Water Supply Vulnerabilities Final Report to the Interim Committee on Water and Natural Resources: New Mexico Bureau of Geology and Mineral Resources, Open-File Report 577, 35 pp.

Clark, Ian D. and Fritz, Peter, 1997, Environmental Isotopes in Hydrogeology: CRC Press, Boca Raton, 328 p.

Coons, L.M., and Kelly, T.E., 1984, Regional hydrogeology and the effect of structural control on the flow of groundwater in the Rio Grande Trough, northern New Mexico; *in* Baldridge, W.S., Dickerson, P.W., Riecker, R.E., and Zidek, J. (eds.), Rio Grande Rift (Northern New Mexico): New Mexico Geological Society, Guidebook 35, pp. 241–244.

Cordell, L., 1978, Regional geophysical setting of the Rio Grande rift: Geological Society of America, Bulletin 89, p. 1073–1090.

Cordell, L. and Keller, G.R., 1984, Regional structural trends inferred from gravity and aeromagnetic data in the New Mexico-Colorado border region; *in* Baldridge, W.S., Dickerson, P.W., Riecker, R.E., and Zidek, J. (eds.), Rio Grande Rift (Northern New Mexico): New Mexico Geological Society, Guidebook 35, p. 21–23.

Daniel B. Stephens and Associates, 2008, Taos Regional Water Plan, Volume 1: Water Plan, January 2007, Online at www.ose.state.nm.us/isc_regional_plans7.html.

Drakos, P., Lazarus, J., Riesterer, J., White, B., Banet, C., Hodgins, M., and Sandoval, J., 2004a, Subsurface stratigraphy in the southern San Luis Basin, New Mexico; *in* Brister, B.S., Bauer, P.W., Read, A.S., and Lueth, V.W., eds., Geology of the Taos Region: New Mexico Geological Society, Guidebook 55, p. 374–382.

Drakos, P., Lazarus, J., White, B., Banet, C, Hodgins, M., Riesterer, J., and Sandoval, J., 2004b, Hydrologic characteristics of basin-fill aquifers in the southern San Luis Basin, New Mexico; *in* Brister, B.S., Bauer, P.W., Read, A.S., and Lueth, V.W., eds., Geology of the Taos Region: New Mexico Geological Society, Guidebook 55, p. 391–404.

Drakos, P., Sims, K., Riesterer, J., Blusztajn, J., and Lazarus, J., 2004c, Chemical and isotopic constraints of source-waters and connectivity of basin-fill aquifers in the southern San Luis Basin, New Mexico; *in* Brister, B.S., Bauer, P.W., Read, A.S., and Lueth, V.W., eds., Geology of the Taos Region: New Mexico Geological Society, Guidebook 55, p. 405–414.

Drakos, P., Riesterer, J., Lazarus, J., and Hodgins, M., 2016, Geologic interpretations from test and production wells drilled at the Town of Taos Rio Pueblo de Taos site, Taos, New Mexico: Glorieta Geoscience, Inc. 2007 technical report prepared for the Town and Taos and Souder, Miller, and Associates, New Mexico Bureau of Geology Open-File Report 585, 28 p. plus appendices.

Drenth, B.J., Grauch, V.J.S., Thompson, R.A., and Bauer, P.W., 2015, 3D gravity modeling of the San Luis Basin, northern Rio Grande rift, Colorado and New Mexico: Geological Society of America Abstracts with Programs, v. 47, no. 7, p. 741.

Dungan, M.A., Muehlberger, W.R., Leininger, L., Peterson, C., McMillan, N.J., Gunn, G., Lindstrom, M., and Haskin, L., 1984, Volcanic and sedimentary stratigraphy of the Rio Grande gorge and the Late Cenozoic geologic evolution of the southern San Luis Valley; *in* Baldridge, W.S., Dickerson, P.W., Riecker, R.E., and Zidek, J. (eds.), Rio Grande Rift (Northern New Mexico): New Mexico Geological Society Guidebook 35, pp. 157–170.

Faulds, J.E., and Varga, R.J., 1998, The role of accommodation zones and transfer zones in the regional segmentation of extended terranes; *in* Faulds, J.E., and Stewart, J.H., (eds.), Accommodation Zones and Transfer Zones: The Regional Segmentation of the Basin and Range Province: Geological Society of America, Special Paper 323, pp. 1–45.

Garrabrant, L.A., 1993, Water resources of Taos County, New Mexico: U.S. Geological Survey, Water-Resources Investigations Report 93–4107, 86 pp.

Glorieta Geoscience, Inc., 2001, Geohydrology of the Vista del Valle Subdivision, Taos County, New Mexico: Unpublished consulting report, 9 p., figures, tables, appendices.

Glorieta Geoscience, Inc., 2002, Drilling and testing report, Bureau of Reclamation 2000-feet deep nested piezometer/exploratory well (BOR-2) and 2100-feet deep production well (BOR-3, RG-74545-expl), Paseo del Cañon west site, Taos, New Mexico: Unpublished consulting report, August 2002, 25 p., figures, appendices.

Glorieta Geoscience, Inc., 2007, Geohydrology of the Estancias Atalaya Subdivision, Taos County, New Mexico: Unpublished consulting report, May 2007, 13 p., figures, appendices.

Grauch, V.J.S., and Keller, G.R., 2004, Gravity and aeromagnetic expression of tectonic and volcanic elements of the southern San Luis Basin, New Mexico and Colorado; *in* Brister, B.S., Bauer, P.W., Read, A.S., and Lueth, V.W. (eds.), Geology of the Taos Region: New Mexico Geological Society Guidebook, 55th Field Conference, Geology of the Taos Region, pp. 230–243.

Grauch, V.J.S., Bauer, P.W., and Kelson, K.I., 2004, Preliminary interpretation of high-resolution aeromagnetic data collected near Taos, New Mexico; *in* Brister, B. S., Bauer, P. W., Read, A. S., and Lueth, V. W. (eds), Geology of the Taos Region: New Mexico Geological Society, Guidebook 55, pp. 244–256.

Grauch, V.J.S., Phillips, J.D., Koning, D.J., Johnson, P.S., and Bankey, Viki, 2009, Geophysical interpretations of the southern Española Basin, New Mexico, that contribute to understanding its hydrogeologic framework: U.S. Geological Survey Professional Paper 1761, 88 p.

Grauch, V.J.S., Bauer, P.W., Drenth, B.J., and Kelson, K.I., 2015, Making rift connections: Geophysical insights into the geometry and temporal evolution of the Embudo transfer zone and the basin-bounding Sangre de Cristo fault, northern Rio Grande rift, New Mexico: Abstract presented at 2015 Fall Meeting, AGU, San Francisco, California,14–18 December.

Hearne, G.A., and Dewey, J.D., 1988, Hydrologic analysis of the Rio Grande Basin north of Embudo, New Mexico, Colorado and New Mexico: U.S. Geological Survey, Water-Resources Investigations Report 86-4113, 244 pp.

Hounslow, A.W., 1995, Water quality data analysis and interpretation: CRC Lewis Publishers, New York, 379 p.

John Shomaker and Associates, Inc., 2008, Water-availability assessment for Miranda Canyon Preserve Subdivision, Taos County, New Mexico: Unpublished consulting report, March 2008, 41 p., figures, appendices.

Johnson, P.S., 1998, Surface-Water Assessment, Taos County, New Mexico: New Mexico Bureau of Geology and Mineral Resources, Open-file Report OF-440, 36 pp., plus tables and appendices.

Johnson, P.S., Koning, D.J., and Partey, F.K., 2013, Shallow groundwater geochemistry in the Española Basin, Rio Grande rift, New Mexico—evidence for structural control of a deep thermal source; *in* Hudson, M. and Grauch, V.J.S. (eds.), New Perspectives on the Rio Grande Rift: From Tectonics to Groundwater: Geological Society of America, Special Paper 494, pp. 261–301.

Kelson, K.I., 1986, Long-term tributary adjustments to base-level lowering in northern Rio Grande rift, New Mexico: Unpublished M.S. thesis, University of New Mexico, Albuquerque, 210 pp.

Kelson, K.I. and Bauer, P.W., 2003, Geologic map of the Los Cordovas 7.5-minute quadrangle, Taos County, New Mexico: New Mexico Bureau of Geology and Mineral Resources, Open-file Geologic Map OF-GM 63, scale 1:24,000.

Kelson, K.I., Unruh, J.R., and Bott, J.D.J., 1996, Evidence for active rift extension along the Embudo fault, Rio Grande rift, northern New Mexico (abs.): Geological Society of America, Abstracts with Program, v. 28, no. 7, pp. A377.

Kelson, K.I., Unruh, J.R., and Bott, J.D.J., 1997, Field characterization, kinematic analysis, and initial paleoseismic assessment of the Embudo fault, northern New Mexico: Final Technical Report to the U.S. Geological Survey from William Lettis and Associates, Inc., 48 pp.

Kelson, K.I., Bauer, P.W., and Aby, S.B., 1998, Geology of the Carson 7.5-minute quadrangle, Taos County, New Mexico: New Mexico Bureau of Geology and Mineral Resources, Open-file Geologic Map OF-GM 22, scale 1:24,000.

Kelson, K.I., Bauer, P.W., Unruh, J.R., and Bott, J.D.J., 2004a, Late Quaternary characteristics of the northern Embudo fault, Taos County, New Mexico; *in* Brister, B. S., Bauer, P. W., Read, A. S., and Lueth, V. W. (eds.), Geology of the Taos Region: New Mexico Geological Society, Guidebook 55, pp. 147–157.

Kelson, K.I., Bauer, P.W., Connell, S.D., Love, D.W., Rawling, G.C., and Mansell, M.M., 2004b, Initial paleoseismic and hydrogeologic assessment of the southern Sangre de Cristo fault at the Taos Pueblo site, Taos County, New Mexico; *in* Brister, B. S., Bauer, P. W., Read, A. S., and Lueth, V. W. (eds.), Geology of the Taos Region: New Mexico Geological Society, Guidebook 55, pp. 289–299.

Konikow, L. F., 2015, Long-term groundwater depletion in the United States: Groundwater, vol. 53, no. 1, p. 2–9.

Lambert, P. W., 1966, Notes of the late Cenozoic geology of the Taos-Questa area, New Mexico; *in* Northrop, S. A., and Read, C. B. (eds.), Taos-Raton-Spanish Peaks Country (New Mexico and Colorado): New Mexico Geological Society, Guidebook 17, pp. 43–50.

Leininger, R.L., 1982, Cenozoic evolution of the southernmost Taos plateau, New Mexico: Unpublished M.S. thesis, University of Texas, Austin, 110 pp.

Lipman, P.W., and Mehnert, H.H., 1975, Late Cenozoic basaltic volcanism and development of the Rio Grande depression in the southern Rocky Mountains: Geological Society of America, Memoir 144, pp. 119–154.

Lipman, P.W., and Mehnert, H.H., 1979, The Taos Plateau volcanic field, northern Rio Grande rift, New Mexico; *in* Riecker, R.C. (ed.), Rio Grande rift—Tectonics and magmatism: American Geophysical Union, Washington D.C., pp. 289–311.

Lipman, P.W., and Reed, J.C., Jr., 1989, Geologic map of the Latir volcanic field and adjacent areas: U.S. Geological Survey, Miscellaneous Investigations Map I-1907, scale 1:48,000.

Machette, M.N., Personius, S.F., Kelson, K.I., Haller, K.M., and Dart, R.L., 1998, Map and data for Quaternary faults in New Mexico: U.S. Geological Survey, Open-file Report 98–521, 443 pp.

Machette, M.N. and Personius, S.F., 1984, Quaternary and Pliocene faults in the eastern part of the Aztec quadrangle and the western part of the Raton quadrangle, northern New Mexico: U.S. Geological Survey, Map MF-1465-B, scale 1:250,000.

Mazor, E., 2004, Chemical and Isotopic Groundwater Hydrology: Marcel Dekker, Inc., Basel, Switzerland, 455 pp.

Menges, C.M., 1988, The tectonic geomorphology of mountain front landforms in the northern Rio Grande rift, New Mexico: Unpublished Ph.D. dissertation, University of New Mexico, Albuquerque, 140 pp.

Menges, C.M., 1990, Late Cenozoic rift tectonics and mountain-front landforms of the Sangre de Cristo Mountains near Taos, northern New Mexico; *in* Bauer, P.W.; Lucas, S.G., Mawer, C.K., and McIntosh, W.C. (eds.), Tectonic Development of the Southern Sangre de Cristo Mountains, New Mexico: New Mexico Geological Society, Guidebook 41, pp. 113–122.

MJDarrconsult, Inc., 2008, Geohydrologic investigation report—proposed Los Llanos subdivision, Taos County, New Mexico: Unpublished consulting report, August 2008, 26 p., figures, tables, appendices.

Miller, J.P., Montgomery, A., and Sutherland, P. K., 1963, Geology of part of the Sangre de Cristo Mountains, New Mexico: New Mexico Bureau of Mines and Mineral Resources, Memoir 11, 106 pp.

Montgomery, A., 1953, Precambrian geology of the Picuris Range, north-central New Mexico: New Mexico Bureau of Mines and Mineral Resources, Bulletin 30, 89 pp.

Montgomery, A., 1963, Precambrian geology; *in* Miller, J.P., Montgomery, A., and Sutherland, P.K., Geology of part of the Sangre de Cristo Mountains, New Mexico: New Mexico Bureau of Mines and Mineral Resources, Memoir 11, pp. 7–21.

Muehlberger, W.R., 1979, The Embudo fault between Pilar and Arroyo Hondo, New Mexico: an active intracontinental transform fault; *in* Ingersoll, R.V., Woodward, L.A., James, H.L. (eds.), Santa Fe Country: New Mexico Geological Society, Guidebook 30, pp. 77–82.

Personius, S.F. and Machette, M.N., 1984, Quaternary faulting in the Taos Plateau region, northern New Mexico; *in* Baldridge, W.S., Dickerson, P.W., Riecker, R.E., and Zidek, J. (eds.), Rio Grande Rift (Northern New Mexico): New Mexico Geological Society, Guidebook 30, pp. 83–90.

Peterson, C. M., 1981, Late Cenozoic stratigraphy and structure of the Taos Plateau, northern New Mexico: Unpublished M.S. thesis, University of Texas, Austin, 57 pp.

Piper, A.M., 1944, A graphical procedure in the geochemical interpretation of water analyses: Transactions (American Geophysical Union), vol. 25, p. 914–923.

Read, A.S., Thompson, R.A., and Mansell, M.M., 2004, Generalized geologic map of southern San Luis Basin, in Brister, B.S, Bauer, P.W., Read, A.S., and Lueth, V.W., eds., Geology of the Taos Region: New Mexico Geological Society, 55th Annual Field Conference, p. 114.

Rehder, T.R., 1986, Stratigraphy, sedimentology, and petrography of the Picuris Formation in Ranchos de Taos and Tres Ritos quadrangles, north-central New Mexico: Unpublished M.S. thesis, Southern Methodist University, Dallas, 110 pp.

Seager, W.R., 1975, Cenozoic tectonic evolution of the Las Cruces area, New Mexico; *in* Seager, W.R., Clemons, R.E., Callender, J.F., (eds.), Las Cruces Country: New Mexico Geological Society, Guidebook 26, pp. 241–250.

Shomaker, J.W. and Johnson, P., 2005, Hydrology and water supply in the Taos region; *in* Price, L.G., Bland, D., McLemore, V.T., and Barker, J.M., (eds.); Mining in New Mexico—the Environment, Water, Economics, and Sustainable Development: New Mexico Bureau of Geology and Mineral Resources, New Mexico Decision-Makers Field Guide No. 4, pp. 16–20.

Sorrell, J.D. and Banet, C., 1993, Karavas Tract exploratory well: U.S. Bureau of Indian Affairs unpublished document, 18 p.

Steinpress, M.G., 1980, Neogene stratigraphy and structure of the Dixon area, Espanola basin, north-central New Mexico; Unpublished M.S. thesis: University of New Mexico, Albuquerque, 127 pp.

Taylor, C.J., and Alley, W.M., 2001, Groundwater-level monitoring and the importance of long-term water-level data: U.S. Geological Survey Circular 1217, 68 pp.

Thompson, R. A., and Machette, M. N., 1989, Geologic Map of the San Luis Hills Area, Conejos and Costilla Counties, Colorado: U.S. Geological Survey, Miscellaneous Investigations Series Map I–1906, scale 1:50,000.

Thompson, R.A., Johnson, C.M., and Mehnert, H.H., 1991, Oligocene basaltic volcanism of the north Rio Grande rift: San Luis Hills, Colorado: Journal of Geophysical Research, v. 96, pp. 13,577–13,592.

Timmons, S.W., Land, L., Newton, B.T., and Frey, B., 2013, Aquifer Mapping Program technical document: water sampling procedures, analysis and systematics: New Mexico Bureau of Geology and Mineral Resources Open-File Report 558, 9 p.

Ulmer, D.S. and Laury, R.L., 1984, Diagenesis of the Mississippian Arroyo Penasco Group, north-central New Mexico; *in* Baldridge, W.S., Dickerson, P.W., Riecker, R.E., and Zidek, J. (eds.), New Mexico Geological Society 35th Annual Field Conference Guidebook, p. 91–99.

Wells, S.G., Kelson, K.I., and Menges, C. M., 1987, Quaternary evolution of fluvial systems in the northern Rio Grande rift, New Mexico and Colorado: Implications for entrenchment and integration of drainage systems; *in* Menges, C., Enzel, Y., and Harrison, B. (eds.), Quaternary tectonics, landform evolution, soil chronologies and glacial deposits—Northern Rio Grande rift of New Mexico: Friends of the Pleistocene, Rocky Mountain Cell, Guidebook, pp. 55–69.

Wilson, L., Anderson, S.T., Jenkins, D., and Lovato, P., 1978, Water availability & water quality, Taos County, New Mexico: Phase A Report: Basic data on geography, climate, geology, surface water, groundwater, water rights, water use, water supply and water quality: Technical Report to the Taos County Board of Commissioners by Lee Wilson & Associates, Inc., 66 pp. plus tables and appendices.

Witcher, J.C., King, J.P., Hawley, J.W., Kennedy, J.F., Williams, J., Cleary, M., and Bothern, L.R., 2004, Sources of salinity in the Rio Grande and Mesilla basin groundwater: Water Resources Research Institute Technical Completion Report No. 330: Las Cruces, New Mexico Water Resources Research Institute, 168 p.

New Mexico Bureau of Geology and Mineral Resources

A division of New Mexico Institute of Mining and Technology

Socorro, NM 87801
(575) 835 5490
Fax (575) 835 6333
geoinfo.nmt.edu